

WL-TR-93-3095

PREFABRICATED ROOF BEAMS FOR  
HARDENED SHELTERS

AD-A278 909



LARRY M. BRYANT  
JOHN B. CAMPBELL  
PAUL F. MLAKAR

JAYCOR  
STRUCTURES DIVISION  
1201 CHERRY STREET  
VICKSBURG MS 39180

AUGUST 1993

FINAL REPORT FOR 06/01/93-08/01/93

APPROVED FOR PUBLIC RELEASE; DISTRIBUTION IS UNLIMITED.

DTIC  
ELECTE  
MAY 04 1994  
S B D

AIR BASE SURVIVABILITY SECTION  
WRIGHT LABORATORY  
139 BARNES DRIVE, SUITE 2  
TYNDALL AFB FL 32403-5323

94-13274



94 5 03 001


## NOTICES

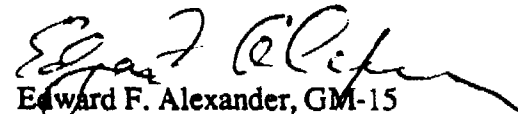
WHEN GOVERNMENT DRAWINGS, SPECIFICATIONS, OR OTHER DATA ARE USED FOR ANY PURPOSE OTHER THAN IN CONNECTION WITH A DEFINITE GOVERNMENT-RELATED PROCUREMENT, THE UNITED STATES GOVERNMENT INCURS NO RESPONSIBILITY OR ANY OBLIGATION WHATSOEVER. THE FACT THAT THE GOVERNMENT MAY HAVE FORMULATED OR IN ANY WAY SUPPLIED THE SAID DRAWINGS, SPECIFICATIONS, OR OTHER DATA, IS NOT TO BE REGARDED BY IMPLICATION, OR OTHERWISE IN ANY MANNER CONSTRUED, AS LICENSING THE HOLDER, OR ANY OTHER PERSON OR CORPORATION; OR AS CONVEYING ANY RIGHTS OR PERMISSION TO MANUFACTURE, USE, OR SELL ANY PATENTED INVENTION THAT MAY IN ANY WAY BE RELATED THERETO.

The Public Affairs Office (PA) has reviewed this report and it is releasable to the National Technical Information Service (NTIS). At NTIS, the report will be made available to the general public, including foreign nations.

This technical report has been reviewed and is approved for publication.

  
RICHARD A. REID, CAPT., USAF  
Project Officer

  
William S. Strickland, GM-14  
Chief, Air Base Survivability Section

  
Edward F. Alexander, GM-15  
Chief, Air Base Systems Branch

If your address has changed, if you wish to be removed from our mailing list, or if the addressee is no longer employed by your organization, please notify WL/FIVC, Tyndall AFB Florida 32403-5319, to help maintain a current mailing list.

Copies of this report should not be returned unless required by security considerations, contractual obligations, or notice on a specific document.

REPORT DOCUMENTATION PAGE			Form Approved OMB No. 0704-0188	
Public reporting burden for this collection of information is estimated to average 1 hour per response, including the time for reviewing instructions, searching existing data sources, gathering and maintaining the data needed, and completing and reviewing the collection of information. Send comments regarding this burden estimate or any other aspect of this collection of information, including suggestions for reducing this burden, to Washington Headquarters Services, Directorate for Information Operations and Reports, 1215 Jefferson Davis Highway, Suite 1204, Arlington, VA 22202-4302, and to the Office of Management and Budget, Paperwork Reduction Project (0704-0188), Washington, DC 20503.				
1. AGENCY USE ONLY (Leave blank)	2. REPORT DATE AUG 1993	3. REPORT TYPE AND DATES COVERED FINAL 06/01/93--08/01/93		
4. TITLE AND SUBTITLE PREFABRICATED ROOF BEAMS FOR HARDENED SHELTERS		5. FUNDING NUMBERS C F08635-91-C-0176 PE 63723 PR 2104 TA 20 WU 03		
6. AUTHOR(S) LARRY M. BRYANT JOHN B. CAMPBELL PAUL F. MLAKAR				
7. PERFORMING ORGANIZATION NAME(S) AND ADDRESS(ES) JAYCOR STRUCTURES DIVISION 1201 CHERRY STREET VICKSBURG MS 39180		8. PERFORMING ORGANIZATION REPORT NUMBER J650-93-014/1717		
9. SPONSORING/MONITORING AGENCY NAME(S) AND ADDRESS(ES) AIR BASE SURVIVABILITY SECTION WRIGHT LABORATORY 139 BARNES DRIVE, SUITE 2 TYNDALL AFB FL 32403-5323		10. SPONSORING/MONITORING AGENCY REPORT NUMBER WL-TR-93-3095		
11. SUPPLEMENTARY NOTES				
12a. DISTRIBUTION/AVAILABILITY STATEMENT APPROVED FOR PUBLIC RELEASE; DISTRIBUTION IS UNLIMITED.			12b. DISTRIBUTION CODE	
13. ABSTRACT (Maximum 200 words)  <p>The objective of this research was to develop a procedure for designing roof beams for a new generation of rapidly erected protective shelters. The cost of these roof elements should be minimized consistent with the performance constraints, and made of lightweight elements.</p> <p>Identifying a concept satisfying the above criteria was accomplished by developing an analysis procedure, designing a number of candidate beams, evaluating their respective performances, estimating costs, and finally performing laboratory tests on prototypes of the recommended concept. The design procedure utilizes a dynamic analysis of the beam based on procedures contained in design manuals, building codes, and a survey of the technical literature. Validation by finite element analysis was done to provide a check of the simplified analysis. Three concepts for prefabricated elements were considered: conventionally reinforced concrete, prestressed concrete, and a steel beam with a composite concrete slab.</p> <p>Based on the results of the concept evaluation, a test program was designed and conducted to validate the steel-concrete composite beam. The prototype beams incorporated special reinforcing designed to confine the concrete and greatly enhance its ductility and ultimate strength. The results of these tests showed that the design procedure accurately predicts the response of the steel-confined concrete composite beam.</p>				
14. SUBJECT TERMS Reinforced Concrete, Prestressed Concrete, Steel-Concrete Composite, Roof Beams, Blast, Survivability, Confined Concrete, Testing			15. NUMBER OF PAGES 186	
			16. PRICE CODE	
17. SECURITY CLASSIFICATION OF REPORT UNCLASSIFIED	18. SECURITY CLASSIFICATION OF THIS PAGE UNCLASSIFIED	19. SECURITY CLASSIFICATION OF ABSTRACT UNCLASSIFIED	20. LIMITATION OF ABSTRACT UL	

# TABLE OF CONTENTS

REPORT DOCUMENTATION PAGE - SF 298 .....	i
TABLE OF CONTENTS .....	iii
LIST OF FIGURES .....	vi
LIST OF TABLES .....	ix
PREFACE .....	x
EXECUTIVE SUMMARY .....	1
SECTION 1. INTRODUCTION .....	4
A. Background .....	4
B. Objective .....	5
C. Scope .....	6
SECTION 2. LITERATURE SURVEY .....	8
A. Analysis Methods .....	8
1. Flexural Strength .....	8
2. Shear Strength .....	8
3. Dynamic Analysis Method .....	9
B. Assumptions and Approximations .....	10
1. Ductility and Support Rotation .....	10
2. Beam Stiffness .....	14
SECTION 3. DESIGN PROCEDURE .....	16
A. Problem Definition .....	16
1. Constraints .....	16
2. Performance Criteria .....	19
B. Dynamic Analysis Method .....	21
1. Calculation of Flexural Resistance .....	21
2. Calculation of Element Stiffness .....	23
3. SDOF Calculation .....	23
C. Additional Design Details .....	25
1. Reinforced Concrete Concept .....	25
2. Prestressed Concrete .....	28
3. Steel-Concrete Composite .....	32
4. Shear and Bending of Top Slab .....	33
SECTION 4. CONCEPT EVALUATION .....	42
A. Design Procedure Analysis of 15-Ton Beams .....	42

For

☒  
☐  
☐

on

Library Codes

Serial and/or

Special

Dist.

A-1

## TABLE OF CONTENTS (Continued)

B. Validation With Finite Element Analysis.....	46
1. Reinforced Concrete.....	49
2. Prestressed Concrete .....	50
3. Steel-Concrete Composite.....	50
C. Cost Estimate and Preliminary Evaluation .....	51
D. Extended Evaluation Criteria.....	55
E. Analysis of Reduced Weight Beams for Original Concepts .....	56
F. Analysis of Fiber Reinforced Beams .....	59
1. Background.....	59
2. Objective and Approach .....	60
3. Concrete Beams with External Carbon Fiber Sheets.....	61
4. Analysis of Bench Scale Experiments.....	63
5. Dynamic Response of Full Size CFRP Reinforced Beams .....	69
6. Pultruded Fiberglass Beams.....	72
7. Conclusions and Recommendations .....	76
F. Final Evaluation .....	77
SECTION 5. ENHANCING BEAM DUCTILITY WITH CONFINED CONCRETE. 81	
A. Confined Concrete Analysis .....	81
1. Background.....	81
2. Analysis of Confined Concrete.....	83
B. Application to Roof Beam Slab.....	92
SECTION 6. PROTOTYPE TEST PROGRAM.....	95
A. Objectives.....	95
B. Design and Fabrication of the Test Beams .....	96
1. Laboratory Setup .....	96
2. Design and Fabrication of Test Beams .....	99
3. Instrumentation of Test Beams .....	106
C. Discussion of Results .....	111
1. Description of Tests .....	111
2. Overall Performance.....	115
3. Response Comparisons.....	120
4. Strain Gage Results .....	125
5. Confined Concrete Slab.....	131

## TABLE OF CONTENTS (Concluded)

SECTION 7. Summary, Conclusions and Recommendations .....	133
A. Summary .....	133
B. Conclusions .....	134
C. Recommendations.....	134
SECTION 8. References .....	135
APPENDIX A - DESIGN PROCEDURE FORMULAS.....	142
A. Reinforced Concrete .....	142
1. Flexural Resistance.....	142
2. Stiffness .....	143
B. Prestressed Concrete.....	146
1. Flexural Resistance.....	146
2. Stiffness .....	147
C. Steel-Concrete Composite.....	150
1. Flexural Resistance.....	150
2. Stiffness .....	151
D. Mass of Roof Beams and overlying Soil .....	153
1. Reinforced Concrete.....	153
2. Prestressed Concrete .....	153
3. Steel -Concrete Composite.....	153
4. Overlying Soil .....	153
5. Mass .....	153
E. Dynamic Analysis.....	154
1. Equivalent Mass and Net Resistance:.....	154
2. Equation of Motion.....	154
3. Dynamic Shear Force .....	155
APPENDIX B. PROTOTYPE BEAM TEST DATA.....	157

## LIST OF FIGURES

Figure 1. Modular Hardened Shelter. ....	5
Figure 2. Ductility Factor For Reinforced Concrete Beams with Varying Amounts of Reinforcing. ....	14
Figure 3. Peak Dynamic Pressure on Shelter Roof From Assumed Threat. ....	17
Figure 4. Idealized Dynamic Structural Loadings for 20- and 50-Foot Roof Spans. ....	18
Figure 5. Effective Width of Slabs for Three Concepts. ....	22
Figure 6. Abutment Requirement for Prestressed Roof Beam to Avoid Tensile Bond Failure. ....	29
Figure 7. Transverse Shear and Flexural Failure Modes of Reinforced Concrete or Prestressed Slab. ....	34
Figure 8. SDOF Model of Cantilevered Roof Slab. ....	35
Figure 9. General Configuration of Reinforcing for Slab Portion of Reinforced Concrete of Prestressed Beam. ....	38
Figure 10. Development of Thrust in Roof Slabs. ....	39
Figure 11. Comparison of Shear Strength Equations for Members Subject to Axial Load. ....	40
Figure 12. Design Procedure Results for 50 Foot Beams. ....	43
Figure 13. ADINA Finite Element Grid for 50 Foot Prestressed Beam. ....	47
Figure 14. Material Models for ADINA Analysis of Beams. ....	48
Figure 15. Reinforced Concrete Load Deflection Results - ADINA and Design Procedure. ....	49
Figure 16. Finite Element Results for 50 foot Prestressed Concrete Beam. ....	50
Figure 17. Finite Element Results for 50 foot Steel Concrete Composite Beam. ....	51
Figure 18. Sensitivity of Overall Beam Cost to Variations in Unit Prices. ....	54
Figure 19. Comparison of Reduced Weight Beams Having Similar Dynamic Resistances. ....	58
Figure 20. Comparison of Dynamic Resistances for Equal-Weight Beams. ....	59
Figure 21. Flexural Strength Model for General Externally Reinforced Concrete Beam. ....	62
Figure 22. Lab Specimen Reinforcement Configurations and Loading Geometries. ....	64
Figure 23. Laboratory Specimen Flexural Strength Models. ....	65
Figure 24. Comparison of Computed and Observed Load Capacities of Laboratory Specimens. ....	66
Figure 25. Full Size CFRP Beams Required for Dynamic Loads. ....	71
Figure 26. Maximum Response Chart for Elastic SDOF Systems Showing CFRP Fiberglass Beam Responses. ....	72
Figure 27. Pultruded Fiberglass Beam Designs for 20-Foot Roof Span. ....	74
Figure 28. Pultruded Fiberglass Beam Designs for 50-Foot Roof Span. ....	75
Figure 29. Proposed Lightweight Two-Way Roof System Using Pultruded Fiberglass Beams. ....	80

Figure 30.	Typical Stress-Strain Curves for Normal to Very High Strength Concrete in Compression. ....	82
Figure 31.	Axial Stress-Strain Curves for $f'_c = 3600$ psi Concrete Under Triaxial Load Conditions. (Reference 48).....	82
Figure 32.	Typical Steel-Concrete Composite Beam Stresses, Strains, and Load-Deflection Response.....	83
Figure 33.	Behavior of Symmetric Axially Loaded Members with Different Levels of Confining Reinforcement.....	85
Figure 34.	Biaxial Confinement in Rectangular Members. ....	87
Figure 35.	Analytical Model of Stress-Strain Curve for Confined Concrete. ....	89
Figure 36.	Measurements Between Laterally Supported Longitudinal Bars from Reference 3. ....	91
Figure 37.	Examples of Transverse Reinforcement from Reference 3 .....	91
Figure 38.	Example Reinforcement Options for 24-Inch-Wide, 6-Inch-thick Normal Strength Concrete Slab. ....	92
Figure 39.	Analytic Stress-Strain Curves for Example Slab. ....	94
Figure 40.	Schematic View of 150-Ton Load Frame Used for Prototype Beam Tests. ....	97
Figure 41.	Three Regions Defined for Displacement Controlled Beam Tests. ....	98
Figure 42.	Prototype Beam Four-Point Load Configuration, Shear, and Moment Diagrams.....	99
Figure 43.	Fabrication Details for Prototype Beams. ....	101
Figure 44.	Prototype Beams During Assembly of Reinforcing Cage and Concrete Placement .....	104
Figure 45.	Sketch of Nomenclature for Strain Gage Levels.....	107
Figure 46.	Details of Strain Gage Instrumentation of Prototype Beams.....	108
Figure 47.	Modified Level 1 (Top of Slab) Strain Gage Locations. ...	109
Figure 48.	Locations of Displacement Monitoring Gages. ....	110
Figure 49.	Concrete Cylinder Strength On Each Day Of Testing.....	111
Figure 50.	Pretest Photograph of Beam 10A Showing Spreader Beam, Load Points and Roller Supports .....	113
Figure 51.	Gimbaled Support Condition After Test Showing Yielded Roller and Bottom Flange.....	114
Figure 52.	Beam 16A at Conclusion of Test Showing Spalled Concrete Layer and Permanent Deformation. ....	115
Figure 53.	Load-Deflection Plots for Beams 10A.....	116
Figure 54.	Load Deflection Plots for Beams 10B .....	117
Figure 55.	Load Deflection Plots for Beams 16A.....	118
Figure 56.	Load Deflection Plots for Beams 16B .....	119
Figure 57.	Beam 16B At Conclusion of Test with 11 Inches of Permanent Deflection. ....	120



Figure 58.	Load-Deflection Curves for 10-Foot Prototype Beams with Design Procedure and ADINA Predictions.....	122
Figure 59.	Load-Deflection Curves for 16-Foot Prototype Beams with Design Procedure and ADINA Predictions.....	123
Figure 60.	Confined Concrete Core with Layer of Spalled Concrete - Beams 16A and 10B. ....	124
Figure 61	Confined Concrete Core with Thin Layer of Spalled Concrete - Beam 16B. ....	125
Figure 62	Location of Auxilliary Strain Gages on Beam 16B. ....	126
Figure 63.	Measured Strain Distribution in Beam 10A at 1/2 Inch Midspan Deflection.....	128
Figure 64.	Moment-Curvature Diagram for Test beams.....	129
Figure 65.	Buckled Longitudinal Rebar in Beam 10A. ....	132

## LIST OF TABLES

TABLE 1.	SUMMARY OF RESULTS FOR 50-FOOT LONG, 15-TON BEAMS .....	42
TABLE 2.	PARAMETER STUDY FOR 15 TON BEAMS .....	46
TABLE 3.	FABRICATION COST ELEMENTS .....	52
TABLE 4.	BEAM FABRICATION COST ESTIMATE.....	53
TABLE 5.	MEAN AND SIMULATED VARIATION IN FABRICATION COST PER UNIT WIDTH OF BEAM.....	54
TABLE 6.	DESIGN PROCEDURE RESULTS FOR 50 FOOT LONG EQUAL CAPACITY BEAMS .....	57
TABLE 7.	PHYSICAL PROPERTIES OF CFRP SHEETS AND EPOXY ADHESIVE.....	63
TABLE 8.	4-POINT BENDING OF EXTERNALLY REINFORCED CONCRETE BEAMS .....	67
TABLE 9.	SINGLE POINT LOAD BEAM TEST RESULTS .....	69
TABLE 10.	SUMMARY OF FULL SIZE CFRP BEAM SHAPES .....	70
TABLE 11.	PHYSICAL PROPERTY RETENTION FOR TYPICAL PULTRUDED BEAMS.....	77
TABLE 12.	SUMMARY INFORMATION FOR CONCEPT EVALUATION.....	78
TABLE 13.	EVALUATION OF CANDIDATE BEAMS .....	79
TABLE 14.	BEAM TEST DISPLACEMENT RATES .....	98
TABLE 15.	CONCRETE MIX PROPORTIONS.....	106
TABLE 16.	SUMMARY OF CONCRETE CYLINDER STRENGTHS.....	112
TABLE 17.	MEASURED DUCTILITY AND SUPPORT ROTATIONS FOR PROTOTYPE BEAMS.....	121
TABLE 18.	LOCATION AND NUMBERING OF STRAIN GAGES .....	126

## **PREFACE**

This report was prepared by JAYCOR, Structures Division, 1201 Cherry Street, Vicksburg, MS 39180, Contract No. FO8635-91-C-0176, for Wright Laboratory, Airbase Survivability Section (WL/FIVCS), Suite 2, Barnes Drive, Tyndall Air Force Base, Florida 32403-5323.

The authors wish to acknowledge the technical support provided by Mr. Stan Strickland of Wright Laboratory Air Base Survivability Section.

The work was performed between June 1991 and August 1993. The WL/FIVCS project officers were Capt. Diane B. Miller and Capt. Richard A. Reid.

## EXECUTIVE SUMMARY

### A. Objective

The objectives of this research effort were to (1) develop a procedure for designing prefabricated roof elements for a rapidly erectable hardened shelter, (2) evaluate five structural concepts to select the most promising, and (3) experimentally validate the design procedure methods, assumptions, and estimates of strength, stiffness, and ductility via static load tests on prototype beams.

### B. Background

The Air Force requires a variety of protective structures to protect against the airblast, ground shock, fragmentation, and cratering effects of increasingly accurate and destructive conventional munitions. Required characteristics of many of these new generation shelters include rapid construction with reduced dependence on skilled labor, high levels of protection from advanced weapons, and concealment. One concept under development consists of an earth-covered shelter constructed with reinforced soil walls and prefabricated roof elements.

### C. Scope

The study developed and validated a design procedure for precast roof elements of the modular hardened shelter.

### D. Methodology

The design procedure developed represents a synthesis of existing analysis and design methodologies described in textbooks, technical manuals, journals and concrete and steel codes. A literature survey supplemented current knowledge and identified key areas for investigation, as described in Section 2 of this report. Recommendations from the literature regarding appropriate performance criteria, i.e., ductility factors and support rotation, and appropriate measures of beam stiffness were considered. The general level of threat, shelter widths, and maximum allowable beam weight were also defined for concept evaluation.

The design procedure and its basis are described in Section 3, with actual formulae for each concept and design mode presented in detail in Appendix A. The dynamic response of the roof beam was determined using an equivalent single degree-of-freedom (SDOF) system, which requires only moderate computational effort and provides sufficient accuracy for this type of system. Additional design details are identified that must be adequately addressed to ensure that the beam can develop its intended flexural strength and ductility. The design procedure is explained and detailed for the five structural concepts considered herein.

Portions of the design procedure were validated by comparison of the static resistance function using the simple procedure with the results of detailed nonlinear finite-element analyses for the initial three structural concepts.

Fiber-reinforced composite beams, including an in-house WL/FIVCS research program to reinforce concrete beams using sheets of carbon-fiber reinforced plastic (CFRP), were

investigated for this application. Pultruded fiberglass beams were also investigated to determine their applicability for the roof elements. Conceptual designs for CFRP reinforced concrete beams and pultruded fiberglass beams to withstand conventional weapons effects were developed and evaluated.

An evaluation of the reinforced concrete, prestressed concrete, and composite steel-concrete concepts based only on estimated fabrication cost indicated that the steel-concrete composite was the most promising candidate for the roof beams. Subjective evaluation of all five concepts, including fiber-reinforced composites and pultruded fiberglass, used a more extensive set of evaluation criteria reflecting cost, weight, handling, storage, erection and confidence and indicated that the steel-concrete composite concept was most promising.

The utility and efficiency of the steel-concrete composite concept was further investigated by consideration of the effects of confinement of the concrete in the top flange slab. The beneficial effects of concrete confinement include a marked increase in strength and ductility. The analytical investigations of this enhancing technology indicated potential benefits worthy of further consideration. In fact, the steel-concrete composite with concrete confinement was selected for experimental verification by a prototype test program.

#### E. Test Description

A prototype test program was developed to provide experimental validation of the steel-confined-concrete composite concept in terms of strength, ductility, and constructability. Specifically, the static flexural resistance function developed analytically using the design procedure relies on full development of theoretical strength and reliability of this strength over a wide range of ductility, a factor yet unproven by experimental verification. In addition to validation of the static resistance function, the overall design procedure was partially validated via prototype testing. Specifically, the non-flexure-related resistance of the concept, including shear and bearing, were verified through the tests.

Prototype steel-confined concrete composite beams were designed using the procedure developed herein. Four beams were tested at the Structures Laboratory, U.S. Army Waterways Experiment Station (WES) in Vicksburg, MS. The prototype test beams were fabricated using standard concrete, reinforcing steel, and plate steel. Standard welds and Nelson shear studs (ASTM A108) were specified. Each beam was instrumented with strain and displacement gages.

#### F. Results

The results of the four prototype beam tests were encouraging. Most importantly, the overall performance of the test specimens met and exceeded expectations as to strength, stiffness, and ductility. Secondly, the test procedures and execution satisfied their intended purpose. All four of the test specimens exhibited considerable ductility, far beyond that observed and calculated for beams without significant confining steel in the concrete. It is important to note that none of the tests were stopped due to imminent or actual failure, but rather due to the loss of rattle space between the beam and the floor or spreader beam. The test program provided (1) a proof-of-concept for the confined concrete-steel composite beam and (2) a baseline to measure the accuracy and appropriateness of the analytical models and methods of this work.

## G. Conclusion

A simple design procedure for precast roof elements was developed and validated by detailed analytical methods and prototype testing. An efficient, prefabricated, structural roof beam was satisfactorily developed that met the logistical and weapons effects criteria established for this project. This steel-concrete composite beam will permit beams with high strength to weight ratio to be designed and constructed using conventional concrete and steel materials, satisfying the desired objectives of this research program.

## H. Recommendations

The design procedure and concept evaluation should be further validated as part of a complete program for full-scale field testing of a family of hardened shelters. The design procedure should be implemented in a computer application for design use. In particular, the design procedure should be adopted for use in design of modular, rapidly-erectable hardened shelters.

## I. Application

The design procedure can be directly applied to design hardened shelter roofs and to evaluate shelter roof concepts for a wide range of weapon threats and shelter geometries.

## J. Benefits

The design procedure and the concept evaluations provide, in a concise and rational format, a practical tool and valuable guidance for design of hardened shelter roofs.

## K. Transferability of Technology

Contractors for DOD projects requiring blast-resistant design of shelter roofs can directly apply the procedures and guidance herein. Civilian projects requiring hardened roofs can also derive design guidance from this study.

## SECTION 1. INTRODUCTION

### A. BACKGROUND

The Air Force requires a variety of protective structures to accomplish its strategic and tactical missions. These facilities, for example, include aircraft shelters, command centers, critical maintenance facilities, and munitions storage. The structures must protect against the airblast, ground shock, fragmentation, and cratering effects of increasingly accurate and destructive conventional munitions. In many applications, such structures must be rapidly erectable. In all cases, the cost of these facilities should be minimized consistent with the performance constraints and, where possible, made of lightweight elements that can be handled easily. In an era of reduced budgets and manpower limitations, the importance of cost effective and efficient structural systems is obvious.

Rapid and unpredictable changes in the scale and geographic diversity of future military involvement requires a new approach to construction of hardened shelters. A high probability exists for operating from forward "bases" which have not previously been used for military purposes, or from rapidly constructed bare bases. It is likely that no hardened shelters will exist beforehand to house aircraft, personnel, and munitions. Therefore, it may be necessary to construct hardened shelters using troop units and equipment already in place or easily obtained/deployed. Required characteristics of these new generation shelters include rapid construction with reduced dependence on labor, high levels of protection from advanced weapons, and concealment. One concept under development consists of an earth-covered shelter constructed with reinforced soil walls and prefabricated roof elements, shown in Figure 1.

The shelter consists of reinforced earthen walls lined with contiguous interlocking modular wall panels that circumscribe the protected space. The structural roof consists of prefabricated beams with an integral slab, placed adjacent to one another on top of the modular wall and part of the soil wall to form a continuous hardened roof. The structure will be covered with soil and may have a burster slab and possibly projectile deflection layers of rock rubble or a concrete deflection grid. The roof beams, wall panels, and additional construction materials would be brought from strategic storage locations by ground, sea, or possibly air transportation. Therefore, it is imperative that the beams be structurally efficient to minimize the individual weight and total number requiring transport and erection.

The modular hardened shelter depicted in Figure 1 should provide a high level of protection from the blast and shock effects of a wide range of conventional, very lethal munitions. This is in contrast to lightweight, rapidly erected "airmobile" shelters which provide environmental protection and only minimal hardening against conventional weapons threats.

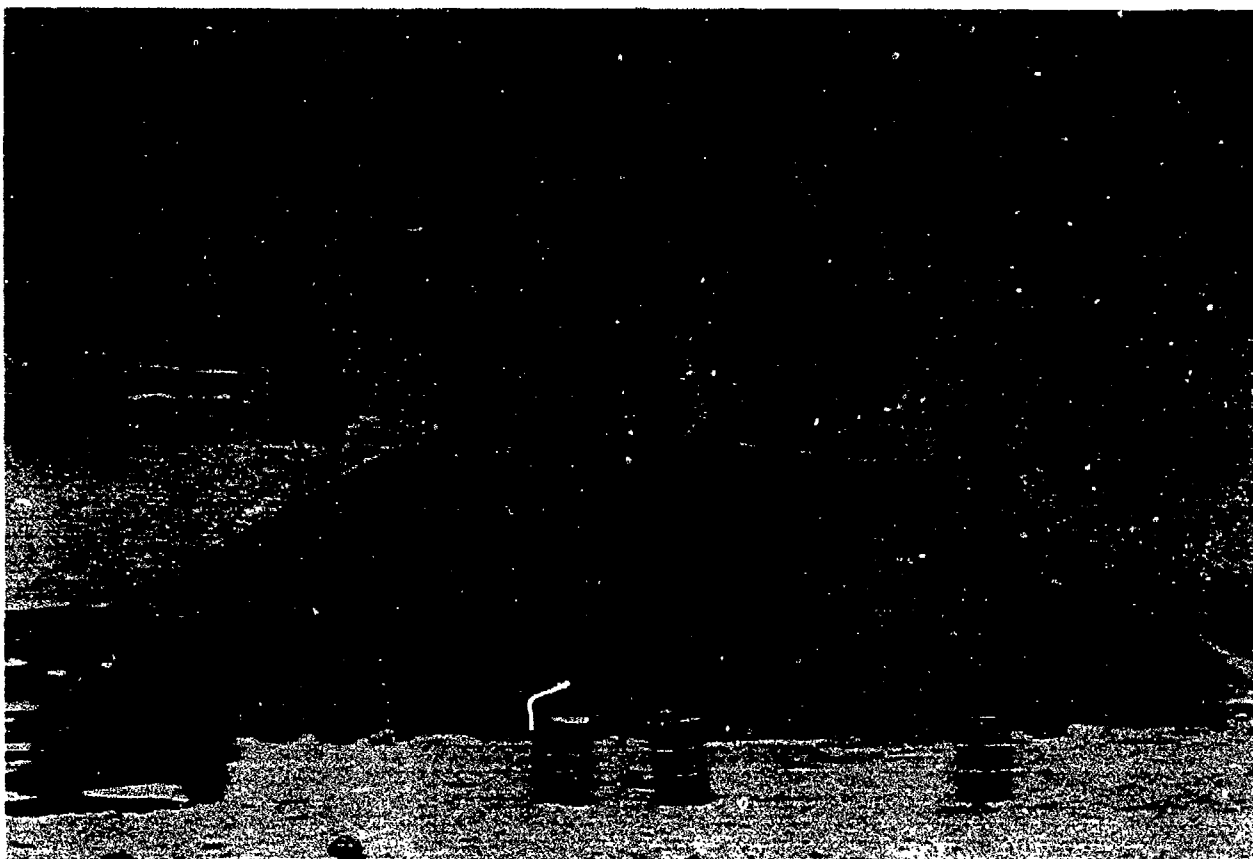


Figure 1. Modular Hardened Shelter (USAF photograph).

## B. OBJECTIVE

The objective of this research effort was to develop a dynamic design procedure for prefabricated roof elements subjected to blast loads. One of the goals in developing the design procedure was to keep the computational effort simple so that the resulting analysis can be carried out in a spreadsheet, or readily programmed in Basic, FORTRAN, or mathematical applications programs such as Mathcad®. This will enable the end user to design roof elements using familiar procedures without resorting to sophisticated computer modeling techniques. In addition, the designer can quickly analyze and refine the roof beam design, or examine the effect of various parameters, without resorting to a computationally intensive method such as finite element analysis.



A second objective of the research was to evaluate five roof beam structural concepts and then to select the structural concept that appeared most promising. A set of criteria and weighting factors was developed for the purpose of selecting the most promising structural roof concept.

### C. SCOPE

The scope of this research was limited to the roof system. The modular wall, reinforced soil, and burster slab were not part of the research effort. Five concepts for prefabricated roof elements were considered: conventionally reinforced concrete, prestressed (pretensioned) concrete, steel-concrete composite, externally reinforced concrete and pultruded fiberglass. Based on the selection process, the steel-concrete composite slab was chosen as the preferred concept. An appropriate design procedure for each concept was documented in the text.

The design procedure represents a synthesis of existing analysis and design methodologies described in textbooks, technical manuals, journals, and concrete and steel codes. A survey of this literature was first conducted to supplement our current knowledge and identify key areas for investigation, as described in Section 2 of this report. During this stage it was also necessary to agree on the general level of threat, shelter widths, and maximum allowable beam weight. Development of the dynamic design procedure included defining the general constraints and formulating structural analysis methods suited to implementation in a spreadsheet or simple computer program, as described subsequently in Section 3. As part of the concept evaluation described in Section 4 of this report, validation of the structural calculations by finite element analysis was conducted to ensure that the design procedure results agreed with those obtained through rigorous analysis. This validation exercise was conducted on example beam designs for each of the initial three concepts. A cost model was developed and applied to the resulting beam designs to evaluate their relative construction costs. Also at this stage several "excursions" were made to investigate a number of issues identified in the literature survey, specifically whether the benefits of using high performance and/or lightweight concrete justified its consideration.

The paramount importance of minimizing beam weight to improve structural efficiency underscored the next stage of development. Smaller, lighter beams for each concept were investigated and a more complete set of evaluation criteria developed and used to evaluate the resulting designs. As described in Section 5, the most promising concept (composite steel and concrete) was further investigated to include the enhancing effects of concrete confinement.

Based on the results of the concept evaluation, a test program was designed and executed to validate the most promising concept. Static load tests were conducted on prototype beams to determine their strength, stiffness, and amount of ductility relative to prediction by the design

procedure and finite element analysis. The prototype test program is described in detail in Section 5.

In Section 7 of this report, conclusions are drawn regarding the development and use of the design procedure and the concept which emerged as the most promising based on structural efficiency and economic considerations. Recommendations regarding future work to improve the overall design of the protective structure are also briefly described.

## SECTION 2. LITERATURE SURVEY

### A. ANALYSIS METHODS

Numerous researchers have previously investigated analysis methods and parameters relevant to the design of modular roof elements. The most relevant of the results and recommendations from the literature concerning flexural strength, shear strength, and dynamic analysis of reinforced concrete, prestressed, and steel composite elements are summarized in the following paragraphs.

#### 1. Flexural Strength

References 1 and 2 describe tests and analysis of singly and doubly reinforced lightweight, high strength, concrete beams. They found that the flexural design provisions of the American Concrete Institute (ACI) were adequate to predict the strength of these beams (Reference 3). The upper range of their experiments was an unconfined compressive strength,  $f'_c=11$  ksi and a ratio of actual to balanced steel,  $\rho/\rho_b<0.54$ .

Reference 4 describes a computational procedure for predicting the flexural resistance and ultimate deflection of concrete beams subject to severe concentrated loads. The model uses linear distribution of strains and detailed constitutive models for the concrete and steel. The concrete model includes the effect of transverse reinforcement in confining the concrete with resultant increases in ultimate strength and corresponding strain, and a correction factor for the effects of web reinforcement. The detailed calculational effort involved in this procedure resulted in very good agreement with experimental results for ultimate strength and deflection.

Reference 5 developed a detailed flexural model to investigate the increased flexural resistance of a concrete section with curvature ductility factors of 10 and 20. This research concluded that the moment capacity at yield from the detailed analysis is within 4% of the nominal moment capacity predicted by ACI, and that the increase in capacity at high ductility varies between 12% and 65%, depending on the amount of transverse reinforcement, ratio of compression to tension reinforcement, and amount of tension reinforcement. The result is also very dependent on the strain-hardening behavior of the reinforcing steel actually used.

#### 2. Shear Strength

Reference 6 investigated the shear strength of rectangular beams made from concrete with  $f'_c=10, 17$ , and 18 ksi. They found that for non-prestressed members subject to

flexure and shear, ACI Code provisions overestimate the nominal shear strength provided by the concrete when the compressive strength is above 17 ksi. For very high concrete compressive strengths, the minimum quantity of shear reinforcing specified in the 1983 edition ACI Code needs to be increased to compensate for the lack of conservatism. At some amount of web reinforcement, the code equations become conservative again, regardless of the deficiency in the  $V_c$  (concrete shear strength) term. Therefore, it appears that the minimum amount of web reinforcing depends on a limiting value of the compressive strength, which was changed in the 1989 edition of the Code.

Reference 7 describes tests of 14 beams and examination of 107 tests in the literature. This study concluded that the ACI Code is conservative for both high strength concrete and normal strength concrete beams. Increasing  $f'_c$  up to 12 ksi does not lower the safety factor, nor does using high tension steel ratios.

### 3. Dynamic Analysis Method

A single degree-of-freedom (SDOF) system is often successfully used to model the dynamic flexural response of a simply supported roof beam. Reference 8 describes a SDOF analysis with load-dependent, variable parameters rather than traditional constant SDOF parameters. This approach requires development of a moment-curvature behavior of the specific cross-section, integrating this for each load step to obtain the deformed configuration, including the effect of end restraints, and then computing the parameters of an equivalent SDOF model. While this approach offers advantages for nonsymmetric cases with complicated boundary conditions and is still fast and convenient relative to multi-degree-of-freedom (MDOF) and finite element models, it was deemed overly detailed for the design procedure analysis. Reference 9 presents an analysis technique for reinforced concrete beams subject to impulsive loads utilizing a nonlocal continuum damage/plasticity model within a Timoshenko beam finite element. Such refinements in the analysis, which replace approximations and simplifications with analytical steps, undoubtedly yield greater accuracy, as seen by the close agreement with laboratory experimental results. While the more advanced techniques improve our understanding of the physical response of structural elements under dynamic loads, the rationale given in Reference 10 for using approximate design methods is still relevant:

"From the viewpoint of practical design, the approximate methods presented here [SDOF constant parameter methods] are extremely important. They should not be regarded as merely crude approximation, to be used for rough or preliminary analysis, nor

should they be regarded as methods to be used only by engineers who lack the training or intellect to employ more sophisticated techniques. Problems in structural dynamics typically involve significant uncertainties, particularly with regard to loading characteristics. Such being the case, complex methods of analysis are often not justified. It is a waste of time to employ methods having precision much greater than that of the input of the analysis."

To ensure that the roof element develops a flexural deformation mode to absorb the blast energy, providing sufficient shear resistance is a must. In this regard, the SDOF analysis method tends to be unconservative when the duration of the dynamic load to the first natural period of the element is less than about 0.4 (Reference 11). Guidelines given by (Reference 12) are:

- For load duration  $t_d$  greater than the first natural structural period  $T_1$ , the first mode governs the response and the approximate analysis can be used.
- For  $t_d < T_1$ , the higher modes should be taken into account, and the Bernoulli-Euler beam theory gives a proper solution.
- For  $t_d \ll T_1$ , very high modes become important in the beam response and rotary inertia and shearing deformation have to be taken into account, and the Timoshenko beam theory is appropriate.

To illustrate, for a Bernoulli-Euler beam, ratios of the contribution from the first and third modes for a uniformly loaded, simply supported beam are  $y_1/y_3=243$ ,  $M_1/M_3=27$ , and  $V_1/V_3=9$ , for the deflections, moments and shears, respectively (Reference 10, pg. 165). While the first mode remains dominant, the higher modes of the beam response include a significant contribution from the high frequency content of the loading impulse. Reference 13 points out that given the approximate method for computing support reactions in Reference 14 may underestimate the maximum value for short duration loads, so this reference (14) was not used.

## B. ASSUMPTIONS AND APPROXIMATIONS

### 1. Ductility and Support Rotation

Previous research regarding appropriate performance criteria for dynamic response of beams was investigated. The relevant findings for selecting appropriate ductility factor and support rotation performance criteria is described in the following paragraphs.

Reference 15 (pg. 637-639) defines the ductility ratio for reinforced concrete elements as the ratio of curvature at ultimate strength to curvature at first yield. This value should be less than 20 for singly and doubly reinforced members. A procedure for calculating this ratio for rectangular singly and doubly reinforced beams is given.

Reference 16 (pg. 6) uses support rotation as a performance criteria for reinforced concrete elements. At  $2^\circ$  of support rotation, the compression concrete crushes. Between  $2^\circ$  and  $4^\circ$ , there is slight loss in moment capacity after the concrete crushes and the compressive force is transferred to the compression reinforcement. This requires an equal amount of compression reinforcement and tension reinforcement. Above  $4^\circ$ , the member loses structural integrity and fails. The preceding applies to members with shear reinforcing that provide shear resistance greater than the flexural resistance and provide restraint of the compressive flexural steel. Ductility factors for beams used as primary support members (versus slabs) for personnel protection should be more restrictive, and are limited to a ductility factor of 10 or  $0.5^\circ$  of support rotation. Structures to protect equipment or explosives may be designed for deflections up to incipient failure.

For steel structures, Reference 17 states that the ductility factor can go as high as 20 and support rotation can go as high as  $12^\circ$ , provided lateral bracing is adequate. For beams where safety of personnel is required, the ductility factor should be less than 10 and support rotation less than  $2^\circ$ . In order to realize this magnitude of plastic behavior, secondary modes of failure must be avoided. These modes are categorized as either instability or brittle modes of failure. Instability includes overall buckling of the member or buckling of component elements (e.g., flange buckling or web crippling). Brittle modes include local stress concentrations and residual stresses, poor welding, notch sensitive steel, shock loading or rapid strain rate sensitive steel, low temperatures, and triaxial tensile stresses in thick gusset plates, webs, and in the vicinity of welds. These brittle modes can be remedied by utilizing a type of steel that conforms to conditions anticipated in service, enforcing high standards in fabrication and workmanship, and careful design of connections.

Reference 18 presents ductility ratios reproduced from Reference 19, except that the ductility factor for reinforced concrete beams responding in flexure with at least  $1/4$  as much compressive as tensile reinforcement is reduced from 7 to 6. Reference 18 recommends using support rotation rather than ductility factor for the design of reinforced concrete members, based on the limiting values from Reference 16. For support rotations ranging from  $0^\circ$ - $2^\circ$  ultimate flexural resistance is maintained. Additional rotation results in crushing of concrete. Rotations from  $2^\circ$ - $4^\circ$  require symmetric tensile and compressive steel with either adequate shear reinforcement or lateral restraint.

Reference 19 presents generally conservative ductility factors resulting from experience in design and evaluation of many protective facilities. For reinforced concrete failing in flexure, with compression reinforcement at least 1/4 the tension reinforcement, a ductility factor up to 7 is allowed. The corresponding value for steel beams failing in flexure, assuming no instability, is 12.

Reference 20 provides a table of ductility factors for impulse and impact loads based on some very early work and analysis. The ductility factor for reinforced concrete beams in flexure is given as  $0.1/(\rho-\rho') \leq 10$ , with the limiting value for slabs given as 30. This format for the ductility ratio first appears in Reference 21 as  $0.1A_c / (A_s - A'_s) < 30$  for reinforced concrete beams. For structural steel, the ductility ratio of 20 is allowed for beams with adequate bracing to prevent local and lateral buckling (Reference 20).

References 1 and 2 describe tests and analysis of lightweight, high strength, singly and doubly reinforced concrete beams. For singly reinforced beams, they found that to achieve a displacement ductility factor of 3,  $\rho/\rho_b$  should not exceed 0.4 for  $f'_c = 8$  ksi, and 0.2 for  $f'_c = 11$  ksi. For doubly reinforced beams, both normal and high strength concrete exhibited a ductility factor less than 3 when reinforced with  $\rho/\rho_b$  greater than 0.4, and beams with  $f'_c = 11$  ksi exhibited a ductility factor that was marginally acceptable when reinforced with  $\rho/\rho_b$  of 0.22.

Reference 22 describes tests on beams with  $f'_c$  of 12 and 15 ksi with reinforcement ratio  $\rho/\rho_b$  values from 0.066 to 0.54. The beams were doubly reinforced with an equal amount of compression and tension reinforcement. They observed ductility factors between 7 and 20, computed as the ratio of the deflection at ultimate to the deflection at first yield of the tension reinforcement. Their results led them to conclude that concerns about the use of high strength concrete possibly resulting in a decrease in member ductility is largely unfounded. The parameter  $\rho/\rho_b$  was found to control the load-deflection behavior and ultimate ductility; members with low  $\rho/\rho_b$  values experienced large deformations at relative constant high loads before the maximum load was attained, whereas beams with high values of  $\rho/\rho_b$  exhibited significant load drop immediately upon crushing of compression concrete, followed by strength gain as the compression steel compensated for the crushed compression concrete.

Reference 23 uses a curvature ductility ratio, defined as the ratio of the curvature at ultimate to the curvature at first yield of the tensile reinforcement, to study the effect of design parameters on the ductility of doubly reinforced concrete beams. This study concluded that the available curvature ductility factor increases with decreasing values of  $\rho$ , increasing values of  $\rho'$ , decreasing values of  $f_y$ , or increasing values of  $f'_c$ . Each of these factors tend to decrease the depth of the neutral axis both at first yield and at ultimate strength. They recommend

$\rho - \rho' < 0.5\rho_b$  for curvature ductility factors greater than 4, and  $\rho - \rho' < 0.75\rho_b$  for ductility factors greater than 2.

In the mid 1960's, reinforced concrete design transitioned from working stress design to ultimate strength design. Results from experimental studies conducted on the strength and ductility of reinforced concrete beams formed the basis for the underlying guidance used in the current ACI Code (References 24, 25, 26 and 27). These experiments verified the validity of using the equivalent concrete stress block, equilibrium of forces, and strain compatibility to calculate the nominal flexural strength of a beam. Formulas were developed to calculate the ultimate strain capacity of the compressed concrete, yield and ultimate curvatures, the length of plastic hinging zone, and inelastic rotation of the beam at ultimate capacity. It was demonstrated experimentally that the rotational capacity of a beam under loading producing a moment gradient is greater than that for a similar beam with constant moment. Further work investigated the effect of ultimate concrete strain and strain hardening of tension reinforcing, and obtained beam rotational capacities of  $4.5^\circ$  to  $5.7^\circ$ . Tests on small and large beams found no evidence of size effect.

In a review of blast-resistant design work in the Peoples Republic of China, ductility ratios for static and dynamic flexural tests are reported to be as high as 10 for beams with small amounts of reinforcement (Reference 28). This study presents a plot of ductility versus  $a/d$ , where "a" is the depth of an equivalent stress block and "d" is the effective depth of the section. A curve fitting this data expresses this relationship as  $\mu = 0.45/(a/d)$ , as shown in Figure 2. A comparison with the results reported by Reference 22 reveals some interesting similarities. Transformation of the  $\rho/\rho_b$  data from Reference 22 into an equivalent  $a/d$  ratio shows that the ductility results from these two investigations agree quite closely (see Figure 2). This transformation is accomplished by expressing balanced failure condition as  $a_b/d = \beta_1(87,000/(87,000 + f_y))$  for singly and doubly reinforced beams, where  $a_b$  is the depth of the stress block for balanced condition,  $\beta_1$  is a function of the concrete compressive strength and  $f_y$  is the yield strength of the reinforcing steel in psi. These results are generally consistent with those reported in Reference 2 for doubly reinforced high-strength, lightweight beams.



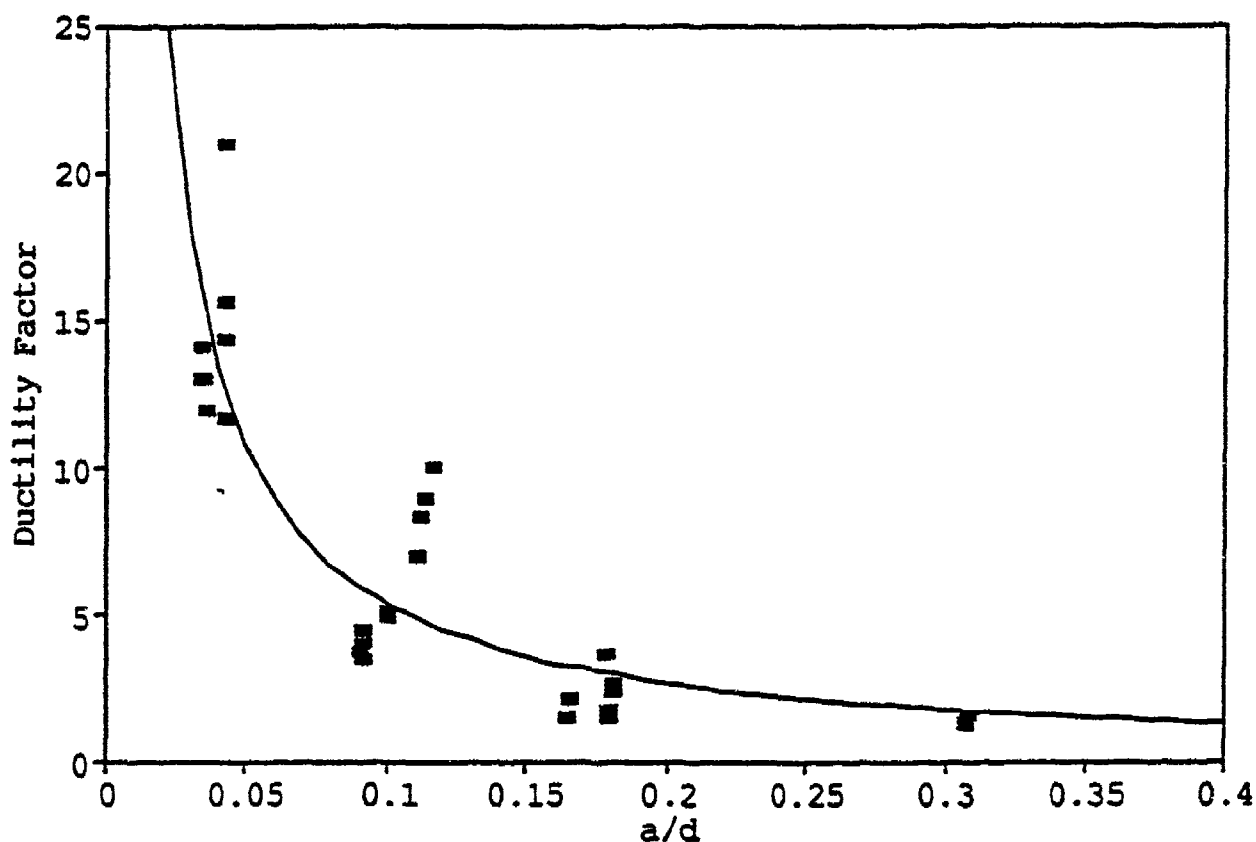


Figure 2. Ductility Factor For Reinforced Concrete Beams with Varying Amounts of Reinforcing.

## 2. Beam Stiffness

Previous research into reinforced concrete beam deflection and stiffness has generally concentrated on short-term static behavior. The relevant research in this area, and the recommendations for consideration of ultimate dynamic response, are summarized in the following paragraphs.

The ACI Code (Reference 3) presents a formula for computing beam deflections at service loads, well below ultimate. Researchers continually publish suggested revisions or alternatives to this formula for effective moment of inertia for short-term deflections. (e.g., References 30, 31). Although the ACI formula and suggested alternatives adequately predict short-term deflections under service loads, they are cumbersome to use and do not explicitly include many parameters that characterize response of reinforced concrete beams (such as reinforcement ratio  $\rho$ ).

For reinforced concrete, Reference 10 recommends the use of the average of the gross and cracked section moment of inertia for SDOF dynamic analyses, and presents a formula for moment of inertia for rectangular, singly reinforced beams, based on Reference 29:

$$I_a = \frac{bd^3}{2}(5.5\rho_s + 0.083) \quad (1)$$

Reference 15 uses the value of average section moment of inertia recommended above by Reference 10.

Similarly, Reference 16 recommends use of the average of the gross (non-transformed) and cracked section moment of inertia where the latter is obtained from formulae and graphs presenting coefficients for various reinforcement ratios and modular ratios for rectangular sections and slabs.

Whereas Reference 18 does not specifically recommend a value for reinforced concrete beam stiffness, a worked example therein uses the approximation given in Reference 10.

Reference 19 presents equations for natural period of concrete beams based on various end conditions, length, reinforcing ratio, and effective depth. This source also provides a correction term for shear deformation. In addition formulae for natural periods of steel beams based on varying end condition, length, weight, moment of inertia, and steel modulus are presented.

### SECTION 3. DESIGN PROCEDURE

The design procedure represents a synthesis of existing analysis and design methodologies described in textbooks, technical manuals, journals, and design codes. Recommendations from the current literature have been incorporated where appropriate. The design procedure is described in this section, with related formulas in Appendix A.

#### A. PROBLEM DEFINITION

The initial step of the design procedure is to define the constraints and performance criteria for a specific type of shelter and threat. Constraints include the geometry of the shelter, blast loading, and maximum allowable weight of the beams. Performance criteria, the allowable limits of dynamic structural response, are based on deflection ductility and support rotation.

##### 1. Constraints

Advantages in fabrication, handling, storage and erection of flat roof elements, coupled with the reinforced earthen wall concept, favored using straight beams versus arched or cambered roof elements. The roof was envisioned to consist of adjacent simply supported beams spanning the short dimension of the shelter. This study considered roof spans of 20 and 50 feet covering the expected range for personnel or aircraft shelters. The roof will likely have a covering of soil and may have additional protective layers. For preliminary comparisons of the initial three roof concepts, the shelter was assumed to have 6 feet of overlying soil with a burster slab.

This design procedure relies on methodologies for threat assessment, weapons effects, and determination of structural loading from other sources. The assumed threat, for preliminary design and concept comparison, was a 1000 lb. general purpose bomb. Guidance in developing detailed structural loading from such a threat, including the effects of soil-structure interaction are contained in References 32 through 36 as well as numerous supplementary papers presented in References 37 through 42. For purposes of this study, the structural load was determined from the soil pressure for the coupled, contact detonation of the bomb at the level of a burster slab, 6 feet above the roof structure surface.

The resulting soil pressures were calculated using the microcomputer implementation of the procedure of Reference 36. Figure 3 shows the computed peak pressure and impulse on the roof for this threat. This pressure distribution, both spatially and temporally nonuniform, is approximated for subsequent analysis purposes by an equivalent spatially uniform

pressure distribution. This equivalent uniform distribution of pressure was chosen to produce a midspan moment identical to that from the nonuniform peak pressure distribution. The duration of the equivalent uniform pressure loading was selected based on the nonuniform impulse at the approximate 1/4 points of the span. Figure 4 shows the resulting zero rise time, triangular pressure pulse magnitudes and durations for the 20 and 50 foot spans. More rigorous techniques for computing structural loading for specific threats, shelter geometry, and material properties would be used once the ranges of required input parameters are established. The current study focuses on development of a procedure for structural design of the roof, and therefore the loads were chosen to simply reflect a reasonable design situation.

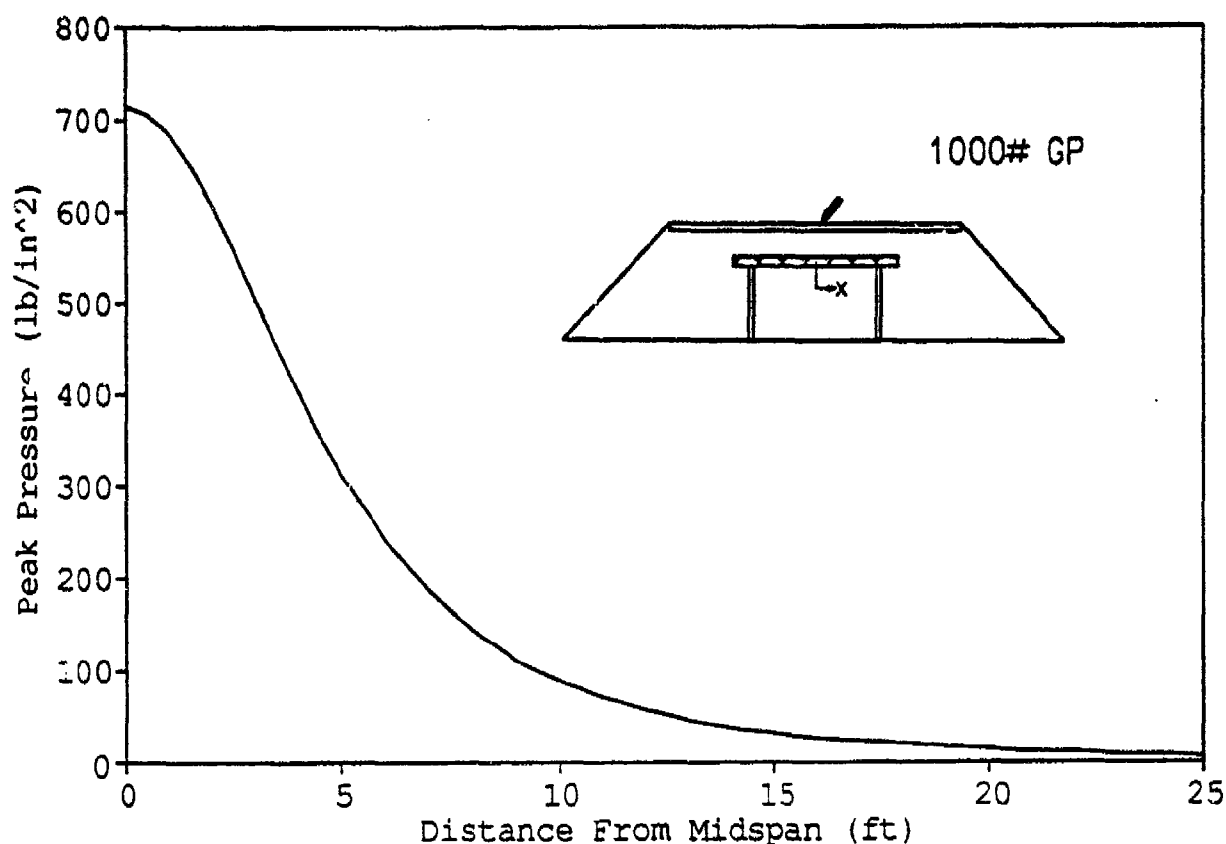


Figure 3. Peak Dynamic Pressure on Shelter Roof From Assumed Threat.

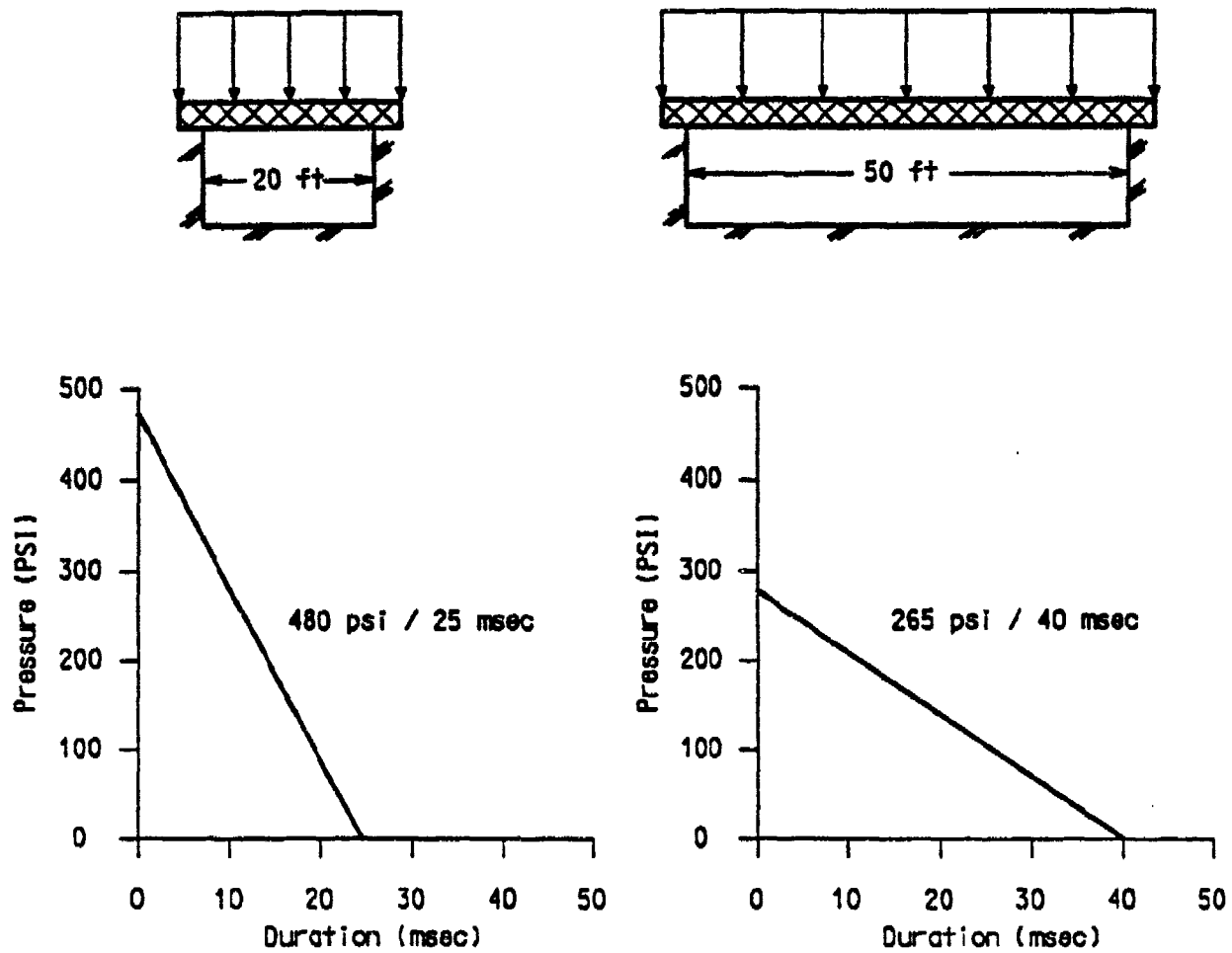


Figure 4. Idealized Dynamic Structural Loadings for 20 and 50 Foot Roof Spans.

Constraints on beam geometry and weight must consider the types of equipment normally available for transportation and erection of the beams. For example, the complement of equipment assigned to an Air Force "Red Horse" unit includes light earth-moving equipment, backhoes, and cranes. With this equipment, beam weights up to 15 tons could be handled. During initial concept development and evaluation, beams were equally sized to weigh 15 tons for comparison. Realistically, however, the availability of a 15 ton crane in a combat situation is practically nil. In addition, committing valuable air and ground transportation capacity to hauling roof beams will require serious consideration. A very direct relationship exists between size and weight of roof beams and the level of protection they provide. Therefore, during an actual design phase, the designer should make a pragmatic study of resources readily available to the field troop units and the level of protection desired to determine a maximum allowable weight and size for the roof beams.

## 2. Performance Criteria

The purpose of this section is to describe the allowable limits of the structural response to dynamic loads. The two primary performance criteria are deflection ductility factor and support rotation. Rationale for these criteria and the allowable limits will be described. Limits will be given for the different materials and structural systems that might possibly be utilized for roof elements.

Ductility measures the capacity of a structure to absorb energy equal to the work done by the applied loading. As seen in Section 2, two common definitions of the ductility factor are (1) the ratio of curvature at ultimate to curvature at first yield, and (2) the ratio of the maximum dynamic deflection to yield deflection. The definition based on curvature is more common in structural analysis with regard to the resistance of structural members and connections to seismic loads. The deflection ductility factor is preferred in blast-resistant design because the analyses usually calculate the deflection of the structural element.

An additional distinction should be made between *material* ductility and *sectional* ductility. Concrete is by-and-large a brittle material; it cracks in tension (and shear) and crushes (often explosively) when its compressive strength is exceeded. Steel, on the other hand, is characterized by yielding followed by significant elongation and contraction in tension and compression. In design of a flexural member, the sectional ductility is the more important; thus, in a reinforced beam, simply increasing reinforcement (materially ductile) and not changing the concrete (materially brittle), will change the section from ductile to brittle behavior. In effect, adding more reinforcement may cause the brittle concrete to govern the section behavior.

Conversely, using higher strength concrete without modifying the reinforcement, has a beneficial effect on sectional ductility even though the material itself is more brittle than normal strength concrete.

The ACI Code (Reference 3) does not directly prescribe ductility limits. Rather, it sets an upper limit on the amount of reinforcement in reinforced concrete and prestressed concrete beams. For reinforced concrete, this limit is 75% of the reinforcement associated with a "balanced" condition. This balance point is the theoretical transition between a ductile failure governed by yielding of the reinforcing steel and a brittle failure governed by crushing of the concrete prior to yielding of the reinforcement. By limiting the amount of reinforcing to 75% of that for a balanced condition, beams designed accordingly will have some ductility. In usual practice, reinforced concrete beams have between 20% to 50% of the "balanced" reinforcement. This ensures that the beam will have a ductility of 3 to 5 (Reference 2). This study adopted a maximum allowable ductility factor of 6. This compares with a value of 7 in Reference 19 for beams with at least 1/4 as much compression steel as tension steel, and a ductility of 6 recommended in Reference 18.

Support rotation, calculated as the angular rotation of a point at midspan relative to an end, provides another useful criteria for assessing structural response. Support rotation roughly corresponds to the amount of curvature in the yielded "hinge" region of the beam where moment is highest. As described in Section 2, the ability of a beam to develop a hinge without significant loss in load capacity requires that the concrete in compression remain relatively intact. This occurs for a normally proportioned reinforced concrete beam when the tension steel yields while the concrete is only moderately strained. Concrete beams with a relatively high ratio of transverse reinforcement, in the form of closed hoops, can experience large curvatures due to the effects of concrete confinement. This enhancing effect will be treated in more detail in Section 5. More commonly, longitudinal reinforcement is placed in the compression zone, with the effect of reducing the concrete area required to balance the tension steel force. Since the beam width is fixed, the position of the neutral axis shifts upwards, causing an increase in the curvature.

The interaction of many factors results in a fairly complex procedure for estimating support rotation (References 24 through 27). In general, normally proportioned reinforced concrete maintains its ultimate flexural resistance for support rotation up to 2°. Achieving support rotation up to 4° requires an equal amount of tension and compression reinforcement, as well as transverse reinforcement to confine the compressive reinforcement and prevent shear failure (References 16 and 18). For this study, a limiting support rotation of 4° was used for evaluation of all concepts.

## B. DYNAMIC ANALYSIS METHOD

The dynamic response of the roof beam is determined using an equivalent single degree-of-freedom (SDOF) model which provides a number of advantages. This approach requires only moderate computational effort yet provides sufficient accuracy for simply supported beams, thus allowing the analyst to investigate a wide range of designs. The analysis may be carried out by hand, with the use of readily available response charts (e.g., References 10, 14, and 43), or with a computer using a beam analysis program (e.g., Reference 44), and SDOF analysis program. This approach is widely used and, therefore, familiar to the design community performing work in this area.

Strain rate effects due to high dynamic loading and response rates tend to increase apparent strength of the construction materials, compared to the nominal strengths measured by static mill tests. This strength increase is typically considered in the dynamic analysis by a percentage increase in the range of 10-15% for steel and concrete (e.g., Reference 16, 19). In this study, a 10% increase is applied to the static strength of concrete and conventional (mild) steel. No increase is applied to prestress strands.

This section briefly summarizes the SDOF analysis method used in the design procedure. The basis for the method, its assumptions, and how it is applied to the current problem of designing roof beams is described. The formulas for determining flexural resistance and stiffness are contained in Appendix A.

### 1. Calculation of Flexural Resistance

The two basic requirements used to calculate flexural resistance are strain compatibility and force equilibrium. Additional assumptions and limitations given in the ACI Building Code (Reference 3) and the American Institute of Steel Construction (AISC) Manual of Steel Construction (Reference 45) provide additional guidance. The assumptions and approximations inherent in the calculation of flexural resistance are:

- 1) Strain is directly proportional to the distance from the neutral axis.
- 2) Concrete compressive stress is modeled by a uniform rectangular stress block with a stress of  $0.85f'_c$  acting over a depth  $a=\beta_1c$ , which should not be greater than the thickness of the top slab, where  $c$  is the depth to the neutral axis.



- 3) Stress in reinforcing steel or plate is proportional to strain up to yield, thereafter, stress is taken as  $f_y$  for the grade of reinforcement used.
- 4) Tension and compression reinforcement are lumped at two depths relative to the top of the beam.
- 5) Maximum usable concrete compressive strain is 0.003.
- 6) Tensile strength of concrete is neglected.
- 7) Flexural strength of a steel-concrete composite section is determined from a plastic stress distribution on the composite section; the web height and thickness must meet a given criterion, and sufficient shear connectors are provided to develop the maximum flexural strength of the composite beam.
- 8) Effective width of the slab  $b_e$  on each side of the centerline of the beam or webs does not exceed one eighth of the beam span or one-half the distance to the adjacent web (see Figure 5).
- 9) The ratio of beam length  $L$  to effective depth  $d$  will not be less than 5.
- 10) No load factors are used, and resistance factors " $\phi$ " are set to unity.

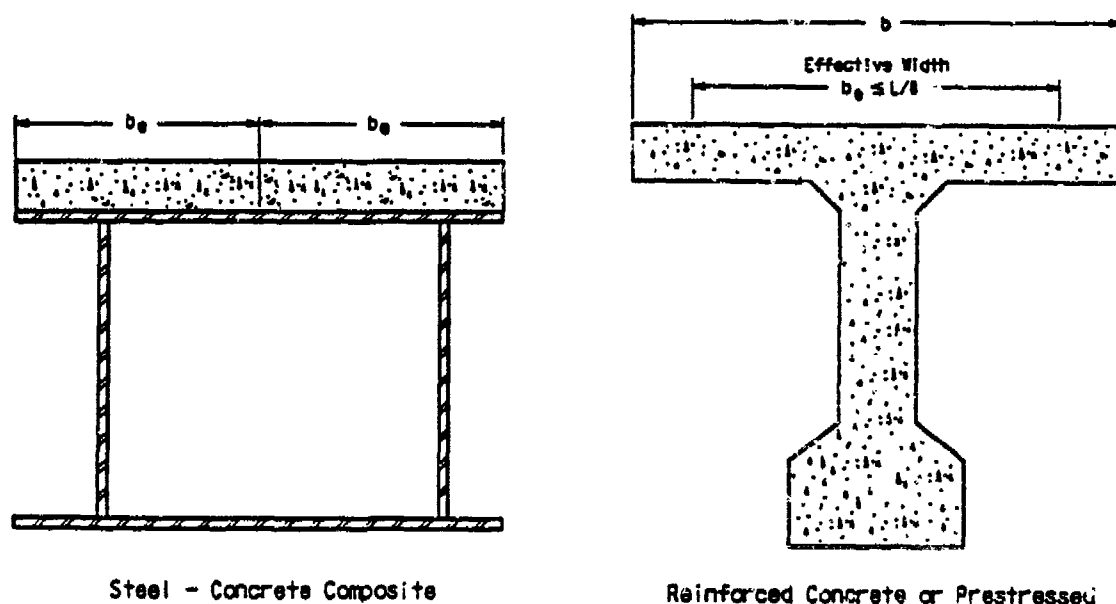


Figure 5. Effective Width of Slabs for Three Concepts.

Appendix A contains details of the closed-form equations for the static resistance for each of the concepts considered. These equations were developed for box or T-shaped reinforced or prestressed concrete sections and include cases in which the compression reinforcement does or does not reach yield. The formulas presented require that the compression zone occurs entirely within the top flange. This results in a more efficient design and avoids ambiguities that arise in computing the depth of the compression block (Reference 46). The formulas for reinforced concrete and steel-concrete composite provide a direct solution; the prestressed concrete formulas generally require one or two iterations to obtain a close estimate of the stress in the prestressing strand. Additional formulas are presented for checking the permissible reinforcing ratio and choosing an adequate steel web for the composite beam.

The nominal moment capacity is then expressed in terms of the maximum force produced by a uniformly distributed load. Subtracting the weight of the beam and overlying soil layer provides the net beam resistance for the SDOF model.

## 2. Calculation of Element Stiffness

Calculating the roof beam stiffness entails making an assumption of the effective moment of inertia  $I_e$ . In dynamic analysis, this is generally taken for reinforced concrete as the average of the gross section moment of inertia  $I_g$  and cracked section moment of inertia  $I_{cr}$ , as described in Section 2. Neglecting the contribution of the reinforcement on the gross moment of inertia has been shown to be a reasonable simplification (Reference 30). The stiffness calculation for the composite steel-concrete beam uses the gross moment of inertia of the transformed section. Finite element analysis provides a means of validating these assumptions, as described later in Section 4. The details of computing beam moment of inertia and stiffness are presented in Appendix A.

## 3. SDOF Calculation

The equivalent SDOF model of the beam is obtained by using transformation factors appropriate for the intended level of response, load distribution, and boundary conditions. The technique for obtaining transformation factors, as well as numeric values for the load-mass transformation factors  $K_{LM}$  that were used, is described in Reference 10. Herein, this method of analysis involves approximating the beam response as elastic-perfectly plastic with a plastic hinge concentrated at midspan, the load as a uniform distribution with some average duration, and the supports on each end as infinitely rigid and strong. These simplifying approximations are

acceptable given the uncertainty associated with threat assessment and determination of the actual, time-dependent structural loads.

Refinements such as those proposed in References 8 and 47 to more accurately represent the nonlinear beam response, nonlinear nonsymmetric support conditions, and soil-structure interaction are justified when greater accuracy is required or when actual construction conditions are better known, such as analysis of lab or field test results. Alternatively, using a refined model during final design allows the engineer to evaluate the design parameters which have the greatest influence on the performance of the shelter. Specific suggestions along these lines are given in Section 8: Conclusions and Recommendations.

The response of the resulting SDOF system can be determined using prepared response charts or numerical integration of the equations of motion. The present study utilized a constant acceleration integration method. This calculation was performed in a spreadsheet that also contained the formulae for beam resistance, mass, and stiffness. By combining the numerical integration with the resistance function procedure, a very useful design tool was obtained. The same result could be accomplished by developing a Basic or FORTRAN program containing the same calculations. A spreadsheet was chosen because of the low-overhead, flexible programming environment, and ad-hoc graphics capabilities. One disadvantage of the spreadsheet format is the inherent difficulty in checking and "debugging" complex formulas.

The results from either graphical or numerical integration were compared with the performance requirements to determine the suitability of a design. Solution of the SDOF system graphically gives the ductility, from which the maximum displacement and support rotation can be obtained. When numerical integration is used, the maximum displacement is obtained directly, from which the ductility and support rotation are calculated. If either requirement was exceeded, the design was modified and the analysis repeated. Once an acceptable design was obtained, it was checked to ensure that flexural failure was the governing response of the beam. This was primarily a matter of providing adequate shear reinforcement.

The design procedure utilizes two methods to estimate the dynamic shear force in the beam. A third method would be used when response charts are used to obtain the system response. The first approach considers the dynamic equilibrium of the load and the beam's resistance and inertia. This approximate method uses the assumed deflected shape to calculate the inertial force. Summing moments about the midspan leads to a simple expression for the dynamic reaction involving the applied force and resistance for both the elastic and inelastic ranges (Reference 10).

The second approach includes the contribution from the higher normal modes which become increasingly important for calculations involving higher derivatives of the deflection expression, as for shear (Reference 10). As described in Section 2: Literature Survey,

for short duration loads that are not purely impulsive, a Bernoulli-Euler beam may be used, and shear deformation and rotational inertia are neglected. In the first step, the natural frequencies for modes one, three, and five for a single span, simply supported beam with uniform mass are determined. Dynamic load factors were then calculated for SDOF systems with these frequencies. The shear force at any given distance was computed by summing the contribution of the modes considered. Specific formulas are given in Appendix A.

Since this approach only applies to an elastic system, this normal mode technique was used to calculate the beam shear for time steps up to the yield point. This was adequate because the high frequency content of short duration dynamic loads causes the maximum shear to occur before the beam has reached the point of maximum resistance. The higher of these two results was then used for designing the shear reinforcement.

A third method would be used when solution is obtained from response charts rather than numerical integration. A conservative approximation for the dynamic shear can be determined by combining the initial load magnitude and maximum resistance using the expression for the dynamic reaction in Reference 10.

### C. ADDITIONAL DESIGN DETAILS

The purpose of this section is to identify and generally describe the structural requirements that must be adequately designed to ensure that the beam can develop its intended flexural strength and ductility. Other limit states, such as shear failure, must be prevented from governing the ultimate strength of the beam. This requires careful investigation of all potential failure modes and designing and detailing the beam such that flexural response governs.

Due to the importance of these design considerations, several conservative assumptions were made; namely, the strength reduction factors from the relevant portions of the concrete and steel design codes (References 3 and 45) were used to factor the nominal strengths and material properties, but were not increased for dynamic load effects. Member sizes were proportioned or checked for conformity with code provisions for concrete cover, rebar, or strand spacing and weld requirements. Some of these associated design considerations are described in the following sections.

#### 1. Reinforced Concrete Concept

Since the design procedure treats shear behavior as a nonductile response mode, the factored shear resistance of the beam must equal or exceed the estimated dynamic shear force. This is exactly the same as the design for conventional loads, and, therefore, the designer

is referred to textbooks for more complete details on designing and detailing shear reinforcement. The discussion herein will touch on some of the issues that are particularly relevant to blast-resistant design.

The shear resistance of a reinforced concrete beam consists of two parts, the concrete shear capacity  $V_c$  and the shear reinforcement capacity  $V_n$ . The ACI code allows  $V_c$  to be taken as:

$$V_c = 2\sqrt{f'_c}(b_w d) \quad (2)$$

where  $b_w$  is the width of the web and  $d$  is the effective depth to the reinforcing. The alternate equation:

$$V_c = (1.9\sqrt{f'_c} + 2500\rho_w \frac{V_u d}{M_u})b_w d \quad (3)$$

where:

$$\rho_w = A_s / (b_w d)$$

$V_u, M_u$  = acting shear and moment at section

should not be used because it underestimates the effect of  $\rho_w$  for beams without web reinforcement and is not entirely correct in its treatment of  $a/d$  (expressed as  $V_u d/M_u$ ). For these reasons, the ACI-ASCE Committee on Shear and Diagonal Tension recommended that this equation not be used (Reference 48) and the ACI Code suggests that the first equation provides a convenient estimate of the concrete shear capacity.

In the section on seismic design, under certain conditions the ACI Code does not allow using the concrete capacity  $V_c$  for computing the shear resistance. This requirement is based on experimental studies that demonstrated that more shear reinforcement is required to insure a flexural failure if the member is subjected to alternating nonlinear displacements in the absence of axial loads. This stratagem is intended to increase the amount of shear reinforcement, not reduce the amount of concrete. In fact, the concrete core may resist all the shear with the shear reinforcement providing confinement and, thus, strengthening the concrete. While it is not suggested that the concrete capacity  $V_c$  be neglected in designing the shear resistance, the designer should be aware that load reversal during rebound and subsequent reloading will cause complex stress patterns that ordinarily do not occur in members under monotonic loads.

Design of shear reinforcement is based on the number of transverse reinforcing bars crossed by a potential diagonal shear crack. The ACI Code gives the amount of shear capacity provided by transverse reinforcing to be:

$$V_s = \frac{A_v f_y d}{s} \quad (4)$$

where  $A_v$  is the total area of the transverse hoop or stirrup,  $f_y$  is the yield strength of the reinforcement and  $s$  is the spacing between hoops or stirrups. Stirrups should not be used, but rather closed hoops or hoops constructed from a stirrup and cross-tie, as described in ACI 318 21.3.3.5. Hoops serve to confine the concrete, engage and laterally support the longitudinal reinforcement, and provide positive anchorage for the vertical legs of the transverse reinforcement. Combining the above equation with the concrete capacity  $V_c$  gives:

$$V_u \leq \phi(V_c + V_s) \quad (5)$$

where  $V_u$  is the shear force computed by the dynamic analysis. Substitution of the expressions for  $V_c$  and  $V_s$  and rearrangement gives the design equation:

$$\frac{A_v}{s} = \frac{(V_u - \phi 2 \sqrt{f'_c} b_w d)}{\phi f_y d} \quad (6)$$

Minimum spacing of transverse reinforcing is given in ACI 318 11.5.4.1 and 11.5.4.3 as the smallest of  $d/2$  or 24 inches, or when  $V_s$  exceeds  $2V_c$ ,  $d/4$  or 12 inches. The latter values also appear in the corresponding code section on seismic design, ACI 21.3.3.2, in addition to such spacing not exceeding eight times the diameter of the smallest longitudinal bars or 24 times the hoop bar diameter. The primary purpose of this requirement is to confine the concrete and maintain lateral support for the longitudinal reinforcing bars in regions where yielding is expected. In the middle of the beam, the requirement for area of reinforcement should be based on the minimum requirement, given as:

$$\frac{A_v}{s} = 50 \frac{b_w}{f_y} \quad (7)$$

Applying this requirement to the case of a simply-supported, single-span, dynamically loaded beam, transverse reinforcing occurs not only near the ends, but also in the middle of the beam. This reinforcement should extend over a length equal to twice the member depth on both sides of a section where flexural yielding is likely to occur.

The ACI Code limits the shear capacity  $V_s$  not greater than  $8\sqrt{f'_c} (b_w d)$  as a means of controlling crack widths at service loads. Since service loads do not represent a significant fraction of the strength of blast-resistant roof beams, this requirement appears

irrelevant. However, a second reason for this limit which does apply to the present case is controlling the stresses that develop in the compression diagonals in the web of a beam. This is accomplished in some codes by limiting the ultimate shear stress to 0.2 to 0.25 times the compressive strength of the concrete. The ACI Code limit on  $V_s$  for crack control provides adequate safety against web crushing in reinforced concrete beams.

## 2. Prestressed Concrete

Design of shear reinforcement for prestressed concrete is performed according to ACI Code Chapter 11.4. Several differences between prestressed and conventional reinforcing include the effect of prestress on the shear capacity of the concrete  $V_c$ , the location of the critical section at  $h/2$  versus  $d$  from the support, and the spacing limits for shear reinforcement of  $3h/4$  versus  $d/2$  for prestressed versus conventional reinforced concrete. The procedure for calculating the shear capacity  $V_c$  will be described. As mentioned earlier, the designer should refer to a concrete design textbook for additional information on shear design and reinforcement detailing.

For the case of a uniformly loaded, simply supported beam, the shear capacity of the concrete  $V_c$  varies according to:

$$V_c = (0.6\sqrt{f'_c} + 700\frac{V_u d}{M_u})b_w d \quad (8)$$

where  $M_u$  and  $V_u$  are the factored moment and shear at the section being investigated.  $V_c$  need not be taken less than  $2\sqrt{f'_c}(b_w d)$  nor greater than  $5\sqrt{f'_c}(b_w d)$ . The quantity  $V_u d/M_u$  is limited to values less than 1.0, and for the case being considered, can be expressed by:

$$\frac{V_u d}{M_u} = \frac{d(l - 2x)}{x(l - x)} \quad (9)$$

where  $l$  is the span length,  $x$  is the distance from the support to the section being investigated, and  $d$  is defined as the distance from the extreme compression fiber to the centroid of prestress reinforcement.

The calculation for  $V_c$  above assumes the prestress is at 100% of its effective value. When the critical section ( $h/2$ ) is closer to the end of the member than the transfer length of the prestressing tendon,  $V_c$  must be reduced accordingly. Within this region the prestress is assumed to vary linearly from zero at the end of the strand to a maximum at a distance of 50 strand diameters,  $d_s$ . This result is used in calculating the web-shear cracking strength  $V_{cw}$ , which is taken as the limiting value for  $V_c$ :

$$V_{cw} = (3.5\sqrt{f'_c} + 0.3f_{pc})b_wd + V_p \quad (10)$$

where:

$f_{pc}$  = compressive stress in the concrete, after allowing for all prestress losses, at centroid of cross section; when centroid lies within the flange,  $f_{pc}$  is calculated at junction of web and flange.

$V_p$  = vertical component of effective prestress force at section (if strands are inclined to axis of beam).

$d$  = distance from the extreme compression fiber to centroid of prestressed reinforcement or  $0.8h$ , whichever is greater.

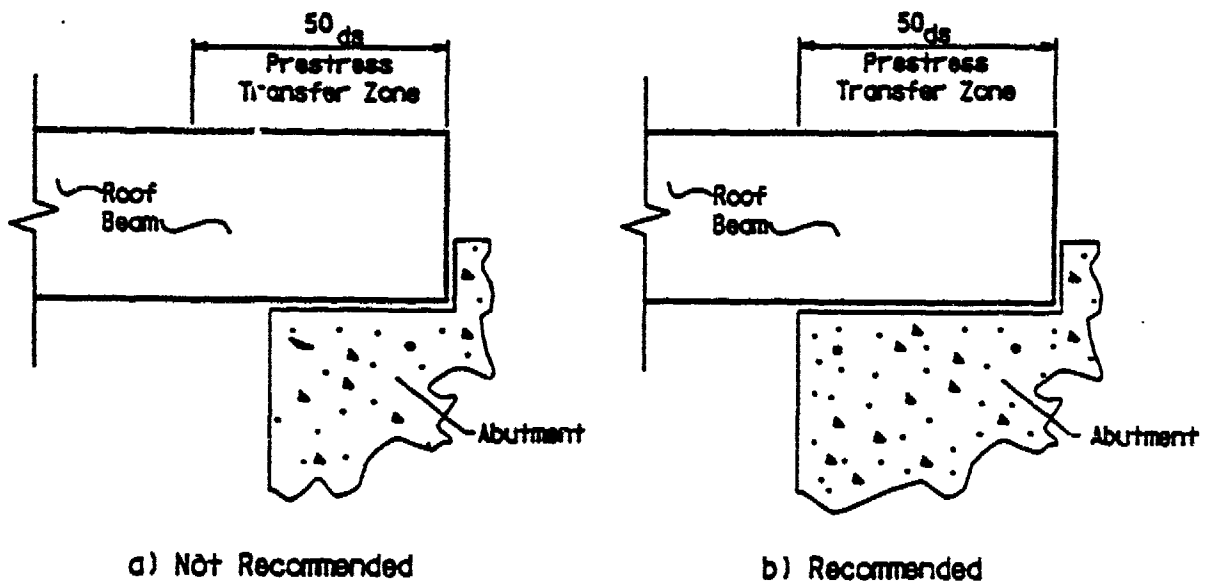


Figure 6. Abutment Requirement for Prestressed Roof Beam to Avoid Tensile Bond Failure.



This situation is depicted schematically in Figure 6a showing a beam resting on a support. The critical section, at  $h/2$  from the support, is within the transfer length of the prestress strand assumed to be  $50d_s$ . Therefore, the shear capacity of the concrete in this critical portion of the beam where shear forces are highest must be reduced. This reduction could be avoided by locating the prestress transfer zone on the outside of the support, as shown in Figure 6b. This design detail is recommended for preventing a brittle failure termed shear-tension, which occurs when shear cracks cross the region of transfer length and destroy the bond between the prestress strand and concrete (Reference 49). When this occurs, the prestress strands are ineffective and the beam will experience a premature, nonductile failure.

A more detailed calculation of the shear capacity of prestressed concrete is given in the ACI Code Section 11.4.2. This approach considers two types of inclined cracking: web-shear cracking and flexure-shear cracking. The corresponding concrete shear capacities are designated as  $V_{cw}$  and  $V_{ci}$ , respectively. The calculation for  $V_{cw}$  has been given above using ACI Eqn. 11-13. This formula is based on the assumption that web-shear cracking occurs due to the shear causing a principal tensile stress of approximately  $4\sqrt{f'_c}$  at the centroidal axis of the cross section. The vertical component of prestress force  $V_p$  is calculated from the effective prestress force without load factors.

The inclined flexure-shear crack capacity,  $V_{ci}$ , is the sum of the shear required to cause a flexural crack plus an additional increment of shear required to change the flexural crack to a flexure-shear crack.  $V_{ci}$  is calculated by:

$$V_{ci} = 0.6\sqrt{f'_c}(b_w d) + V_d + \frac{V_i M_{cr}}{M_{max}} \quad (11)$$

where:

- $V_d$  = shear force at section due to unfactored dead load
- $V_i$  = factored shear force at section due to externally applied loads occurring simultaneously with  $M_{max}$
- $M_{cr}$  = moment causing flexural cracking at section due to externally applied loads
- $M_{max}$  = maximum factored moment at section due to externally applied loads

For the present case of a noncomposite, uniformly loaded beam, ACI Eqn. 11-11 reduces to:

$$V_{ci} = 0.6\sqrt{f'_c}(b_w d) + \frac{V_u M_{ct}}{M_u} \quad (12)$$

where:

- $V_u$  = factored shear force at section  
 $M_u$  = factored moment at section  
 $M_{ct}$  = total moment, including dead load, required to cause cracking at the extreme fiber in tension, given by

$$M_{ct} = (I/y_t)(6\sqrt{f'_c} + f_{pe}) \quad (13)$$

where:

- $I$  = moment of inertia of section  
 $y_t$  = distance from centroidal axis of gross section to extreme fiber in tension  
 $f_{pe}$  = compressive stress in concrete due to effective prestress force at extreme fiber of section where tensile stress is caused by externally applied loads

In design either ACI Eqn. 11-10 would be used, or the lower of  $V_{cw}$  or  $V_{ci}$  if a more detailed calculation is performed, to determine the contribution of the concrete capacity  $V_c$  to the shear capacity. Design of the shear reinforcement for prestressed beams uses the same procedure as described for reinforced concrete in the preceding section.

Two additional design considerations specific to prestressed concrete include the permissible concrete tensile stresses after prestressing and the permissible stresses in prestressing tendons. Permissible concrete tensile stresses are applicable immediately after transfer of the prestressing force and are limited to control serviceability; limiting the tensile stresses reduces the occurrence of cracking which degrades the beam's stiffness and corrosion resistance. The purpose of limiting the stress in prestress tendons is to provide an adequate safety factor under service conditions.

Permissible concrete tensile stresses immediately after prestress transfer should not exceed:

$0.6f'_{ci}$  for extreme fiber stress in compression;

$3.0\sqrt{f'_{ci}}$  at extreme fiber in tension, except at ends of simply supported members

this value may be  $6.0\sqrt{f'_{ci}}$ ;

where  $f'_{ci}$  is the compressive strength of concrete at time of initial prestress.

When investigating stresses at the section where the prestress load is transferred, strain and stress are assumed to vary linearly across the gross cross-section. When the resulting

tensile stresses exceed permissible values, auxiliary reinforcement must be provided in the tensile zone to resist the tensile force in the concrete. The stress in this tension reinforcement should not exceed  $0.6f_{yt}$  nor 30,000 psi (in order to control crack widths). Normally the amount of tension reinforcement provided for rebound, constructability and concrete confinement meets this requirement.

Permissible stresses in the prestressing tendons are not allowed to exceed:

$0.94f_{py}$  due to jacking force,

$0.82f_{py}$ , but not greater than  $0.74f_{pu}$ , immediately after prestress transfer,

where  $f_{py}$  and  $f_{pu}$  are the yield and ultimate tensile strengths of prestressing strands, respectively.

### 3. Steel-Concrete Composite

The shear capacity of the steel-concrete composite beam is assumed to be provided by the plate girder portion of the beam. Within the plate girder, the web carries the majority of the shear, and therefore, the shear capacity of the beam is determined from the shear resistance provided by the web(s). Calculation details are contained in Appendix A, taken from References 45 and 50.

Composite action is accomplished by providing adequate shear connectors between the plate girder and the concrete slab. The number of shear connectors is determined by the smaller of the compressive force in the concrete ( $0.85f'_c A_c$ ) or the tensile force in the girder, assuming all the steel has yielded ( $A_s F_y$ ). In normal situations the first of these two conditions will apply. For stud-type shear connectors, the strength of one shear stud is given by:

$$Q_n = 0.5A_{sc}\sqrt{f'_c E_c} < A_{sc}F_u \quad (14)$$

where

$A_{sc}$  = cross-sectional area of stud, in.<sup>2</sup>

$f'_c$  = compressive strength of concrete, ksi

$F_u$  = minimum specified tensile strength of a stud shear connector, ksi

$E_c$  = modulus of elasticity of concrete, ksi.

For a channel shear connector, the nominal strength is given as:

$$Q_n = 0.3(t_f + 0.5t_w)L_c\sqrt{f'_c E_c} \quad (15)$$

where:

$t_f$  = flange thickness of channel shear connector, in.

$t_w$  = web thickness of channel shear connector, in.

$L_c$  = length of channel shear connector, in.

The number of shear connectors,  $n_{sc}$ , required between the section of maximum bending moment and zero bending moment for the usual case is:

$$n_{sc} = \frac{0.85f'_c A_c}{Q_n} \quad (16)$$

For the case of a simply-supported, uniformly loaded beam,  $n_{sc}$  shear connectors would be uniformly distributed on each side of the beam starting at midspan. Thus, the total number of shear connectors equals twice the number calculated above. Summarizing the AISC requirements for shear connector placement and spacing:

- 1) At least 1 inch of lateral concrete cover;
- 2) Diameter of shear stud not greater than 2.5 times flange thickness, unless located directly over the web;
- 3) Minimum center-to-center spacing along longitudinal and transverse directions not less than 6 and 4 stud diameters, respectively;
- 4) Maximum center-to-center spacing not greater than 8 times the total slab thickness.

#### 4. Shear and Bending of Top Slab

This final topic addresses design of the top slab for transverse shear and bending behavior. Up to now, the primary failure modes considered have been longitudinal bending and vertical shear of the entire beam. Considerable emphasis has been placed on providing adequate shear strength to insure that the beam will experience a ductile flexural failure mode. In a similar vein, the roof beam must be designed to resist transverse shear cracking or flexural failure within the top slab.

Figure 7 shows a schematic cross section of a reinforced concrete or prestressed concrete roof beam. The overhanging portion of the top flange was considered a cantilever for analysis and design purposes. Reinforcement must be provided to preclude a flexural failure or a shearing failure as shown. The analysis and design described in the following sections include calculation of loads, SDOF approximation of a cantilever, and flexural and shear design details.

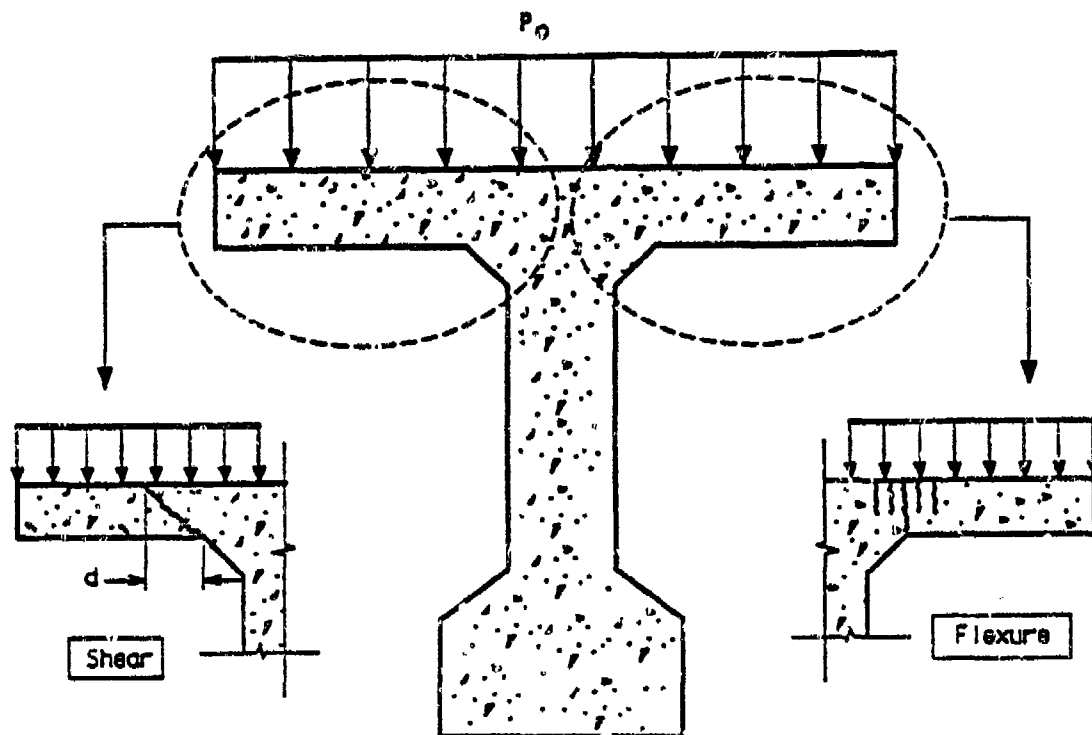


Figure 7. Transverse Shear and Flexural Failure Modes of Reinforced Concrete or Prestressed Slab.

a. Structural Loading

The equivalent structural load used for determining the overall flexural beam strength was dependent on span length. Thus, the loadings for 20 and 50 foot spans are not the same. For design of the slab for transverse bending and shear, the span length does not

directly influence the design load on the cantilevered portion of the slab. Of greater importance is the distance from the blast.

The most severe loading for designing the overall flexural beam resistance was represented by a direct hit over the middle of the beam. However, the likelihood of a hit in the middle is not any greater than a hit at any other location. Therefore, it seems logical and conservative that the top slab transverse bending and shear strength must be uniform along the entire beam length. The corresponding design load would be the peak pressure and duration from the blast. For the present case, this design load was a linear decreasing pressure of 675 psi with a duration of 20 msec.

#### b. Equivalent SDOF Model of a Cantilever

Analysis of the slab dynamic response is accomplished by using an equivalent SDOF model that matches the maximum displacement of the tip of the cantilever under uniform pressure loading. Figure 8 shows a model of the real and equivalent systems which were used to derive transformation factors according to the procedure given in Reference 10.

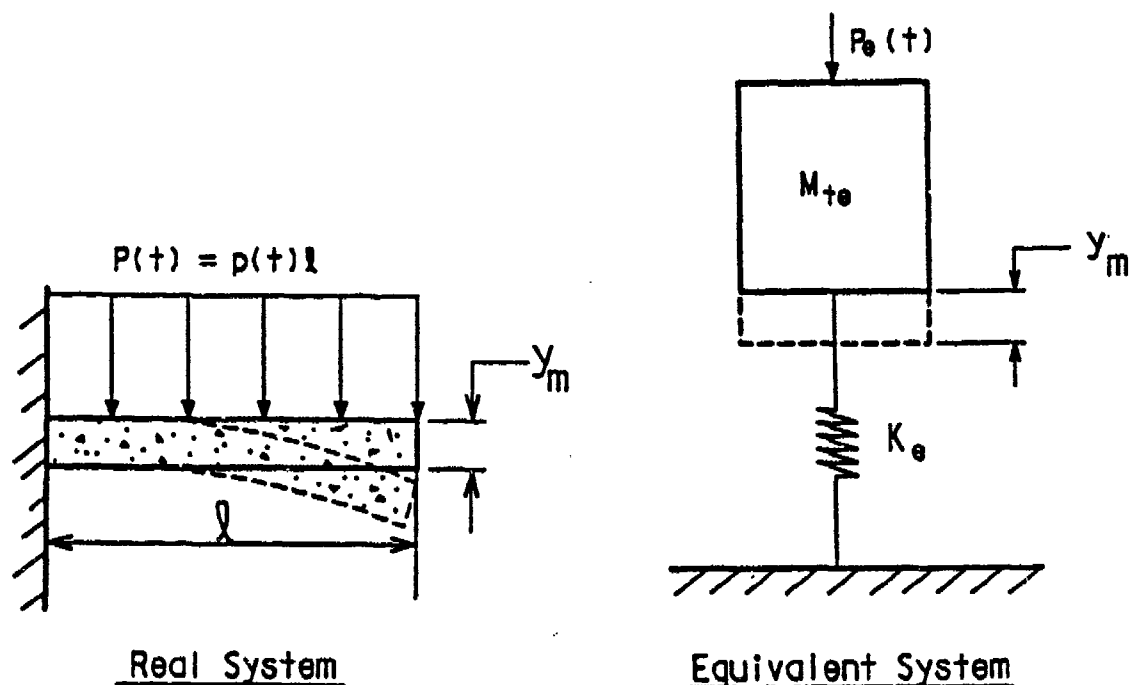


Figure 8. SDOF Model of Cantilevered Roof Slab.

Neglecting shear distortion, the shape function used to evaluate the transformation factors is:

$$\phi(x) = \frac{x^4 - 4L^3x + 3L^4}{3L^4} \quad (17)$$

where  $x$  is measured from the cantilever tip and  $L$  is the total length. For a structure with uniform mass ( $m$ ) along its length, the mass factor  $K_m$  is determined by:

$$K_m = \frac{M_e}{M_t} = \frac{\int m\phi^2(x)dx}{mL} \quad (18)$$

and equals 0.26. The load factor  $K_L$  for a uniformly distributed load  $p(x)$ , calculated by:

$$K_L = \frac{F_e}{F_t} = \frac{\int p(x)\phi(x)dx}{pL} \quad (19)$$

equals 0.4. The load-mass factor  $K_{LM}$  is the quotient of the mass factor and load factor and is, therefore, 0.65. The maximum resistance, in terms of unit width of the slab being considered, is expressed by  $R_m = 2M_p/L$ , where  $M_p$  is the maximum transverse moment capacity at the support. Lastly, the stiffness of the cantilever is  $k=8EI/L^3$ . The moment of inertia  $I$  was taken as the average gross and cracked section moment of inertia, and for the rectangular cross-section was approximated by:

$$I_a = \frac{bd^3}{2}(5.5\rho + 0.083) \quad (20)$$

where:

- $b$  = unit width of slab
- $d$  = distance from extreme compression fiber to centroid of tensile reinforcement
- $\rho$  = tensile reinforcement ratio =  $A_s/bd$

The dynamic reaction at the support was derived using the procedure in Reference 10 for the dynamic equilibrium of the element considering the applied loading, resistance developed by the element, and the inertial force. For elastic response, the shear force is  $V(t) = 0.59R(t) + 0.31F(t)$ , where  $R(t)$  and  $F(t)$  are the time dependent resistance and loading functions.

c. Flexural Design

Resistance to flexural failure is provided by transverse reinforcement on both top and bottom of the slab. The amount of reinforcement should limit the dynamic response to a ductility and end rotation that will not result in significant deterioration of the concrete. Performance criteria for this response were chosen as 3 for ductility and 2° for rotation at the support.

The ultimate moment capacity  $M_p$  was calculated per unit width using the formula for a singly-reinforced rectangular beam:

$$M_p = A_s f_y (d - a / 2) \quad (21)$$

where:

$A_s$  = area of reinforcing steel per unit width

$f_y$  = yield strength of reinforcing steel

$a$  = depth of rectangular stress block

$$a = \frac{A_s f_y}{0.85 f'_c b} \quad (22)$$

Note that the load causes a negative moment condition, hence in the above equation  $d$  is measured from the bottom face of the slab to the middle of the top transverse reinforcing. This reinforcing should be continuous across the top and bottom of the slab to insure development of the rebar. It was assumed that this reinforcement would be placed on top of the longitudinal bars and shear hoops, depicted schematically in Figure 9. The purpose of this arrangement is to increase the effective depth and use a smaller area of steel. Maximum spacing followed the ACI Code for slab reinforcement, which is the smaller of three times the slab thickness or 18 inches. In general, smaller bars with a closer spacing will perform better than larger bars. The tighter spacing will serve to confine the concrete and the smaller bars will develop their strength in a shorter distance.



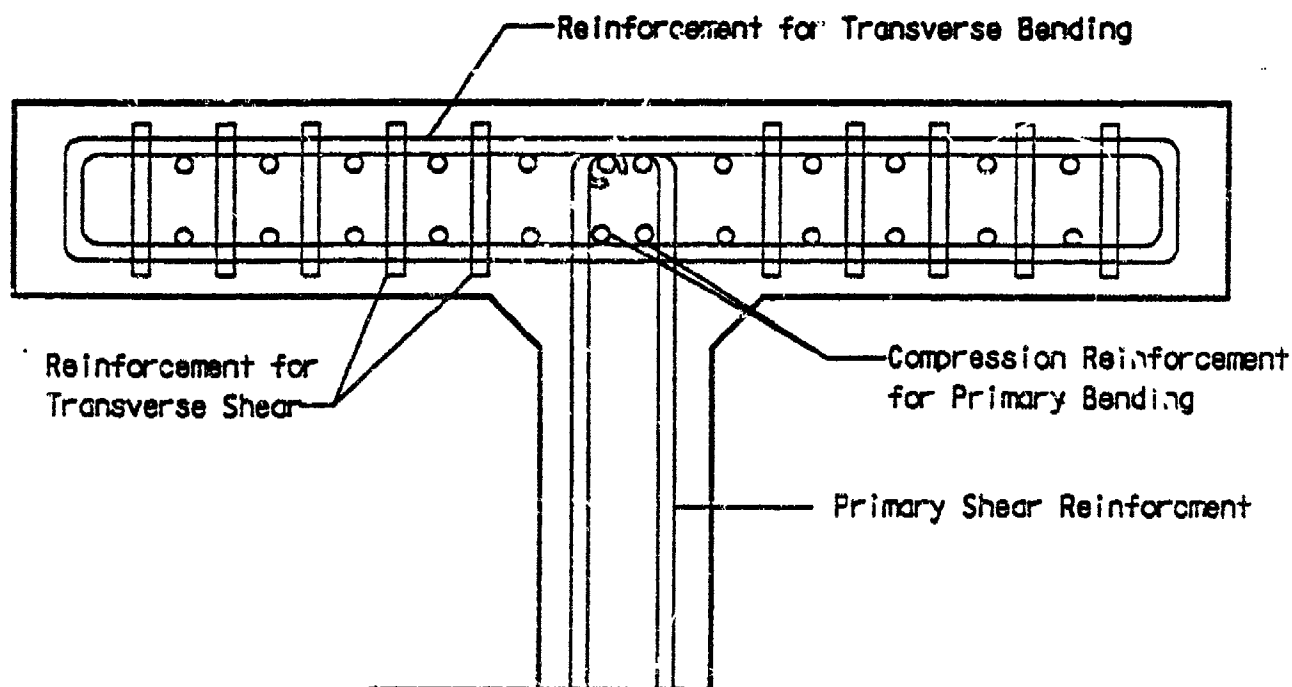


Figure 9. General Configuration of Reinforcing for Slab Portion of Reinforced Concrete of Prestressed Beam.

#### d. Shear Design

The transverse shear capacity of the top flange is analyzed and designed using the formula in 3.C.1 for computing the concrete contribution and required reinforcement. The use of ACI Eqn. 11-3 may underestimate the shear capacity of the concrete in this case. As shown in Figure 10, slabs in the interior of the roof rotate during loading and interference with the adjacent slabs causes thrust to develop. This thrust will be beneficial to the shear capacity of the concrete  $V_c$ . The ACI Code provides several formulas for calculating  $V_c$  for members with axial compression with flexure (ACI Eqn. 11-6 modified with Eqn. 11-7), and without flexure (ACI Eqn. 11-4 and 11-8). Figure 11, taken from the ACI Code (Figure 11.3), shows a comparison of the shear strength equations for members subject to axial load. This figure clearly indicates that ACI Eqn. 11-3 is a conservative lower bound for the shear capacity of concrete for even small values of compressive stress.

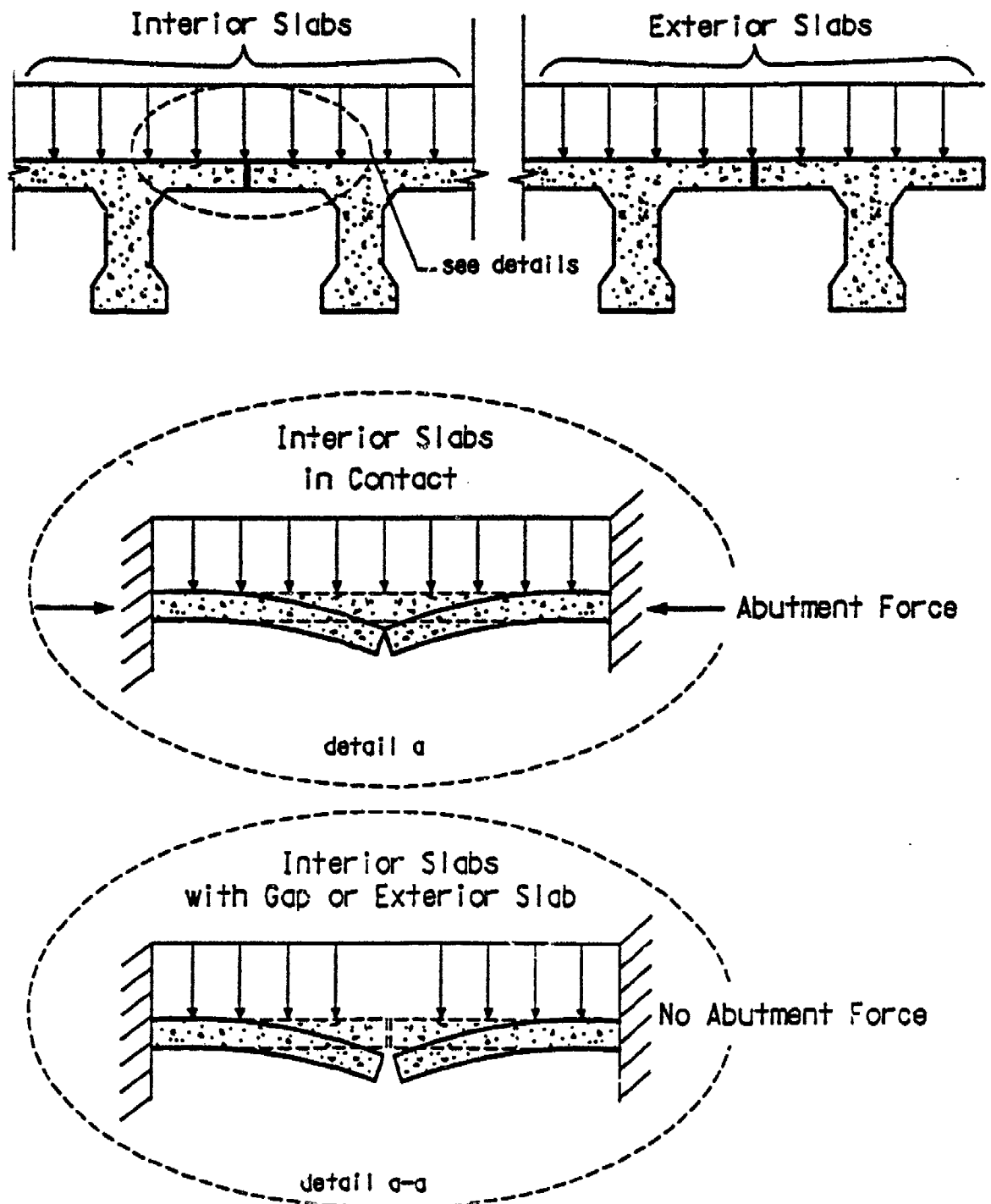


Figure 10. Development of Thrust in Roof Slabs.

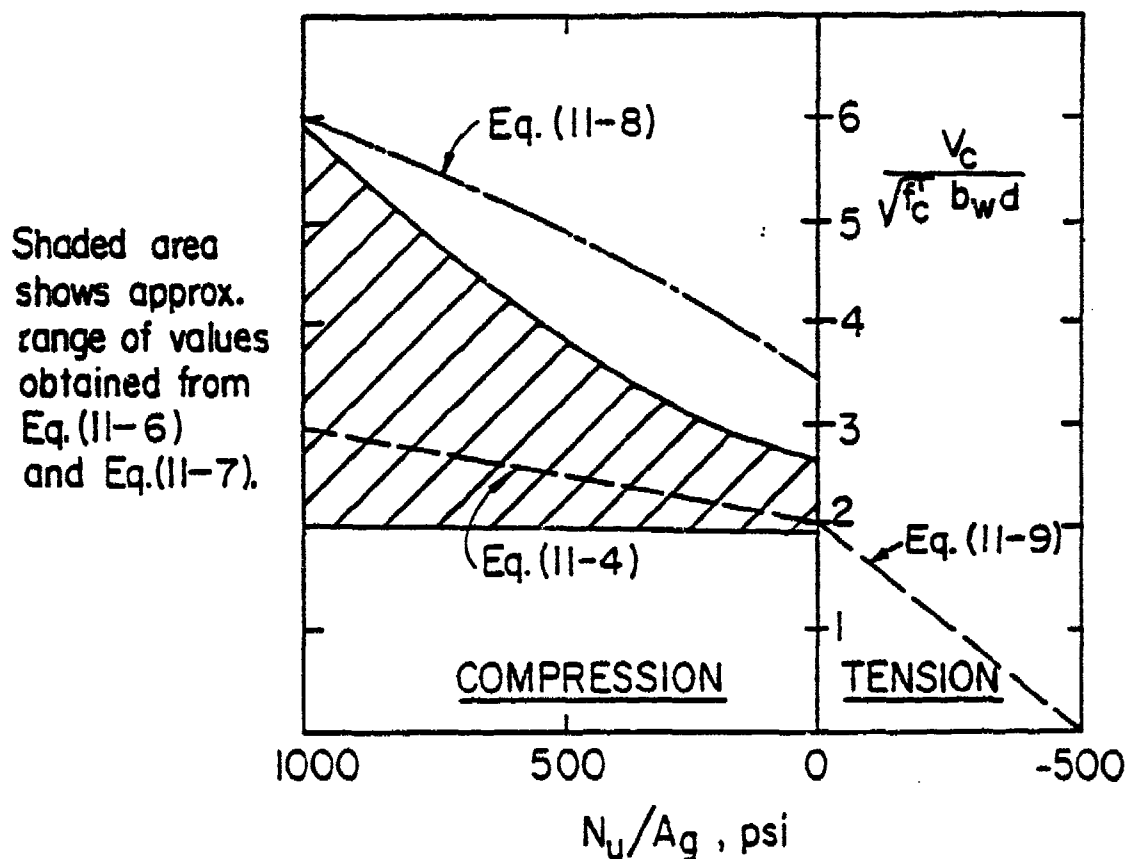


Figure 11. Comparison of Shear Strength Equations for Members Subject to Axial Load.

Development of an approach to quantify and take advantage of thrust in calculating the concrete shear capacity encountered several difficulties. An accurate determination of the thrust presents the first problem. Reference 51 presents an iterative analytical procedure for calculating the thrust developed in a jointed material that could possibly be modified for the present case.

A second problem is that the thrust could not develop near the ends of the structure or where slabs are not in contact initially. In order for the thrust to develop, a rigid abutment must exist, such as where an interior beam is in intimate contact with adjacent beams which are also in contact with their neighbors. Near the ends of the roof, neighboring beams are not fully restrained from translation or rotation. This would also occur in the interior where gaps might exist. Since maximum dynamic shear occurs very early, it is unlikely that closure of gaps as the beams and slabs deform over a longer duration will be of any benefit. In light of these

problems, the influence of axial thrust was neglected in calculating the shear capacity of the concrete  $V_c$ .

The shear resistance of the slab, given by  $V_n = (V_c + V_s)$  must exceed the peak dynamic shear  $V(t)$ , after a strength reduction factor  $\phi = 0.85$  has been applied:  $V(t) \leq \phi V_n$ . Such strength reduction factors are not usually included in blast-resistant design where ductility is allowed. However, since it is essential that brittle failure not occur, some conservatism was introduced here by including  $\phi$ .

Because of the difficulty (hence cost) associated with placing shear reinforcement in conventional slabs, the required strength is usually achieved by increasing the thickness of the concrete. This is not a viable option in the present case due to the overall weight constraints. Anchorage of the shear reinforcement in slabs less than 10 inches thick requires that stirrups or ties enclose a longitudinal bar at each corner or end. The longitudinal bars being enclosed are those required for the flexural resistance of the cantilevered slab. Figure 9 shows a schematic of the flexural and shear reinforcing in the slab.

## SECTION 4. CONCEPT EVALUATION

### A. DESIGN PROCEDURE ANALYSIS OF 15-TON BEAMS

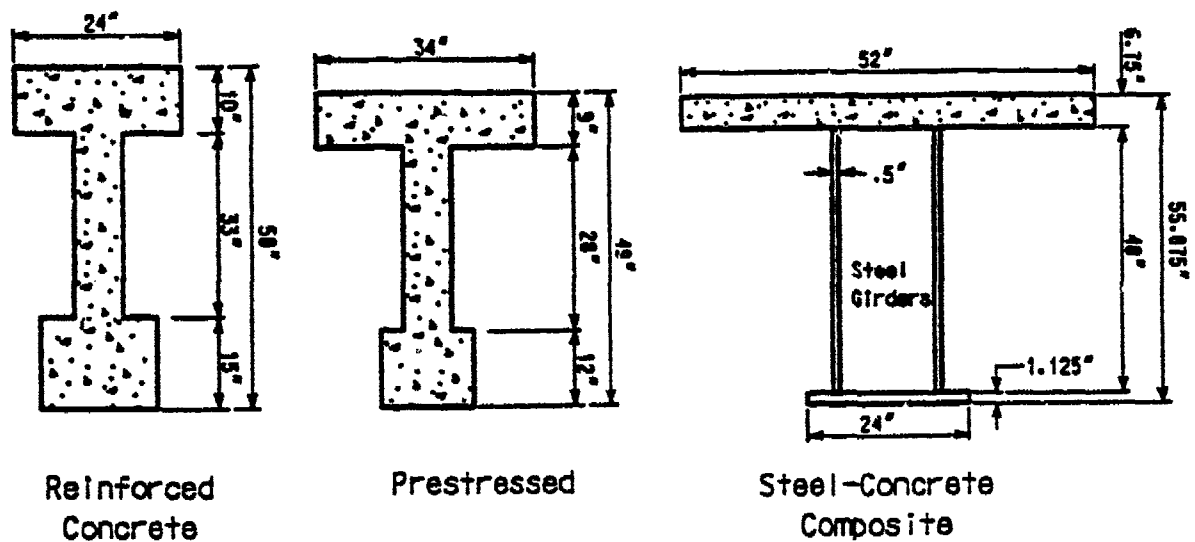
This portion of the report describes application of the design method described in Section 3 to a specific problem and set of construction materials. Evaluation criteria were used to identify the most promising roof beam concept. This evaluation initially considered three concepts (reinforced concrete, prestressed concrete, and composite steel-concrete) and was based only on fabrication cost. Beam weight was constrained to be 15 tons for comparison purposes. Subsequently, two other concepts were investigated and the evaluation criteria expanded to consider additional factors.

The design procedure utilized an iterative approach to proportion the beams and select the reinforcement. The basic design variables were width of slab, depth of the beam, and amount of reinforcement. Sufficient concrete must be provided to adequately anchor and provide minimum spacing for the reinforcing steel, as well as to meet the code requirements for shear capacity. After a suitable beam was determined, it was then necessary to design the web reinforcement for the peak dynamic shear. If the web needed additional thickness to accommodate the shear stresses, it was necessary to reanalyze the dynamic response with the modified web.

Beams designed for a 50-foot span for each concept are shown in Figure 12. These beams all weigh 15 tons and satisfy both the ductility and support rotation criteria as indicated in the figure. The graphs present the calculated SDOF response for the predicted midspan deflection and dynamic shear. The conventionally reinforced beam has the stiffest response, followed by the steel-concrete composite and then prestressed concrete. Table 1 summarizes the results for the 50-foot-long beams. Note that for the constant weight constraint, the steel concrete composite beam has a significantly wider top flange, i.e., it is more structurally efficient.

TABLE 1. SUMMARY OF RESULTS FOR 50 FOOT LONG, 15-TON BEAMS

	Top Width (in)	Maximum Resistance (kips)	Maximum Deflection (in)	Ductility	End Rotation (deg.)	Dynamic Reaction (kips)
Reinforced Concrete	24	987.5	12.5	5.9	2.5	615
Prestressed Concrete	34	1,126	19.6	5.1	3.9	701
Steel-Concrete Composite	52	1,756	18.8	6.4	3.7	1,210



a). Beam Cross Sections

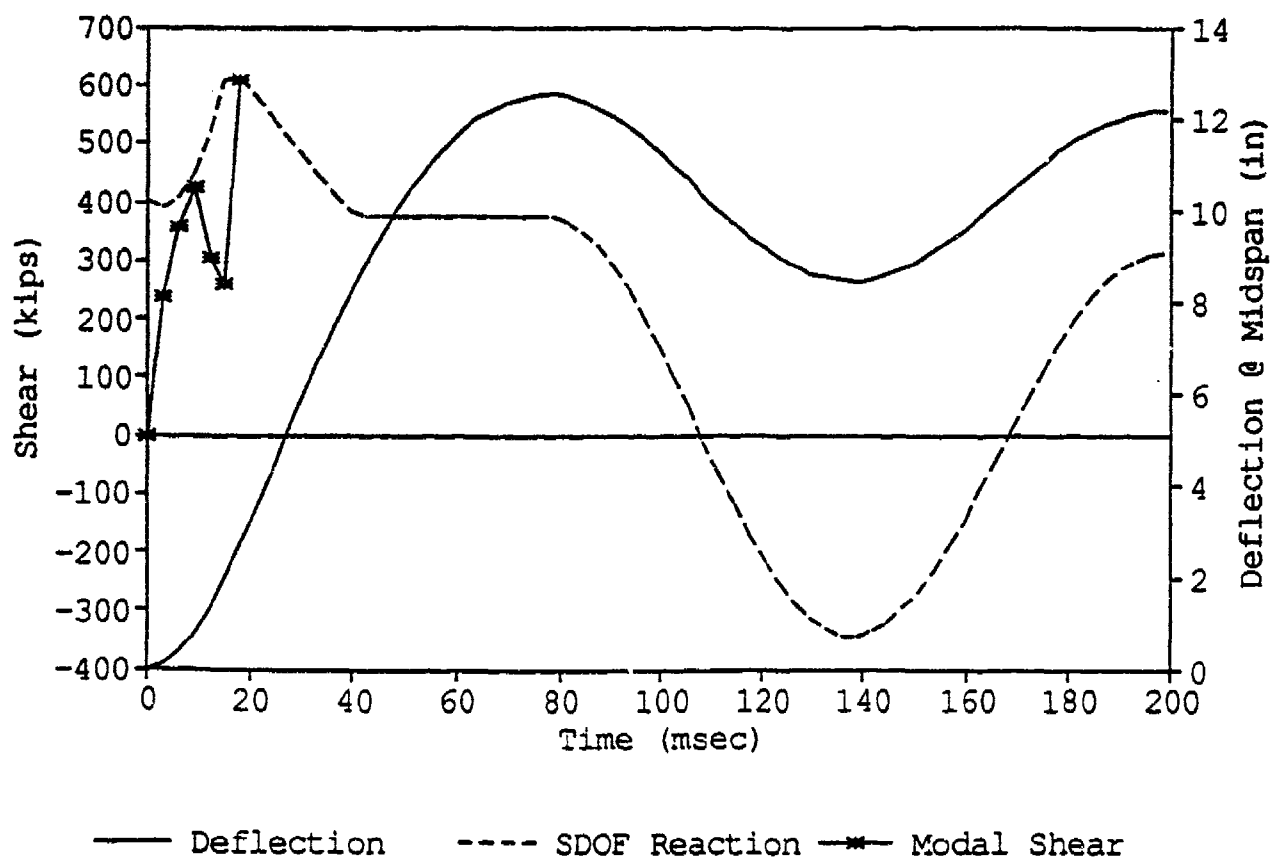


Figure 12. Design Procedure Results for 50-Foot Beams. (Continued)

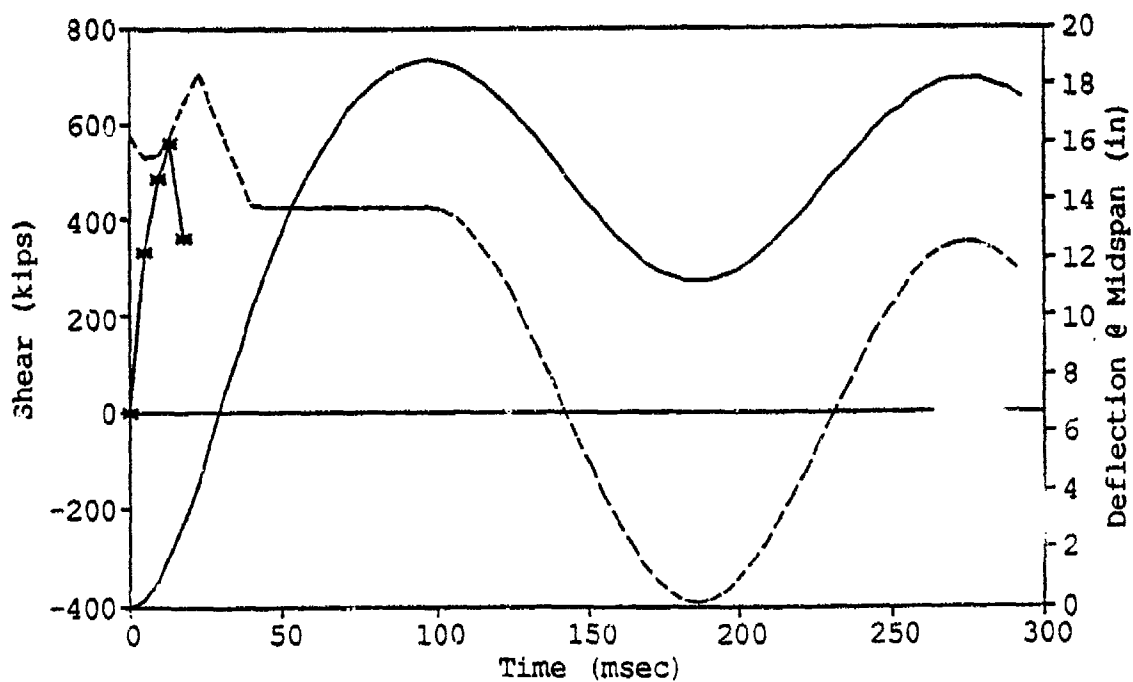
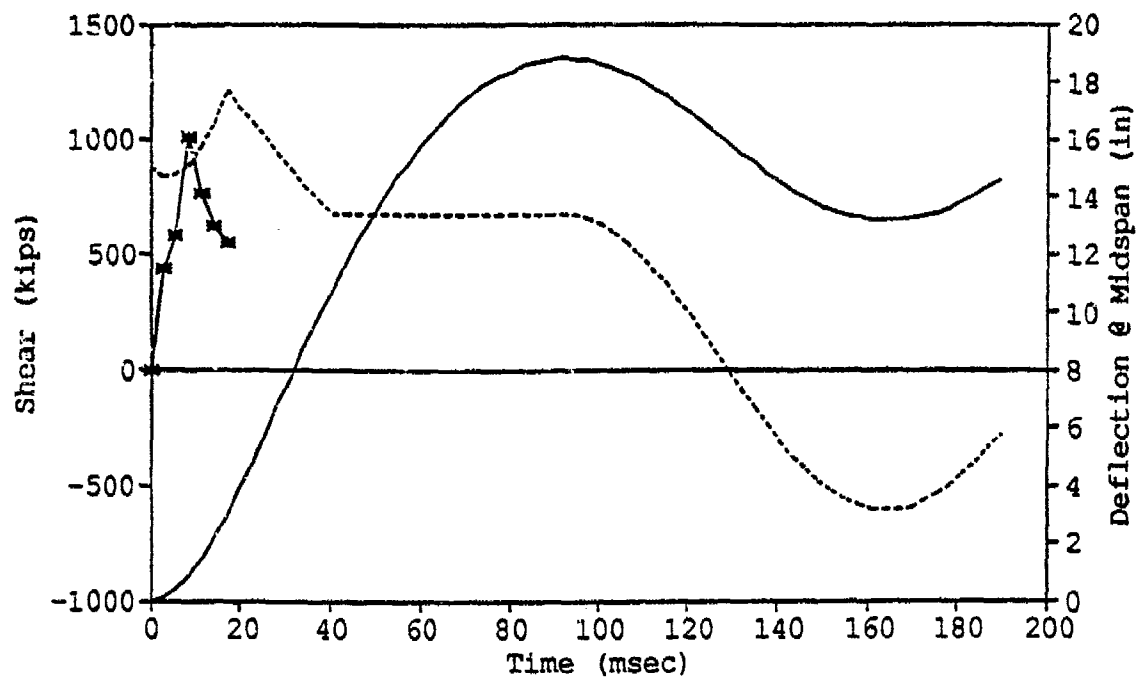


Figure 12. Design Procedure Results for 50-Foot Beams. (Concluded)

A parameter study to evaluate the effects of concrete weight, compressive strength, and tensile strength was conducted for the 15-ton beams. As summarized in Table 2, the study encompassed both beam lengths under consideration (20 ft and 50 ft) and the first two reinforcement concepts (conventional and prestressed). Calculations considering normal weight ( $150 \text{ lb/ft}^3$ ), high strength (10,000 psi) concrete, with zero tensile resistance capacity were taken as a baseline to consider these effects. These baseline cases are numbered 1, 6, 11, and 16 in Table 2. From each of these baseline cases, we considered singly the effects of these three parameters, and then the combined effect (most advantageous) of the three. Specifically, we considered lightweight ( $115 \text{ lb/ft}^3$ ) concrete, higher compressive strength (12,000 psi), and inclusion of tensile strength.

For inclusion of concrete tensile strength, we assumed a tensile stress-strain curve generally similar to that sometimes described for fiber-reinforced concrete. Specifically, we assumed a linear portion up to the modulus of rupture, and a plastic portion out to a failure strain defined by a ductility factor of 10.

The feature of merit for this parameter study was taken as the top width of the precast roof element, since this is an inverse direct measure of the number of beam elements required to cover a given shelter area. Each roof element was sized for the combination of parameters shown in the table, while maintaining consistent performance criteria and beam weight.

The results of this parameter study indicate the following:

1. A decrease in concrete weight to  $115 \text{ lb/ft}^3$  provided an increase in beam width of 19-45 percent.
2. An increase of compressive strength to 12,000 psi provided an increase in beam width of 0-8 percent.
3. Consideration of concrete tensile strength, even for fiber-reinforcement, did not significantly affect ultimate performance. In general, beam bending resistance was increased less than 1 percent by including this effect.
4. The increase in beam width for the advantageous consideration of all three effects was 23-45 percent.

This study indicated that the most benefit appears to come from a decrease in concrete weight, assuming that high compressive strength can be maintained.



**TABLE 2.     PARAMETER STUDY FOR 15-TON BEAMS**

ITEM			CONCRETE PARAMETERS			ANALYSIS RESULTS	
CASE NO.	BEAM LENGTH (FT)	REINFORCEMENT TYPE	WEIGHT (PCF)	COMP. $f_c$ (PSI)	TENSILE $f_t$ (PSI)	TOP WIDTH (IN)	PERCENT GAIN
1	20	Conventional	150	10000	0	52	-
2	20	Conventional	115	10000	0	69	32.7%
3	20	Conventional	150	12000	0	56	7.7%
4	20	Conventional	150	10000	1049	52	0.0%
5	20	Conventional	115	12000	804	70	34.6%
6	20	Prestressed	150	10000	0	67	-
7	20	Prestressed	115	10000	0	89	32.8%
8	20	Prestressed	150	12000	0	67.5	0.7%
9	20	Prestressed	150	10000	1049	68	1.5%
10	20	Prestressed	115	12000	804	90	34.3%
11	50	Conventional	150	10000	0	16.5	-
12	50	Conventional	115	10000	0	24	45.5%
13	50	Conventional	150	12000	0	16.5	0.0%
14	50	Conventional	150	10000	1049	17	3.0%
15	50	Conventional	115	12000	804	24	45.5%
16	50	Prestressed	150	10000	0	28.5	-
17	50	Prestressed	115	10000	0	34	19.3%
18	50	Prestressed	150	12000	0	29	1.8%
19	50	Prestressed	150	10000	1049	28.5	0.0%
20	50	Prestressed	115	12000	804	35	22.8%

#### B.     VALIDATION WITH FINITE ELEMENT ANALYSIS

Finite element modeling to validate the static resistance functions embodied in the design procedure utilized the nonlinear analysis program ADINA (Reference 52). The finite element model consisted of plane-stress two-dimensional elements representing the steel and concrete portions of the beam while truss elements modeled the shear connectors and longitudinal reinforcing. Figure 13 depicts a typical finite element mesh for one of the 50-foot prestressed beams. This particular model includes 400 plane-stress elements for the concrete, 50 truss elements each for the prestress tendons and compression steel, and 288 truss elements for the transverse steel.

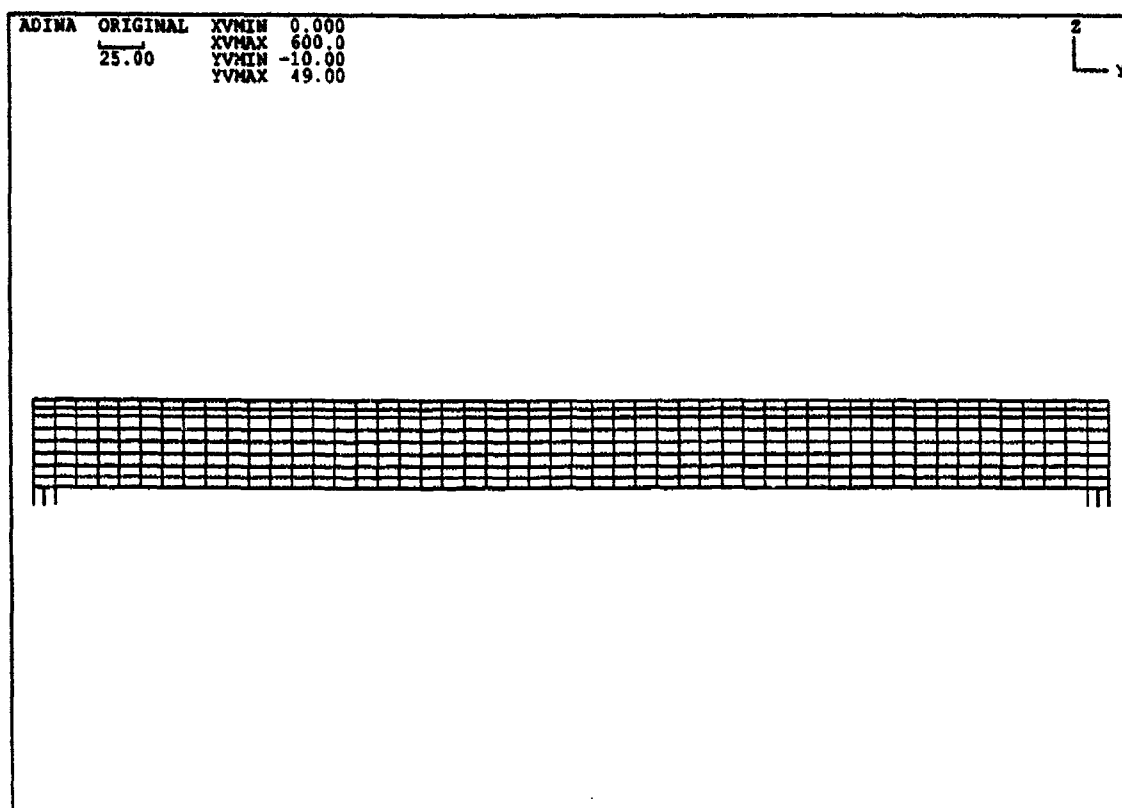


Figure 13. ADINA Finite Element Grid for 50 Foot Prestressed Beam.

Modeling of the support conditions used spring gap elements to distribute the reaction from the beam to fixed boundary conditions. The gap elements separate when in tension but otherwise take compressive forces. This modeling device avoids the high stress concentrations of supporting the end at one point, or the indeterminacy and possible tensile support of multiple fixed points. The shortening of the spring elements is subtracted from the results when calculating the midspan deflection. In addition, the clear span distance is taken from the middle of the support springs, one half element away from the end of the beam.

Load is applied incrementally in the form of a uniform pressure over the top surface of the modeled beam. For each load increment, the analysis program performs successive iterations until a measure based on the largest displacement difference is smaller than a specified threshold. In the elastic range, this requires one or two iterations. As the beam begins to yield, 5 to 10 iterations are required and the incremental load step sizes are reduced. The analysis continues until the solution fails to converge within 100 iterations for a small load step. The nonlinear analysis procedure requires definition of material stress-strain curves representing the linear and post-yield behavior of the concrete, rebar, and plate steel. Figure 14 depicts the stress-strain curves for confined concrete, 60-ksi yield strength rebar, prestress strand, and GR50 plate steel. The yield points have been factored by the dynamic increase factor of 1.1 adopted in the analysis.

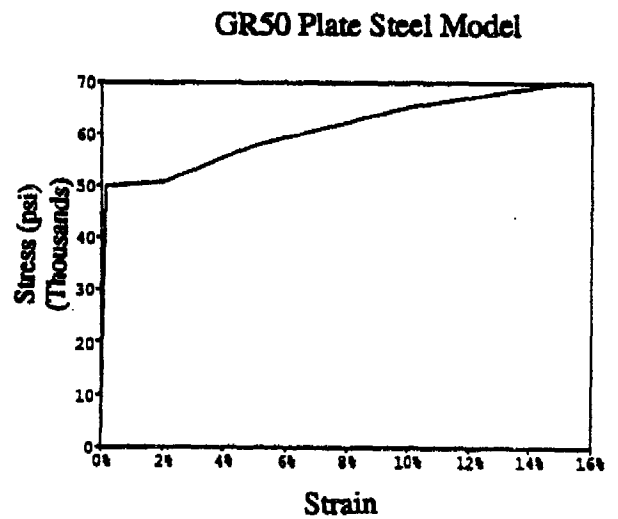
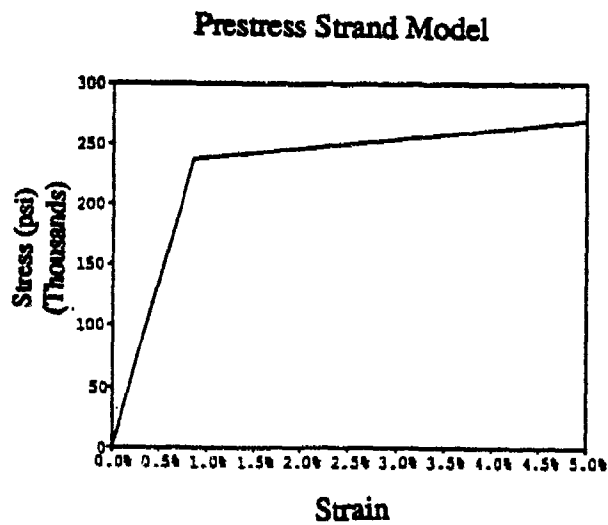
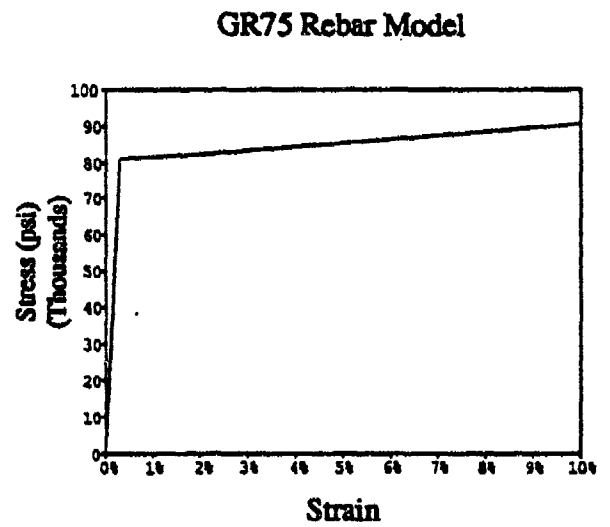
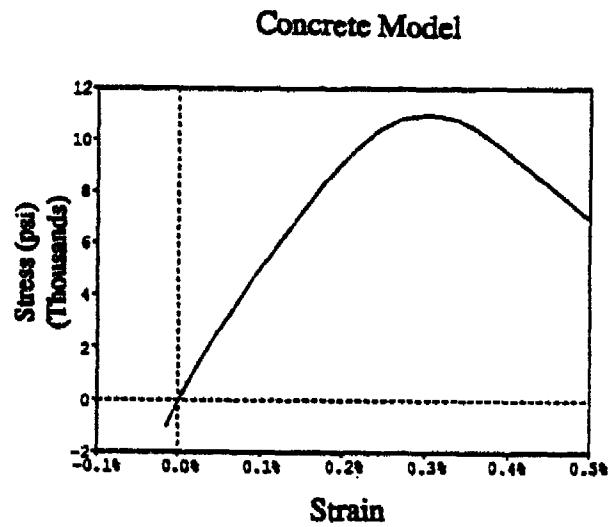


Figure 14. Material Models for ADINA Analysis of Beams.

## 1. Reinforced Concrete

Finite element analysis of the 50-foot conventionally reinforced concrete beam predicts initial cracking at approximately 300 kips, reducing the beam stiffness from about 566,000 lb/in to about 220,000 lb/in, a reduction of about 61%. Then, at approximately 95% of the design procedure ultimate resistance, the finite element calculation predicts yield of the reinforcement and a pronounced softening of the beam. The calculation proceeds at load increments of 1/2 psi until the beam reaches 7 inches of deflection and convergence of the solution is not attained. This incremental load for this step represents approximately 0.7% of the total load. At the last converged load step, the compressive strain in the concrete and tensile strain in the reinforcing are 0.004 and 0.012 micro strains, respectively, i.e., above crushing and yield.

Comparison of the design procedure and finite element predictions show quite close agreement. Figure 15 shows the finite element load deflection results and the bilinear resistance function utilized in the design procedure for the 50-foot conventionally reinforced beam.

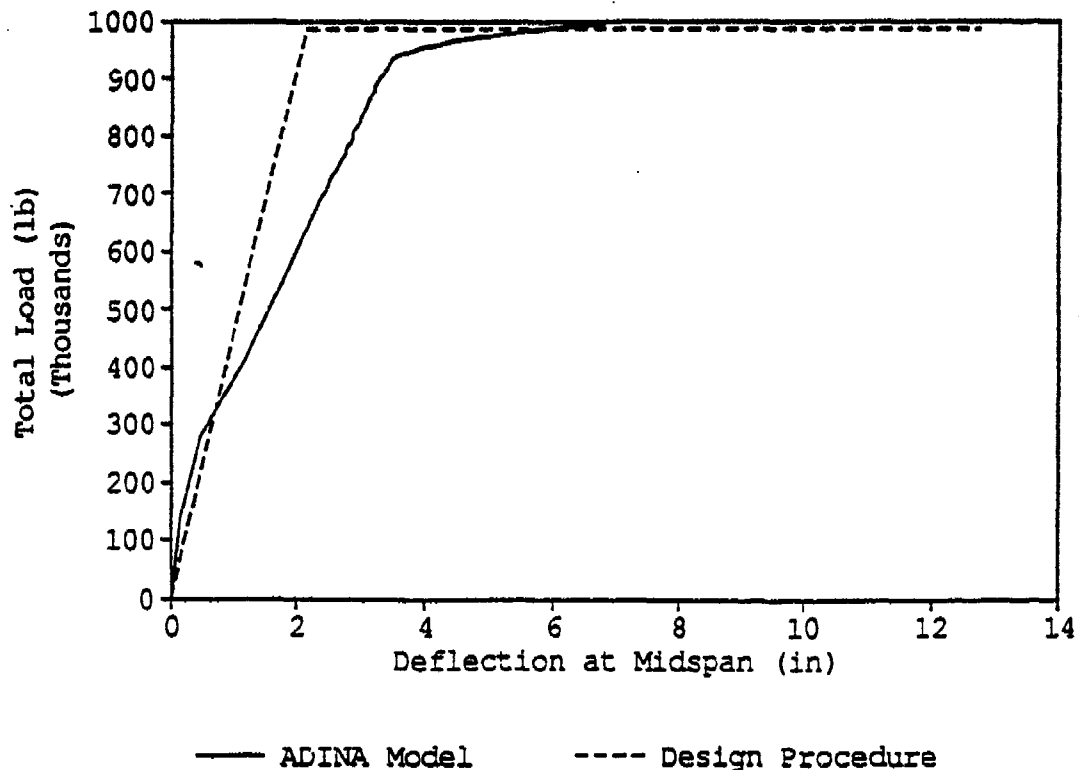


Figure 15. Reinforced Concrete Load Deflection Results - ADINA and Design Procedure.

## 2. Prestressed Concrete

Results from the ADINA analysis of a 50-foot prestressed beam appear in Figure 16. The finite element model attained an ultimate load only 8% higher than the design procedure value. The computed strain distribution shows very good agreement with the design procedure maximum and minimum strains and computed location of the neutral axis. Likewise, the stresses in the concrete, reinforcing steel and prestress strands were also very close to those predicted by the design procedure. Note that both procedures account for beam camber (negative deflection) in the unloaded state.

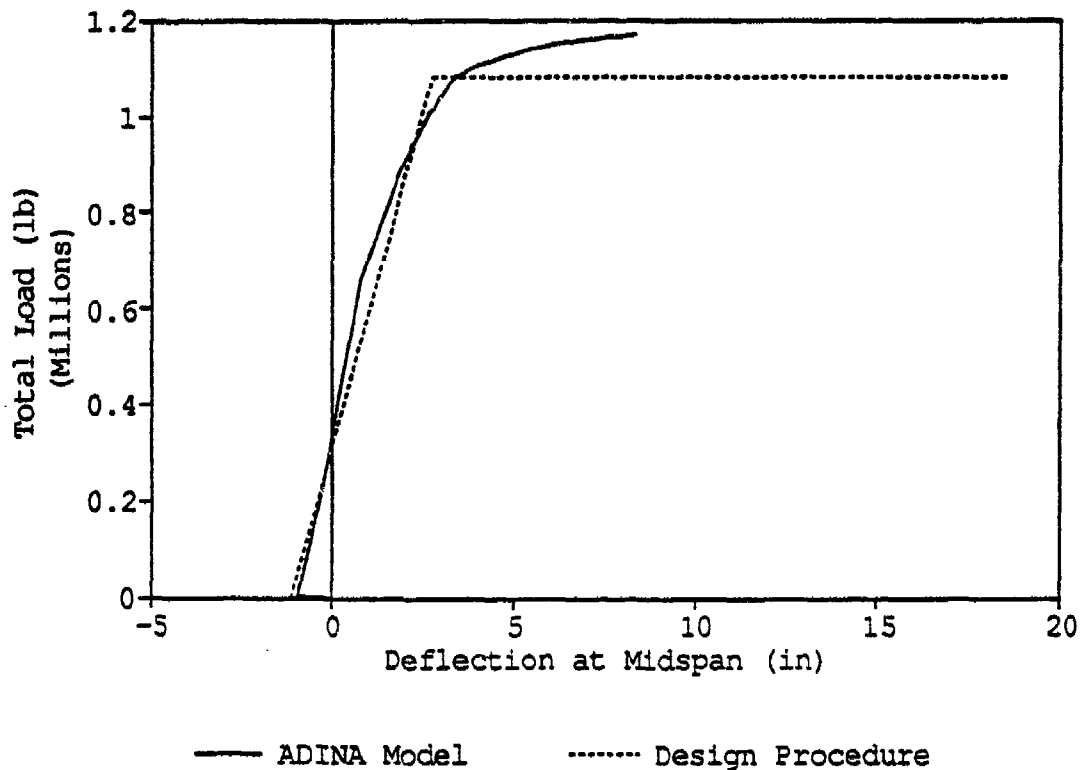


Figure 16. Finite Element Results for 50-foot Prestressed Concrete Beam.

## 3. Steel-Concrete Composite

The predicted load deflection response of the composite steel-concrete beam is shown in Figure 17. The finite element prediction agrees very well with the design procedure results. The energy computed by integrating the load deflection response for the design procedure is only 3.4 % less than that computed by the more sophisticated analysis, out to a ductility factor of about 6.

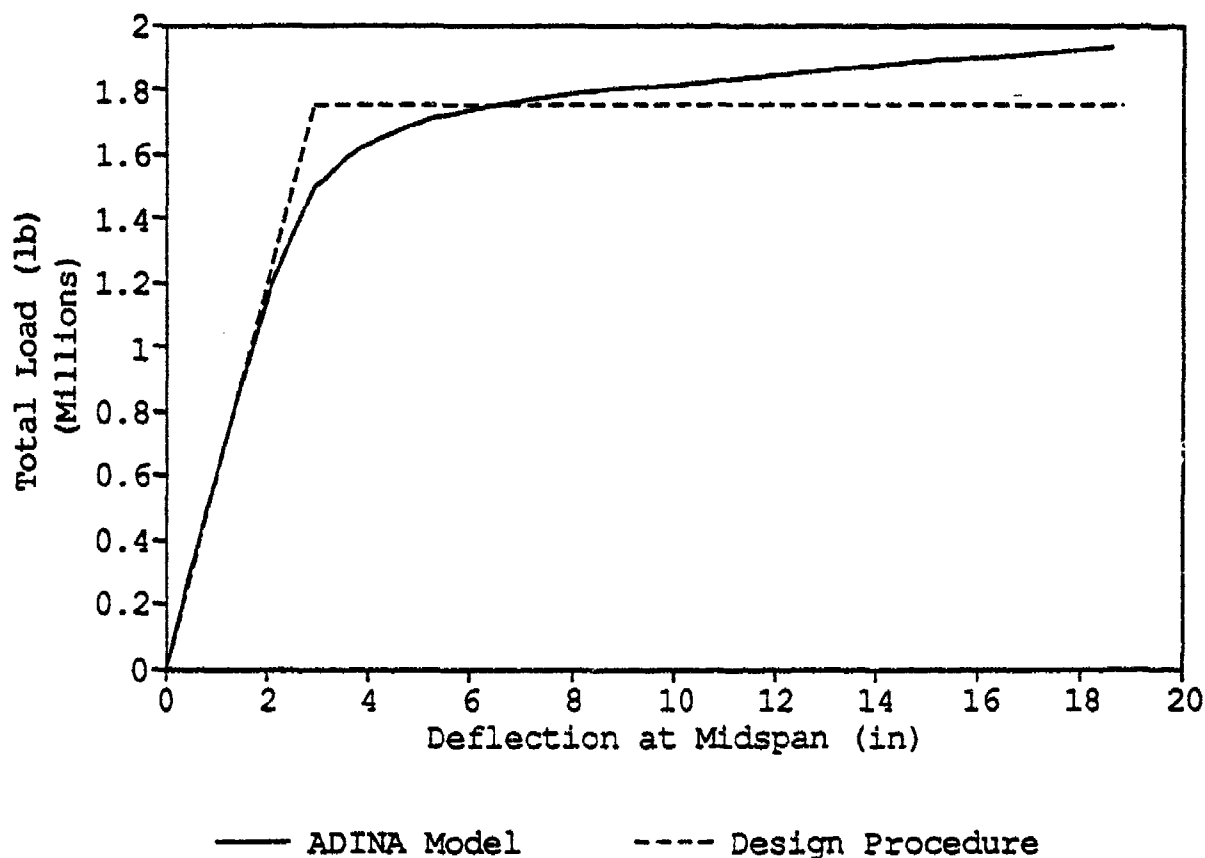


Figure 17. Finite Element Results for 50-foot Steel Concrete Composite Beam.

### C. COST ESTIMATE AND PRELIMINARY EVALUATION

During the initial phase of developing the design procedure and concept evaluation, a criteria of 15 tons was imposed on beam weight. This constraint originated from the expected availability of a 15 ton crane for placing the roof beams. Allowing each beam to weigh 15 tons meant that covering a shelter would require fewer beams since each beam could have a wider slab and stockier web and bottom flange. Furthermore, enforcing a fixed weight on all three concepts facilitated evaluation based on fabrication cost alone. Thus, a fabrication cost model was developed for each concept which included material and labor for the items shown in Table 3.

**TABLE 3. FABRICATION COST ELEMENTS**

<b>Item</b>	<b>Unit</b>	<b>Unit Price</b>
<b>Rebar (GR75)</b>	<b>lb</b>	<b>\$0.72</b>
<b>Rebar (GR60)</b>	<b>lb</b>	<b>\$0.69</b>
<b>Prestress Tendons</b>	<b>lb</b>	<b>\$2.00</b>
<b>Lightweight Concrete</b>	<b>cy</b>	<b>\$227.25</b>
<b>Forms</b>	<b>sf</b>	<b>\$4.00</b>
<b>Plate Steel (GR50)</b>	<b>lb</b>	<b>\$0.55</b>
<b>Shear Studs</b>	<b>ea</b>	<b>\$1.50</b>
<b>Stiffeners</b>	<b>lb</b>	<b>\$0.80</b>
<b>Welding of girder</b>	<b>lf</b>	<b>\$6.67</b>
<b>Welding of stiffeners</b>	<b>lf</b>	<b>\$10.00</b>
<b>Coating</b>	<b>sf</b>	<b>\$1.75</b>

The unit prices in the table are derived from industry standard figures (Reference 53) and generally cover the major cost components for the three concepts. Estimating fabrication costs probably overestimates the price per beam compared to the price of several suppliers bidding on 100 or 1000 such beams. In such a case, equipment and form costs would be amortized over a large number of beams, and lower material and labor unit costs would likely result from efficiencies in purchasing raw materials and in streamlining labor-intensive processes. Since this efficiency would likely be realized for all three concepts similarly, the estimated fabrication costs are useful for comparing the three concepts and providing a relative ranking.

Cost estimates were made for the three beam types for both 20- and 50-foot span lengths. Preliminary design of the concrete beams prior to calculating costs included selecting primary reinforcement to satisfy the design procedure, designing the web shear reinforcement, and designing the reinforcement in the slabs to resist flexure and shear in the transverse direction. Similarly, design of the composite steel-concrete beams addressed requirements for shear connectors, bearing and intermediate web stiffeners, welding and concrete slab reinforcement.

Table 4 summarizes the estimated costs for the six beams. On a unit width cost basis, the composite and the prestressed beams were the least expensive followed by the conventional concrete beam. Comparing the short versus long spans, the 20-foot concrete beams include a large amount of shear reinforcement, making them more expensive overall than the 50-foot beams. Concrete costs were governed by the constant 15-ton weight, and consequently were nearly identical for the 20- and 50-foot spans.

**TABLE 4. BEAM FABRICATION COST ESTIMATE**

Item	RC20	RC50	PS20	PS50	COM20	COM50
Rebar (GR75)	\$3,289	\$3,313	\$ 3,091	\$1,845	\$ 1,365	\$ 96
Rebar (GR60)	2,290	572	2,674	336	437	152
Prestress Tendons	0	0	1,124	2,072	0	0
Lightweight Concrete	2,186	2,174	2,193	2,168	1,447	1,026
Forms	1,660	2,600	1,312	2,300	644	792
Plate Steel (GR50)	0	0	0	0	5,432	7,868
Shear Studs	0	0	0	0	660	345
Stiffeners	0	0	0	0	901	650
Welding (girder)	0	0	0	0	1,067	2,668
Welding (stiffeners)	0	0	0	0	690	640
Coating	0	0	0	0	320	875
Total Cost	\$9,425	\$8,659	\$10,394	\$8,722	\$12,964	\$15,111
Width	69 in	24 in	89 in	34 in	110 in	52 in
Cost per unit width (\$/ft)	\$1,639	\$4,329	\$1,401	\$3,078	\$1,414	\$3,487

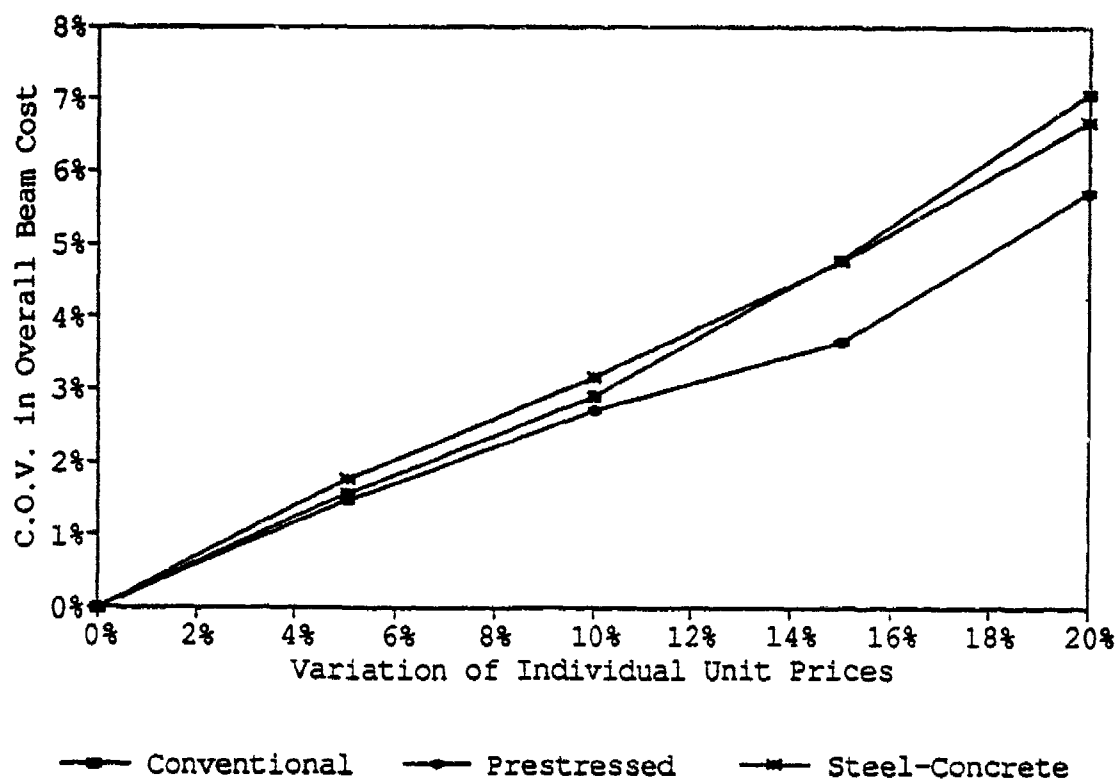
The effect of variations in the unit costs on the overall cost was also investigated. Each unit price was assumed to be a uniform random variable within a given range. For example, the unit price of concrete might take on any value within  $\pm 5\%$  of the average value in Table 4. At the same time, the price of reinforcing and all other materials and labor were also assumed to vary within the same range. A random number generator was used to determine this variation and the resulting unit costs were used in a simulation to compute the beam cost for 100 trials. The results in Table 5 contain the mean fabrication cost, the standard deviation, and the coefficient of variation (C.O.V.) for four ranges of uncertainty in the unit prices,  $\pm 5\%$ ,  $\pm 10\%$ ,  $\pm 15\%$ , and  $\pm 20\%$ .

Figure 18 displays the C.O.V. for the three concepts versus the range of uncertainty. The prestressed concept shows slightly less sensitivity to the uncertainties while the other two concepts exhibit practically the same variation.



**TABLE 5. MEAN AND SIMULATED VARIATION IN FABRICATION  
COST PER UNIT WIDTH OF BEAM**

Range	Mean Price (\$/ft)	RC50 4329	PS50 3078	COM50 3487
$\pm 5\%$	Std. Deviation C.O.V.	68 \$/ft 1.6%	45 \$/ft 1.5%	51 \$/ft 1.8%
$\pm 10\%$	Std. Deviation C.O.V.	126 \$/ft 2.9%	83 \$/ft 2.7%	110 \$/ft 3.1%
$\pm 15\%$	Std. Deviation C.O.V.	208 \$/ft 4.8%	112 \$/ft 3.6%	166 \$/ft 4.7%
$\pm 20\%$	Std. Deviation C.O.V.	307 \$/ft 7.1%	176 \$/ft 5.7%	233 \$/ft 6.7%



**Figure 18. Sensitivity of Overall Beam Cost to Variations in Unit Prices.**

#### D. EXTENDED EVALUATION CRITERIA

This section describes the factors, both quantitative and qualitative, which comprise the extended framework for evaluating results from the design process. Each criteria has an associated importance factor or weight which expresses its importance relative to the other factors.

*Fabrication Cost (25%)* As previously discussed, fabrication cost includes material, labor, and equipment used in fabrication. Conventionally reinforced and prestressed concrete beams require forming, utilizing "casting beds" which consist of 100- to 500-foot-long steel side forms and bottom plates bolted or clamped together after positioning of the reinforcing steel. Casting beds for prestressed concrete incorporate massive reaction blocks and hydraulic equipment for applying the prestress forces to the steel strands. Many precast yards have forms for standard shaped beams typically used for highway bridges which, if used or modified for the roof beams, could result in substantial savings.

Fabrication of the steel-concrete composite beams requires the facilities of a steel fabrication yard for shearing the plate steel, templates to hold the pieces together, welding equipment and a sandblast/paint shop. Additionally, the sides of the concrete slab are formed and reinforcing steel bent and tied in position in preparation for placing the concrete in the form or the composite slab. The steel plate must be protected against corrosion by sandblasting and painting.

*Handling (15%)* Handling includes moving beams from one stage to another, i.e., fabrication, storage, and erection and includes special precautions and equipment. Heavier beams require greater lifting capacity. Prestressed concrete requires special precautions (and possibly special equipment and procedures) during the handling to prevent cracking due to the camber and tensile stresses caused by prestress forces.

*Storage (15%)* Storage addresses life-cycle costs of stockpiling and maintaining the beams in a ready condition. Besides considering physical space requirements, storage includes resistance to corrosion and freeze-thaw deterioration of materials and strength properties, prestress losses from creep and shrinkage, protection from ultraviolet (UV) degradation, and maintenance of protective coatings.

**Erection (25%)** Erection pertains to the degree of difficulty and resources required to erect the beams on the shelter walls, and includes the influence of weight, number of beams required per shelter, resistance to breakage, and connection details.

**Reliability (20%)** As used here, reliability implies the level of confidence in the design and performance of a given concept or material. Extensive empirical and theoretical knowledge of the behavior of specific steel and concrete materials give these traditional concepts an advantage over newer and less well known concepts.

## **E. ANALYSIS OF REDUCED WEIGHT BEAMS FOR ORIGINAL CONCEPTS**

During the course of performing this analysis and evaluation, the overall beam weight became a design parameter of extreme importance rather than simply a constraint. The rationale for this shift was simple: in deploying the shelters, every pound is critical, therefore, the overall weight of the roof should be as small as possible; similarly, the individual beams should be as light as possible to facilitate handling, transportation, and erection. Since this change did not involve reducing the threat, the only change that could occur was in more efficient utilization of the construction materials and structural concepts. In addition to the original three concepts, two additional concepts utilizing fiber reinforced plastic (FRP) were analyzed. This section describes the results of the analysis for the three original concepts; the FRP analysis and results are described in Section F.

The design procedure described in Section 3 was used to design 50-foot beams providing the same level of protection as before but achieving some weight reduction through optimizing the design. A similar analysis described in Part A of this Section found that lightweight concrete provided a significant benefit over normal weight concrete. However, using concrete with compressive strengths over 10,000 psi and including fibers to enhance the tensile strength had negligible benefits.

All three concepts were analyzed for a top slab width of 24 inches, i.e., all have the same applied load. The thickness of the top slab was primarily determined by the depth of the compression zone required to balance the tension reinforcement. The thickness of the web must satisfy shear and stability (for steel) requirements. Figure 19 and Table 6 summarize the results which show the steel-concrete composite to have the lowest ratio of weight-to-coverage (lb per square foot) of the three concepts, because the materials could be more efficiently utilized. The reinforced and prestressed concrete concepts use a significant volume of concrete for anchoring and covering the tension and shear reinforcement and prestress strands. Concrete also contributes only about 1/2 the shear capacity of the web, with the rest carried by steel

reinforcing. Conversely, the steel-concrete composite benefits from the combined shear and tension capacity of the web. In the beam mid-span, where shear is low, the web will yield in flexure, and significantly improve the moment capacity of the beam. Closer to the supports, the steel web is very efficient in resisting shear.

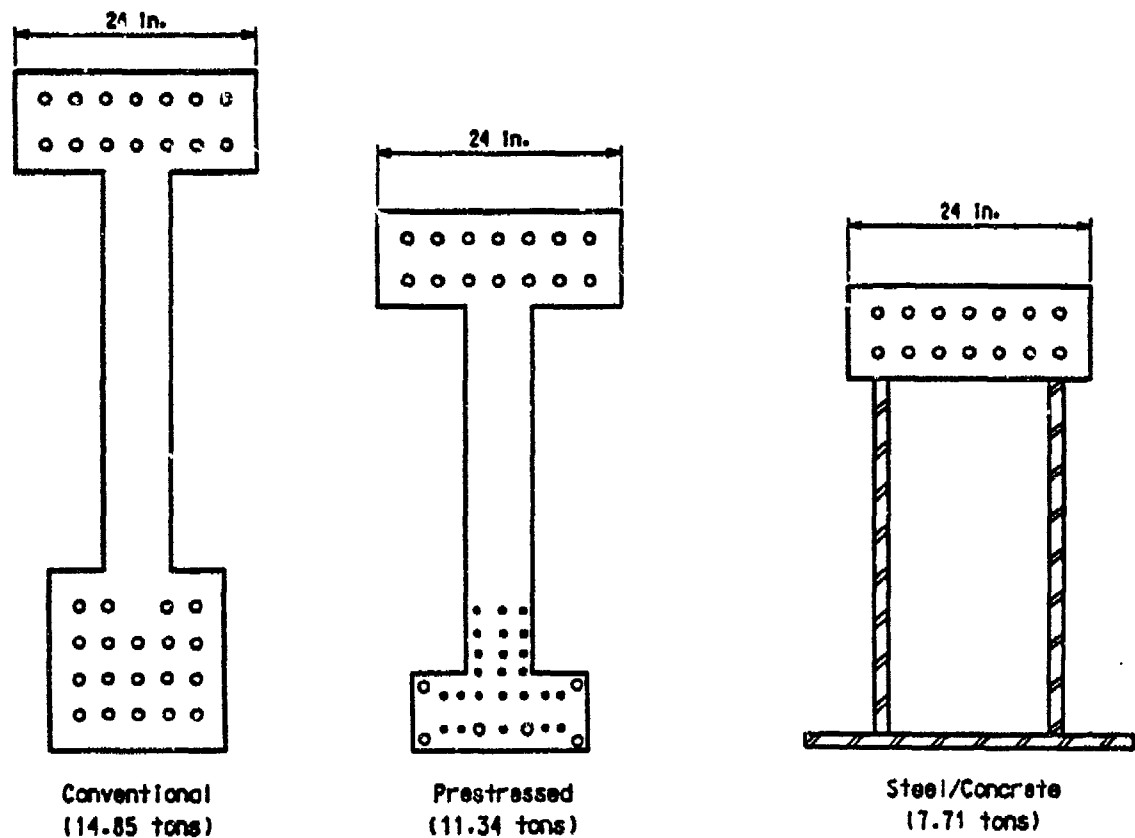
TABLE 6. DESIGN PROCEDURE RESULTS FOR 50-FOOT  
LONG EQUAL CAPACITY BEAMS

CONCEPT	TOP WIDTH (IN)	MAX. DEFLECT (IN)	DUC- TILITY	SUPPORT ROTATION (DEGREES)	BEAM WEIGHT (TONS)	BEAM WEIGHT (LB/SF)
Reinforced Concrete	24	13.8	6.0	3.4	14.06	281
Prestressed Concrete	24	21.0	5.6	4.0	11.34	226
Steel-Concrete Composite	24	21.2	5.2	4.0	7.71	154

This same conclusion was observed from the earlier 15-ton, 50-foot beam calculations (see Table 1) which had slab widths for the reinforced concrete, prestressed concrete, and steel-concrete composite of 24, 34, and 52 inches, respectively. Corresponding weight per unit area values were 297, 209, and 130 pounds per square foot. Thus the steel-concrete composite roof beam covers slightly more than twice the area of an equal weight reinforced concrete roof beam.

An analysis was also performed comparing the dynamic resistance for reinforced and prestressed concrete beams which weigh approximately the same as the reduced weight steel-composite beam (e.g. 7.71 tons). In performing this analysis, the slab width remained 24 inches. The results of these analyses are shown graphically in Figure 20, which plots the bilinear resistance functions for the three resulting beams. The steel-concrete composite beam had a ductility of 5.2 and end rotation of 4°. The reinforced and prestressed concrete roof beams are plotted with their elastic deflection and ultimate resistance out to a center span deflection of 25 inches. It is evident from this graph that neither of the latter concepts provides anywhere close to the dynamic resistance provided by an equivalent weight steel-concrete composite beam.

## Beams Having Equivalent Dynamic Capacity



Note: Total weight of each 50-foot-long beam is shown in tons.

Figure 19. Comparison of Reduced Weight Beams Having Similar Dynamic Resistances.

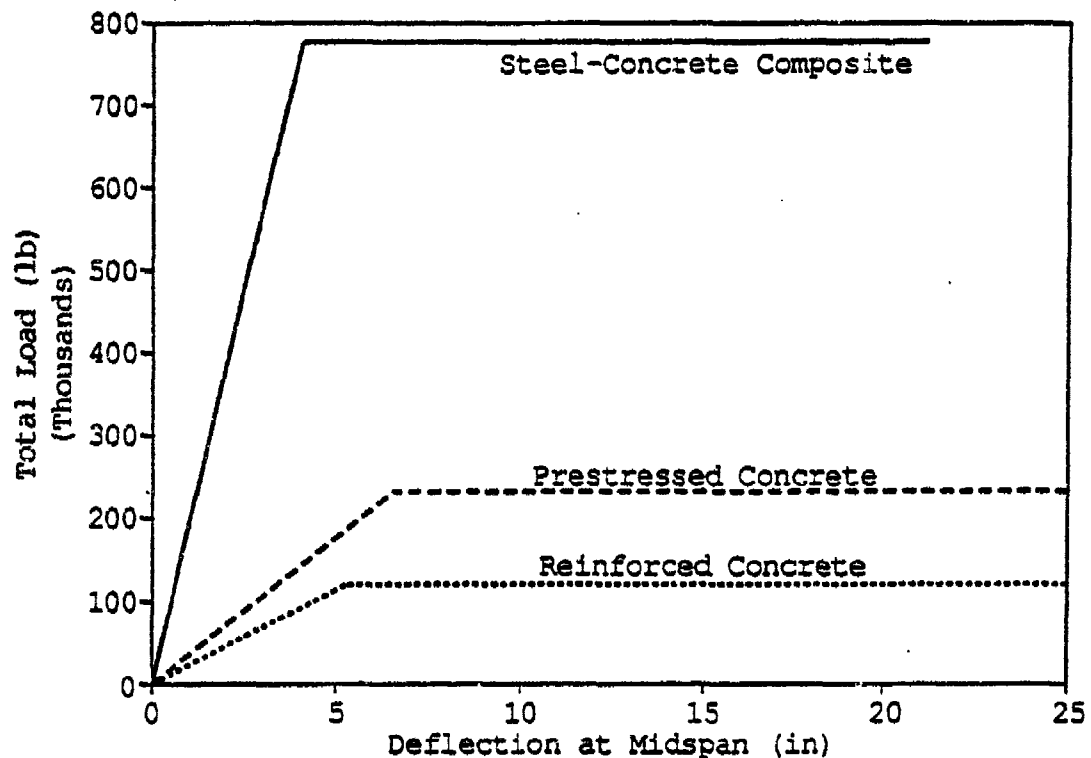


Figure 20. Comparison of Dynamic Resistances for Equal-Weight Beams.

## F. ANALYSIS OF FIBER REINFORCED BEAMS

Presented in this section are the work and findings from the analysis of two concepts which utilize advanced fiber composites for reinforcement (in this section, the term "composite" is used to refer to a material that contains oriented fibers in a matrix of either plastic or epoxy). A resistance function for each concept was developed and an equivalent SDOF model was used to determine the dynamic response for beam design.

### 1. Background

The development of high-strength, lightweight fibers, such as E and S fiberglass, aramid, and carbon has prompted a number of studies of how these materials might be used in lieu of steel reinforcing, or perhaps wholesale replacement of concrete and steel, to produce

lighter and perhaps stronger beams. In applications where chemical and electrical neutrality are crucial, such advanced composites offer the strength advantage of steel and the corrosion resistance of aluminum. For example, replacing steel strands or rods with composite strands or rods of nonmetallic materials would extend the useful life of bridge beams subject to attack by deicing salts or marine environments (especially salt water). However, tensioning and anchorage systems are relatively new and unproven, and the high cost of fibers has slowed implementation of composites in the majority of applications where conventional materials provide a technically suitable solution.

## 2. Objective and Approach

The difficulty associated with anchoring the composite reinforcement may possibly be solved by using a thin sheet of composite material attached to the outside of the beam with adhesive. Such an approach has been the focus of several research efforts, including an in-house FIVCS research program to reinforce concrete beams using sheets of carbon-fiber, reinforced plastic (CFRP). Using this approach, the composite reinforcement is bonded to the bottom and side surfaces of plain concrete beams where it serves as the tension and shear reinforcement for the beam.

The second concept considered in this investigation consisted of beams made from pultruded fiberglass. In this type of beam, continuous filaments (called rovings) of fiberglass are embedded in a matrix of plastic (polyester) which is thermally cured in a die. The die can have an open or closed cross-section, creating I-beam or hollow rectangular shapes.

The overall objective of this research investigation was to develop conceptual designs for CFRP reinforced concrete beams and pultruded fiberglass beams to withstand conventional weapons effects, and to evaluate their suitability as roof beams for the protective shelter.

The technical approach follows the general description given in Section 3.B. First, the static resistance function for the structural element is determined from ultimate strength analysis with appropriate material models. The resulting strength and stiffness describe a multi-linear response path when the element is loaded dynamically. The dynamic response is obtained using an equivalent SDOF model, and the resulting maximum deflection and support rotation compared with the performance requirements. These steps are repeated to obtain a suitable design, and then criteria such as shear resistance and overall beam weight are addressed. With the beam geometry and reinforcing details determined, the fabrication cost was estimated and values of quantitative and qualitative evaluation criteria assigned.

### 3. Concrete Beams with External Carbon Fiber Sheets

Computation of the flexural strength of concrete beams reinforced with CFRP sheets assumes a linear strain distribution through the cross-sectional depth, a rectangular compressive stress distribution, and linear stress-strain behavior for the CFRP material up to tensile rupture. This method of computing flexural capacity follows the guidelines established in Sections 10.2 and 10.3 of Reference 3 (with the exception that conventional steel reinforcing is replaced with the CFRP).

This approach has been used to calculate the flexural strength of concrete beams reinforced externally with fiber reinforced plastic (FRP) plates (References 54 through 56), and prestressed sheets (References 57 and 58). Much of this research has focused on developing a suitable bond between the concrete and external reinforcing plate or sheet. Frequently, premature failure occurs when tensile cracks form in the concrete prior to reaching the ultimate strength of the external reinforcing, and the sheet "peels away" from the beam. This failure mode represents a significant technical challenge that has yet to be solved.

Assuming for the present that no other failure mode will occur, the flexural strength determination is very similar to that for a conventionally reinforced beam. The location of the neutral axis, " $c$ ," is computed by defining the compressive and tensile forces in terms of the distance  $c$ , as in Figure 21. Enforcing equilibrium gives an equation that can be reduced to quadratic form and solved to obtain the neutral axis location. Alternatively, equilibrium of the concrete compressive force, bottom strip tensile force, and side strip tensile force can be evaluated by an iterative "solver" available in some spreadsheets. This provides a separate check of the analytical solution. Detailed formulas for this solution are contained in the corresponding section of Appendix A. The moment capacity can then be determined by the product of the compression and tensile forces and their respective distances from the neutral axis.

The beam stiffness was calculated by using the average of the gross and cracked section moments of inertia. The latter is obtained by taking the first moment of area of the compression and tension areas with respect to the location of the cracked section neutral axis " $c$ ." After solving the resulting quadratic for " $c$ " the cracked section moment of inertia was determined using the parallel axis theorem.



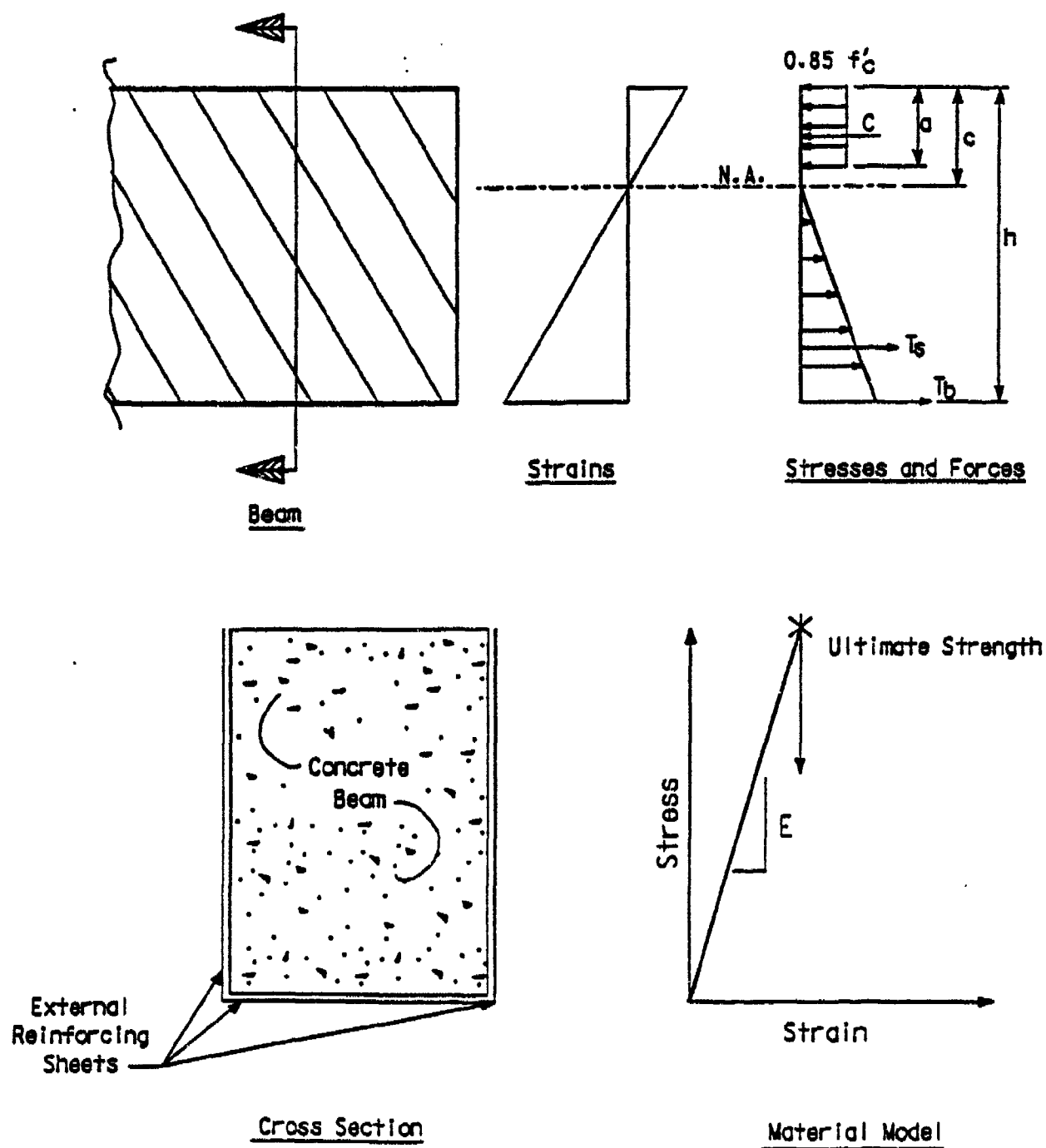


Figure 21. Flexural Strength Model for General Externally Reinforced Concrete Beam.

#### 4. Analysis of Bench Scale Experiments

Validation of this procedure was accomplished by analyzing the results from a series of bench-scale beam tests (References 59 and 60). These beams measured 2.0 inches by 2.0 inches by 12.0 inches and were made from a nominal 4200 psi compressive strength concrete (small aggregate), with a 28-day compressive strength reported to be 4256 psi ("G-mix"). The beams were reinforced with single-ply CFRP sheets, 0.0075 inches (7.5 mil) thick, attached to the beams in various configurations (labeled Beam a through f) and shown schematically in Figure 22. Physical properties of the CFRP sheets and epoxy paste adhesive used to bond them to the beams are given in Table 7.

TABLE 7. PHYSICAL PROPERTIES OF CFRP SHEETS AND EPOXY ADHESIVE

Item	Adhesive <sup>1</sup> @ 73°F	5.2 mil thick CFRP sheet <sup>2</sup> @ 77°F
Compressive Strength (28 days)	12,000 psi	N.A.
Compressive Modulus (28 days)	830,000 psi	N.A.
Tensile Strength (14 days)	3,600 psi; 0.4% elongation	310,000 psi; 1.4% elongation
Tensile Modulus (14 day)	750,000 psi	21.5x10 <sup>6</sup> psi
Flexural Strength (14 day)	4,400 psi	260,000 psi
Tangent Modulus in Bending	100,000 psi	18.5x10 <sup>6</sup> psi
Shear Strength (14 day)	3,400 psi	N.A.
Bond Strength (2 day dry cure)	3,300 psi	N.A.
Bond Strength (14 day moist cure)	2,400 psi	N.A.

<sup>1</sup> Sikadur® 31, Hi-Mod Gel, Sika Corporation, Lyndhurst, NJ.

<sup>2</sup> Magnamite Graphite Prepreg Tape AS4/3501-6, Hercules Inc., Wilmington, DE.

Loading was applied in two locations, 1-1/2 inches from the centerline, as shown in Figure 22. This load configuration causes a 3.0-inch-long constant moment zone in the middle of the beam. Shear spans of 3.0 inches between the points of load application and the supports cause these beams to be classified as "deep" beams in terms of their shear behavior. Unless otherwise reinforced, the behavior of such beams is governed by the shear capacity of the concrete rather than the flexural strength developed by the tensile reinforcement and compression concrete (Reference 48, pp 177 and 191). It was assumed that the external reinforcing provided additional shear capacity so that the beams would fail in flexure. Flexural strengths were

determined for the different reinforcement options using the simplified models shown in Figure 23. The measured and computed capacities for these beams are summarized in Table 8 and in Figure 24.

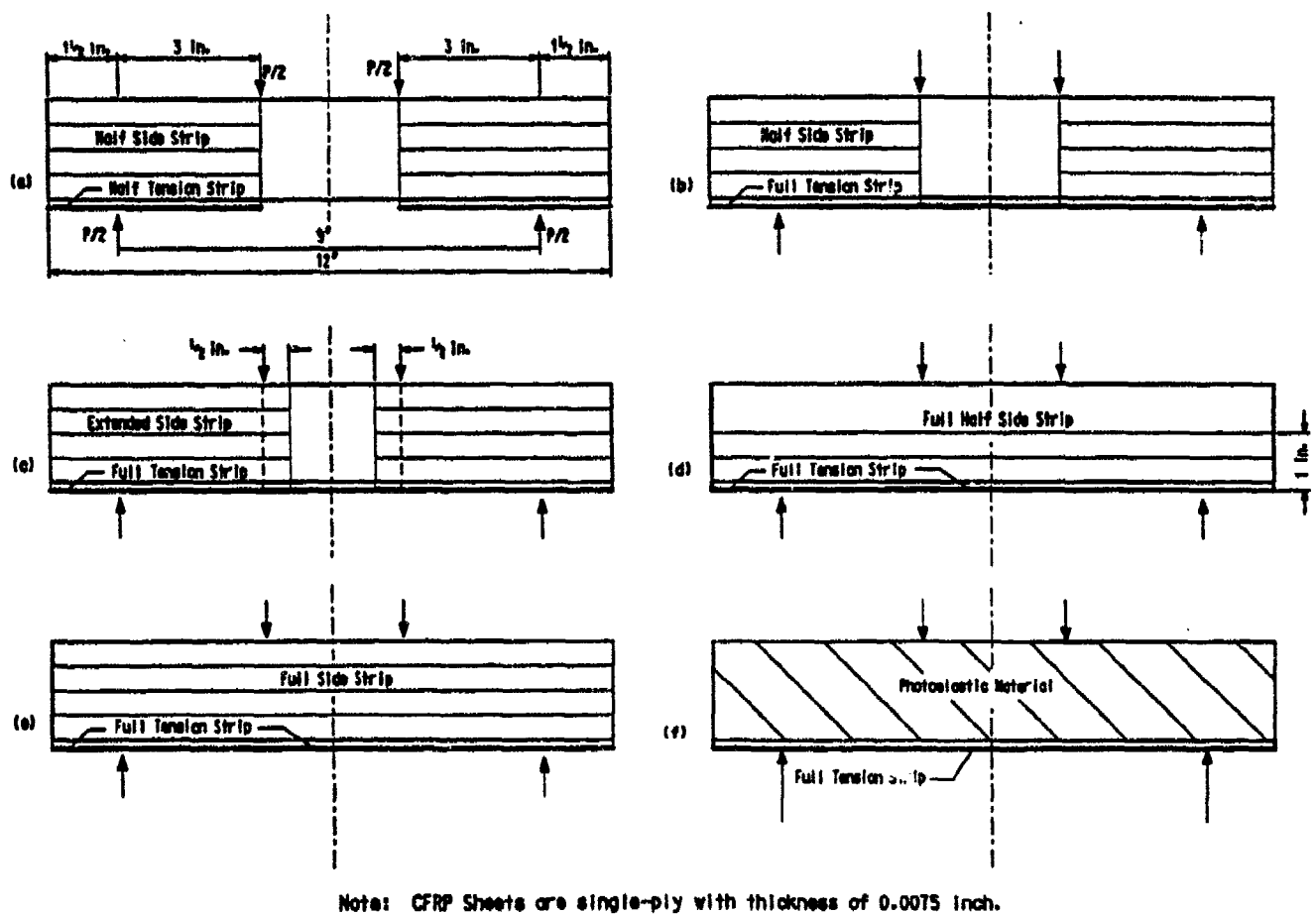
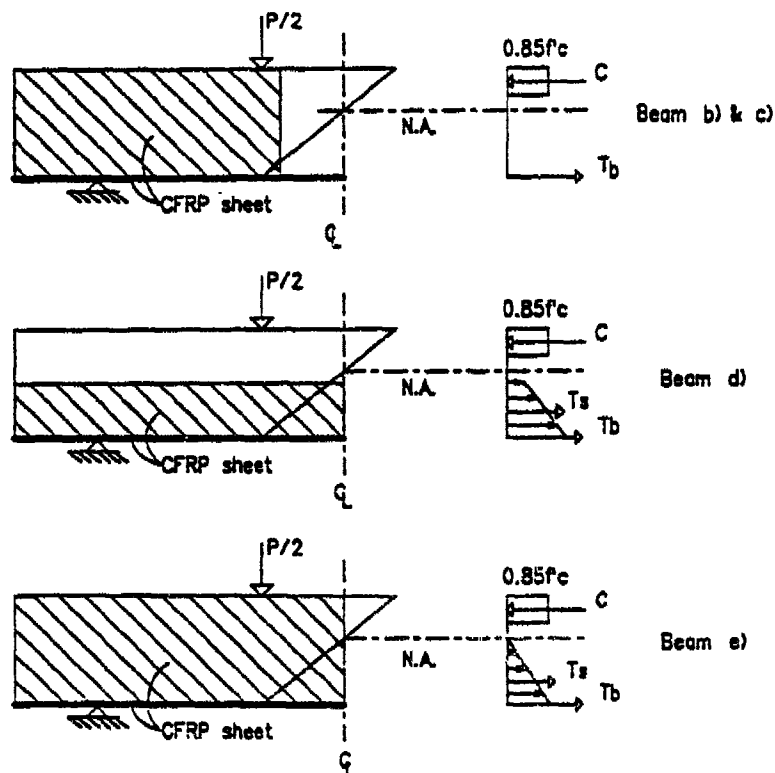


Figure 22. Lab Specimen Reinforcement Configurations and Loading Geometries.

## LAB TEST ANALYSIS PROCEDURE



### Assumptions:

- 1) Strains vary linearly from neutral axis to extreme fibers
- 2) Compressive stress modeled as rectangular stress block
- 3) Maximum compressive strain in concrete of 0.003
- 4) Tensile stress in CFRP sheet computed by assuming a linear stress-strain response with modulus  $21.5 \times 10^6$  psi
- 5) Tensile force in side sheet acts at centroid of trapezoidal or triangular stress distribution.

Figure 23. Laboratory Specimen Flexural Strength Models.

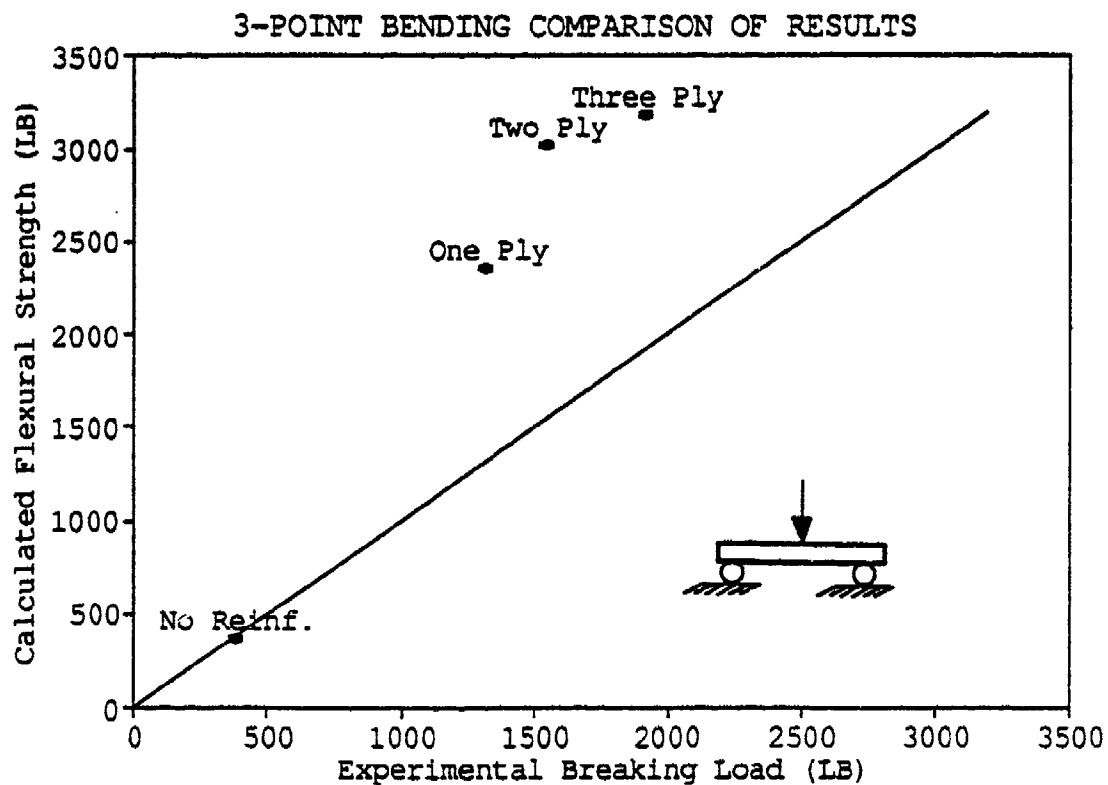
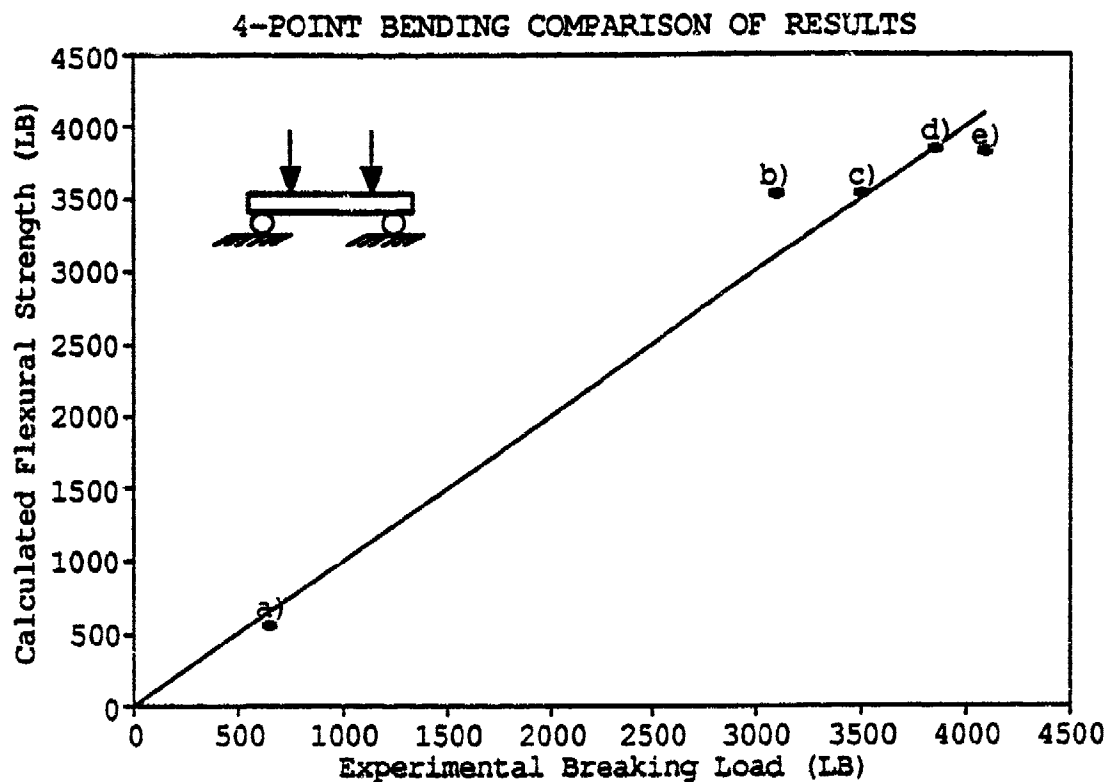


Figure 24. Comparison of Computed and Observed Load Capacities of Laboratory Specimens.

**TABLE 8. 4-POINT BENDING OF EXTERNALLY REINFORCED CONCRETE BEAMS**

Unit	Measured Ultimate Load (lb)	Computed Flexural Capacity (lb)
No Reinf.	560	564
Beam a)	650	564
Beam b)	3100	3534
Beam c)	3500	3534
Beam d)	4100 4100	3818 (neglecting compressive CFRP) 4024 (including compressive CRFP)
Beam d)	3860	3850
Beam f)	2650 (shear)	3534

The computed capacities generally agree with the measured ultimate loads. Specific observations for each case are summarized below:

*Beam a):* CFRP sheets bonded to bottom and sides of shear spans, but not the center span, did not improve the flexural capacity compared to an unreinforced beam. The flexural capacities are based on a modulus of rupture of 635 psi, or approximately  $10\sqrt{f'_c}$  which is typical (Reference 61).

*Beam b):* A CFRP sheet bonded the full length of the bottom and on the sides of the shear spans improved the load capacity. The nominal shear capacity of the concrete beam without shear reinforcing is approximately 520 pounds (based on ACI Eqn. 11-3). Thus, a shear failure would occur at a load of 1040 pounds without any benefit from the external reinforcing. Since the beam failed at approximately three times this load, the CFRP strips on the bottom and on the sides apparently contributed to the shear capacity of the concrete.

*Beam c):* This beam configuration had CFRP sheets bonded the full length of the bottom and the sheets on the sides covered the shear spans and overlapped 1/2 inch onto the middle span. The measured load agrees within 1% of the theoretical flexural capacity.

*Beam d):* CFRP sheets were bonded the full length of the beam on the bottom on lower half of the sides. Measured and calculated ultimate loads agree within 0.3%.

*Beam e):* This beam was entirely covered with CFRP sheets except for the top surface. Including the contribution of compressive stress in the CFRP strip above the neutral axis, the computed flexural capacity agrees within 2% of the actual measured ultimate load. If the compressive stresses are neglected due to possible buckling of the thin strip, the calculated capacity is 7% lower than the measured load at failure.

*Beam f):* This beam had a full length CFRP sheet on the bottom and no CFRP sheets on the sides. Instead, at least one side was completely covered by a photoelastic laminate. It is postulated that this beam failed due to shear cracking, and that the bottom CFRP sheet, and possibly the photoelastic sheet, provided additional shear strength to the concrete.

The preceding flexural calculations predict that stress in the CFRP sheets never reaches the reported ultimate strength of 310 ksi, and hence capacity is limited by the concrete in compression. Computed strains in the bottom CFRP sheets were between 0.007 and 0.009, corresponding to stresses between 150 and 200 ksi. These stresses are approximately 1/2 to 2/3 of the ultimate strength of the CFRP material. In conventional reinforced concrete, this condition corresponds to an over reinforced section, wherein the tensile reinforcement does not yield before the concrete reaches a maximum compressive strain. The thicknesses of CFRP sheets required to attain an extreme fiber tensile stress of 310 ksi simultaneously with 0.003 compressive strain in the concrete were calculated to be 3.3 mils for Beams b) & c), 1.96 mils for Beam d) and 1.83 mils for Beam e).

An analysis of conventionally reinforced beams with comparative flexural strengths was also performed. This analysis was based on singly reinforced beams with 60 ksi rebar and an effective depth  $d = 1.8$  inches. To develop the same moment capacity, the reinforcing ratio  $\rho = A_s/bd$  for Beams c), d) and e) were found to be 1.55%, 1.74%, and 1.88%, respectively. These represent normally reinforced beams with reinforcing ratios in the neighborhood of 50% of "balanced failure," as defined by the ACI Code. Typical beams have 35 to 50% of balanced reinforcement, or 1 to 1.5%. Therefore, similar flexural capacities could be attained with a modest amount of conventional reinforcing.

In addition to the two-point load tests described above, tests were also performed on beams where the load was placed in the middle of a simply supported span. These beams were made from the same nominal 4200 psi compressive strength concrete and reinforced with CFRP sheets with one, two, and three plies of unidirectional carbon fibers bonded to the bottom of the beams. The thicknesses of these sheets were 0.0075 inches, 0.015 inches, and 0.0175 inches

respectively. The results of these calculations are summarized in Table 9 and the lower half of Figure 24.

**TABLE 9. SINGLE POINT LOAD BEAM TEST RESULTS**

<b>Unit</b>	<b>Experimental Ultimate Load (lb)</b>	<b>Computed Flexural Load (lb)</b>
<b>No Reinf.</b>	376	376
<b>One Ply</b>	1315	2356
<b>Two Plies</b>	1543	3023
<b>Three Plies</b>	1916	3182

The experimental breaking loads were lower than the predictions for flexural capacity for the beams with reinforcing probably due to shear failure. Increasing the amount of reinforcing from one to three plies gives the beam increased shear resistance, but the increase is much less than for beams with shear reinforcing on the sides.

Conventionally reinforced beams with no shear reinforcement show a trend of greater shear capacity with increasing amount of reinforcing. Greater reinforcing ratios cause inclined cracks to be narrower, and hence aggregate interlock accounts for some improvement in the shear capacity (Reference 48). This same phenomenon could account for the somewhat higher breaking loads exhibited by the two- and three-ply reinforced beams. This conclusion is supported by single point load tests on similarly reinforced beams made from cement paste without aggregate. In these tests, a smaller incremental strength gain occurred going from one to two plies, and no strength gain occurred going from two to three plies.

#### **5. Dynamic Response of Full Size CFRP Reinforced Beams**

The dynamic response of full size CFRP beams was analyzed to determine whether this concept offered any potential for use as roof elements for protective structures. Since CFRP has a unit weight which is a fraction of steel, has extremely high tensile strength, and can be placed on the bottom surface, there exists a potential for weight savings. Therefore, using the procedure for calculating flexural strength and the dynamic analysis method previously described, 20- and 50-foot-long beams were designed for the assumed loading.

In computing the flexural capacity it was assumed that tensile rupture of the carbon fiber sheet or crushing of the compression concrete would control the ultimate strength of the beam. Consistent with these assumptions, the dynamic response of the beam was limited to a



ductility factor no greater than 1.0. This represents a significant performance penalty, nevertheless, the mechanical behavior of the CFRP reinforced concrete beam precludes the allowance for any higher ductility.

It was also assumed that shear failure of the beam would be completely prevented by either the CFRP sheets or conventional shear reinforcement and also that the CFRP sheets were perfectly bonded to the concrete. Additional assumptions were the same as before with respect to dynamic load magnitudes and durations, transformation to an equivalent single-degree-of-freedom model, concrete strength and soil cover. No dynamic increase factor was applied to the carbon fiber strength.

Analyses were conducted for 24-inch wide, 20- and 50-foot-span lengths reinforced with thin (1/4") and thick (2") layers of CFRP bonded to the bottom and sides of the web. These two thicknesses were chosen so as to obtain some idea regarding the range of possible design outcomes. Note that the CFRP sheets used in the lab scale tests were very thin (approximate thickness 0.0075 inches). To obtain a 1/4-inch-thick reinforcing layer would require a different manufacturing process more like the pultrusion process. The required beam sizes summarized in Table 10 and shown in Figure 25, indicate that the concept of using carbon fiber sheets to reinforce concrete beams requires very heavy beams. Included in the table for comparison are the results from the preliminary analysis of 15-ton conventionally reinforced concrete (RC) beams.

TABLE 10. SUMMARY OF FULL SIZE CFRP BEAM SHAPES

CASE	CFRP Thickness	Beam Weight	Weight per SF
20' CFRP	1/4 inch	6.2 tons	309 lb/sf
20' CFRP	2 inches	6.4 tons	318 lb/sf
20' RC	N.A.	15 tons	261 lb/sf
50' CFRP	1/4 inch	33.8 tons	675 lb/sf
50' CFRP	2 inches	38.3 tons	766 lb/sf
50' RC	N.A.	15 tons	300 lb/sf

The size of the beams is attributed to the inherently nonductile and stiff flexural behavior of the beams. In order to develop the necessary strength and stiffness, the beams must be very deep, resulting in a large amount of concrete in the web. Figure 26, from Reference 10, plots the maximum response of an elastic SDOF system subjected to a triangular load pulse with zero rise time. Plotted on this graph are the 20- and 50-foot 1/4-inch CFRP reinforced beams. The combination of mass and stiffness for these beams cause their natural periods to be close to

the duration of the load pulse. This condition requires the maximum beam resistance to be greater than the applied load for a ductility of 1.0. Consequently, these externally reinforced concrete beams have a poorer weight to coverage ratio than the least efficient of the three previously considered concepts discussed in Parts A and E of this section.

An estimate of the cost to fabricate these beams was based on the cost of the fibers and the concrete forming and placing costs. The price of carbon fibers depends on the process and quality of the fibers, with a possible range of \$12 to \$85 per pound (Reference 62). The low-cost, high-strength graphite fibers used for reinforcing the lab-scale beams have an approximate cost of \$25 per pound. Unidirectional continuous fibers (tows) that might be used for pultrusion would be in the \$15 per pound range, whereas woven fibers having biaxial strength are in the range of \$80 per pound (Reference 63). For the present case, a price of \$20 per pound was assumed for the carbon fibers, and the fiber content was assumed to be 60% by volume of the reinforcement. Since the fiber cost dominates the price of the composite, the composite cost considered the fiber cost only. Manufacturing the reinforcing sheets and bonding them to the concrete beam would incur additional cost, but since these are completely unknown, they were not included in the estimate. Therefore, the estimated cost represents a very approximate lower bound.

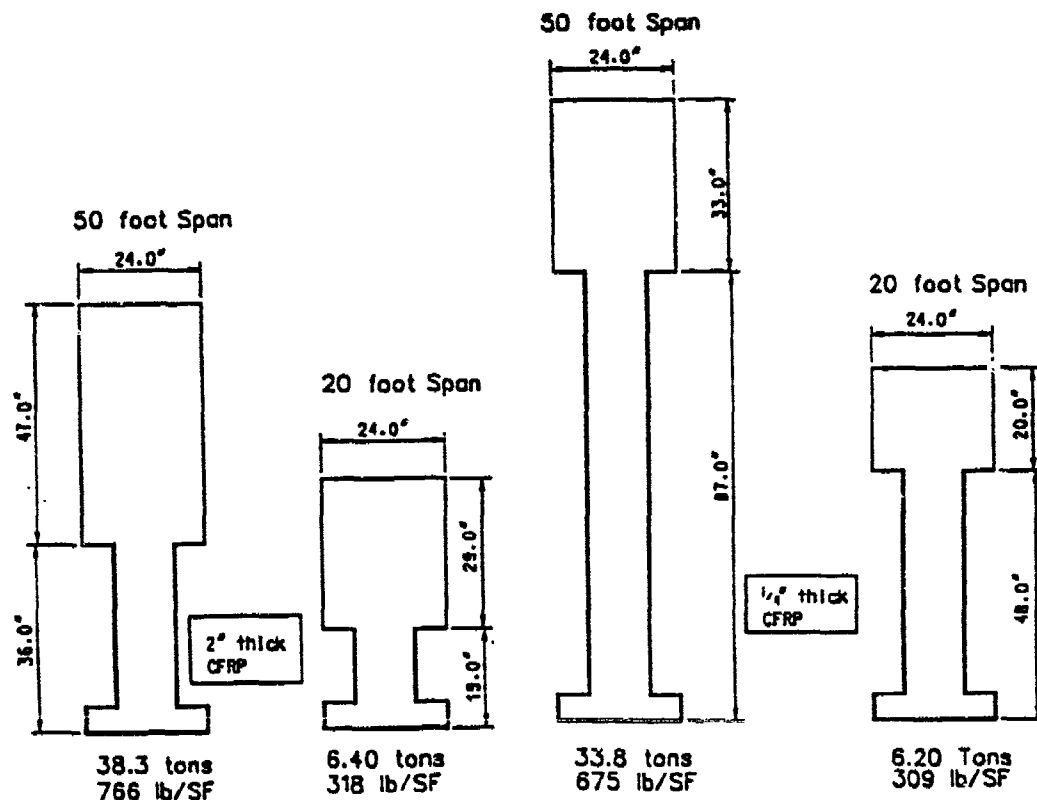


Figure 25. Full Size CFRP Beams Required for Dynamic Loads.

Estimates were made for the 20- and 50-foot beams with 1/4 inch of CFRP reinforcement. The analysis showed no benefit from using thick sheets of reinforcing. The estimated costs of these two beams are \$7150 (20 foot) and \$33,650 (50 foot), which equates to \$71.50 per square foot and \$336.50 per square foot of coverage, respectively. For both beams the fiber cost represents approximately 73% of the total cost of the beam.

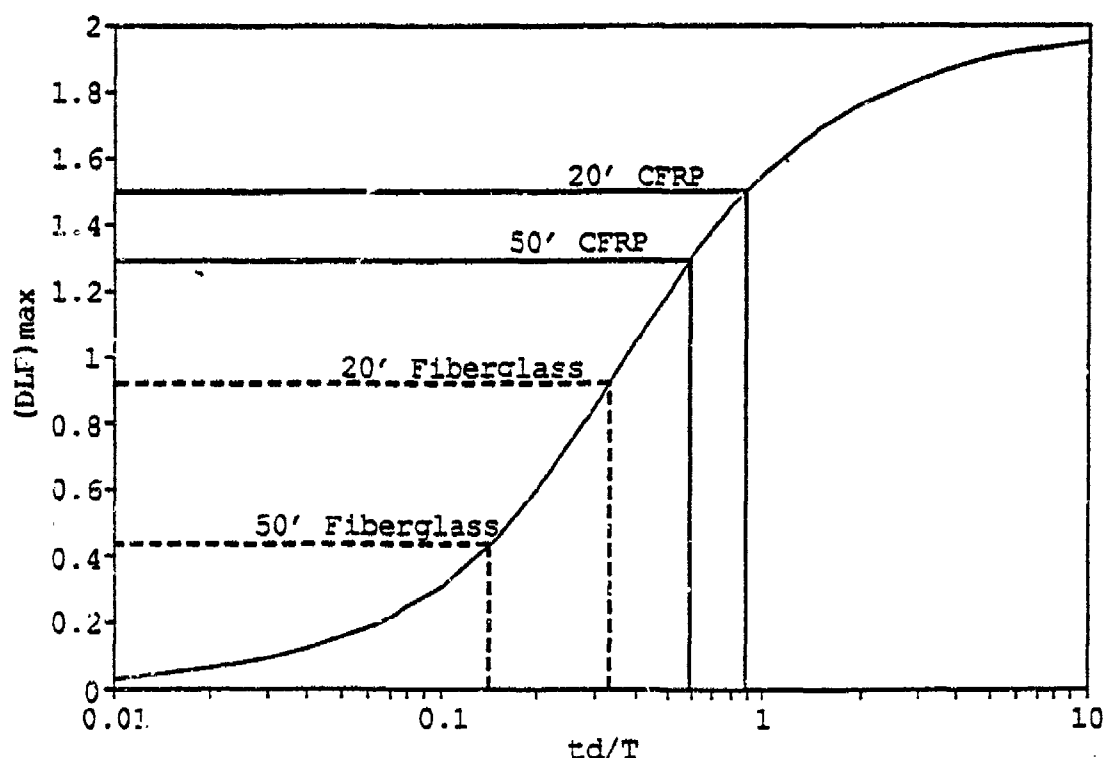


Figure 26. Maximum Response Chart for Elastic SDOF Systems Showing CFRP and Fiberglass Beam Responses.

## 6. Pultruded Fiberglass Beams

Pultruded fiberglass beams are commercially manufactured in a variety of structural shapes and compete with steel, wood, and aluminum in applications where strength, light weight, corrosion resistance, and electrical non-conductivity are required. Because of its good strength to weight ratio, pultruded fiberglass beams were investigated for roof beam elements for protective structures.

The starting point for this investigation was to evaluate the dynamic capacity a commercially available product. The largest rectangular section available from a manufacturer of such products (Reference 64) has dimensions 9 inches wide by 11 inches deep with 3/4 inch wall thickness. This beam weighs approximately 500 pounds for a 20 foot span. Analysis showed that a 20 foot beam would resist a dynamic load of approximately 120 psi with 25 msec duration (Reference 65), roughly the equivalent of a hit from a 250 lb GP bomb. The same beam spanning 50 feet will support static load from slightly under 2 feet of soil with no extra capacity. Therefore, to resist greater dynamic loading, such as those used for the other concepts, a thicker and heavier beam would be required.

The design of such a beam used design assumptions developed in Reference 64 and summarized as follows:

- 1) Flexural strength is determined by the maximum allowable stress in the flange; this may be governed by tensile failure in the tension flange or buckling of the compressive flange. The flexural strength is:

$$F_u = \frac{E}{16(b/t)^{0.85}} \leq 35,000 \text{ psi} \quad (23)$$

where:

- $F_u$  = ultimate flexural stress, psi
- $E$  = modulus of elasticity for material  
=  $3 \times 10^6$  psi
- $b$  = width of beam, inch
- $t$  = wall thickness, inch

The allowable bending stress  $F_b$  has a factor of safety of 2.5:

$$F_b = \frac{F_u}{2.5} \quad (24)$$

- 2) Shear strength is determined from the allowable shear stress  
 $F_v = 4000/3.0 = 1,333$  psi.

This approach is based on empirical results from tests on many beams by one manufacturer, and is appropriate for the preliminary investigations described herein. A more rigorous and general analysis is presented in Reference 66 for designing pultruded beams with

open and closed cross sections, different fiber and matrix materials, and various fiber orientations. The procedure is rather lengthy and was not used in this preliminary investigation.

For the dynamic analysis, tensile and shear strength values  $F_b$  and  $F_v$  were not reduced by the factors of safety given above. The ductility factor was limited to no more than 1.0 because of the brittle response associated with tensile rupture, buckling and shear failure.

A box-beam was considered for several reasons. With two webs to carry shear, the ultimate strength is less likely to be controlled by shear. The box beam shape is also more stable in resisting lateral-torsional buckling due to the increased stiffness of the top flange. Thirdly, the top flange of an I-beam might need special attention to resist the transverse bending and shear stresses from the blast pressure acting on the cantilevered flanges.

Two cross-sections designed for a 20-foot span are shown in Figure 27 along with the 9 inch by 11 inch commercially available beam mentioned earlier. Both beams have overall dimensions of 12 inch wide by 28 inch deep but differ in wall thickness and number of webs. The single-box beam was governed by shear and required a wall thickness of 2.7 inches. The double-box beam required a wall thickness of 2 inches to achieve adequate resistance for a ductility of 1.0. The two beams weigh 1.57 tons and 1.61 tons respectively with ratios of weight per area of 157 and 161 pounds per square foot.

Doubling the width of the beam from 12 inches to 24 inches required a cross-section 38 inches deep with four webs, each 2.5 inches thick. Shear governed the thickness of the webs, therefore, the flexural ductility was slightly less than 1.0. The weight of this beam was 3.78 tons, resulting in an areal weight of 189 pounds per square foot.

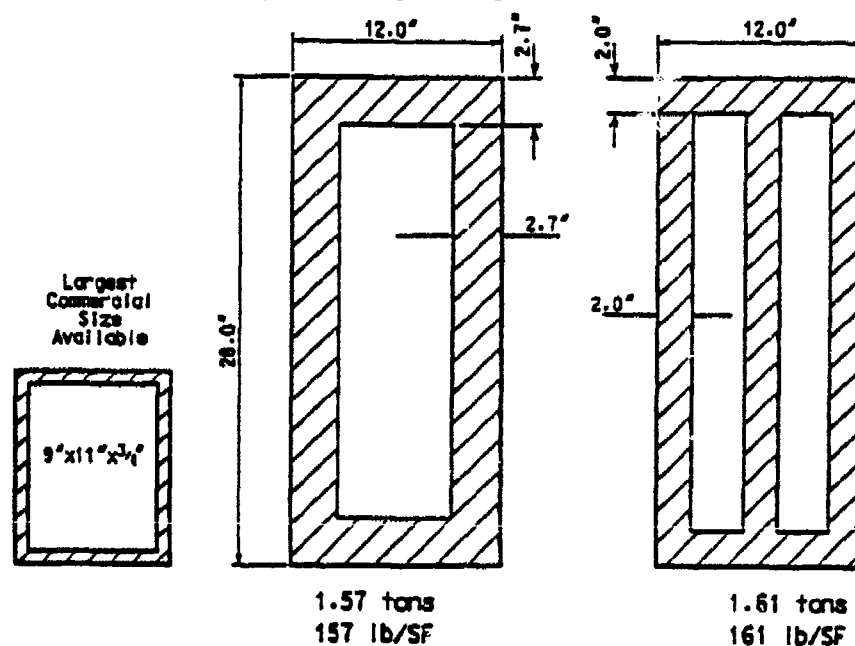


Figure 27. Pultruded Fiberglass Beam Designs for 20-Foot Roof Span.

Achieving a 50-foot span required the beam cross-section shown in Figure 28. This double-box beam has overall dimensions of 18 inches wide by 44 inches deep with 2.15-inch-thick walls. This beam weighs 6.88 tons and has a weight per area ratio of 183 pounds per square foot.

Estimating the fabrication cost for these conceptual beams is very speculative, because of the unknown cost of tooling and other equipment required to produce extremely large custom shapes. An estimate was, therefore, made using the cost of the fibers, assuming that this will represent the bulk of the material cost. Using \$0.75 per pound for E-glass, and a 50% by volume fiber content, the weight of fibers was estimated for the beams described above. The 20-foot-long, 9-inch by 11-inch by 3/4-inch beam would cost approximately \$230. The 20-foot-long single-box beam has a fiber cost of \$1540 (\$77 per square foot) and the 50-foot-long double-box beam has a fiber cost of \$6750 (\$90 per square foot).

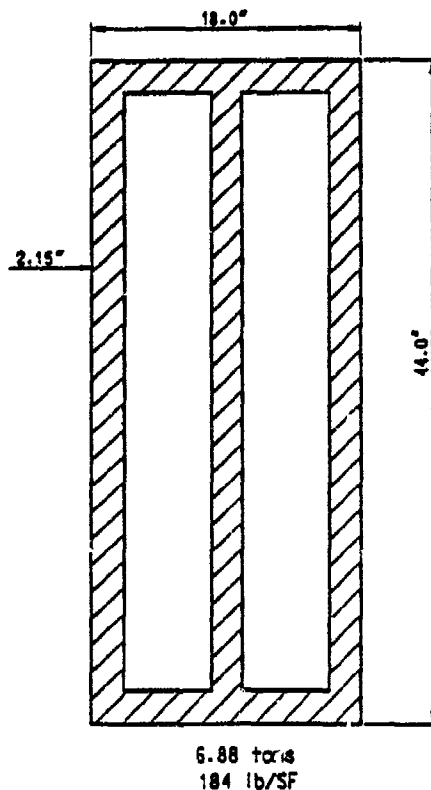


Figure 28. Pultruded Fiberglass Beam Designs for 50-Foot Roof Span.

## 7. Conclusions and Recommendations

The use of concrete beams with external CFRP reinforcing does not represent a viable concept for roof beams at this time. The ultimate flexural strength is characterized by brittle failure modes, either in tension rupture of the CFRP fibers or crushing of the concrete. Therefore, such beams must remain elastic. In blast-resistant and seismic design, members designed for relatively large ductilities require a fraction of the static strength of an elastic member and are, therefore, much more economical.

Pultruded FRP beams were also analyzed, and found to have acceptable performance and weight, even though they also were limited to a ductility factor less than 1.0. The characteristics of these beams which permits them to work are their flexibility and low mass. These beams had relatively long natural periods compared to the duration for the dynamic load. Figure 26 shows a SDOF response graph with the  $t_d/T$  ratios for the 20-foot and 50-foot beams and their corresponding dynamic load factors. For these two beams, the required resistances are 90% and 40% of the applied load.

While beams with wall thicknesses of 2.5+ inches were designed, manufacturing is limited to sections with wall thickness less than 1-1/4 inches. This limitation is related to the thermoset curing process which is exothermic and very rate sensitive. Problems occur with void inclusions when thick sections are manufactured. Another limitation in the manufacturing process is the overall size of the beam. As the overall beam size increases, larger pulling forces are required to overcome surface friction within the tool. The largest rectangular shape currently available is 9-inch-wide by 11-inch-deep with 3/4-inch wall thickness. The largest open cross-section is an I-beam with 24 x 3/8 inch web and 7 x 3/4 inch flanges.

The thick-wall shapes were designed using a very simple design procedure that applies to a specific manufacturers' standard products. Customization of the fiber and matrix composition could possibly reduce the thickness of the walls and overall size of the beams. The required design procedure becomes more complex, as the beam must be treated as an orthotropic laminated material. Should there be a need to pursue this concept, it should include a rigorous analytical and experimental effort to quantify the global behavior of the beam and local behavior of its individual components. An example of such an investigation is described in Reference 66 which found that local buckling of the compression flanges introduced a failure mode that eventually resulted in material degradation and total failure of the beam. This source developed analytical solutions to predict this behavior based on either measured or computed material properties.

Another consideration associated with pultruded beams is the effect of temperature on retention of physical properties. This characteristic is highly dependent on the composition of the matrix material. Recommended approximate values for retention of ultimate stress and modulus of elasticity for several proprietary resin systems are given in Table 11 below.

TABLE 11. PHYSICAL PROPERTY RETENTION  
FOR TYPICAL PULTRUDED BEAMS

Temperature	Resin System "A"	Resin System "B"
<b>Ultimate Stress</b>		
100° F	85%	90%
125° F	70%	80%
150° F	50%	75%
<b>Modulus of Elasticity</b>		
100° F	100%	100%
125° F	90%	95%
150° F	85%	90%

## F. FINAL EVALUATION

Five concepts were considered for roof beams for a rapidly erectable protective shelter. This section briefly reviews the results from the preceding analysis, and evaluates those results within the framework of the evaluation criteria described in Section 4.D. Reasons are given for the ratings given to each concept. The objective of this evaluation was to select the most promising concept for further validation with laboratory tests on prototype beams.

The five concepts considered in this study were: reinforced concrete (RC), prestressed concrete (PS), steel-concrete composite (SC), concrete with external carbon fiber plastic reinforcement (CFRP), and glass fiber reinforced plastic beams (GFRP). The criteria and weighting factors by which the concepts were evaluated consisted of: fabrication cost (25%), handling (15%), storage (15%), erection (25%), and reliability (20%). A relative rating between one and five, with five representing the best and one representing the poorest, was assigned to each concept for each criteria. A final score was then obtained by summation of the products of the weighting factors times the ratings.

In arriving at the relative rankings, the summary information in Table 13 was considered along with other subjective factors. In fabrication, mass production and low material costs favor



prestressed, steel-concrete composite, and GFRP. While reinforced concrete and CFRP concepts can be mass produced, they require more labor-intensive fabrication related to installing larger quantity of shear reinforcement or bonding of external reinforcing. Evaluation of handling was based on weight and toughness of the beam. Reinforced concrete and CFRP beams weigh the most, while prestressed is subject to breakage because of prestressed-induced tensile stresses, and the CFRP and GFRP can be damaged by abrasion or gouging of the fibers. On the other hand, steel concrete composite had medium-weight and could withstand fairly rough handling without significant damage.

TABLE 12. SUMMARY INFORMATION FOR CONCEPT EVALUATION

CONCEPT	COST (\$/SF)		EFFICIENCY (LB/SF)	
	20 FOOT	50 FOOT	20 FOOT	50 FOOT
RC	82	87	260	281
PS	70	62	202	226
SC	71	70	163	154
CFRP	72	336	310	675
GFRP	77	90	160	183

In storage, reinforced concrete appeared to be the least sensitive to exposure and long-term effects. Prestressed will undergo time-dependent creep which may increase the amount of camber for high levels of prestress; in addition, prestressed would likely have narrow cracks in the top slab due to tensile stresses that could allow water and moisture into the beam. The steel-concrete composite beams would require coating to seal the steel girder from moisture and, thus, corrosion. CFRP and GFRP have temperature and UV sensitive matrix materials, and unless properly stored could experience strength loss over the expected 20-year lifetime.

Rankings under the erection criteria were related to total beam weight and weight per area. GFRP beams were rated the highest because of their overall light weight and smaller size. Steel-concrete composite, prestressed, reinforced concrete, and CFRP were ranked according to their weight per unit area. Consideration was not given to integration with the shelter wall; however, this will most likely be an important design consideration when the roof beams and reinforced soil wall are combined. Design of the abutment and ends of the beam will take into account bearing and shear stresses, anchorage of tensile reinforcement, and anchorage for rebound.

Finally, the reliability criteria subjectively ranks the confidence one has in the concept to perform as designed. This includes a knowledge of the component materials (steel, concrete,

GFRP, and CFRP), the way these materials are combined into a structural member, and knowledge of the past performance of similar structural elements under static and dynamic loads. Steel-concrete composite received the highest ranking; in this concept two very well understood materials are combined in the least complicated system of the five concepts. Reinforced concrete is ranked next, and shares the same advantages of steel-concrete composite. However, this concept relies extensively on high performance, lightweight concrete to reduce the weight of the beam. Although recent research supports the validity of traditional design assumptions, actual design experience is relatively sparse. This same logic applies to prestressed, with the additional uncertainty that protective structures historically have not utilized prestressed concrete. Finally, GFRP and especially CFRP concepts have significant uncertainties and assumptions that must be further investigated before they can be used with confidence for blast-resistant structures. The final rankings for each concept, considering all of these factors is presented in Table 13.

TABLE 13. EVALUATION OF CANDIDATE BEAMS

CRITERIA	WEIGHT	RC	PS	SC	CFRP	GFRP
Fabrication	25%	2	5	4	1	3
Handling	15%	2	3	5	1	4
Storage	15%	5	3	4	1	2
Erection	25%	2	3	4	1	5
Reliability	20%	4	3	5	1	2
Total		2.85	3.5	4.35	1.0	3.3

The combination of low fabrication cost, structural efficiency, and confidence gives steel-concrete composite the highest ranking of the five concepts. The importance given to weight of the beams is apparent by the relative scores for reinforced concrete and GFRP. Reinforced concrete has been and will continue to be a predominant construction method for protective structures. However, GFRP appears promising and warrants further investigation because of its low weight and good strength properties. One possible use might be in a two way roof system for a reduced threat scenario. Such a roof, shown in Figure 29, would consist of primary steel-concrete composite girders on 15, 20 or 25 foot centers supporting lightweight, elastic beams placed on top of the girders to form the roof of the shelter. GFRP beams, or custom built FRP composite panels, would be a leading candidate for the lightweight elastic beams.

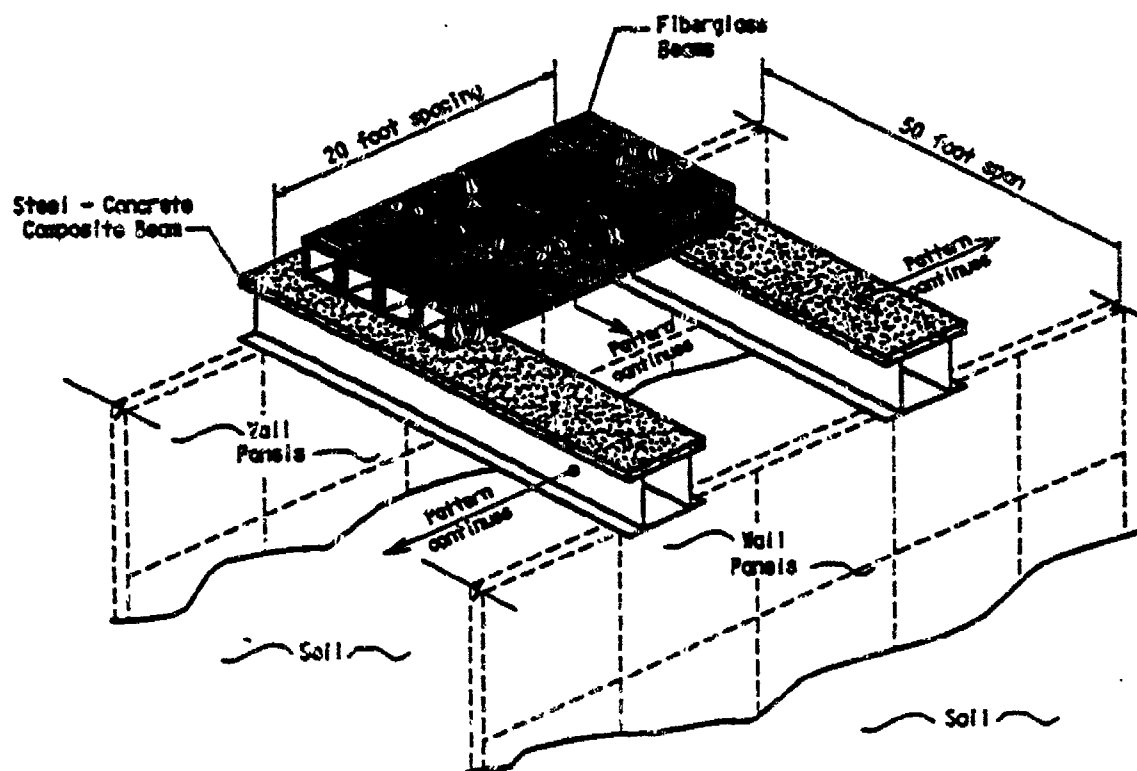


Figure 29. Proposed Lightweight Two-Way Roof System Using Pultruded Fiberglass Beams.

## SECTION 5. ENHANCING BEAM DUCTILITY WITH CONFINED CONCRETE

### A. CONFINED CONCRETE ANALYSIS

Design procedures for reinforced concrete are predicated on the assumption that concrete exhibits brittle failure at small strains. Design of structural elements to respond in a ductile mode has been accomplished by limiting the effective tensile reinforcing ratio and through the addition of compression reinforcement. Design of columns and joints to resist seismic induced loading relies on the use of transverse reinforcing to confine an interior concrete core. The effect of closely spaced shear reinforcement in conjunction with compression reinforcement in beams has been recognized for some time (References 26 and 27). As a result, seismic provisions of the ACI Code (Reference 3) require closely spaced hoops in flexural members where yielding is likely to occur (21.3.3.1 and 21.3.3.2). In the present study, an analytical method was used to quantify the effect of using confining reinforcement on the strength and ductility of the concrete slab in the steel-concrete composite concept.

#### 1. Background

The compressive strength of concrete  $f'_c$  is determined from axial compression tests of cylindrical specimens. Stress-strain curves (Reference 48) for typical concrete specimens of various strengths are shown in Figure 30. Normal strength concrete has peak stress values of 3,000 to 4,000 psi at a corresponding strain of 0.2%. After the peak load is reached, the concrete gradually loses strength and will completely fail at strains between 0.3% to 0.4%. When concrete is tested under triaxial loading, with lateral confinement provided by a pressurized fluid, two changes occur: the strength improves dramatically and the peak and ultimate strains become very large. For example, Figure 31 shows stress-strain curves (Reference 48) for a concrete with  $f'_c = 3600$  psi under increasing triaxial pressures. These test results suggest that the longitudinal stress at failure,  $\sigma_1$ , increases linearly with the confining pressure,  $\sigma_3$ , viz.,

$$\sigma_1 = f'_c + 4.1 \cdot \sigma_3 \quad (25)$$

In addition, strain at peak stress tends to increase with increasing confining stress. The benefit of this phenomenon in structural applications has been studied extensively, with particular regard to seismic design of columns and beam-column joints. A comprehensive state-of-the-art review of this subject is contained in Reference 68.

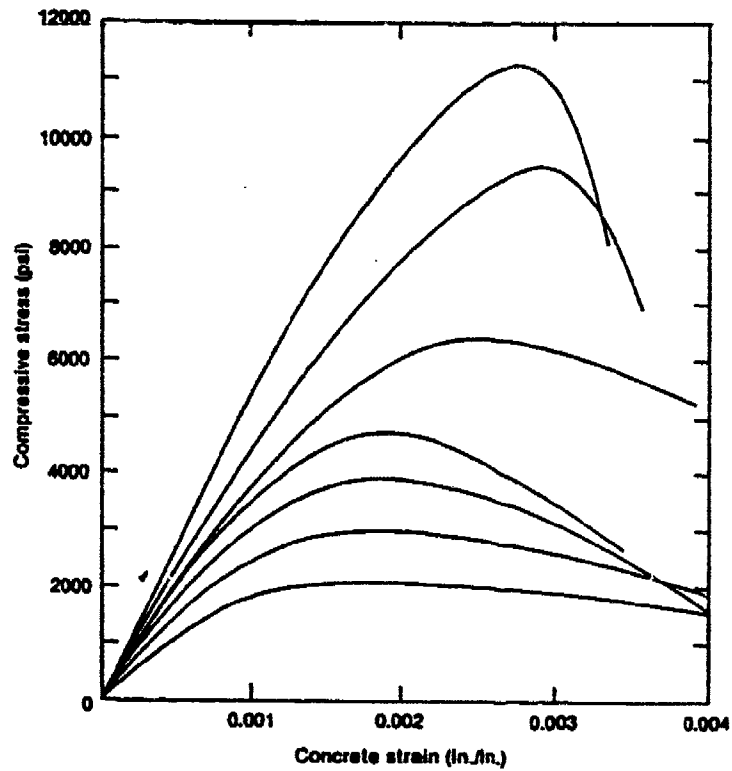


Figure 30. Typical Stress-Strain Curves for Normal to Very High Strength Concrete in Compression.

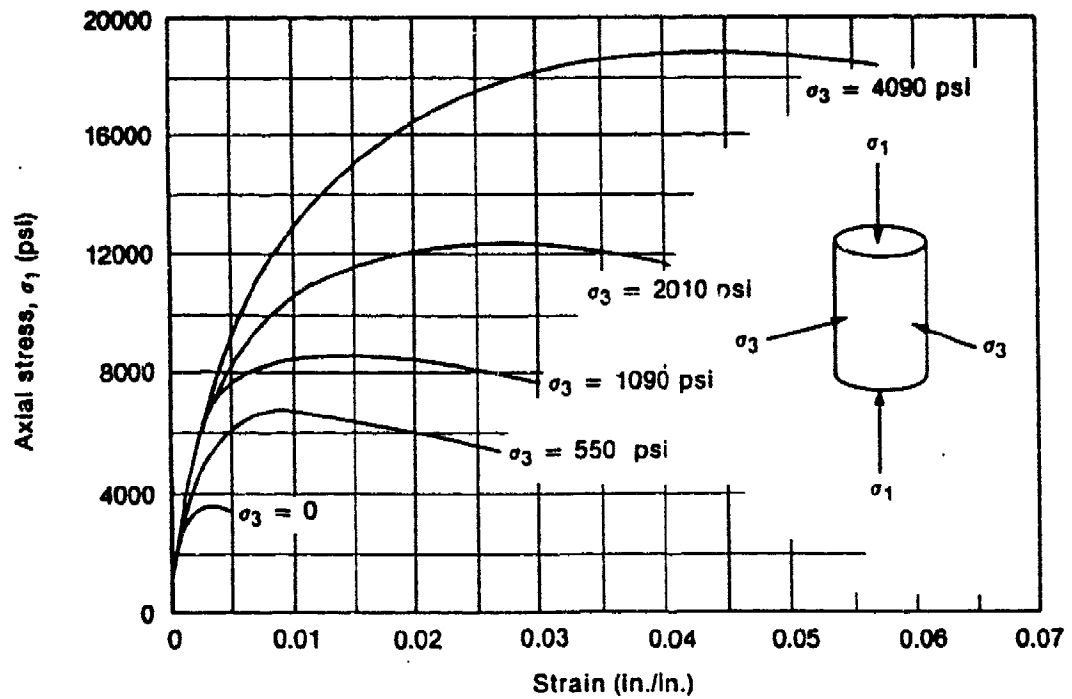


Figure 31. Axial Stress-Strain Curves for  $F'_c = 3600$  psi Concrete Under Triaxial Load Conditions. (Reference 48)

## 2. Analysis of Confined Concrete

The concrete slab portion of the steel-concrete composite roof beam experiences compressive stresses similar to a column under axial load. While the strain distribution is not uniform from bottom to top, the stress distribution approaches a nearly uniform distribution. This condition is illustrated schematically in Figure 32 showing the idealized linear strain distribution and corresponding stresses for a steel-concrete composite beam near its ultimate capacity with its neutral axis in or near the top flange of the girder. A schematic load-deflection curve in the figure shows three general response levels, an initial elastic region prior to yielding of the tension flange, a plastic region where the steel section progressively yields, and a post-peak region after crushing of the concrete. After the concrete slab loses integrity, the residual load capacity is determined by the steel girder, including any local failure modes. The last region of response is not of interest in design.

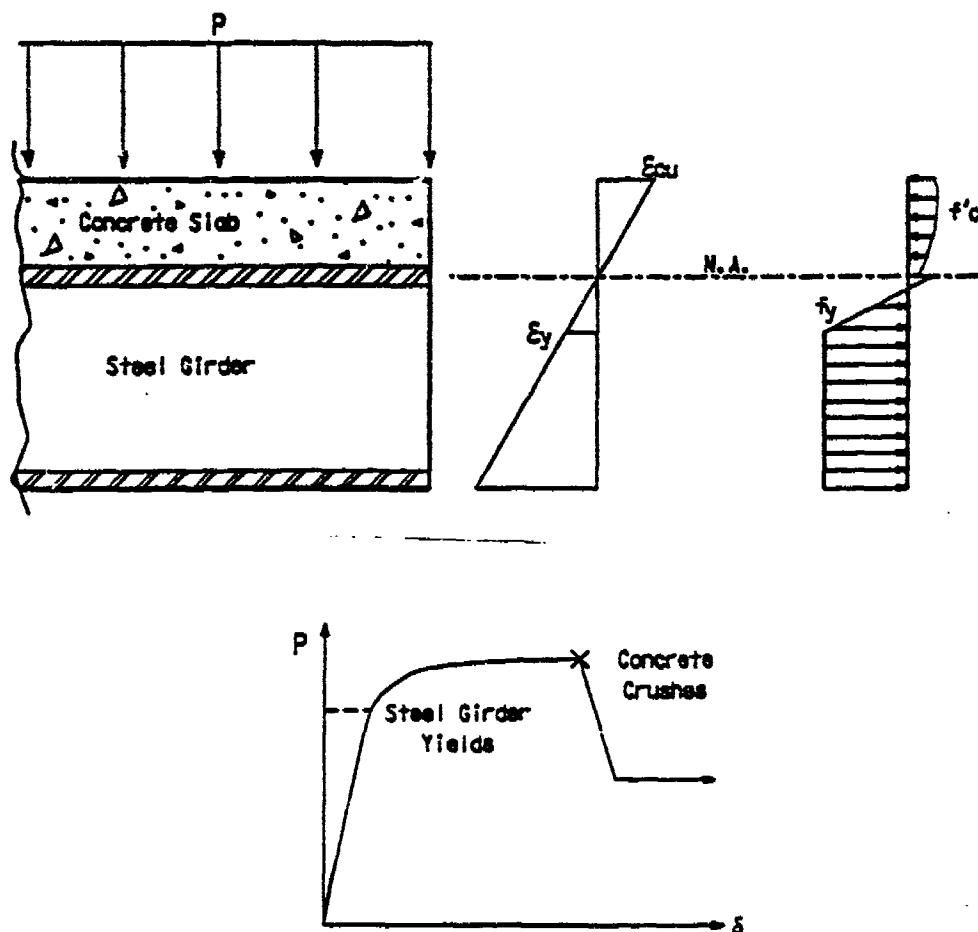


Figure 32. Typical Steel-Concrete Composite Beam Stresses, Strains, and Load-Deflection Response.

As the concrete becomes compressed in the longitudinal direction due to development of the internal moment, it expands in the transverse direction (similar, but to a smaller degree as a rubber eraser gets fatter when squeezed). This lateral expansion can be resisted by external pressure, as in a triaxial load test, by an external jacket (Reference 69), or by internal reinforcing. In circular cross-sections, spiral rebar cages are very effective, and for square or rectangular cross-sections, hoops and cross-ties have been used very successfully. The transverse reinforcing provides stiffness to and enables the longitudinal bars to confine the concrete core. Figure 33 illustrates schematically a square column under axial compression with various configurations of longitudinal and transverse reinforcing. The longitudinal rebar is stiffened by closely spaced transverse hoops and ties and develops significantly more confinement than if they were absent. This confinement is depicted for three different cases along with typical stress-strain curves for the confined concrete core. In general, an increase in transverse reinforcement and/or a decrease in tie spacing increases the strength and ductility of the confined concrete core. The analysis described next characterizes this effect and estimates the resultant stress-strain behavior of the confined concrete.

Many models have been proposed to describe the interaction of concrete and confining reinforcing. Rather than evaluate the merits of all the confined concrete models, a model was chosen that had moderate complexity and good predictive capability based on comparison with a large number of experimental results. This model computes the peak stress and strain for specific geometric and material parameters, and uses these values to estimate the stress-strain behavior of the confined concrete. The analysis described next is taken from Reference 70.

a. Generalized confined compressive strength.

The analysis replaces the coefficient 4.1 and value of confining pressure  $\sigma_3$  in the previously described linear relation between concrete strength and confining stress with computed values, i.e.,

$$f'_{cc} = f'_{co} + k_1 f_{le} \quad (26)$$

where:

$$\begin{aligned} f'_{cc} &= \text{confined compressive strength} \\ f'_{co} &= \text{unconfined compressive strength} \\ k_1 &= \text{coefficient determined by calculation} \\ f_{le} &= \text{equivalent confining stress by calculation} \end{aligned}$$

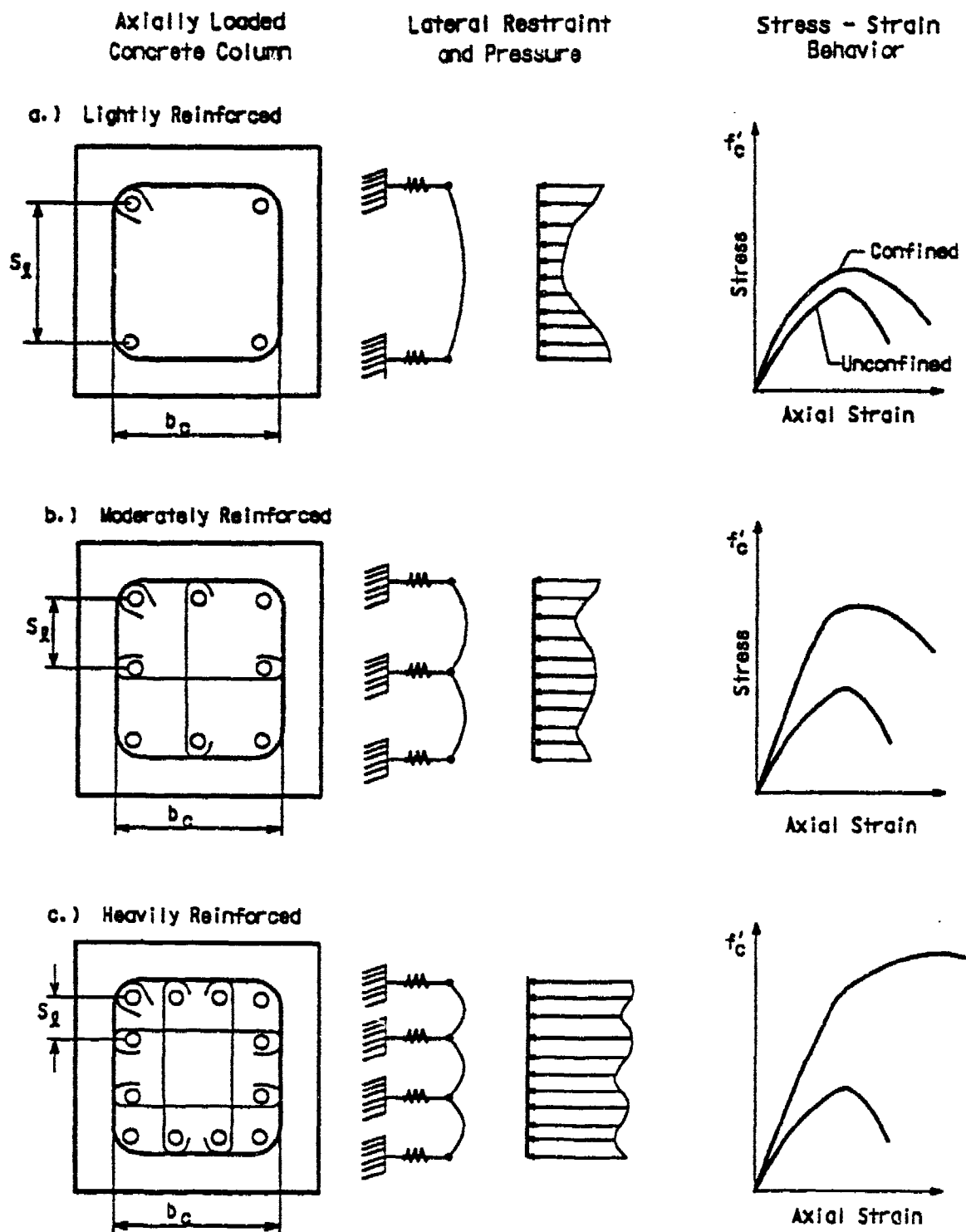


Figure 33. Behavior of Symmetric Axially Loaded Members with Different Levels of Confining Reinforcement.



b. Square, Symmetrically reinforced columns.

The equivalent confining stress,  $f_{le}$ , approximates the variable stress (lateral restraint) shown in Figure 33 with an equivalent uniform value. For the case of closely spaced bars and cross-ties in Figure 33, the pressure distribution is indeed close to uniform. Where the reinforcing consists only of corner bars tied with perimeter hoops at large spacing, the confining pressure is much more variable in both directions. Therefore, an equivalent uniform pressure was estimated by:

$$f_{le} = k_2 f_l \quad (27)$$

where:

$$k_2 = 3.1 \sqrt{\left(\frac{b_c}{s}\right)\left(\frac{b_c}{s_l}\right)\left(\frac{1}{f_l}\right)} \leq 1.0 \quad (28)$$

and:

$$f_l = \frac{\sum A_s f_{yt}}{sb_c} \quad (29)$$

$b_c$  = center to center distance of perimeter hoop reinforcement.

$A_s$  = area of transverse reinforcement in one direction.

$f_{yt}$  = yield stress of transverse reinforcement, psi.

$s, s_l$  = spacing between transverse ties and longitudinal bars respectively.

The coefficient  $k_1$  in Equation 26 is then calculated as:

$$k_1 = 15.6(f_{le})^{-0.17} \quad (30)$$

The equation for  $f_{le}$ , applies to square columns with equal reinforcing in both directions.

c. Rectangular, Unsymmetrically Reinforced Column.

For the rectangular cross-section shown in Figure 34, the previous relationships for square columns were modified to account for different widths, i.e.,  $b_{cx}$  and  $b_{cy}$ . An equivalent lateral pressure is calculated as:

$$f_{le} = \frac{f_{lex} b_{cx} + f_{ley} b_{cy}}{b_{cx} + b_{cy}} \quad (31)$$

This relationship is shown in Figure 35. The values in this equation are calculated for each direction using modified forms of equations 27 through 29.

$$f_{lex} = k_{2x} f_{lx}$$

$$k_{2x} = 3.1 \sqrt{\left(\frac{b_{cx}}{s}\right) \left(\frac{b_{cx}}{s_{lx}}\right) \left(\frac{1}{f_{lx}}\right)} \leq 1 \quad (32)$$

$$f_{lx} = \frac{\sum A_{sx} f_{yt}}{s b_{cx}}$$

Similar equations are used for  $f_{ley}$ .

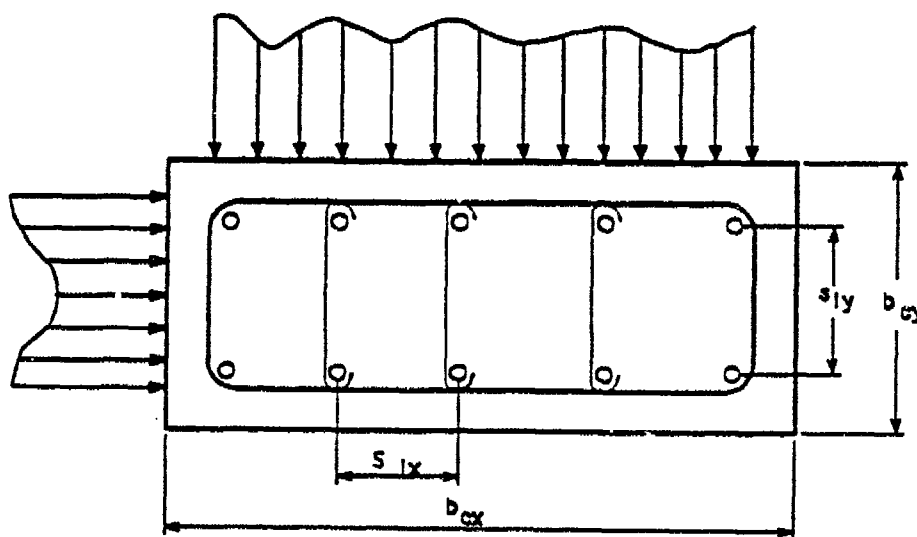


Figure 34. Biaxial Confinement in Rectangular Members.

d. Confined concrete stress-strain curve.

After calculating the maximum strength  $f'_{cc}$ , the corresponding strain is calculated by the expression:

$$\epsilon_1 = \epsilon_{01}(1 + 5K) \quad (32)$$

where:

$\epsilon_1$  = strain at peak stress

$\epsilon_{01}$  = strain corresponding to peak stress  $f'_{co}$  determined under same rate of loading as that used for the confined concrete

$\equiv 0.002$  for low rate of loading

and:

$$K = \frac{k_1 f_{le}}{f'_{co}} \quad (33)$$

The parabolic rising branch of the stress-strain curve is then

$$f_c = f'_{cc} \left[ 2 \left( \frac{\epsilon_c}{\epsilon_1} \right) - \left( \frac{\epsilon_c}{\epsilon_1} \right)^2 \right]^{1/(1+2k)} \leq f'_{cc} \quad (34)$$

as shown in Figure 35. The linear descending branch is defined by the strain at 85% of  $f'_{cc}$ . Analysis of column tests were used to determine the relationship for this strain as:

$$\epsilon_{85} = 260 \rho \epsilon_1 + \epsilon_{085}$$

Where  $\epsilon_{085}$  = the strain at 85% of the unconfined compressive strength after the peak

$\epsilon_1$  = peak strain for confined concrete

$\rho$  = transverse reinforcing ratio

$$= \frac{\sum A_s}{s(b_{cx} + b_{cy})}$$

The summation indicates the total area of transverse reinforcement in two directions crossing  $b_{cx}$  and  $b_{cy}$ . If  $\epsilon_{0.85}$  is not determined by tests under the same rate of loading as the confined concrete, a value of 0.0038 may be appropriate for slow loading rate. The post-peak strength descends linearly to 20% of the peak value  $f'_{cc}$ , after which it is assumed constant.

The linear descending branch is highly influenced by the amount of transverse reinforcement providing restraint to the longitudinal bars. As the outer skin of concrete is assumed to be failed, sufficient lateral restraint must be provided to keep the longitudinal bars from buckling. This is an extremely important point, in that if the longitudinal bars buckle, they can no longer confine the concrete and the descending branch of the stress-strain curve is steep and rapid, i.e., failure is rapid and catastrophic.

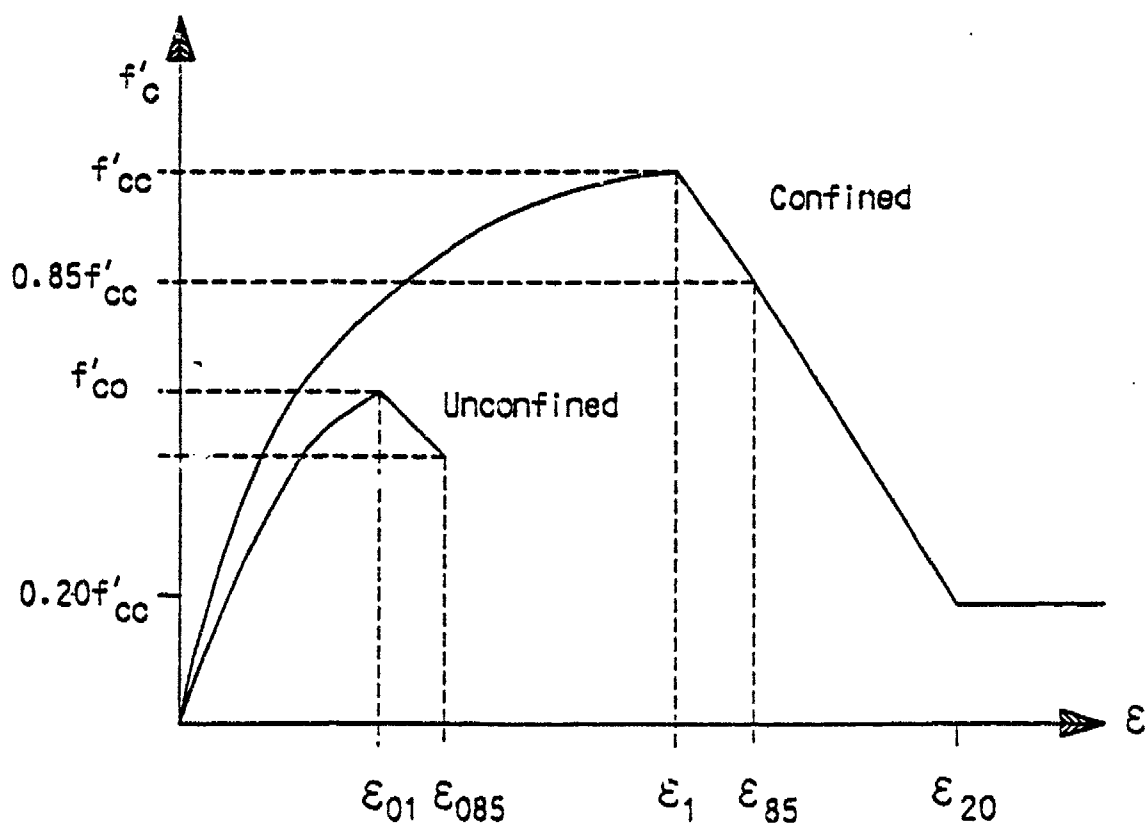


Figure 35. Analytical Model of Stress-Strain Curve for Confined Concrete.

e. Maximum spacing for ties.

The maximum spacing for transverse reinforcing in the ACI Code under Section 7.10.5 - Lateral Reinforcement for Compression Members - Ties is given as "spacing of ties shall not exceed 16 longitudinal bar diameters, 48 tie bar or wire diameters, or least dimension of the compression member." The ties should be arranged such that every corner and alternate longitudinal bar is enclosed by a corner of a tie with an included angle of not more than 135°. Spacing between unsupported longitudinal bars should not be greater than 6 inches clear on each side along the tie from a laterally supported bar. Figure 36 from the ACI Code (Fig. 7.10.5) is provided to clarify the foregoing remarks. The seismic design portion of the ACI Code for transverse reinforcement of members subjected to axial and bending, Section 21.4.4.2, states that "Transverse reinforcement shall be spaced at distances not exceeding (a) one-quarter of the minimum member dimension and (b) 4 inches." Additionally, the total cross-sectional area of transverse reinforcement (including crossties) should be greater than the values given by the following equations:

$$A_{sh} = 0.3(sh_c) \left( \frac{A_g}{A_{ch}} - 1 \right) \left( \frac{f'_c}{f_{yh}} \right) \quad (36)$$

$$A_{sh} = 0.09(sh_c) \left( \frac{f'_c}{f_{yh}} \right) \quad (37)$$

where:

- $A_{sh}$  = minimum area of transverse reinforcement.
- $A_g$  = gross area of concrete cross-section.
- $A_{ch}$  = area of concrete core, measured to outside of confining reinforcing.
- $f_{yh}$  = yield strength of hoop reinforcement.
- $h_c$  = cross-sectional dimension of concrete core measured center-to-center of confining reinforcement.
- $s$  = spacing of transverse reinforcement.

Such transverse reinforcement shall consist of hoops and optional crossties of the same bar size and spacing as the hoops. Each end of the crosstie shall engage a peripheral longitudinal bar, as shown in Figure 37 taken from ACI (Fig. 21.4.4).

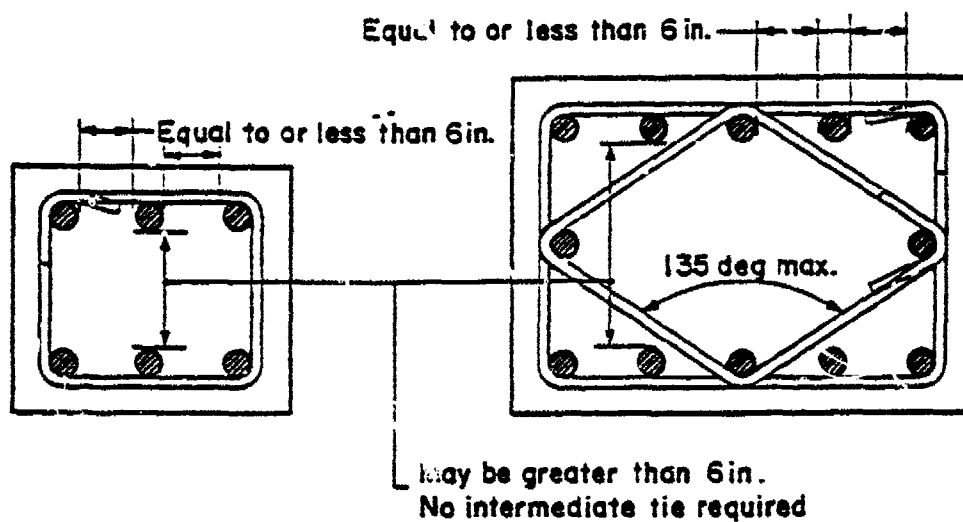


Figure 36. Measurements Between Laterally Supported Longitudinal Bars from Reference 3.

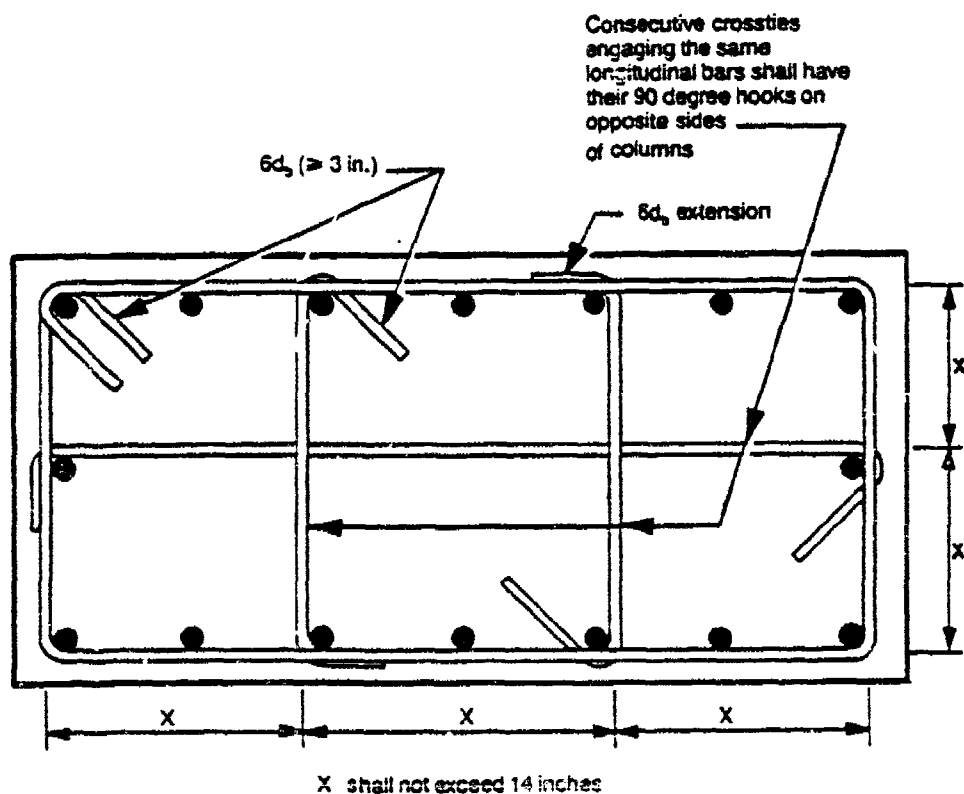


Figure 37. Examples of Transverse Reinforcement from Reference 3.

## B. APPLICATION TO ROOF BEAM SLAB

The foregoing analysis procedure was used to design reinforcement for the top slab of the steel-concrete composite beam. Examples of a typical slab with two different reinforcement layouts are described in the following to illustrate the use and benefits of this concept.

Figure 38 shows a cross-section of a 24-inch-wide 6-inch-deep concrete slab such as could be used for a roof beam. Grade 60 #3 (3/8 inch diameter) rebar was used for both the longitudinal and transverse reinforcing. The concrete was assumed to have an unconfined compressive strength  $f'_{co}$  of 4000 psi. The two cases described herein represent using maximum spacing between the transverse hoops of either 6 inches, according to ACI Sec. 7.10.5, or 1.5 inches, if Sec. 21.4.4.2 is followed. It should be noted that spacing based on 1/4 the width of a column is reasonable, but not really practical for thin slabs. The corresponding amount of transverse reinforcing, in the form of a perimeter hoop and cross-ties, is based on the minimum amount required to satisfy ACI Eqn. 21-3 or 21-4. After selecting this reinforcing, the procedure from Reference 70 was used to estimate the strength and ductility.

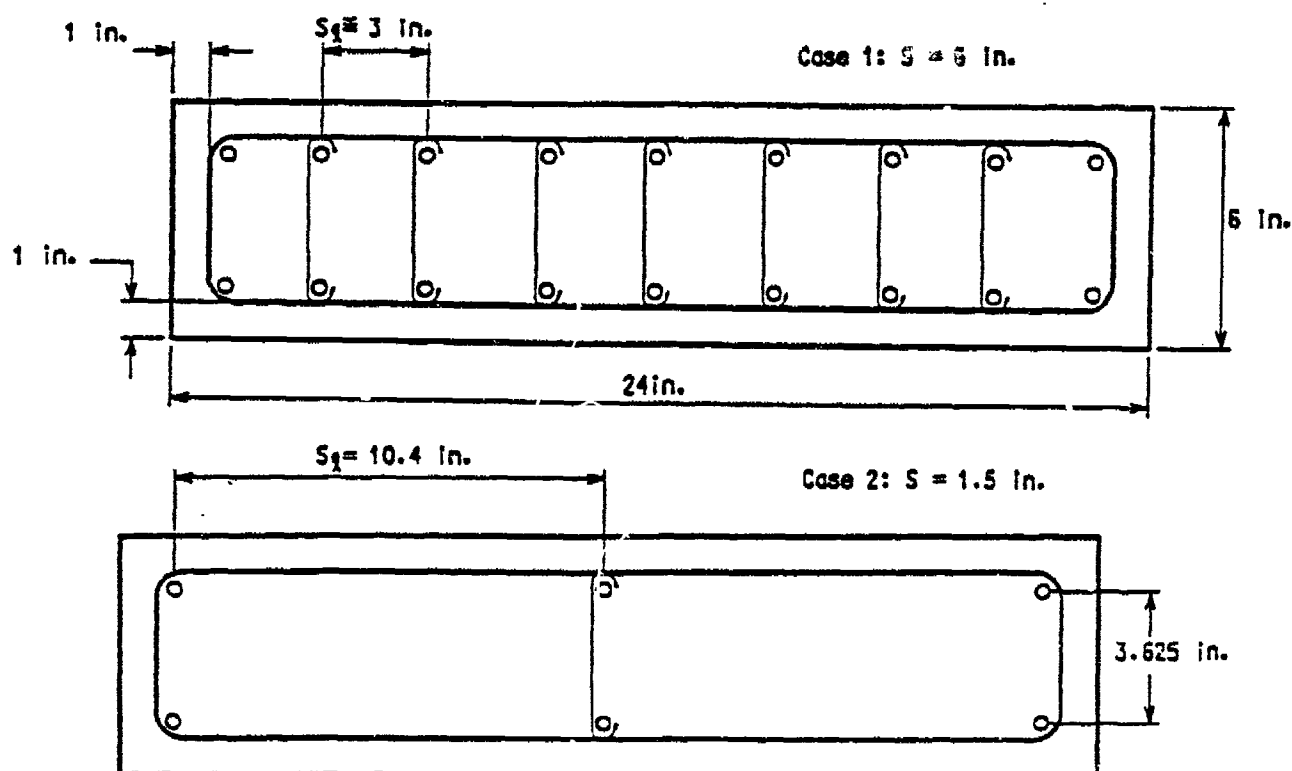


Figure 38. Example Reinforcement Options for 24-Inch-Wide, 6-Inch-Thick Normal Strength Concrete Slab.

For Case 1 (Figure 39), with  $s = 6$  inches, the minimum area of reinforcement determined by ACI Equations 21-3 and 21-4 was  $0.782 \text{ in}^2$ . This result was determined by using  $h_c = 21.625$  inches, the center-to-center distance in the long dimension. This requirement can be satisfied by one perimeter hoop and six crossties as shown for case 1. The resulting reinforcing has eight longitudinal bars in each face on spacing  $s_l$  of approximately 3 inches. The minimum area of reinforcing in the short direction was satisfied by the perimeter hoop alone. These parameters lead to a peak confined compressive strength of nearly 5700 psi at a strain of 0.6%. This represents a 42% gain in strength and peak strain 3 times the value of  $\epsilon_{01} = 0.2\%$  assumed for the unconfined concrete. The reinforcement ratio,  $\rho_{sh}$ , defined here as:

$$\rho_{sh} = \frac{A_{sh}}{s h_c}, \quad (38)$$

is equal to 0.68% for this case.

The second case used the more conservative spacing of 1.5 inches between transverse hoops. ACI Equations 21-3 and 21-4 give a minimum area of reinforcing of  $0.196 \text{ in}^2$ , which would be satisfied by the No. 3 perimeter hoop ( $A_{sh} = 0.22 \text{ in}^2$ ). However, ACI Sec. 21.4.4.3 requires that crossties or legs of overlapping hoops cannot be spaced more than 14 inches on center perpendicular to the longitudinal axis of the member, see Figure 37. Therefore, one crosstie is used in addition to the perimeter hoop and the resulting reinforcing has three longitudinal No. 3 bars in each face with spacings of 10.44 inches in the long direction and 3.625 inches in the short direction (see Figure 38).

Computing the confined concrete strength and ductility using the previously defined equations leads to a peak confined compressive strength of 6234 psi at a strain of 0.8%. This represents a strength gain of 56% at a ductility of nearly 4 times the unconfined case. The reinforcing ratio  $\rho_{sh}$  equals 1.07% for this case.

A third analysis was made using the perimeter hoop and crossties from Case 1, but centered on 1.5-inch spacing as determined from Case 2. The resulting confined strength was 9335 psi with a strain of 1.5% at peak stress. The strength has more than doubled and ductility is nearly 8 times the unconfined value for a reinforcing ratio  $\rho_{sh}$  of 2.7%. Figure 39 summarizes these results by showing the computed stress-strain behavior for the unconfined concrete and the three confined cases. The obvious benefits of adequate confinement are a dramatic gain in strength with increasing strain, and much greater material ductility. These characteristics are ideal for the steel-concrete composite beam. While this same approach could be applied to the reinforced concrete and prestressed beams, it is likely that severe rebar congestion would occur due to the required shear stirrups and transverse shear and flexural reinforcement.



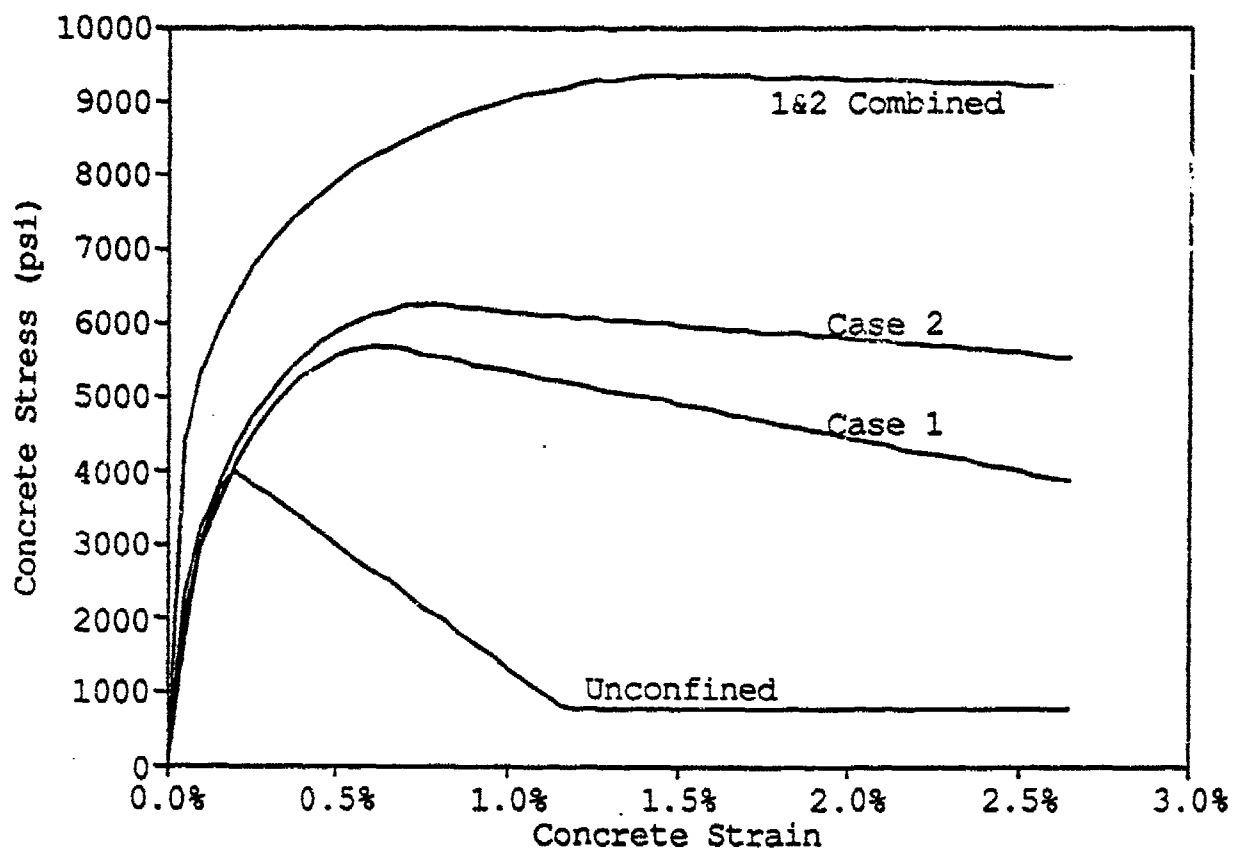


Figure 39. Analytic Stress-Strain Curves for Example Slab.

## SECTION 6. PROTOTYPE TEST PROGRAM

As described in the preceding sections, the steel-concrete composite cross-section with confined concrete presents a potentially attractive concept for blast-resistant roof beams. In general, the two key individual components of this concept, i.e., steel-concrete composite and confinement of concrete have been applied and proved individually for each component for applications different from that considered herein. The combination of these components, applied to the extremely high resistance/weight requirement for the shelter roof, has not yet been proven. Due to this lack of proof-of-concept, a prototype beam test program was developed and implemented.

### A. OBJECTIVES

The test program was developed to provide experimental validation of the concept in terms of strength, ductility, and constructability. Specifically, the static flexural resistance function for this concept was developed analytically using the procedures and assumptions described in the previous sections. Whereas the analytical development was known to be fundamentally sound, the performance of the concept relies on full development of theoretical strength and reliability of this strength over a wide range of ductility. Neither the analytical procedure nor previous research could prove the applicability of the concept to meet these requirements. Ultimate confidence in the analytically derived static resistance function could be achieved only through experimental validation.

In addition to validation of the static resistance function, the overall design procedure can be partially validated via prototype testing. Specifically, the nonflexure resistance of the concept, including shear and bearing, could be verified through the tests.

Finally, the constructability of this particular concept has not been proven since the confinement of the concrete portion of a steel-concrete composite beam has not been previously seen in practice. The potential fabrication problem of this combination that would benefit from design and construction of the test specimens is the possible interference of the considerable longitudinal and transverse reinforcement required to produce confinement of the concrete and the shear studs required for transfer of the horizontal shear between the concrete and the steel section. The level of difficulty in fabrication of this detail could be investigated and determined by design and fabrication of actual large-scale prototypes.

## B. DESIGN AND FABRICATION OF THE TEST BEAMS

### 1 Laboratory Setup

The prototype beams were to be tested at the facilities of the Concrete Technology Division (CTD), Structures Laboratory, U.S. Army Waterways Experiment Station (WES) in Vicksburg, MS. These facilities include a large structural test floor, various loading frames, reaction frames, loading rams, deflection gages, and load control and data acquisition devices. The capabilities and limitations of the facilities and available equipment provided a framework and boundaries for cost-effective prototype beam test design.

The structural test floor has a large open area with embedded threaded connectors for attachment of load frames, reaction frames, and other test equipment. The physical dimensions of the test area were more than adequate and imposed no restraint on the design or handling of the test specimens. A large overhead gantry crane and available forklift provided adequate capacity for moving any of the proposed test specimens.

The grid of connectors embedded in the floor is on a 3-foot spacing in both directions, as illustrated in Figure 40. Each threaded connector and the structural floor is designed for a maximum vertical load (upward or downward) of 100,000 pounds at each grid point. Various components of load and reaction frames and other laboratory equipment were available that were specifically designed to work in this threaded connector system. The spacing of the connectors and the load limit per connector played no minor role in design of the test specimens. The impact of these constraints are described in the following section.

Whereas the WES laboratory had a number of various loading and reaction frame components and several sizes and types of loading rams, the most practicable setup involved using the load frame shown in Figure 40, with a single loading ram with 150-ton capacity. This loading frame is supported on four columns on 6-foot spacing and was specifically designed for the 150-ton ram capacity. The clear spacing between columns provides sufficient room for any prototype beam design. Other available loading frames and rams were of considerably less capacity and would not be suitable for this program.

Likewise, a limited number of reinforced steel beams were available to act as reaction beams or spreader beams for the loading. The geometry and capacity of the available beams indicated one large 8-foot beam would be adequate for use as a spreader beam and several smaller beams could be used as reaction beams.

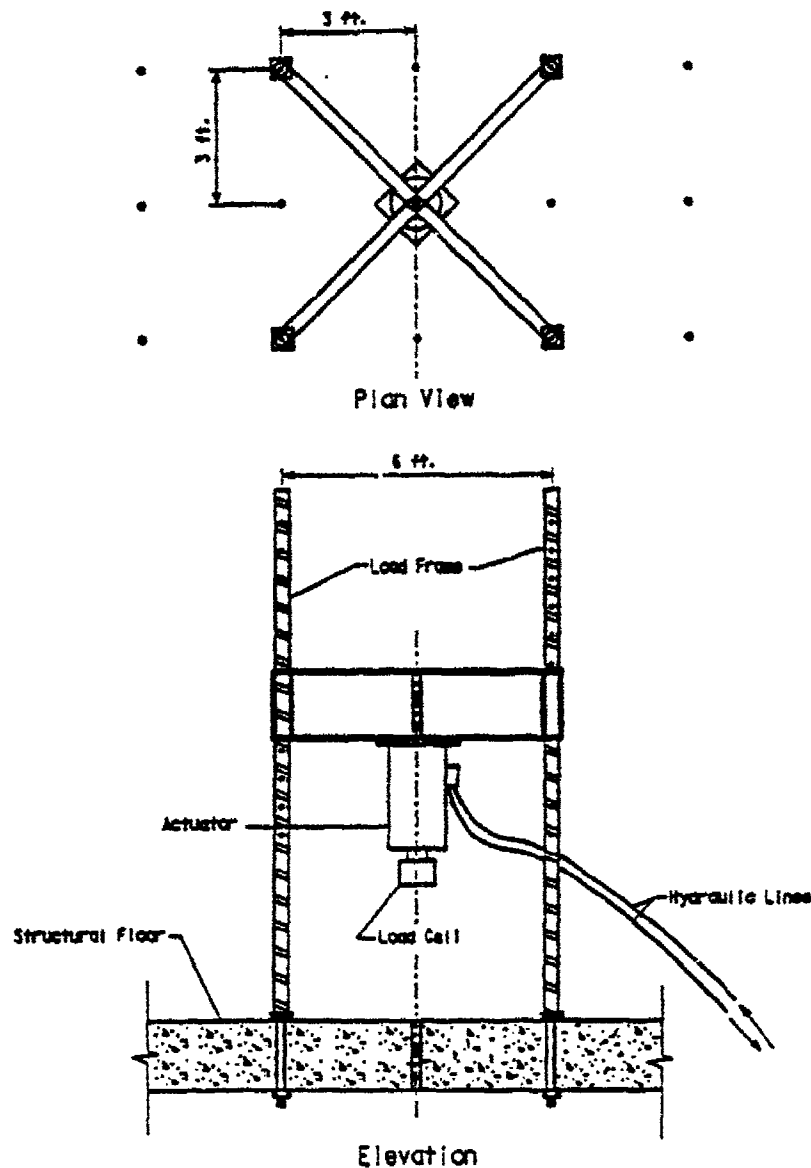


Figure 40. Schematic View of 150-Ton Load Frame Used for Prototype Beam Tests.

Loading was accomplished with the 150-ton ram under displacement control. The hydraulics were controlled by a recently installed microcomputer based system. The actuator and pump were reconditioned just prior to the beam tests. The new system monitored ram displacement and load as control variables.

Separate data acquisition facilities at the WES lab were capable of monitoring up to 40 channels of data simultaneously at a fixed sampling rate. Data was acquired from strain gages attached to the beam, displacement gages, and the load cell via an analog to digital and signal conditioning system interfaced to a data acquisition computer.

Since the data sampling rate was constant, the ram displacement rate was set to provide a reasonable number of data points in the three primary regions of response, i.e. linear elastic, yield, and plastic. A slow ram displacement rate was prescribed in the linear region due to the relatively stiff response. A slower displacement rate was prescribed for the crushing/yielding region to permit good definition of this region of significant changes in the stiffness of the system. The displacement rate was significantly increased in the postyield region to permit timely completion of the test and to acquire only a reasonable number of data points in this region of large displacements. Figure 41 and Table 14, taken from the test plan, show the selected displacement rates and deflection regions for the tests.

TABLE 14. BEAM TEST DISPLACEMENT RATES.

Region	Displacement Rate (in/sec)	Deflection Range (in)		Number of Samples	
		10-foot	16-foot	10-foot	16-foot
I	.001	0-0.5	0-1	50	100
II	.0005	0.5-1.0	1-2	100	200
III	.002	1-4	2-6	150	200

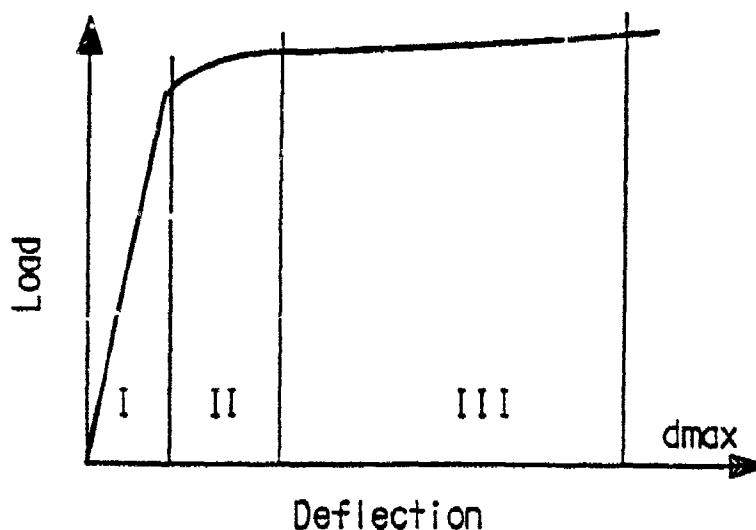


Figure 41 Three Regions Defined for Displacement Controlled Beam Tests.

## 2. Design and Fabrication of Test Beams

The test beams were designed using the procedure developed herein. As the loading would be static and nonuniform, the design was primarily based on the ultimate flexural capacity and stiffness of the test beam. The limitations imposed by available equipment, primarily the 150-ton total vertical load capacity, restricted the prototype design to a small family of test beams. Additionally, the beam weight and size was to be limited somewhat to permit reasonable handling with limited facilities of potential fabricators and allow a reasonable number of beams to be built within the budget.

The basic beam design considered a symmetrical, simply supported beam with two point loads to produce pure bending in the center section, as shown in Figure 42. The maximum applied moment was, thus, a function of the distance between a load point and nearest support, and the maximum vertical load. The distance between load points was maintained at values greater than twice the beam depth to minimize localized load effects. Two different beam designs were developed to investigate response for different length/depth ratios. The beam lengths selected corresponded approximately to half- and third-scale for the expected prototypes. However, the beam designs were not to be scale models, rather they represent prototypes somewhat shorter than the spans of 20 and 50 feet. For each beam design, two specimens were fabricated to provide replication and backup.

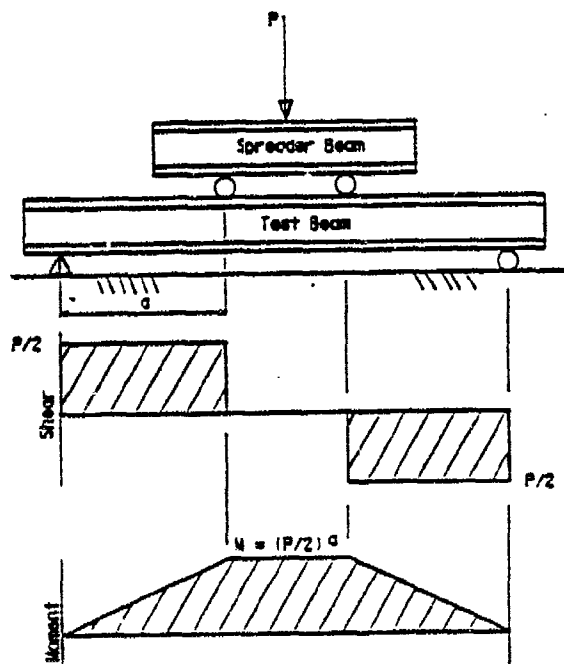


Figure 42. Prototype Beam Four-Point Load Configuration, Shear, and Moment Diagrams.

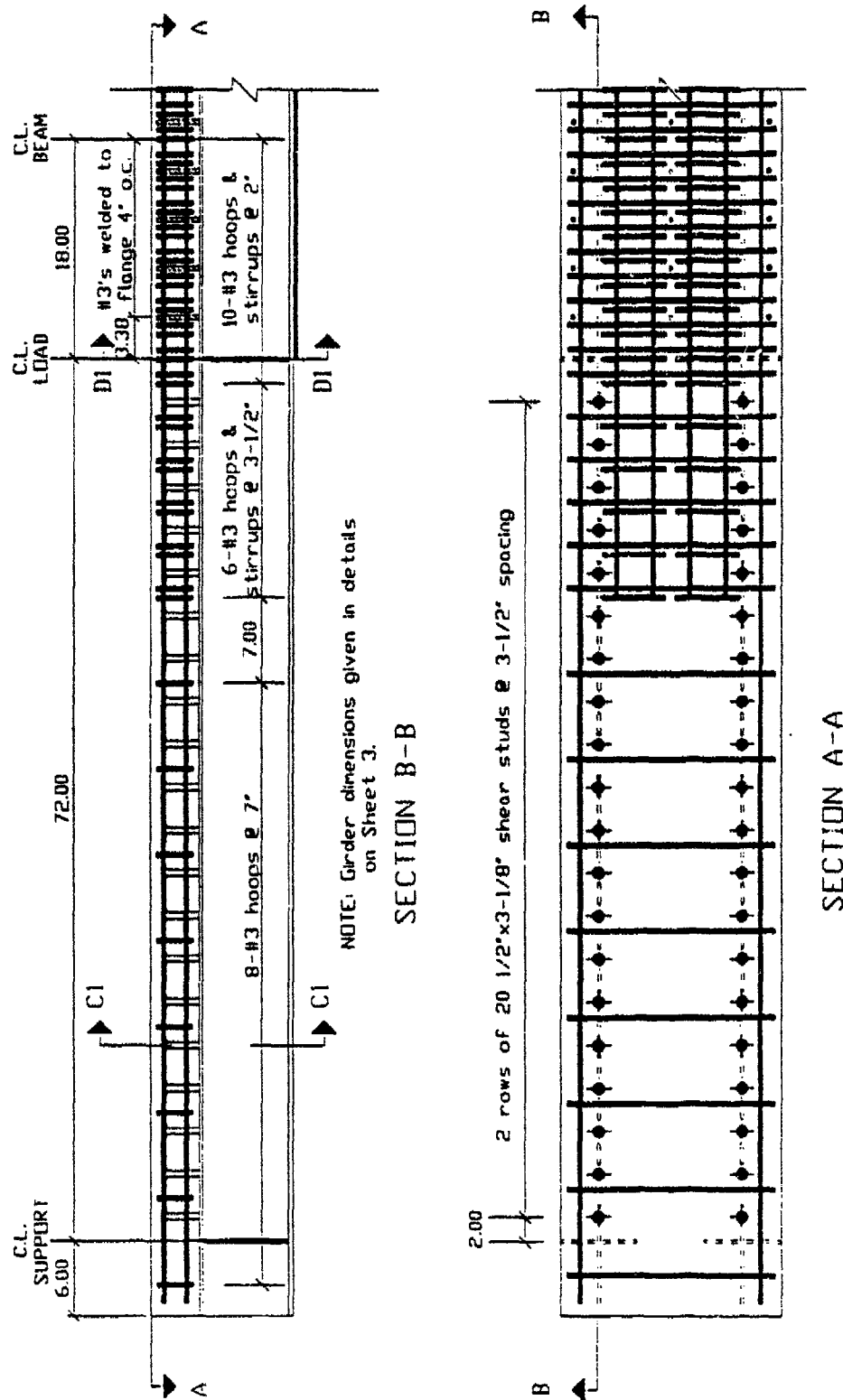
Each beam was designed to ensure flexural response, i.e., all other response modes were carefully designed to prevent premature failure in another mode. Specifically, the shear studs, web shear, reaction point and load point bearing, welds, and flange buckling were conservatively designed to carry more than the expected maximum load. This conservatism for nonflexural modes was consistent with the design procedure to ensure flexural response and ductility.

The prototype test beams were fabricated using standard concrete, reinforcing steel, and plate steel. Specifically, the concrete was specified to have a 28-day strength of 4000 psi. The reinforcement used standard bars with a nominal yield strength of 60 ksi (ASTM A615). The plate steel was typical of plate girder construction with a nominal yield strength of 50 ksi (ASTM A572). Standard welds and Nelson shear studs (ASTM A108) were specified.

The two prototype beams were 10 feet and 16 feet long with clear spans between supports of 9 feet and 15 feet. The constant moment section between load points was 2 feet for the 10-foot beam and 3 feet for the 16-foot beam. The resulting maximum moments that could be applied to the two prototype beams, determined by one-half the maximum ram capacity times the shear span, were 6.3 and 10.8 million inch-pounds, respectively. Beam cross-sections for the two lengths were checked against these limiting values during design.

The dynamic capacity of each beam was determined by scaling the duration of the load pulse by the geometric scale factor (e.g., 0.45x25 msec for the 9-foot-clear span and 0.3x40 msec for the 15-foot-clear span) in the design procedure analysis. It should be emphasized that these were not "scaled experiments" in a precise definition of the term. The beams were to be fabricated using conventional materials to avoid the complexities and cost of scaling the physical properties. For example, the size and properties of the concrete slab and confining reinforcement (bar size and spacing) were representative of a full size beam as opposed to a scaled model.

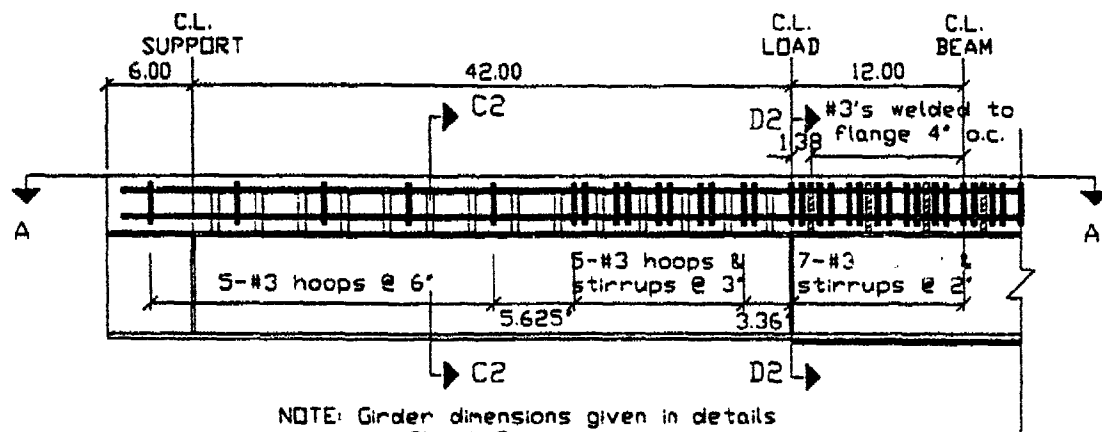
It was found that both prototype beam designs could use the same cross-section, thus, simplifying the design and fabrication of the test articles. Figures 43a and 43b show elevation and plan views of the two beams, which have the cross section depicted in Figure 43c. This cross-section has a predicted ultimate moment capacity of 3.6 million inch-pounds, with a ductility factor of 9 and support rotation of 4° for the shorter beam, while the longer beam had a ductility factor of 5.5 and support rotation of 4°. The resulting predicted ultimate loads for the two point load configuration were 172 kips and 101 kips, respectively, for the 10-foot and 16-foot-long beams, both well within the capacity of the 150-ton ram and load frame.



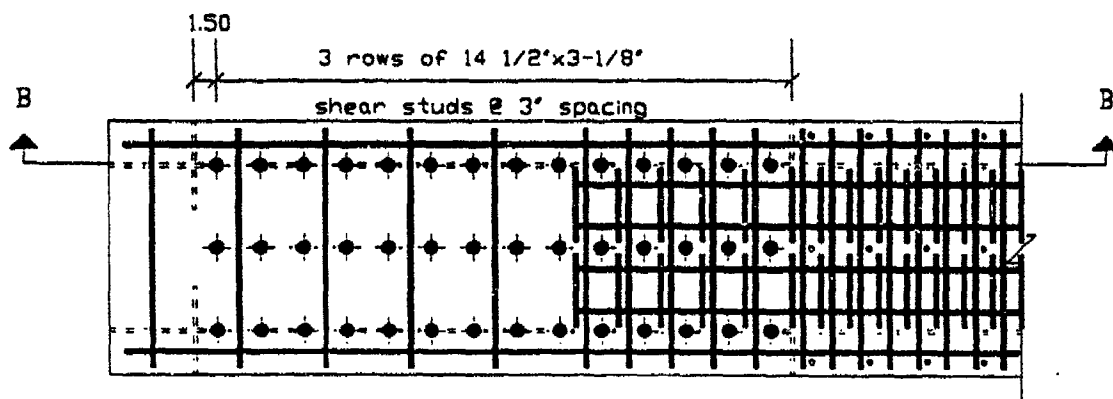
a. 16 Foot Beam

Figure 43. Fabrication Details for Prototype Beams. (Continued)



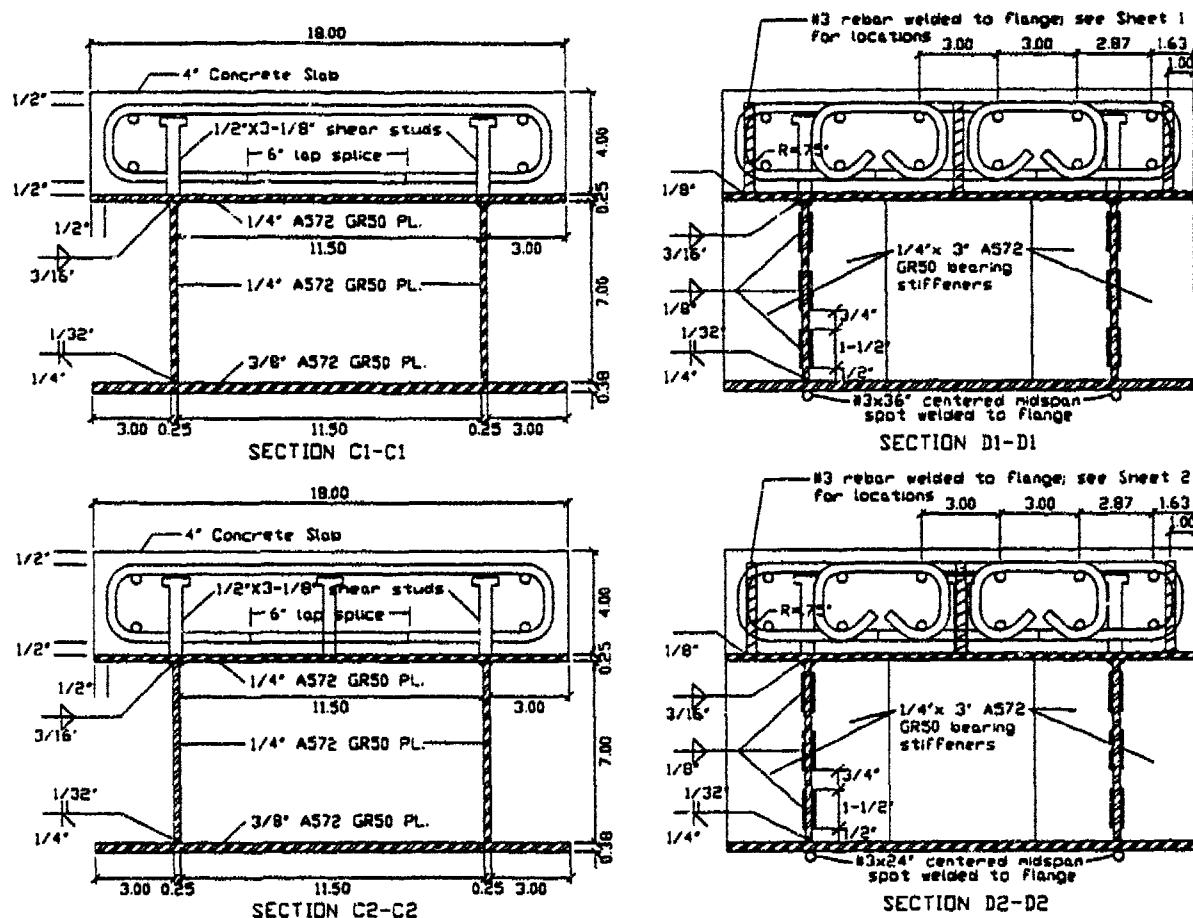


NOTE: Girder dimensions given in details on Sheet 3.



b. 10 Foot Beam.

Figure 43. Fabrication Details for Prototype Beams. (Continued)



- NOTES: 1) Use E70XX low-hydrogen electrodes.  
 2) Use A572 GR50 or equiv. strength for all flanges, webs, and stiffeners.  
 3) Shear connectors are 1/2"x3/8" Nelson Studs.  
 4) Use #3 GR60 rebar for longitudinal bars, stirrups and hoops; bends are 1-1/2" dia.  
 5) Concrete shall be 4000 psi compressive strength with maximum water-cement ratio of 0.44.

### c. Cross Sections.

Figure 43. Fabrication Details for Prototype Beam. (Concluded)

The associated design details, including the number and layout of shear connectors, size of bearing stiffeners, and size of welds were determined using standard design procedures contained in References 45, 50, and 71, and summarized in Section 3.C.3. Design of the reinforcing to provide confinement of the concrete slab was done according to the procedure described in Section 5. Closely spaced hoops and stirrups were placed in the constant moment section, as shown in Figures 43 and 44. Outside of this section the spacing of confining rebar was increased to conveniently fit with the shear connectors (3 to 3.5 inches) for a distance of about one-and-a-half beam depths, beyond which only nominal reinforcing was used. The shear connectors were placed only in the shear span between the load points and end supports. The short beam had a 3 x 14 (42 total) pattern while the longer beam had a 2 x 20 pattern (40 total).

Fabrication was achieved by two different fabricators. The method of construction was generally not constrained except by the specification of final product. Fabricating procedures were generally typical and essentially left up to the two fabricators. The steel plate girder section was fabricated first by a local steel fabricator. The web and flange plates were cut and welded to form the steel girder. Nelson studs were then welded to the top flange in accordance with the design specifications. The steel fabricator also cut and bent the reinforcing steel that would be placed in the concrete slab.

After the steel girder sections were complete, they were moved to the second contractor shop building where the strain gages were applied and concrete slab placed. The strain gaging used standard procedures for preparation of the metal surfaces and gage bonding. Strain gages were applied to flat milled surfaces on the rebars. Protective layers were then applied to waterproof the gages and resist abrasion during subsequent concrete work. Strain gaging the top surface of the concrete was done after approximately 21 days of cure. The concrete surface at each gage location was first prepared by applying a layer of epoxy cement which was then finished to a smooth, hard surface.



Figure 44. Prototype Beams During Assembly of Reinforcing Cages and Concrete Placement. (Continued)



Figure 44.     Prototype Beams During Assembly of Reinforcing  
                 Cages and Concrete Placement. (Concluded)

After the strain gages had been applied, the steel reinforcing cages were assembled and tied. As the cages were constructed, the strain gaged pieces were placed at the appropriate locations for each beam design. After the cages were tied and placed among the studs, the alignment and placement was inspected for conformance with the specifications. The beams were carefully leveled and the sides of the slab portions were formed with wood forms. The ready-mix concrete with mix properties given in Table 15 was placed and consolidated using a vibrator, then trowel finished. Standard cylinders (6 inch diameter x 12 inch tall) were made for testing at 7, 14, 21, and 28 days. The slabs and cylinders were covered with plastic and moist-cured for a period of 28 days at the fabricator shop. The photograph in Figure 44 shows one of the 16 foot beams on the left and a 10-foot beam on the right as the reinforcing cages were being assembled. The shear studs are visible as rows of pegs with heads attached to the top surface of the steel girders. Figure 44 also shows the concrete being consolidated with a vibrator as it is placed in a 10-foot beam. Strain gage lead wires are visible coming out of the top surface of the slabs. In the background, the two 16-foot beams already have concrete in place.

TABLE 15. CONCRETE MIX PROPORTIONS

Portland Cement (lb)	828
Flyash (lb)	255
Sand (lb)	2492
Gravel (lb)	3812
Air (oz)	3
Water Reducer (oz)	32
Water (gal)	35

### 3. Instrumentation of Test Beams

Instrumentation consisted of strain gages attached to the test beams, displacement gages mounted at points under the beam, a displacement gage to measure ram travel and a load cell under the hydraulic loading ram. Uniaxial strain gages were placed at seven levels throughout the depth of the beam (Figure 45). Specifically, gages were placed (1) on the top of the concrete slab, (2) on a longitudinal bar in the concrete approximately 1.25 inches from the top surface, (3) on a hoop bar at mid height in the slab, (4) on the top surface of the girder flange, (5) & (6) on the side of the web plate 1.5 inches below the top and above the bottom flanges, and (7) on the bottom surface of the girder flange, as shown in detail in Figure 46.

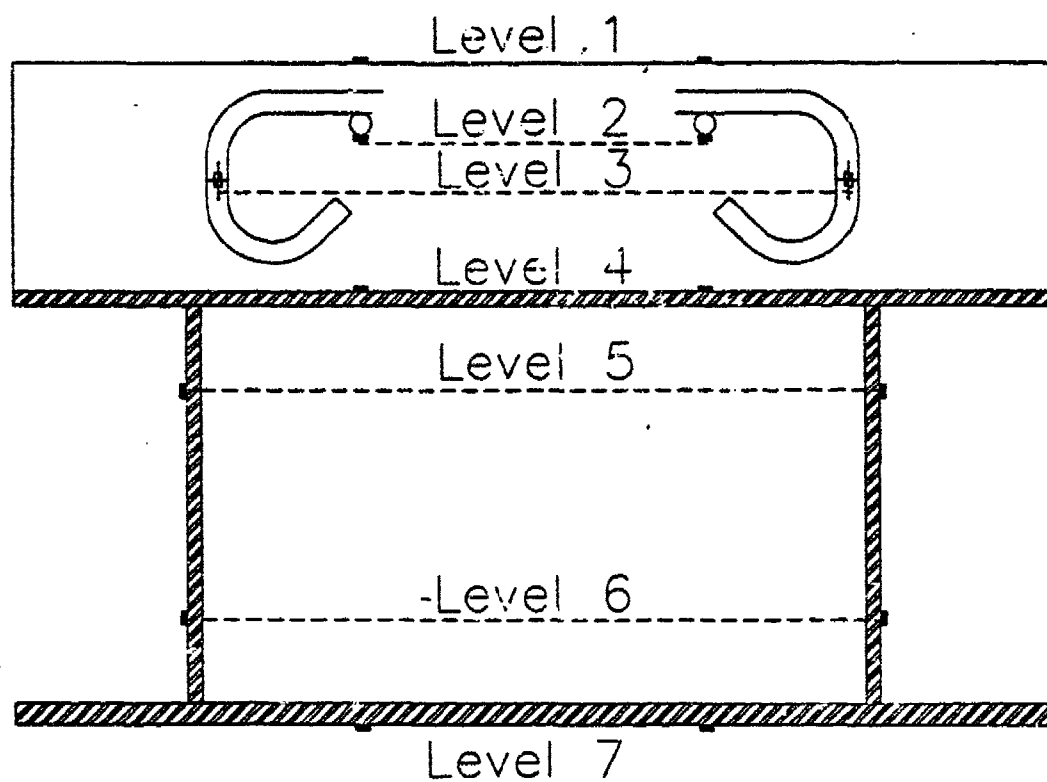


Figure 45. Sketch of Nomenclature for Strain Gage Levels.

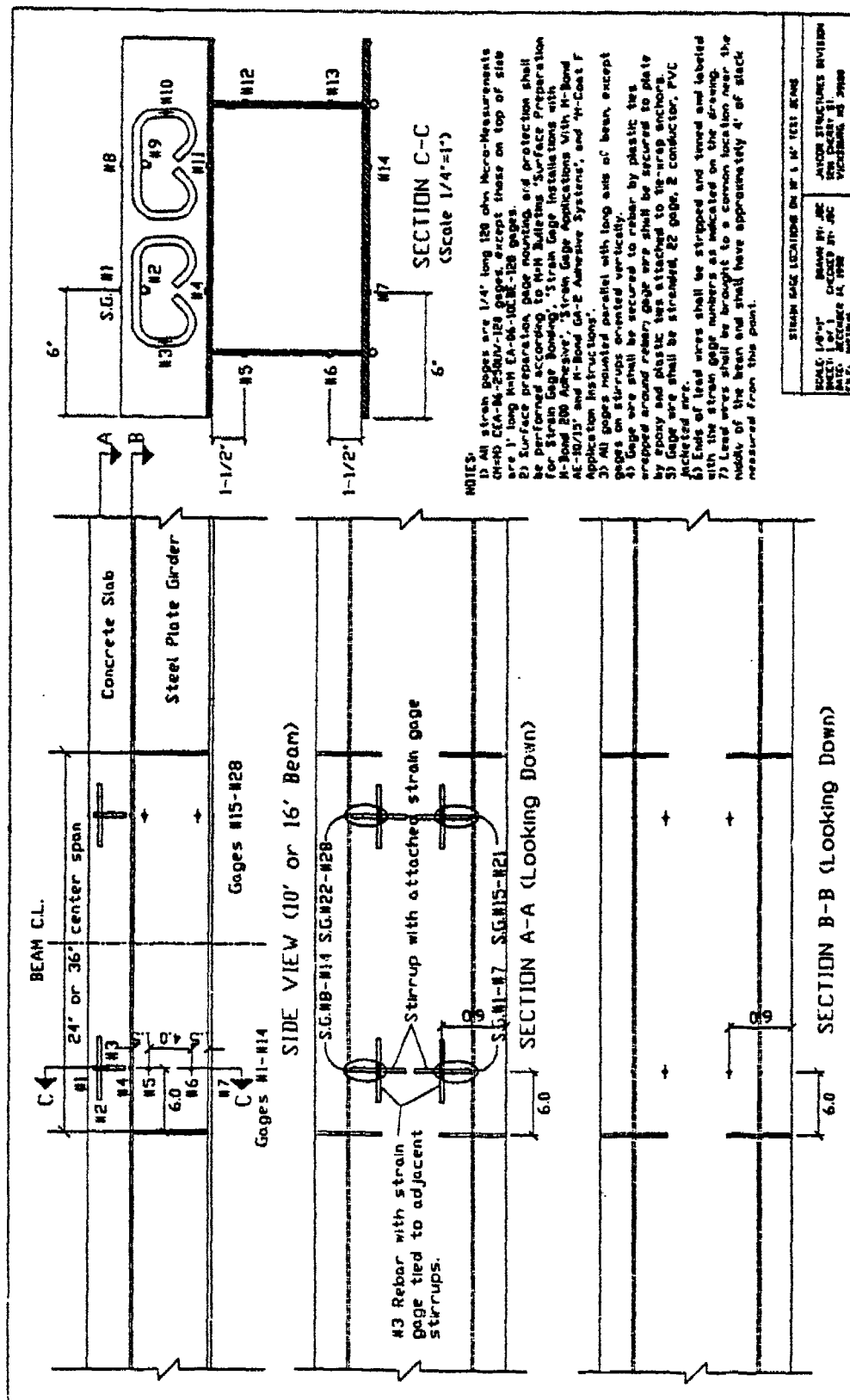


Figure 46. Details of Strain Gage Instrumentation of Prototype Beams.

Gages 1, 2, and 4 through 7 were oriented parallel with the long axis of the beam while gage 5 was oriented vertically on the hoop bar. For replication and backup purposes, gages were placed doubly symmetric about the beam length and width centerlines. Thus, a total of 28 strain gages were attached to each beam. This duplication permitted accounting for imperfections or nonsymmetry of the beam or loading and also served as a backup in case of gage failures during fabrication or testing. Due to the irregular finish resulting from bringing the gage wires out the top of the slab, the location of the strain gages on the slab surface were adjusted as shown in Figure.47.

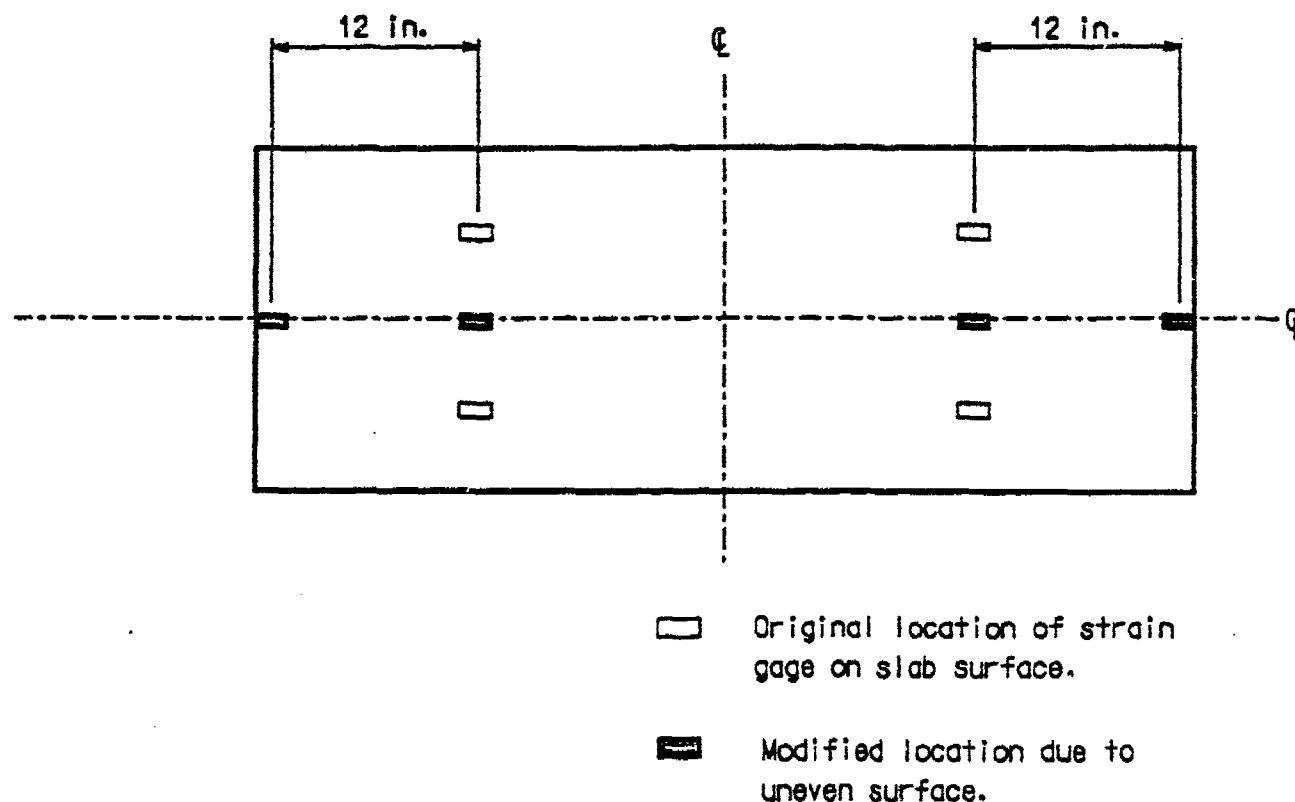


Figure 47. Modified Level 1 (Top of Slab) Strain Gage Locations.

Prior to testing, deflection gages were placed at five locations along the length of each beam. These locations, shown in Figure 48, include the beam centerline, load points, and midway between the load points and reactions. At midspan, two gages were used to measure any twist of the beam. The redundancy and symmetry of the deflection gage placement accounted for nonsymmetric loading or response.



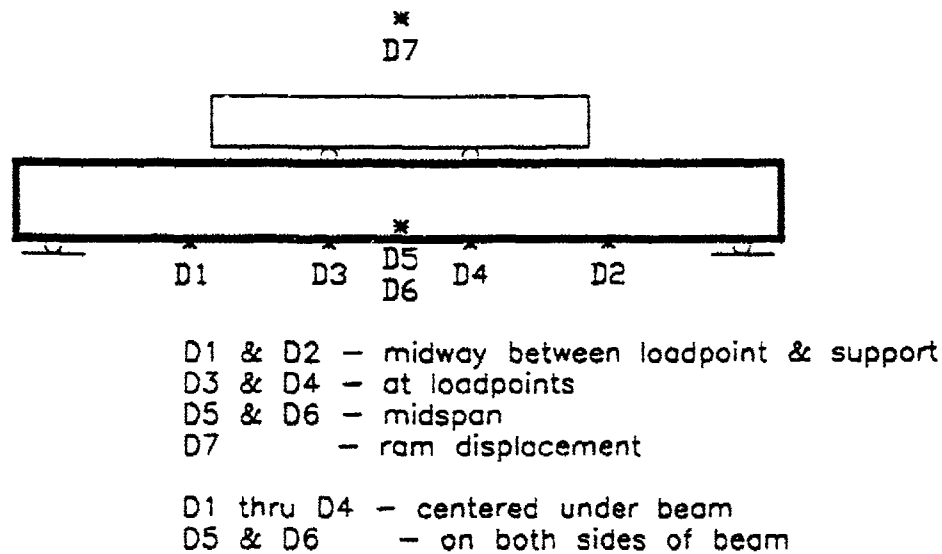


Figure 48. Locations of Displacement Monitoring Gages.

The deflection gages were placed as previously described and linked to the data acquisition system. The strain gage wires were similarly linked to this interface. The entire system was checked for continuity, including the interface with the load cell and ram displacement gage. The output from the load cell and midspan deflection gages were connected to an analog plotter to provide a real-time plot of the load-deflection response. Video and still photography were used for additional test documentation. The video camera faced one side of the beam and included digital output of the load cell and ram displacement prominently in view.

## C. DISCUSSION OF RESULTS

### 1. Description of Tests

During the period of concrete curing, concrete cylinders were broken after 7, 14, 21, and 28 days. On each of these days, three cylinders were selected at random from those available and tested to compressive failure at the WES CTD laboratory. The results of these three tests were averaged to estimate the progress of strength gain of the concrete. The results of these tests are presented in Table 16 and Figure 49. As seen in this figure, the concrete steadily gained strength and reached the prescribed strength in 28 days. These results indicated that the tests could proceed at anytime after the minimum imposed 28 days. In addition, cylinders were broken on each beam test day to determine the appropriate concrete strength for comparison with the design value in hindcast analysis of the test results.

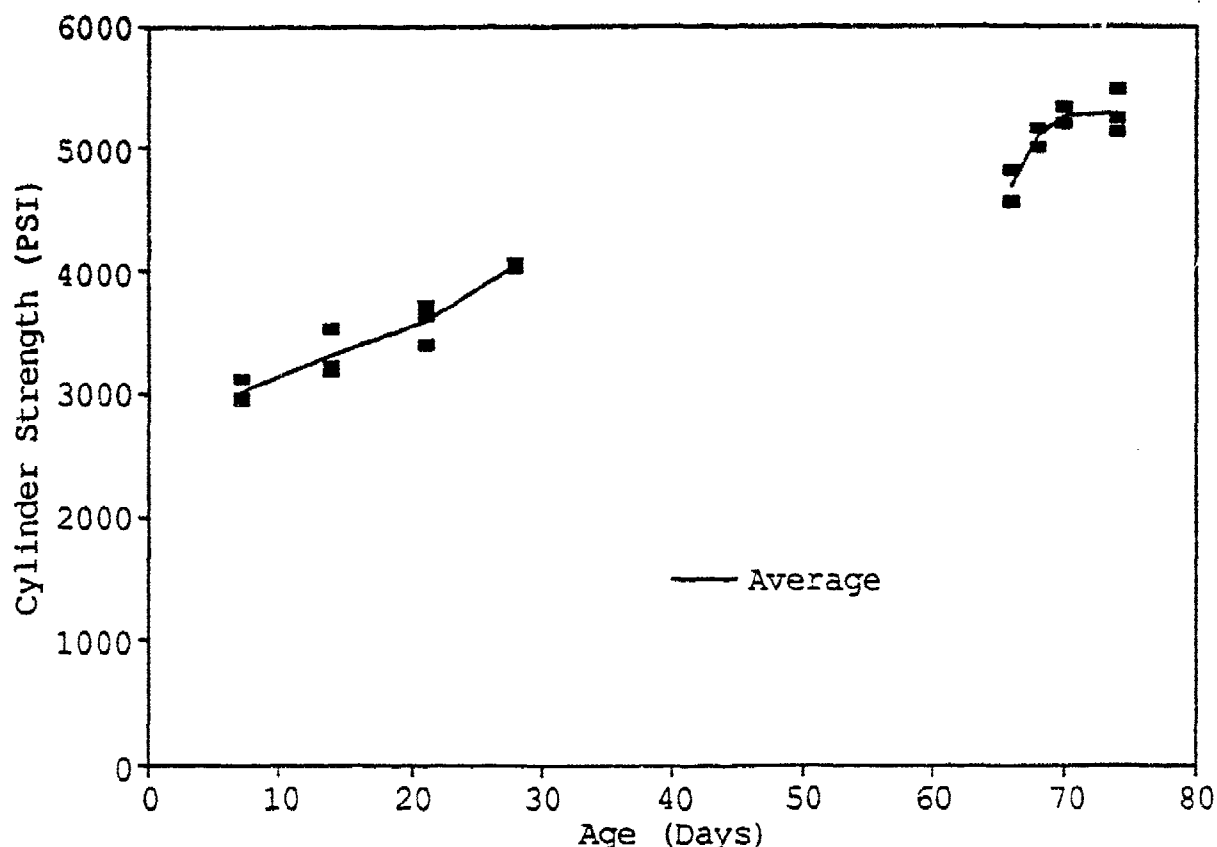


Figure 49. Concrete Cylinder Strength On Each Day Of Testing.

TABLE 16. SUMMARY OF CONCRETE CYLINDER STRENGTHS

AGE (DAYS)	CYLINDER (PSI)	CYLINDER (PSI)	CYLINDER (PSI)	AVERAGE (PSI)	
7	2950	2970	3130	3016	
14	3540	3180	3240	3320	
21	3400	3640	3730	3590	
28	4030	4070	4050	4050	
66	4560	4830	na	4695	Beam 16A
68	5020	5160	na	5090	Beam 10B
70	5200	5340	na	5270	Beam 10A
74	5480	5130	5250	5290	Beam 16B

The four beams and remaining cylinders were transported to the laboratory after the concrete had cured about 21 days. Delays in installation of the new test system at the WES laboratory delayed the first beam test to day 66 after the concrete was placed. The first beam tested, Beam 16A, was set up and inspected two days prior to the test. The general arrangement of the test setup is depicted in the pictures in Figure 5C of Beam 10A. The force from the ram was distributed through the spreader beam to the slab surface by 1.5-inch-diameter steel bars and bearing plates (Figure 50 top shows the ram in the top middle of the photo in contact with the spreader beam; the spreader beam in turn is resting on the two round bars in contact with the top surface of the test beam slab). The beam ends reacted through similar rollers to beams resting on the floor, as shown in Figure 50 bottom. Spacer plates were inserted as required to provide additional clearance between the spreader beam and the test article, and between the beam and the floor.

The maximum ram travel of under six inches was less than the anticipated beam deflection. Therefore, an unloading/reloading cycle was also included in the loading program to permit placement of spacers between the ram and the spreader beam. After the spacers were in place, the beam was reloaded for continued testing.

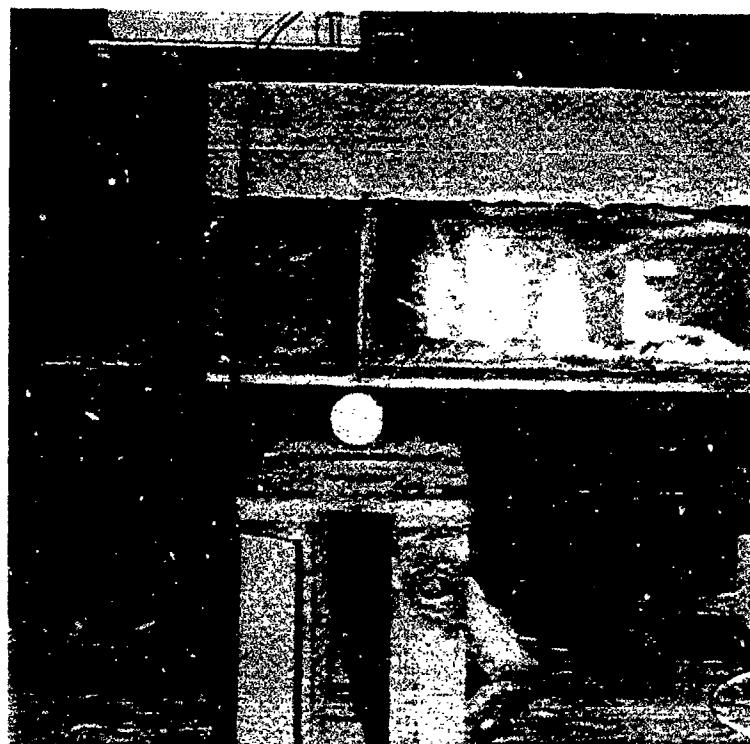
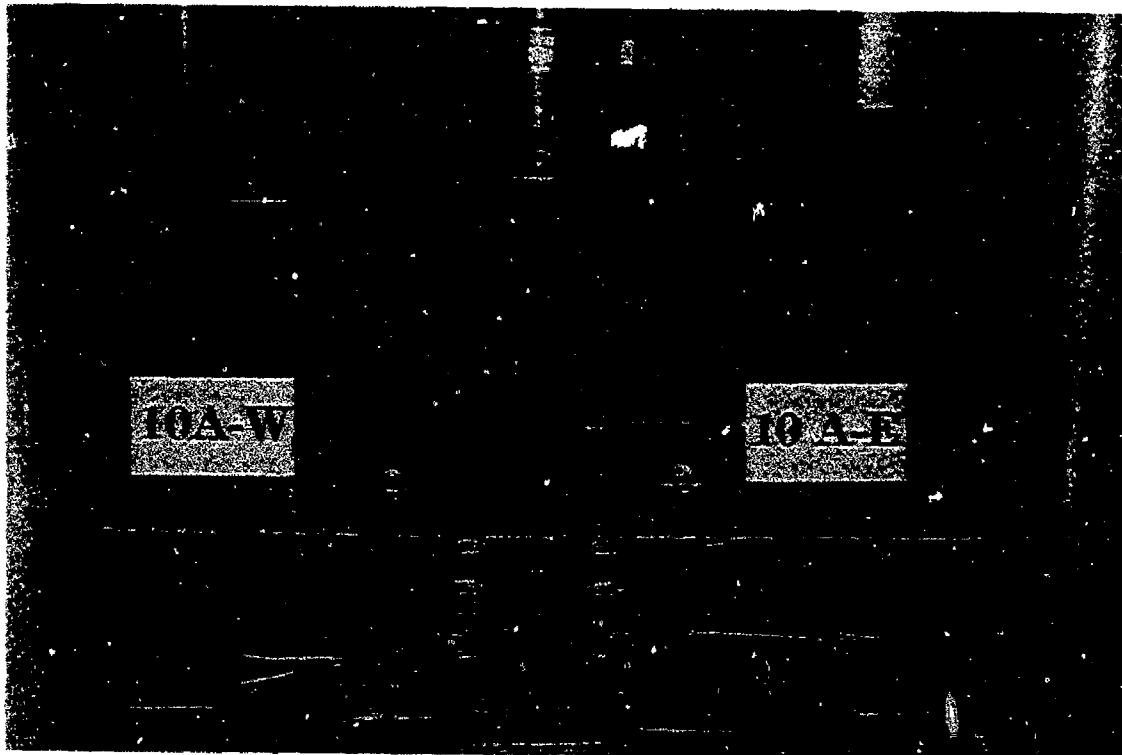


Figure 50. Pretest Photograph of Beam 10A Showing Spreader Beam, Load Points and Roller Supports.

Beam 16A was tested first. Subsequent tests of beams 10B, 10A, 16B were conducted on two-day intervals to allow beam removal and setup and quick-look analyses of the previous test results. Lessons learned from each test were used to improve the testing procedure for subsequent tests. For example, the gimbaled end support used to allow some rotational freedom about the longitudinal axis was severely deformed after the test on Beam 10B (Figure 51). This support was replaced in subsequent tests with a roller and plate. The first two tests (16A and 10B) were terminated when the beam bottom flange reached the concrete blocks that were used to protect the displacement gages underneath the beam (Figure 52). The second two tests (10A and 16B) were temporarily stopped at this point and the blocks and displacement gages were removed. The test was resumed and continued until the beam reached the floor or the ends of the spreader beam contacted the test article.

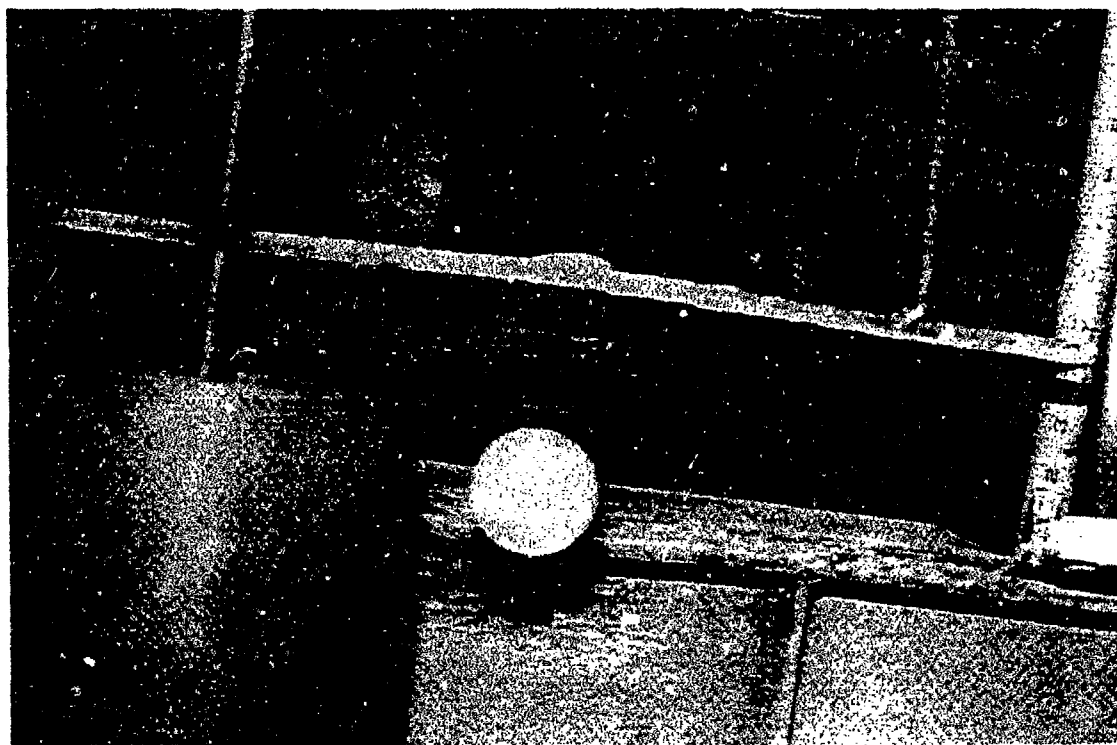


Figure 51. Gimbaled Support Condition After Test Showing Yielded Roller and Bottom Flange.



Figure 52. Beam 16A at Conclusion of Test Showing Spalled Concrete Layer and Permanent Deformation.

## 2. Overall Performance

The results of the four prototype beam tests were encouraging from a number of standpoints. Firstly, and most importantly, the overall performance of the test specimens met expectations as to strength, stiffness, and ductility. Secondly, the test procedures and execution proved to be excellent for the intended purpose. Very few problems were evidenced during the tests and each was of a generally minor nature. Testing proceeded essentially as planned and data acquisition appeared to be very consistent. An overall appreciation of the test results can be gained from a study of the measured load-deflection relationships.

a. Beam 10A

The load-deflection results for test beam 10A are shown in Figure 53. From the initiation of loading up to a load of about 170 kips the beam responded quite linearly. At this load gradual softening occurred due to initiation of yield of the steel girder. Between this point and just over 200 kips, the slight softening continued until the concrete above the confining steel spalled off, relieving some of the load and causing the "peak" in the response. In the plastic region the response reflects progressive yielding of the confined concrete and of yielding in the steel girder. The load rises only gradually in this region due to strain-hardening of the girder steel as the beam curvature and strains increase. At a deflection of about 3.5 inches, the beam was unloaded to permit addition of spacers to continue the test. The unloading/reloading segments are relatively linear and the generally plastic response continued when the load and deflection returned to the unloading point. The test was paused at about 5.5 inches of deflection (not unloaded/reloaded as before) while the deflection gages beneath the beam were removed to allow continued deflection (indicated on the curve by a downward spike). Since the deflection gages were removed, the last portion of the load-deflection curve was obtained by extrapolating the ram travel data. The test continued until the space between the spreader beam and the test article was exhausted (displacement  $\approx$  6 inches). This last segment indicated a slight increase in load followed by an equal decrease in the load over the final 0.5 in of deflection.

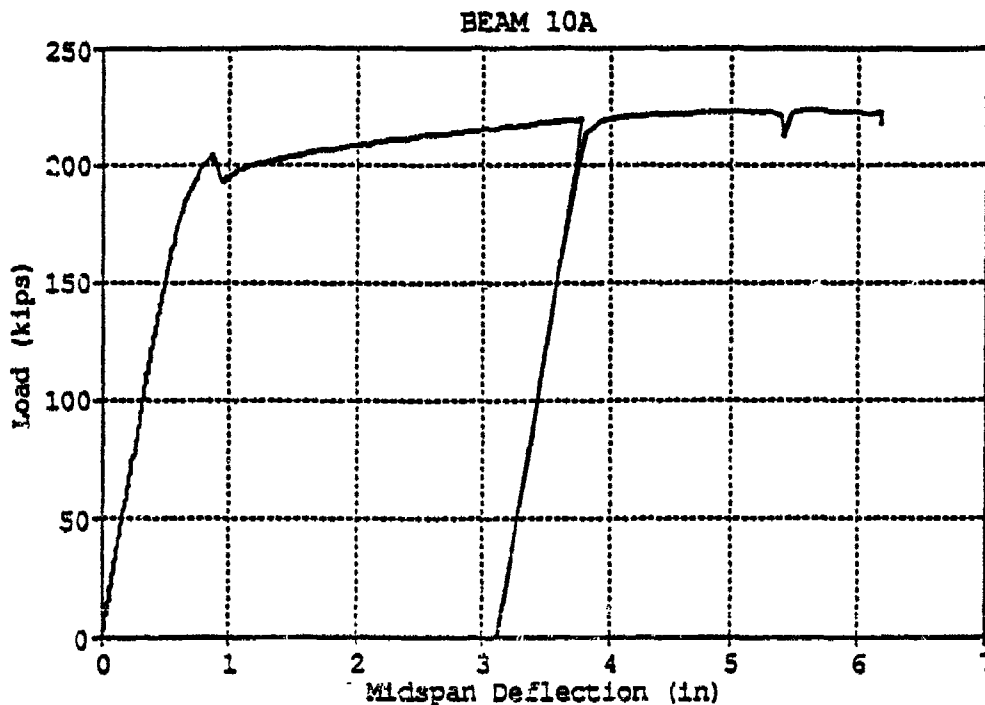


Figure 53. Load-Deflection Plots for Beam 10A.

b. Beam 10B

The response of Beam 10B, shown in Figure 54, was very similar to Beam 10A. The linear and initial softening regions are essentially the same as for 10A. The straight portion of the response between about 1 inch and 2 inches deflection reflects a problem that occurred with the hydraulic system at this critical stage of the test. Just before the top layer of concrete began to crush, the hydraulic system *appeared* to have reached maximum capacity and the load became constant. Meanwhile, the controller program continued to run, accumulating approximately 1 inch of discrepancy between the actual and rate controlled deflections. After a check of the hydraulic system by the WES and MTS technicians, the problem was found to be a closed valve for developing higher pressure at the pump. The valve was opened very slowly, but unfortunately the accumulated error caused a significant jump in the applied load and deflection. This problem did not occur in the first test, Beam 16A, due to the lower load capacity of the longer beam. Loading continued normally after this point up to unloading and reloading at about 3.5 inches to accommodate ram extension. The test was terminated at about 5 inches of displacement due the lack of space between the concrete blocks on the floor and the beam.

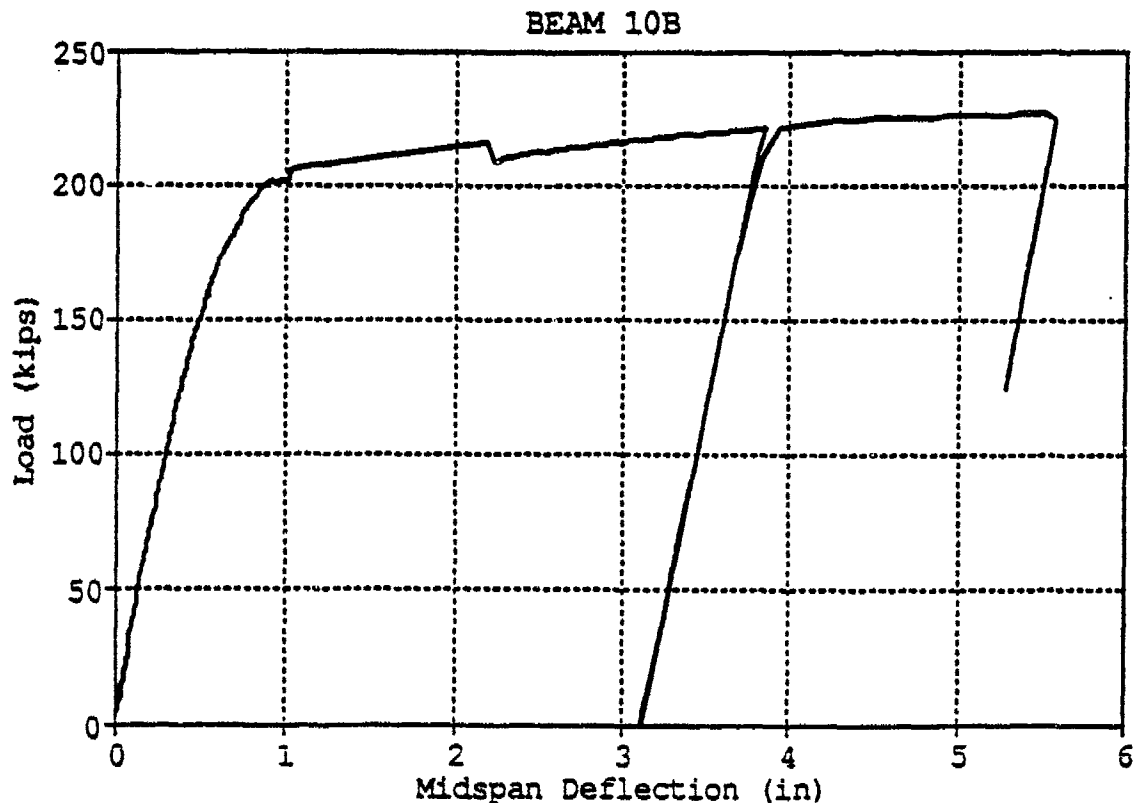


Figure 54. Load-Deflection Plots for Beam 10B.



c. Beam 16A

The test results for beam 16A, shown in Figure 55, indicate the same general regions of response, i.e., linear, softening/crushing, plastic, and unloading/reloading, as previously described. Naturally, for the longer beams, the loads are less and the deflections greater than the shorter 10-foot beams. The crushing of the concrete above the confining steel occurred more abruptly in this test than in the others and occurred in two distinct stages between about 2 to 3 inches of deflection. After the unload/reload cycle, loading continued to about 7.5 inches, where the test was terminated due to lack of rattle space between the beam and the floor.

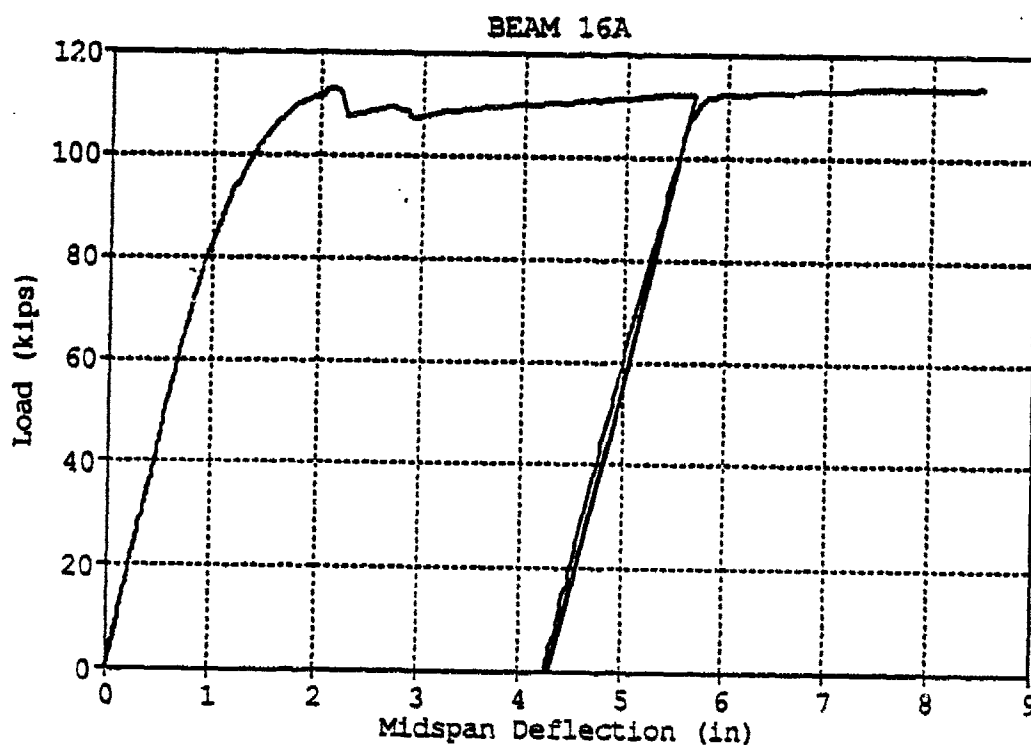


Figure 55. Load Deflection Plots for Beams 16A.

d. Beam 16B

The results of the final beam test (16B) are shown in Figure 56. Compared to the previous tests, this test produced probably the most reliable and useful data. The crushing/softening behavior was less pronounced in this test, probably due to somewhat less concrete failing outside the confined region. This test was set up with more space between the beam and floor to permit testing further into the plastic range. As a result, the beam was unloaded twice, as shown, to permit addition of spacers at the ram. Reloading consistently returned to the original response at unloading and continued plastically. The test was terminated at about 12 inches of deflection due to interference between the beam and the concrete floor. Even at this large deflection, the beam was continuing to accept load. Figure 57 shows the beam after the termination of the test with approximately 11 inches of permanent deflection at midspan.

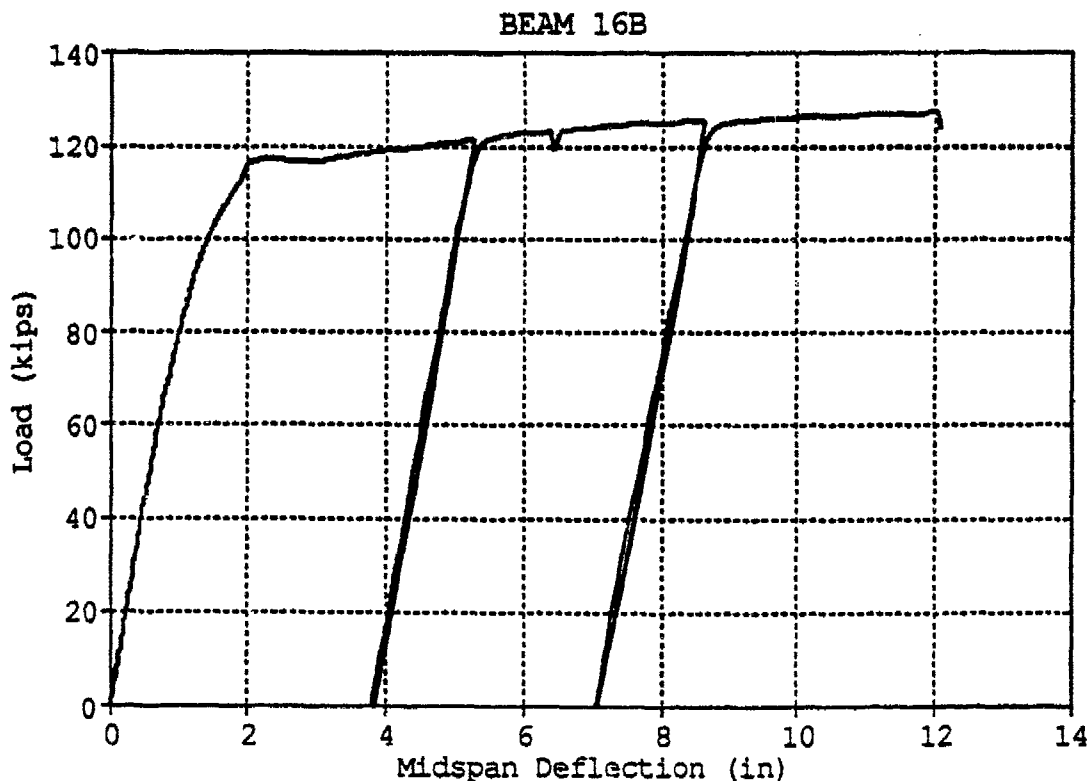


Figure 56. Load Deflection Plots for Beams 16B.

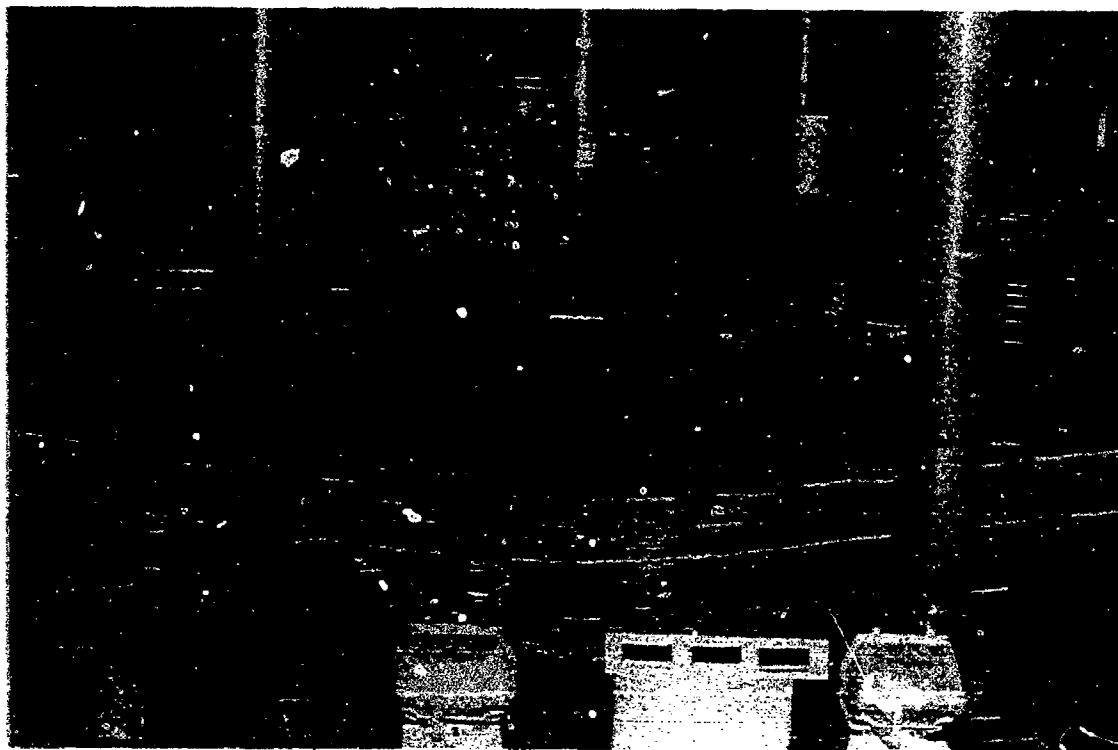


Figure 57. Beam 16B At Conclusion of Test with 11 Inches of Permanent Deflection.

### 3. Response Comparisons

All four of the test specimens exhibited considerable ductility, far beyond what might be expected for beams without significant confining steel in the concrete. Table 17 summarizes the measured maximum midspan deflections, computed ductilities, and support rotations for each test. It is important to note that none of the tests were stopped due to imminent or actual failure, but rather due to the loss of rattle space between the beam and the floor or spreader beam. One cannot say from these results how much more ductility could have been achieved from these beams, only that the measured ductility was considerable at test termination.

**TABLE 17. MEASURED DUCTILITY AND SUPPORT ROTATIONS  
FOR PROTOTYPE BEAMS**

Beam	$\delta_y$ Elastic Deflection (inches)	$\delta_u$ Maximum Deflection (inches)	$\mu$ Ductility $\delta_u/\delta_y$	$\phi$ Support Rotation (degrees)
10A	0.42	6.2	14.8	6.5
10B	0.42	5.5	13.0	5.8
16A	1.1	8.5	7.7	5.4
16B	1.1	12.0	10.9	7.6

The goals of the test program were to provide (1) a proof-of-concept for the confined concrete-steel composite beam and (2) provide a baseline to measure the accuracy and appropriateness of the analytical models and methods of this work. As shown, the test results indicate that the first goal was adequately met. The second goal was assessed by comparing the test results with analytical predictions. The comparison of results for the two 10-foot and two 16-foot test beams with analytical predictions are discussed next.

a. Beams 10A and 10B

The overall response for the 10-foot beams are compared with the analytical predictions in Figure 58. This figure plots the load deflection results for both tests with the predictions from ADINA and the simplified design procedure. The ADINA posttest analysis and simplified procedure results were based on the concrete and steel material properties as measured from concrete cylinders and steel coupons. As seen in the figure, the ADINA results compare extremely well with the test results. ADINA does not predict the peak just before the concrete crushes, rather the smeared concrete model used in the analysis predicts a smoother transition from the linear to relatively plastic response regions. Also, there was no attempt to reproduce the unloading/reloading cycle required by the test procedure in the ADINA analysis. The comparison clearly shows the capability of the finite element analysis to very reasonably predict the overall response of the beams. The simplified procedure predicted reasonable, though

slightly conservative, values for the stiffness and ultimate resistance of the beams. The simplified prediction is shown for a design ductility of 6, and clearly indicates the much higher ductility achieved by the test articles. These comparisons provide a large measure of confidence in both prediction methods. The maximum ductility factor utilized in the simplified procedure could easily be increased.

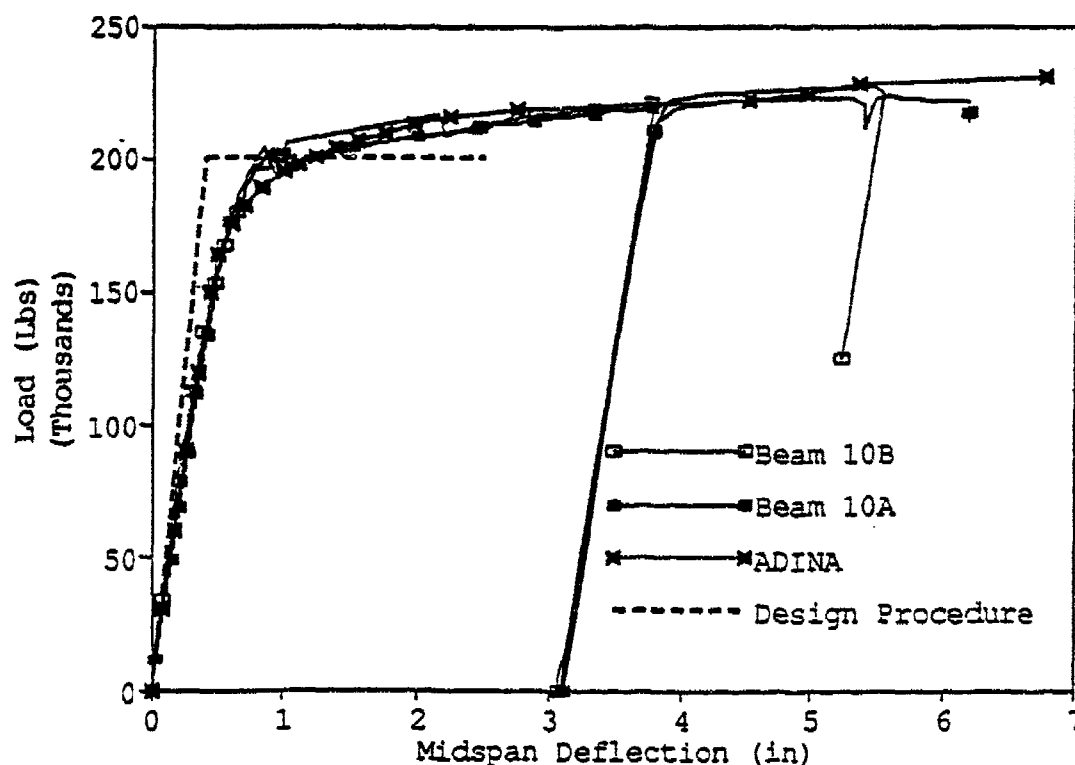


Figure 58. Load-Deflection Curves for 10-Foot Prototype Beams with Design Procedure and ADINA Predictions.

b. Beams 16A and 16B

A similar comparison of test results and analytical predictions for the 16-foot beams is shown in Figure 59. This comparison also indicates the excellent capabilities of the analytical methods to predict the overall response. In fact, the most striking difference in results is the difference in ultimate resistance of the two test articles, i.e., the ultimate resistance for test Beam 16B was approximately 10-12 percent higher than beam 16A. From posttest observations of the test articles, it appeared that Beam 16B had a slightly larger area of confined concrete than

Beam 16A. This conclusion was based on the different behavior and appearance of the scabbed-off layer of concrete outside the reinforcing cage. Beams 10A, 10B, and 16A developed cracks in the outer layer near the load points that peeled-off intact pieces of concrete (Figure 60). In contrast, the exterior concrete from Beam 16B did not have any large, intact pieces (Figure 61). The resulting thinner shell of unconfined concrete also reduced the abrupt drop in peak load characteristic of the other beams. In spite of this variability between the results from the two 16 foot beams, the ADINA analysis did an excellent job of predicting the overall response. The simplified procedure also produced a very reasonable, slightly conservative static resistance function. As previously seen for the 10-foot prototype, the maximum ductility factor utilized in the design procedure was very conservative.

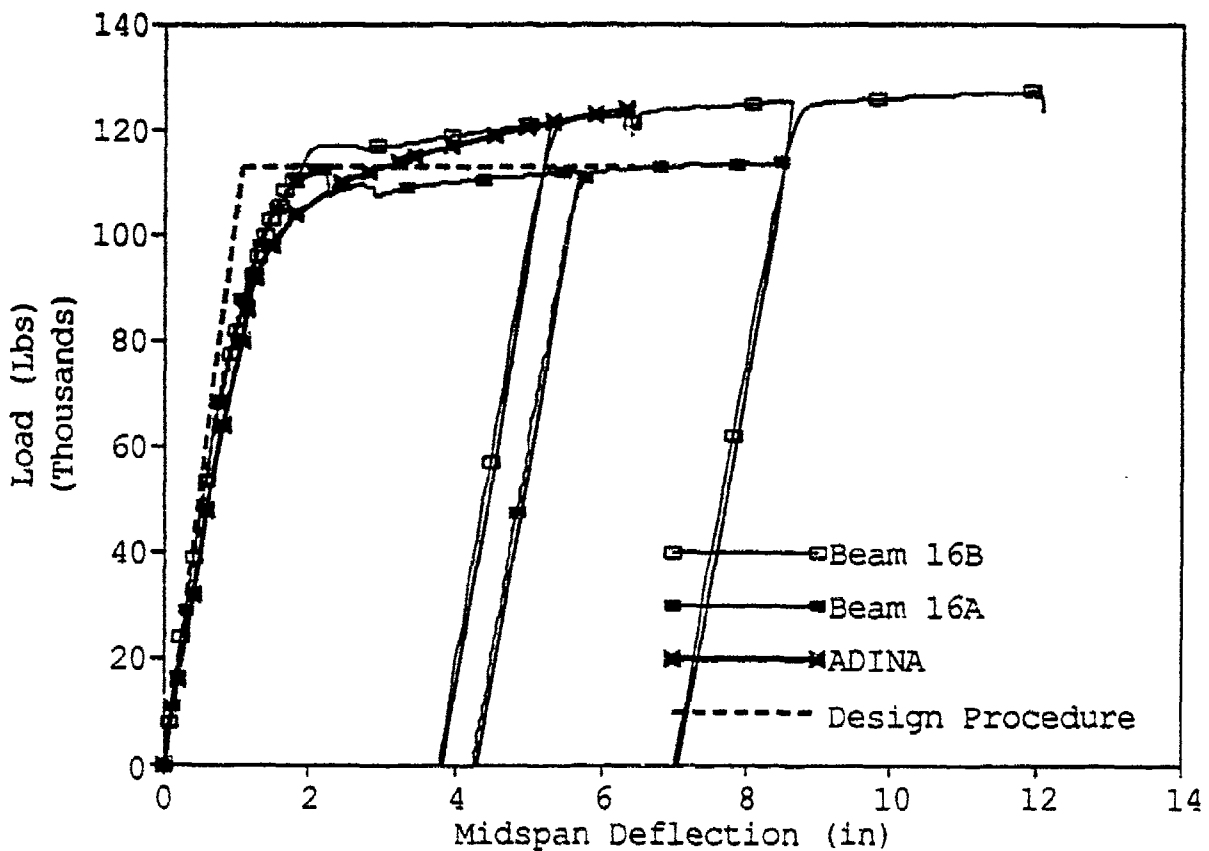


Figure 59. Load-Deflection Curves for 16-Foot Prototype Beams with Design Procedure and ADINA Predictions.

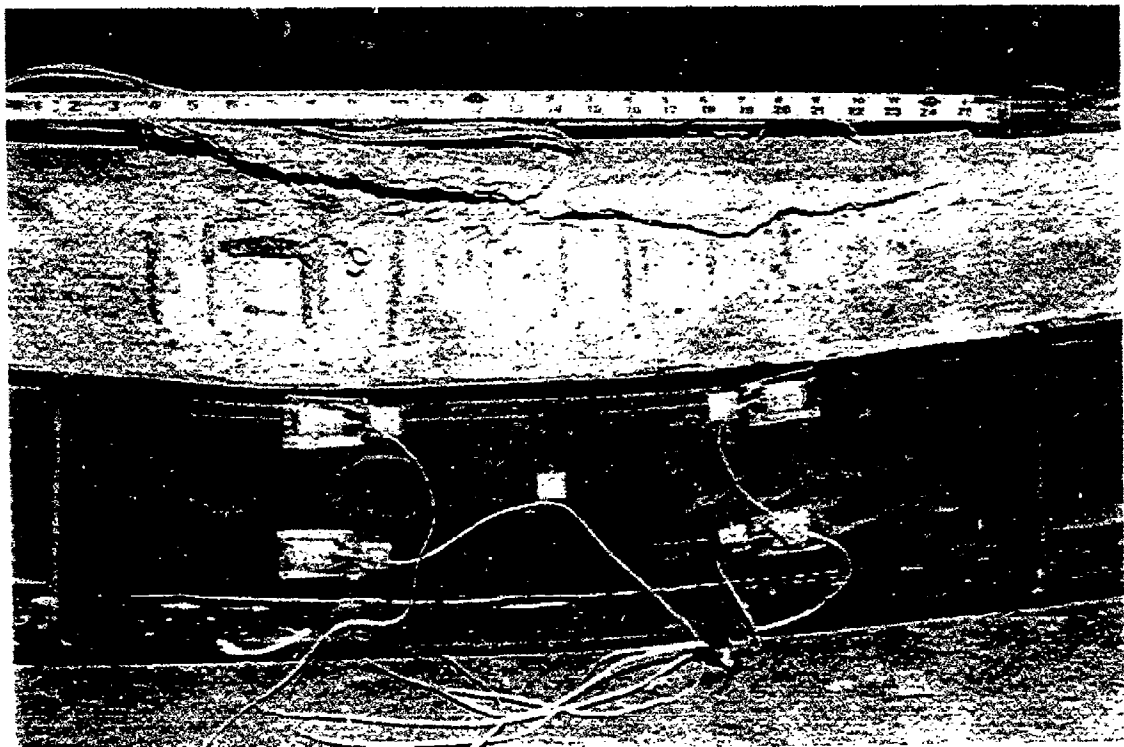
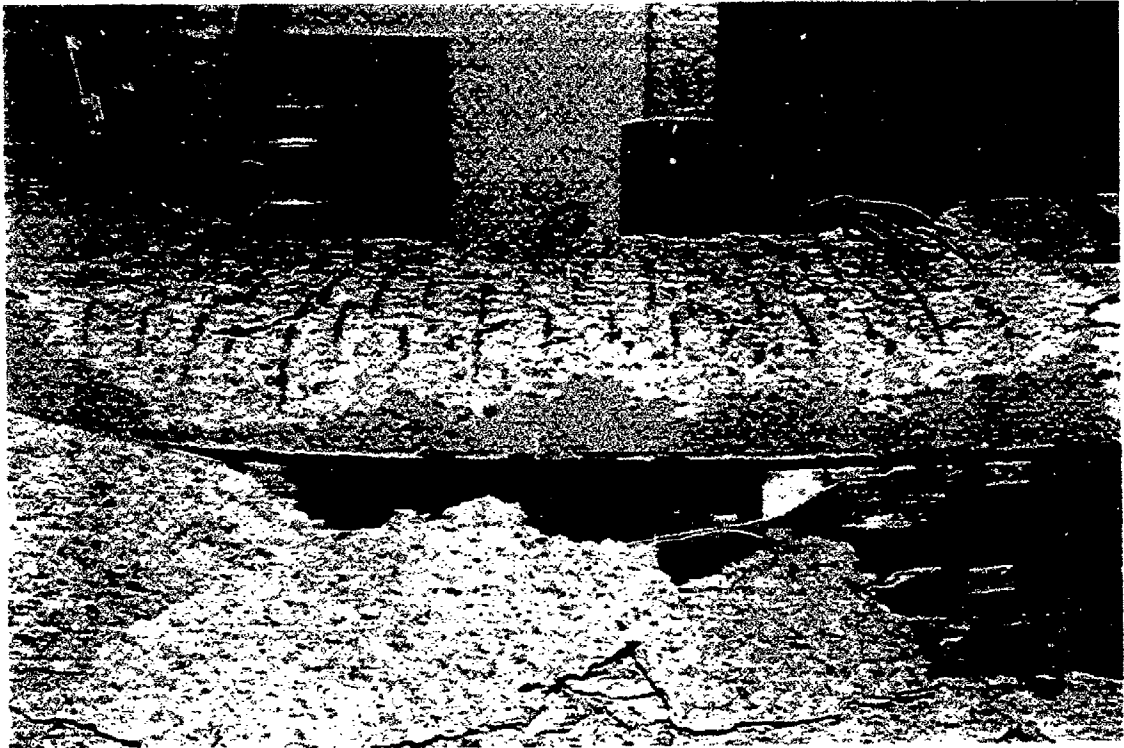


Figure 60. Confined Concrete Core with Layer of Spalled Concrete -  
Beams 16A and 10B.

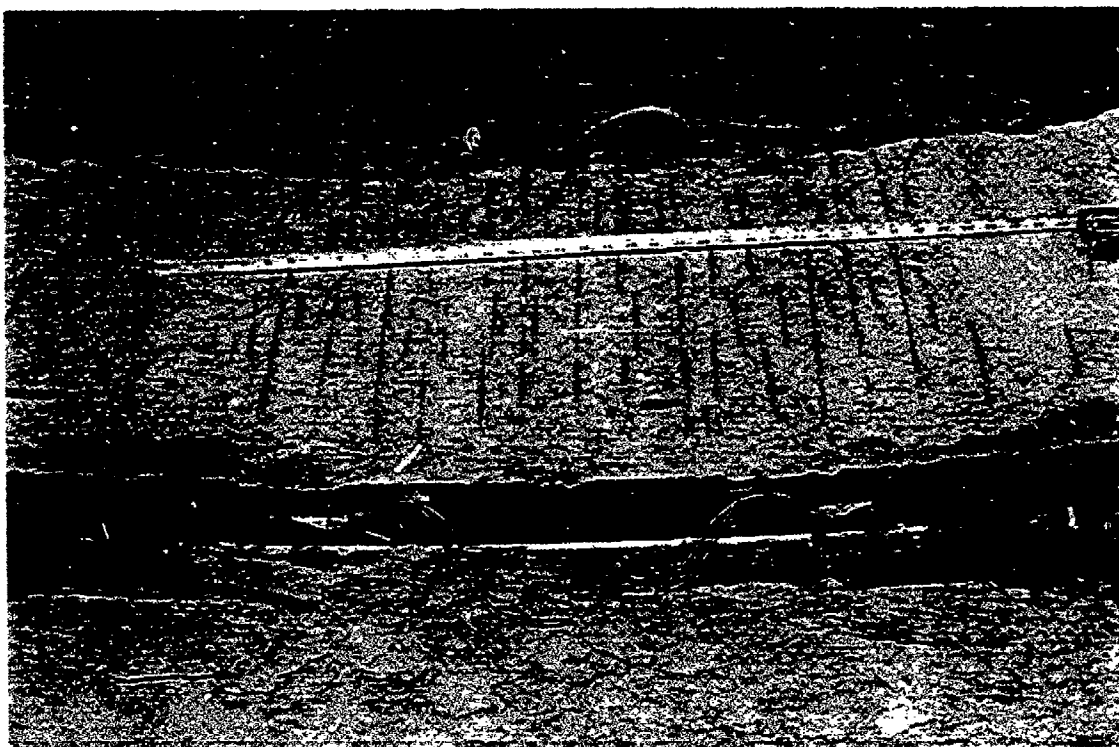


Figure 61. Confined Concrete Core with Thin Layer of Spalled Concrete - Beam 16B.

#### 4. Strain Gage Results

Data from the strain gages are contained in Appendix B and discussed briefly here. First, the gage numbering is reviewed, and units of measurement and sign convention are explained. Then, some observations regarding the strain measurements are presented. Finally, analysis of the strain gage data is presented in the form of moment-curvature relationships for the test beams as compared to the behavior predicted by ADINA.

The location and numbering of gages were described earlier in Section 6.B.3 and shown in Figure 46. The gages were configured and numbered in four groups of seven. Table 18 summarizes the gage locations and numbers. Gages were oriented to measure strains in the longitudinal direction, except Level 3, which measured the strain in hoop reinforcement in the vertical direction. Level 1 gages deviated from the pattern used for the other levels, as explained earlier. These gages were positioned on the longitudinal centerline of the beam 6 inches either side of the line of load application; gages 1 and 22 were outside the loads and gages 8 and 15 were inside the constant moment section, as shown previously in Figure 47.



TABLE 18. LOCATION AND NUMBERING OF STRAIN GAGES

Location	Level	Gage Numbers			
		1	8	15	22
Top of Concrete Slab	Level 1	1	8	15	22
Concrete, 1.25 inches from top	Level 2	2	9	16	23
Mid height of slab (vertical)	Level 3	3	10	17	24
Top surface of upper flange	Level 4	4	11	18	25
Web, 1.5 in. from top	Level 5	5	12	19	26
Web, 1.5 in. from bottom	Level 6	6	13	20	27
Bottom surface of lower flange	Level 7	7	14	21	28

On Beam 16B, the Level 1 gages were not used. Instead, these four channels were used for four additional strain gages on the steel girder web and bottom flange to improve the prediction of strain distribution. Gages 1 and 15 supplemented the gages on Levels 5 and 6, respectively. Gage 8 was located in the center of the web, and gage 22 was positioned on the top surface of the lower flange (Figure 62).

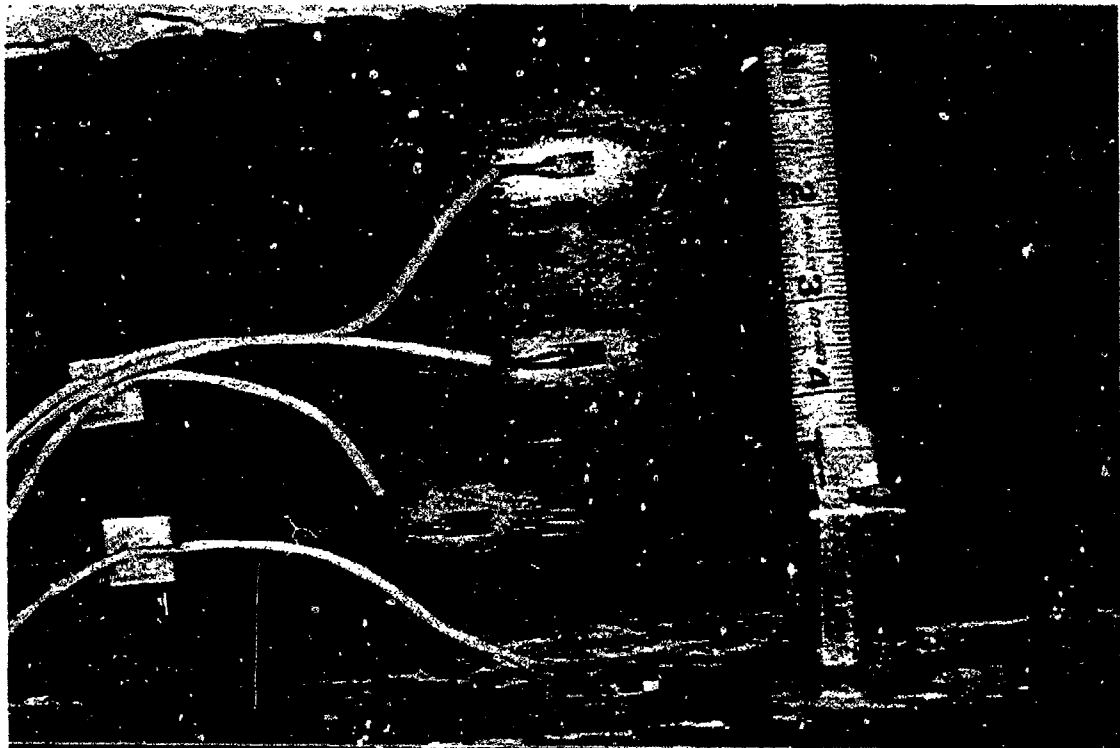


Figure 62. Location of Auxilliary Strain Gages on Beam 16B.

Tensile strains were negative values and conversely, compressive strains were positive. Units of measurement were micro strains, equal to  $10^{-6}$  in/in. For example, the yield point in tension for 50-ksi steel corresponds to approximately -1700 micro strains (-0.17%).

Generally, the strain gage results were in good agreement with the overall response of the beams. For example, at the peak load prior to crushing of the concrete, ultimate compressive strains at the concrete surface, measured by gages 8 and 15, were about 3000 micro strains (0.003). The beginning of nonlinear load-deflection behavior corresponds to onset of yield strains in the lower flange. Maximum longitudinal strains in the slab, measured by Level 2 gages, indicated concrete strains in excess of 10,000 micro strains (1%), which agrees with the confined concrete model prediction.

Unfortunately, the strain gages on the confining reinforcement (Level 3) performed poorly and evidenced a high gage failure rate. Although the reason for this failure is not known, it was observed that only two Level 3 gages performed as expected (Beam 10A, gages 24 and 10), indicating strains that approached or exceeded yield of the stirrups. The hoops containing these two gages were oriented such that the gages were towards the middle of the slab rather than towards the edge of the slab as were all the rest. One plausible explanation for the survival of these gages is that the lateral expansion of the concrete towards the edges of the slab squeezed the protective tape which was adhered to the gages and lead wires.

The strain gage data was useful in analyzing the moment-curvature behavior of the beams. Moment is the product of the load times the distance between load and support locations. Curvature is determined by the strain distribution in the cross-section, and is defined as the quotient of strain divided by distance from the neutral axis. The moment-curvature relationship is somewhat analogous to the stress-strain response of a material in that the external load (stress/moment) is plotted as a function of the internal deformation (strain/curvature). A brittle material/member has little or no postpeak response, whereas a ductile material/member evidences some form of plastic load resistance.

Curvatures were computed from the measured strains by fitting a straight line ( $y=ax+b$ ) to the data from Levels 2, 4, 5, 6, and 7. This line estimates a linear strain distribution in the beam. The coefficient "a" representing the line slope corresponds to the curvature. Strain values from the four gages on each level were typically averaged together to obtain a single value for the strain. Since many of the gages produced erratic data as the tests progressed, it was necessary to disregard some measurements. Figure 63 depicts a representative result for the strains in Beam 10A at 1/2-inch midspan deflection. The figure plots strain versus distance from the bottom of the beam. The average strain values appear as "x," and the line which best fits this data is plotted through the points. Where this line passes through zero strain marks the location of the neutral axis, in this case approximately 6.5 inches from the bottom surface of the beam.

The curvature is determined by dividing the strain in the lower flange, -2000 micro strains, by the distance to the neutral axis, giving a curvature of about 300 micro strains/inch.

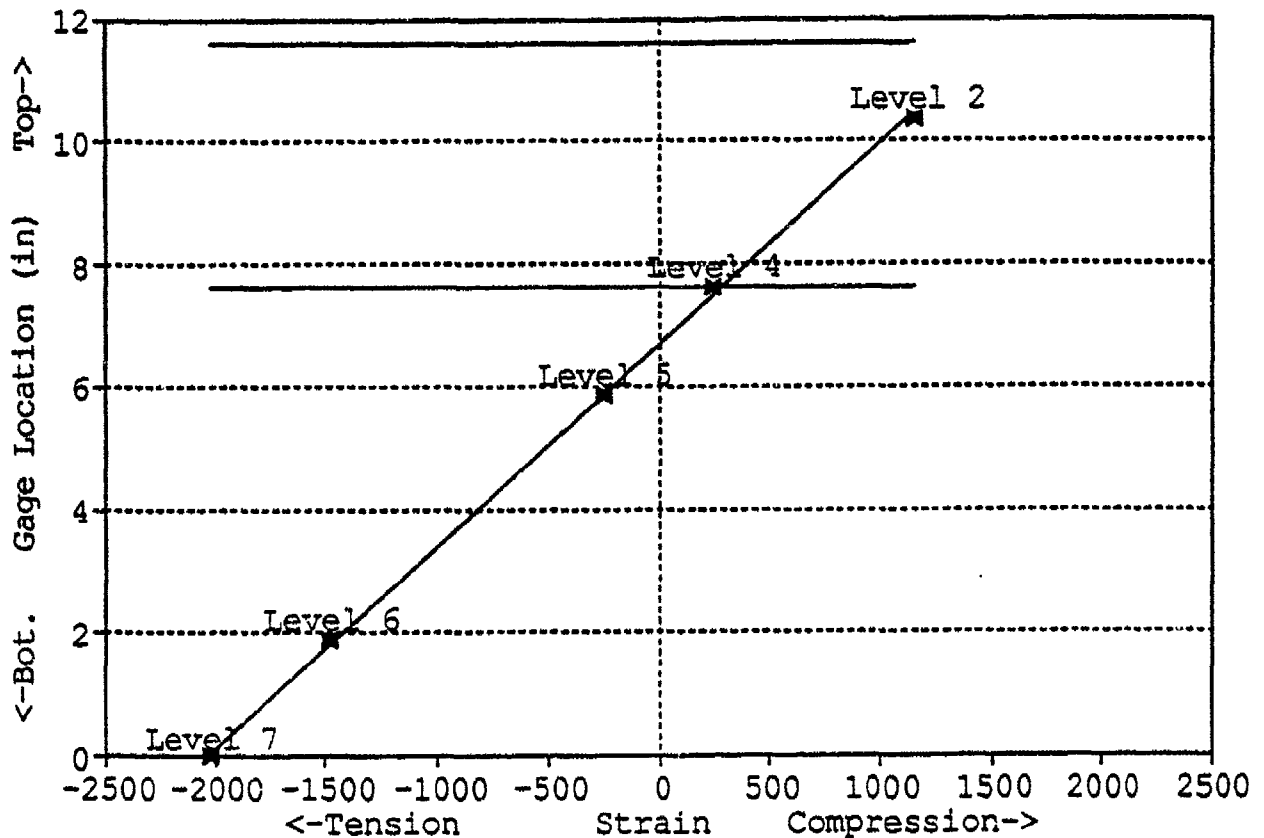


Figure 63. Measured Strain Distribution in Beam 10A at 1/2-Inch Midspan Deflection.

Repeating this strain/curvature analysis at frequent intervals of displacement leads to the moment-curvature plot for the beam response shown in Figure 64. A similar calculation from the ADINA strain results is shown as a continuous curve in the figure. The ADINA moment-curvature plot has a more gradual softening behavior, but is otherwise in very good agreement with the experimental results. Similar plots for the other test beams are shown in the continuation of Figure 64. In each case, the experimental and analytical results show excellent agreement.

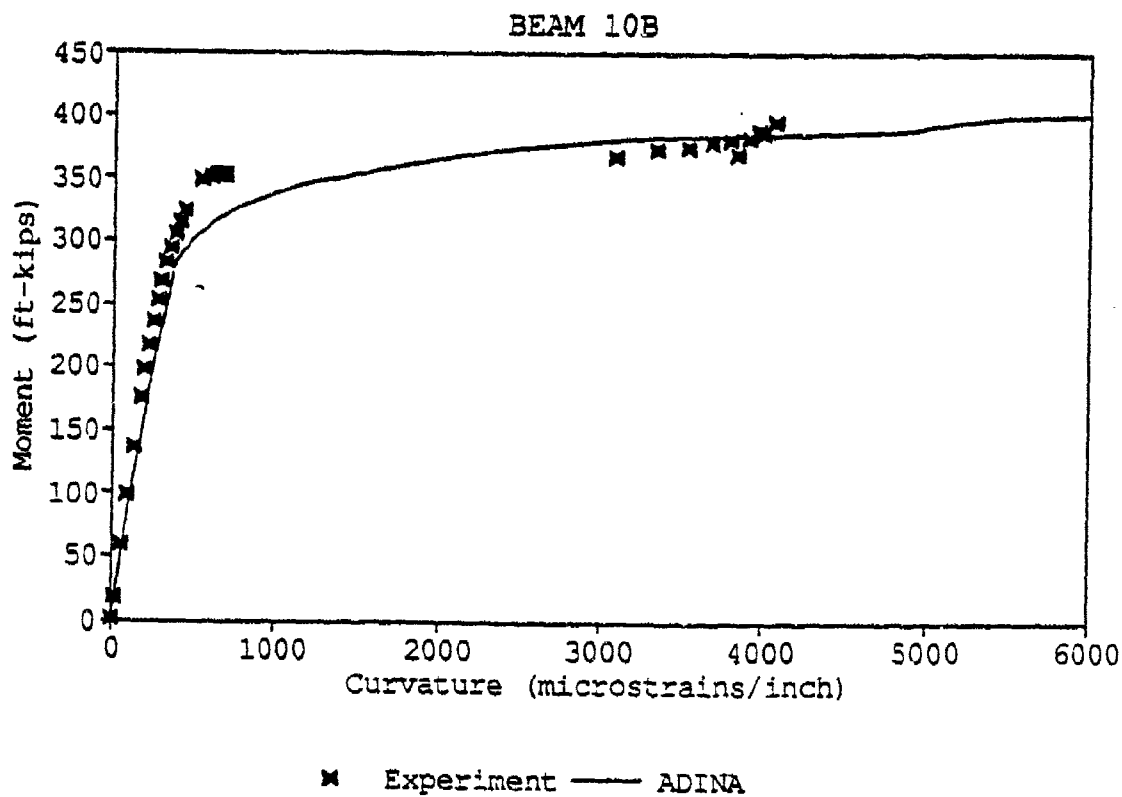
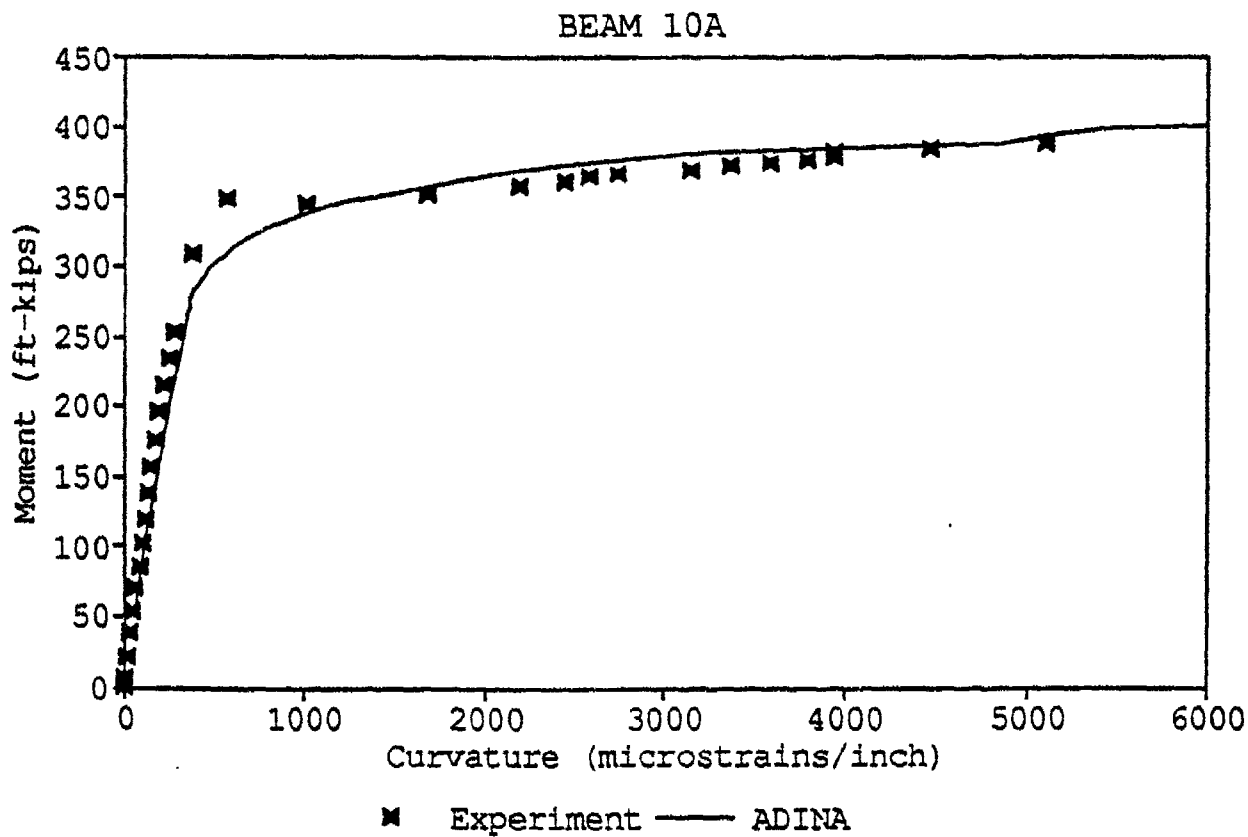


Figure 64. Moment-Curvature Diagrams for Test Beams. (Continued)

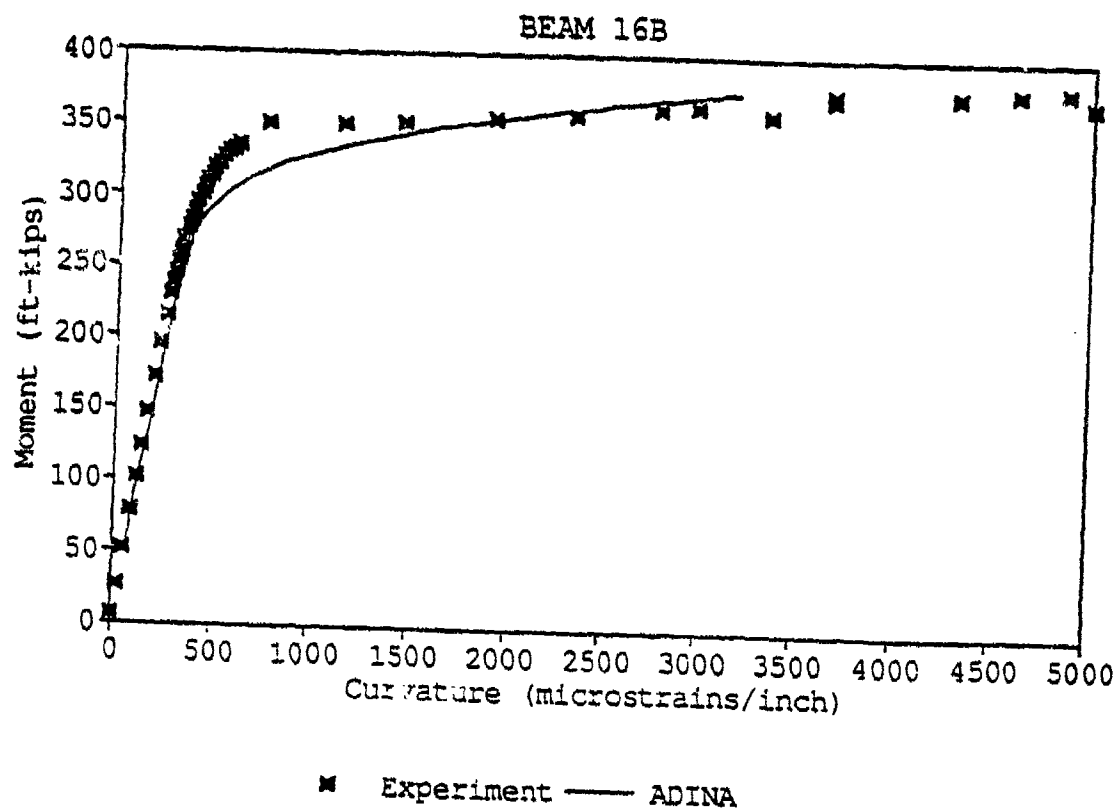
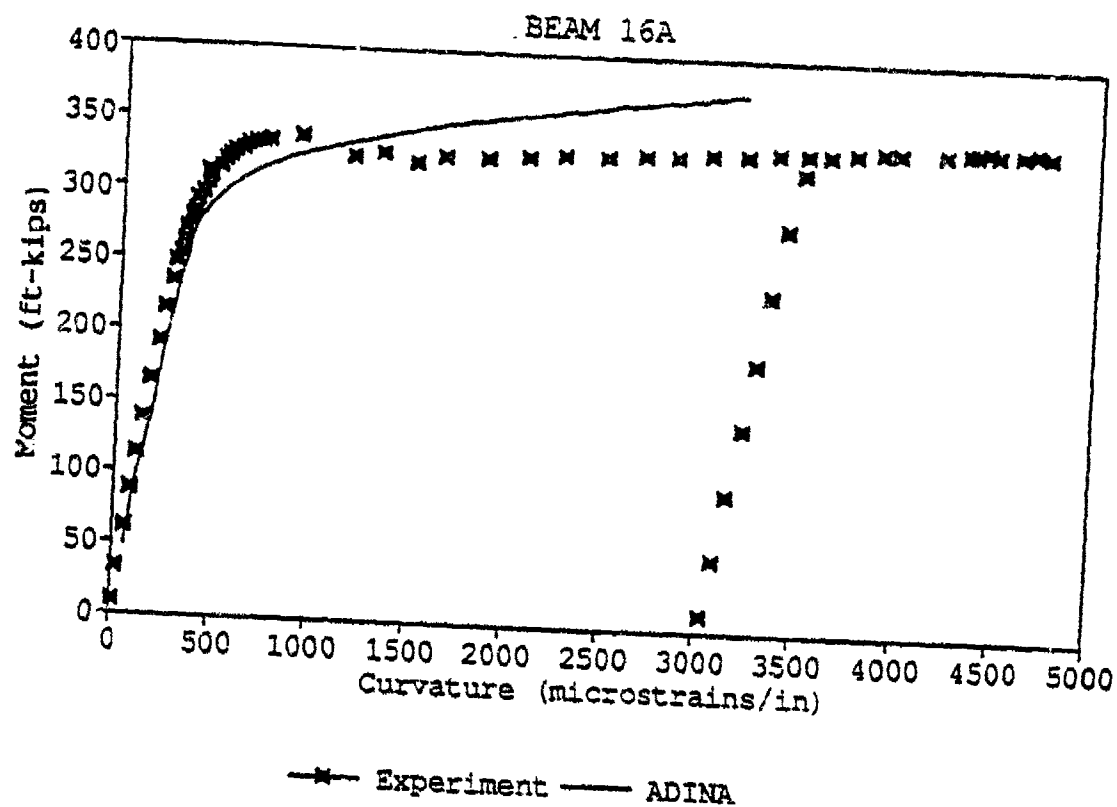


Figure 64. Moment-Curvature Diagrams for Test Beams. (Concluded)

## 5. Confined Concrete Slab

As previously discussed, the overall performance of the prototype beams was more than satisfactory. This was in large part due to the very ductile behavior of the confined concrete slab. A conventional steel-composite beam (i.e., without confining reinforcing) would have experienced a significant loss in load capacity following the initial load peak. It would still have a significant amount of ductility due to the long-yield plateau of the steel girder, but at a reduced load corresponding to the plastic moment capacity of the steel girder only.

Strain gages embedded in the concrete slab indicated that maximum strains of 1.5 to 2.0% were achieved (see Level 2 strain gage histories in Appendix B). Based on physical measurements of the final dimensions of the beams, the slab between load points shortened by 4.2%, 3.4%, 2.3%, and 2.4% for Beams 10A, 10B, 16A, and 16B, respectively. This represents an order of magnitude increase in the amount of strain possible with unconfined concrete. An appreciable increase in the concrete strength probably occurred, though direct measurements could not be made. The strength gain was inferred by the good agreement between predicted and measured load capacities.

Beam 10A was the only beam that experienced a drop in load resistance very near the end of the test. An examination of the beam after the test revealed that one of the top corner longitudinal rebar was buckled outward. As shown in Figure 65, the spacing between the perimeter hoops at this location was not uniform as designed, consequently the buckled bar had an unsupported length of about 3 inches rather than the 2-inch nominal spacing. When the bar buckled, this resulted in a loss of confinement and local crushing of the concrete within the confined core. Even so, the overall beam response was barely affected, with a drop in load of approximately 0.5%, and the experiment was terminated because of interference between the spreader beam and test beam rather than imminent "failure" of the test beam.



Figure 65. Buckled Longitudinal Rebar in Beam 10A.

## **SECTION 7. SUMMARY, CONCLUSIONS AND RECOMMENDATIONS**

### **A. SUMMARY**

A design procedure for design of blast-resistant roof beams of a modular protective structure was developed. This procedure incorporates current methods and recommendations for blast-resistant design in a relatively simple form to permit rapid analysis of candidate concepts. This procedure was applied to evaluate different structural concepts for roof beams for two shelter sizes for a typical threat level.

In all, five different roof beam element concepts were evaluated:

1. Conventionally reinforced concrete.
2. Prestressed (pretensioned) concrete.
3. Steel-concrete composite having a solid concrete top flange integrally connected to a welded plate girder.
4. Concrete beams reinforced externally with carbon fiber sheets.
5. Pultruded fiberglass beams.

The dynamic design procedure utilizing a single-degree-of-freedom analysis for the beam concepts was applied to determine the structural efficiency and effectiveness of the concepts to blast induced shock loads. In addition to structural efficiency, other evaluation criteria including cost, constructability, handling, storage, erection, and reliability were used to select the most effective of the five concepts considered.

The structural response predicted by the simplified procedure compared very favorably to that of a more sophisticated finite element analysis. This favorable comparison verified and added confidence in the simplified design procedure.

Based on the results of the concept evaluation, the steel-concrete composite beam was determined to be the most promising. A test program was designed and conducted to further validate the steel-concrete composite beam concept. The prototype beams incorporated special reinforcing designed to confine the concrete slab and greatly enhance its ductility and ultimate strength. The results of these tests verified that the design procedure accurately predicts the response of the steel-confined concrete composite beam. The enhanced strength and ductility of this concept will permit relatively light-weight beams to be constructed using conventional concrete and steel materials, satisfying the desired objectives of this research program.



## B. CONCLUSIONS

- The simplified dynamic design procedure developed herein was validated for use in designing prefabricated roof elements to resist air blast induced shock loadings.
- A method was presented that can be used to predict the significant strength enhancement achieved by using confining reinforcement for concrete slab elements.
- Of the five concepts studied, the steel-composite concrete roof beam was found to be the most efficient and effective to meet the blast and shock requirements for this program.
- The static test results (resistance function, load -deflection, and strain) of the four prototype steel-composite concrete roof beams compared very favorably with predictions made by the simplified design procedure and finite element analyses.
- The overall objectives of the study were met extremely well.

## C. RECOMMENDATIONS

- The simplified design procedure should be used for the design of roof beams used for the prefabricated protective shelter proposed by the Air Force.
- A user friendly computer program should be written to implement the design procedure developed and validated in this study.
- Details for attaching the roof beam to the earth-wall system of the concept shelter need to be developed and verified.
- Consider the use of light-weight cross beams to span over the roof beam concept recommended from this study to determine if savings in cost and weight can be achieved.
- Design a full size shelter concept and subject it to a series of weapon effects field tests.
- Develop a family of design charts for various shelter configurations and threats.

## SECTION VIII. REFERENCES

1. Ahmed, S. H. and Barker, R., "Flexural Behavior of Reinforced High-Strength Lightweight Concrete Beams," ACI Structural Journal, Vol. 88 No. 1, January-February 1991.
2. Ahmed, S. H. and Batts, J., "Flexural Behavior of Doubly Reinforced High-Strength Lightweight Concrete Beams with Web Reinforcement," ACI Structural Journal, Vol. 88 No. 3, May-June 1991.
3. Building Code Requirements for Reinforced Concrete, (ACI 318-89) and Commentary.
4. Krauthammer, T., Shahriar, S., and Shanaa, H. M., "Analysis of Reinforced Concrete Beams Subjected to Severe Concentrated Loads," ACI structural Journal, Vol. 84 No. 6, November-December 1987.
5. Russo, G., "Beam Strength Enhancement at Design Ductility Factor Demands," Journal of Structural Engineering, Vol. 116 No. 12, American Society of Civil Engineers, December 1990.
6. Roller, J. R. and Russell, H.G., "Shear Strength of High-Strength Concrete Beams with Web Reinforcement," ACI Structural Journal, Vol. 87 No.2, March-April 1990.
7. Sarsam, K.F. and Al-Musawi, J.M., "Shear Design of High and Normal Strength Concrete Beams with Web Reinforcement," ACI Structural Journal, Vol 89 No. 6, November-December 1992.
8. Krauthammer, T., Shahriar, S., and Shanaa, H.M., "Response of Reinforced Concrete Elements to Severe Impulsive Loads," Journal of Structural Engineering, Vol. 116 No. 4, American Society of Civil Engineers, April 1990.
9. Stevens, D. J. and Krauthammer, T., "Nonlocal Continuum Damage/Plasticity Model for Impulse-Loaded RC Beam," Journal of Structural Engineering, Vol. 115 No. 9, American Society of Civil Engineers, September 1989.
10. Biggs, J.M., Introduction to Structural Dynamics, McGraw-Hill Book Company, New York, 1964.

11. Mercx, W.P.M., "The Normal Mode Technique: Applications for the Analysis of Transient Loaded Structures," Proceedings of the Fourth International Symposium on the Interaction of Non-nuclear Munitions with Structures, Panama City Beach, FL, 17-21 April 1989.
12. Karthaus, W., and Leussink, J.W., "Dynamic Loading: More Than Just a Dynamic Load Factor," Proceedings of the International Symposium on the Interaction of Non-nuclear Munitions with Structures, U.S. Air Force Academy, CO, 10-13 May 1983.
13. Carroll, T.P., "The Importance of Dynamic Reactions in the Design of Explosively Loaded Flexural Members," Proceedings of the Fourth International Symposium on the Interaction of Non-nuclear Munitions with Structures, Panama City Beach, FL, 17-21 April 1989.
14. Structures to Resist the Effects of Accidental Explosions, Volume III, Principles of Dynamic Analysis, TM 5-1300, prepared by Ammann & Whitney, New York, NY, for ARDEC, Dover, NJ, June 1984.
15. The Air Force Manual For Design and Analysis of Hardened Structures, AFWL-TR-74-102, prepared by Civil Nuclear Systems Corporation, Albuquerque, NM, for Air Force Weapons Laboratory, Air Force Systems Command, Kirtland Air Force Base, NM, October 1974.
16. Structures to Resist the Effects of Accidental Explosions, Volume IV, Reinforced Concrete Design, TM 5-1300, prepared by Ammann & Whitney, New York, NY, for ARDEC, Dover, NJ, April 1987.
17. Structures to Resist the Effects of Accidental Explosions, Volume V, Structural Steel Design, TM 5-1300, prepared by Ammann & Whitney, New York, NY, for ARDEC, Dover, NJ, May 1987.
18. Protective Construction Design Manual: Resistance of Structural Elements (Section IX), ESL-TR-87-57, prepared by Applied Research Associates, Albuquerque, NM, for Engineering and Services Laboratory, Air Force Engineering and Services Center, Tyndall AFB Florida, November 1989.
19. Design of Structures to Resist Nuclear Weapons Effects, Manual No. 42, Task Committee on Updating Manual 42 of the Committee on Dynamic Effects of the Structural Division of the American Society of Civil Engineers, American Society of Civil Engineers, New York, NY, 1985.

20. Structural Analysis and Design of Nuclear Plant Facilities. Manual No. 58, Committee on Nuclear Structures and Materials of the Structural Division of the American Society of Civil Engineers, American Society of Civil Engineers, New York, NY, 1980.
21. Newmark, N.M., "An Engineering Approach to Blast-Resistant Design," Transaction of the American Society of Civil Engineers, Vol. 121, pp. 45-61, 1956.
22. Shin, S., Ghosh, S.K., and Moreno, J., "Flexural Ductility of Ultra-High Strength Concrete Members," ACI Structural Journal, Vol. 86. No. 4, July-August 1989.
23. Park, R. and Ruitong, O., "Ductility of Doubly Reinforced Concrete Beam Sections," ACI Structural Journal, Vol. 85 No. 2, March-April 1988.
24. Mattock, A.H., "The Rotational Capacity of Hinging Regions in Reinforced Concrete Beams," in Flexural Mechanics of Reinforced Concrete, Proceedings of 10-12 Nov 1964 ASCI-ACI International Symposium, Miami, FL, 1965. Also published as SP-12, American Concrete Institute, Detroit, MI, pp. 143-181.
25. Mattock, A.H., Discussion of "Rotational Capacity of Reinforced Concrete Beams" by W.G. Corley, Proceedings, ASCE, Vol.93, ST2, April 1967, pp. 519-522.
26. Corley, W.G., "Rotational Capacity of Reinforced Concrete Beams," Proceedings, ASCE, Vol.92, ST2, October 1966, pp. 121-146.
27. Cohn, M.Z. and Ghosh, S.K., "Flexural Ductility of Reinforced Concrete Sections," Publications, International Association for Bridge and Structural Engineering, Zurich, Vol. 32-II, 1972, pp. 53-83.
28. Chen Zhao-yuan, and Wang Shang-jin, "Progress in Blast-Resistant Structures Research," Proceedings of the Fourth International Symposium on the Interaction of Non-nuclear Munitions with Structures, Panama City Beach, FL, 17-21 April 1989.
29. Norris, C. H., Structural Design For Dynamic Loads, McGraw-Hill, New York, 1958.

30. Al-Zhaikh, A.H. and Al-Zaid, R.Z., "Effect of Reinforcement Ratio on the Effective Moment of Inertia of Reinforced Concrete Beams," ACI Structural Journal, Vol. 90 No. 2, March-April 1993.
31. Duan, L., Wang, F., and Chen, W., "Flexural Rigidity of Reinforced Concrete Members," ACI Structural Journal, Vol. 86 No. 4, July-August 1989.
32. Protective Construction Design Manual: Airblast Effects (Section IV), ESL-TR-87-57, prepared by Applied Research Associates, Albuquerque, NM, for Engineering and Services Laboratory, Air Force Engineering and Services Center, Tyndall AFB Florida, November 1989.
33. Protective Construction Design Manual: Groundshock and Cratering (Section V), ESL-TR-87-57, prepared by Applied Research Associates, Albuquerque, NM, for Engineering and Services Laboratory, Air Force Engineering and Services Center, Tyndall AFB Florida, November 1989.
34. Protective Construction Design Manual: Loads on Structures (Section VII), ESL-TR-87-57, prepared by Applied Research Associates, Albuquerque, NM, for Engineering and Services Laboratory, Air Force Engineering and Services Center, Tyndall AFB Florida, November 1989.
35. Structures to Resist the Effects of Accidental Explosions. Volume II. Blast Fragment and Shock Loads, TM 5-1300, prepared by Ammann & Whitney, New York, NY, for ARDEC, Dover, NJ, December 1986.
36. Fundamentals of Protective Design For Conventional Weapons, TM 5-855-1, U.S. Army Engineer Waterways Experiment Station, Vicksburg, MS, 1986.
37. Proceedings of the Symposium on the Interaction of Non-nuclear Munitions with Structures, U.S. Air Force Academy, CO, 10-13 May 1983.
38. Proceedings of the Second Symposium on the Interaction of Non-nuclear Munitions with Structures, Panama City Beach, FL, 15-18 April 1985.
39. Internationales Symposium Interaktion Konventioneller Munition mit Schutzbauten, Mannheim, Germany, 9-13 March 1987.

40. Proceedings of the Fourth International Symposium on the Interaction of Non-nuclear Munitions with Structures, Panama City Beach, FL, 17-21 April 1989.
41. Internationales Symposium Interaktion Konventioneller Munition mit Schutzbauten, Mannheim, Germany, 22-26 April 1991.
42. Proceedings of the Sixth International Symposium on the Interaction of Non-nuclear Munitions with Structures, Panama City Beach, FL, 3-7 May 1993.
43. Protective Construction Design Manual: Dynamic Response of Structures (Section X), ESL-TR-87-57, prepared by Applied Research Associates, Albuquerque, NM, for Engineering and Services Laboratory, Air Force Engineering and Services Center, Tyndall AFB Florida, November 1989.
44. CRSI PC Software Catalog, Concrete Reinforcing Steel Institute, Schaumburg, IL, 1993.
45. Manual of Steel Construction - Load and Resistance Factor Design, First Revised Edition, American Institute of Steel Construction, Inc., Chicago, 1991.
46. Naaman, A.E., "Unified Design Recommendations for Reinforced, Prestressed, and Partially Prestressed Concrete Bending and Compression Members," *ACI Structural Journal*, Vol. 89 No. 2, March-April 1992.
47. Wong, W.S. and Weidlinger, P., "Design of Underground Shelters Including Soil-Structure Interaction Effects," Proceedings of the Symposium on the Interaction of Non-nuclear Munitions with Structures, U.S. Air Force Academy, CO, 10-13 May 1983.
48. MacGregor, J.G., Reinforced Concrete Mechanics and Design, Prentice Hall, Englewood Cliffs, NJ, 1988.
49. Kaufman, M.K. and Ramirez, J.A., "Re-evaluation of the Ultimate Shear Behavior of High-Strength Concrete Prestressed I-Beams," *ACI Structural Journal*, Vol.85 No.3, May-June 1988.
50. Salmon, C.G., Johnson, J.E., STEEL STRUCTURES: Design and Behavior. Emphasizing Load and Resistance Factor Design, 3rd ed., Harper Collins Publishers Inc., New York, 1990.

51. Brady, B.H.G., and Brown, E.T., Rock Mechanics for Underground Mining, George Allen & Unwin, London, 1985, pp. 214-218.
52. ADINA Theory & Modeling Guide, ADINA R&D, Inc., Watertown, MA, December 1987.
53. Means Building Construction Cost Data, 50th Annual Edition, R. S. Means Company, Inc., Kingston, MA, 1991.
54. Ritchie, P.A., Thomas, D.A., Lu, L., and Connelly, G.M., "External Reinforcement of Concrete Beams Using Fiber Reinforced Plastics", ACI Structural Journal, 88(4), pp 490-500, 1991.
55. Saadatmanesh, H., and Ehsani, M.R., "RC Beams Strengthened With GFRP Plates. I: Experimental Study," J. Struc. Engrg., ASCE, 117(11), pp 3417-33, 1991.
56. Wei An, Saadatmanesh, H., and Ehsani, M.R., "RC Beams Strengthened With FRP Plates. II: Analysis and Parametric Study," J. Struc. Engrg., ASCE, 117(11), pp 3434-55, 1991.
57. Triantafillou, T., Deskovic, N., "Innovative Prestressing With FRP Sheets: Mechanics of Short-Term Behavior," J. Engrg. Mech., ASCE, 117(7), pp 1652-72, 1991.
58. Triantafillou, T., Deskovic, N., Deuring, M., "Strengthening of Concrete Structures with Prestressed Fiber Reinforced Plastic Sheets," ACI Structural Journal, 89(3), pp 235-244, 1992.
59. Ross, C. A., "Concrete Beams Reinforced with Graphite/Epoxy Uniaxial Fibrous Composite Material," briefing for JAYCOR and AF CESA/RAC... October 1992
60. Memorandum for Record to Mr. William S. Strickland, IPA Program Report, Fall 1992.
61. Freedman, S., "Properties of Materials for Reinforced Concrete," in Handbook of Concrete Engineering, 2nd Edition, Mark Fintel, ed., Van Nostrand Reinhold, New York, 1985.
62. Schwartz, M.M., Composite Materials Handbook, 2nd ed., McGraw-Hill, Inc., New York, 1992.
63. Faylor, D., Morrison Molded Fiberglass Company, 4 October 92 telephone conversation regarding pultrusion costs, materials, and process limitations.

64. Design Manual. EXTREN® Fiberglass Structural Shapes, Morrison Molded Fiber Glass Company, Bristol, Virginia, 1989.
65. JAYCOR, unclassified letter, Captain Richard Reid, AFCEA, Subject: Dynamic Response of Buried Composite Material Beams Subjected to Blast Loads, 1 October 1992.
66. Barbero, E.J., Shin-Ham Fu, and Raftoyiannis, I., "Ultimate Bending Strength of Composite Beams," ASCE Journal of Materials in Civil Engineering, Vol.3 No. 4, November 1991.
67. Kent, D.C. and Park, R., "Flexural Members with Confined Concrete," ASCE Journal of the Structures Division, Vol. 97 No. ST7, pp. 1969-1990, Jul 1971; Closure to Discussion, Vol. 98 No. ST12, pp.2805-2810, December 1972.
68. Sakai, K. and Sheikh, S.A., "What Do We Know About Confinement in Reinforced Concrete Columns" (A Critical Review of Previous Work and Code Provisions)," ACI Structural Journal, Vol. 86 No. 2, March-April 1989.
69. Ge, H. and Usami, T., "Strength of concrete-Filled Thin-Walled Steel Box Columns: Experiment," J. Struct. Div., ASCE, 118 (11), pp. 3036-3054, November 1992.
70. Saatcioglu, M. and Razvi, S.R., "Strength and Ductility of Confined Concrete," J. Struct. Div., ASCE, 118(6), pp. 1590-1607, June 1992.
71. Nelson, Q., Embedment Properties of Headed Studs, TRW Inc, 1977.



## APPENDIX A - DESIGN PROCEDURE FORMULAS

### A. REINFORCED CONCRETE

Refer to Figure A-1 for definition of symbols.

#### 1. Flexural Resistance

Case 1: Compression Reinforcement Yields:

$$C_c = 0.85f'_c(ab_t - A_{st})$$

$$C_s = A_{st}f_y$$

$$T_s = A_{sb}f_y$$

$$a = \frac{A_{sb}f_y - A_{st}(f_y - 0.85f'_c)}{0.85f'_c b_t}$$

$$\text{Check that: } \epsilon_{st} = \epsilon_{cu} \left(1 - \frac{\beta_1 d_t}{a}\right) \geq \frac{f_y}{E_s}$$

Case 2: Compression Reinforcement Does Not Yield:

$$C_c = 0.85f'_c(ab_t - A_{st})$$

$$C_s = A_{st}f_{st}$$

$$T_s = A_{sb}f_y$$

$$a = \frac{T_s - \epsilon_{cu} E_s A_{st} \sqrt{(T_s - \epsilon_{cu} E_s A_{st})^2 + 4(0.85f'_c b_t)(\epsilon_{cu} E_s A_{st} \beta_1 d_t)}}{2(0.85f'_c b_t)}$$

$$\text{Check that: } \epsilon_{st} = \epsilon_{cu} \left(1 - \frac{\beta_1 d_t}{a}\right) \leq \frac{f_y}{E_s}$$

Moment capacity:

$$M = C_c(d_{tot} - d_b - \frac{a}{2}) + C_s(d_{tot} - d_b - d_t)$$

## 2. Stiffness

- a. Moment of Inertia of Uncracked Section  $I_g$ :  
Location of neutral axis from bottom of beam:

$$\bar{y} = \frac{\Sigma A \cdot y}{\Sigma A}$$

$$\Sigma A \cdot y = t_t b_t (d_{tot} - \frac{t_t}{2}) + d_w t_w (\frac{d_w}{2} + t_b) + t_b b_b (\frac{t_b}{2}) + (n-1) A_{st} (d_{tot} - d_t) + (n-1) A_{sb} d_b$$

$$\Sigma A = t_t b_t + d_w t_w + t_b b_b + (n-1)(A_{st} + A_{sb})$$

Moment of Inertia  $I_g$ :

$$I_g = \frac{1}{12} (b_t t_t^3 + b_b t_b^3 + t_w d_w^3)$$

$$+ b_t t_t (d_{tot} - \bar{y} - \frac{t_t}{2})^2 + b_b t_b (\bar{y} - \frac{t_b}{2})^2 + t_w d_w (t_b - \bar{y} + \frac{d_w}{2})^2$$

$$+ (n-1) [A_{st} (d_{tot} - \bar{y} - d_t)^2 + A_{sb} (\bar{y} - d_b)^2]$$

- b. Moment of Inertia of Cracked Section:

Case 1: Neutral Axis in Top Flange:

Solve the quadratic  $c = \frac{-B + \sqrt{B^2 - 4AC}}{2A}$  to find the distance "c" from the top of the beam to the neutral axis, where:

$$A = \frac{b_t}{2}$$

$$B = (n-1) A_{st} + n A_{sb}$$

$$C = -[(n-1) A_{st} d_t + n A_{sb} (d_{tot} - d_b)]$$

Check that "c" is less than  $b_t$ , and if not, the cracked section neutral axis is in the web and is solved for below.

$$I_{cr} = \frac{b_t c^3}{3} + (n-1) A_{st} (c - d_t)^2 + n A_{sb} (d_{tot} - c - d_b)^2$$

**Case 2: Neutral Axis in Web:**

Solve the quadratic above with the terms defined by:

$$A = \frac{t_w}{2}$$

$$B = b_t d_t - t_t t_w + (n-1)A_{st} + nA_{sb}$$

$$C = -\left[\frac{t_t^2}{2}(b_t - t_w) + (n-1)A_{st}d_t + nA_{sb}(d_{tot} - d_b)\right]$$

$$I_{cr} = \frac{b_t t_t^3}{12} + b_t t_t \left(c - \frac{t_t}{2}\right)^2 + (n-1)A_{st}(c - d_t)^2 \\ + nA_{sb}(d_{tot} - c - d_b)^2 + \frac{t_w (c - t_t)^3}{3}$$

c. Average Moment of Inertia and Stiffness:

$$I_{avg} = \frac{I_g + I_{cr}}{2}$$

Stiffness for a beam carrying a uniformly distributed load is:

$$K = \frac{384 E_c I_{avg}}{5 L^3}$$

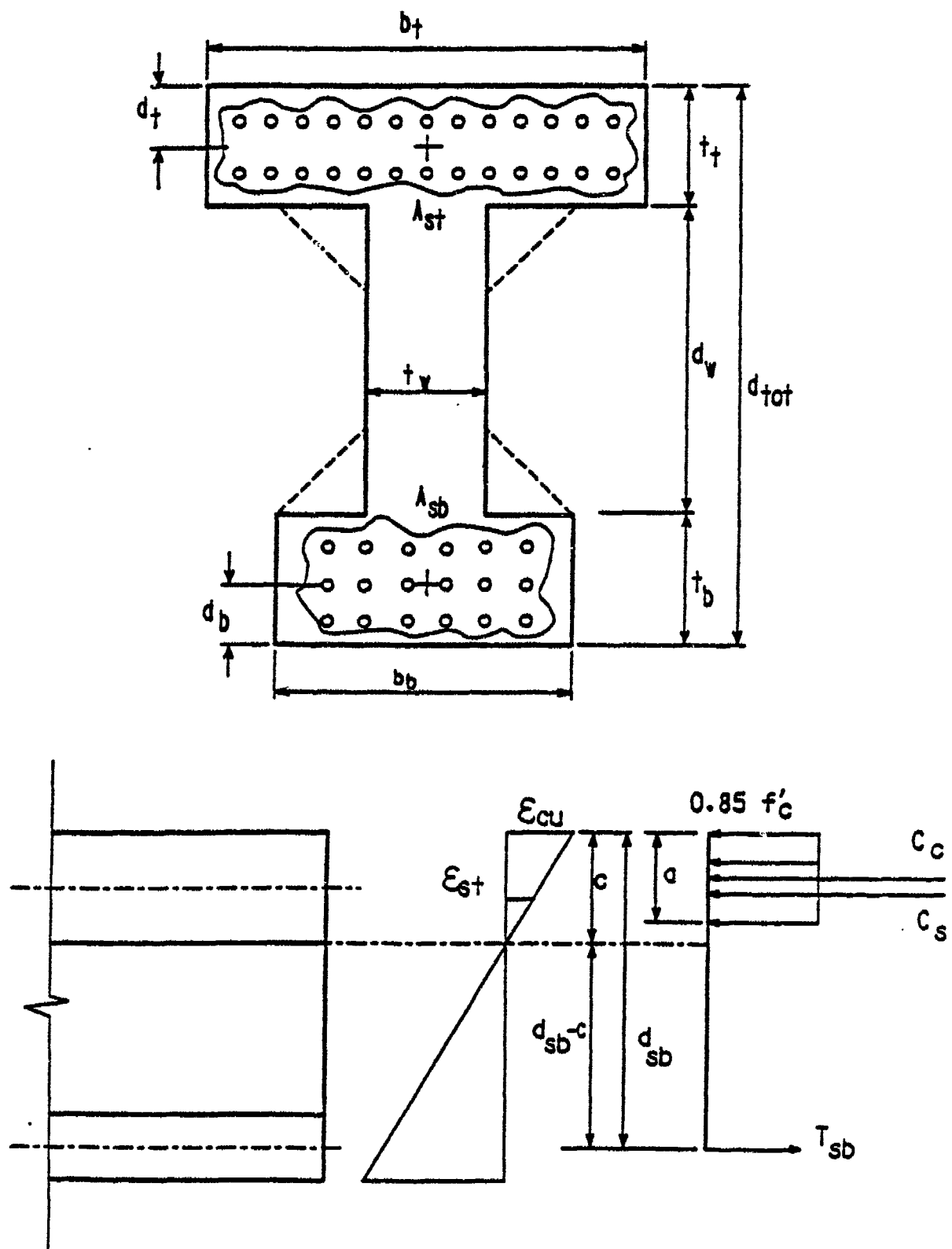


Figure A-1. Definition of Formula Symbols for Reinforced Concrete Concept.

## B. PRESTRESSED CONCRETE

Refer to Figure A-2 for definition of symbols.

### 1. Flexural Resistance

#### Case 1: Compressive Reinforcement Yields:

$$C_c = 0.85 f'_c (ab_t - A_{st})$$

$$C_s = A_{st} f_y$$

$$T_{sb} = A_{sb} f_y$$

$$T_{ps} = A_{ps} f_{ps}$$

$$a = \frac{A_{sb} f_y + A_{ps} f_{ps} - A_{st} (f_y - 0.85 f'_c)}{0.85 f'_c b_t}$$

$$\text{Check that: } \epsilon_{st} = \epsilon_{cu} \left(1 - \frac{d_t}{c}\right) \geq \epsilon_y = \frac{f_{dy}}{E_s}$$

#### Case 2: Compression Reinforcement Does Not Yield:

$$\text{From summation of forces, and } \epsilon_{st} = \epsilon_{cu} \frac{a - \beta_1 d_t}{a}:$$

$$0.85 f'_c b_t a^2 + (\epsilon_{cu} E_s A_{st} - A_{ps} f_y) a - \epsilon_{cu} E_s A_{st} \beta_1 d_t = 0$$

Solve this quadratic for  $a$  and  $c = \frac{a}{\beta_1}$ .

Since  $f_{ps}$  is not known, the solution is obtained by trial and error, with  $f_{ps}$  defined for 270 ksi 7-wire stress-relieved low-relaxation strand:

$$\epsilon_{ps} = \frac{(d_{sp} - c)}{c} \epsilon_{cu}$$

$$f_{ps} = 28,000 \epsilon_{ps} \text{ (ksi), when } \epsilon_{ps} \leq 0.008$$

$$f_{ps} = 268 - \frac{0.075}{\epsilon_{ps} - 0.0065} < 0.98 f_{pu} \text{ (ksi) when } \epsilon_{ps} > 0.008$$

An estimate of  $f_{ps}$  is made which allows the calculation of the position of the neutral axis for either Case 1 or Case 2. The strain  $\epsilon_{ps}$  and stress  $f_{ps}$  is then calculated and compared with the initial estimate, which is then refined if need be and the calculation repeated until good agreement (<5%) is achieved.

Moment capacity:

$$M = T_{ps}(d_{tot} - \frac{a}{2} - d_p) + T_{sb}(d_{tot} - \frac{a}{2} - d_b) - C_s(d_t - \frac{a}{2})$$

where  $C_s = A_{st}f_y, \epsilon_{st} > \epsilon_y$

$$= A_{st} \epsilon_{st} E_s, \epsilon_{st} < \epsilon_y$$

## 2. Stiffness

### a. Moment of inertia of Uncracked Section $I_g$ :

Location of Neutral Axis from Bottom:

$$\bar{y} = \frac{\sum A \cdot y}{\sum A}$$

$$\sum A \cdot y = t_t b_t (d_{tot} - \frac{t_t}{2}) + d_w t_w (\frac{d_w}{2} + t_b) t_b b_b (\frac{t_b}{2})$$

$$+ (n-1)A_{st}(d_{tot} - \frac{t_t}{2}) + (n-1)A_{sb}d_b + (n_{ps}-1)A_{ps}d_b$$

$$\sum A = t_t b_t + d_w t_w + t_b b_b + (n-1)(A_{st} + A_{sb}) + (n_{ps}-1)A_{ps}$$

Moment of Inertia  $I_g$ :

$$I_g = \frac{1}{2}(b_t t_t^3 + t_w d_w^3 + b_b t_b^3)$$

$$+ b_t t_t (d_{tot} - \bar{y} - \frac{t_t}{2}) + b_b t_b (\bar{y} - \frac{t_b}{2}) + t_w d_w (t_b - \bar{y} + \frac{d_w}{2})$$

$$+ (n-1)[A_{st}(d_{tot} - \bar{y} - d_t)^2 + A_{sb}(\bar{y} - d_b)^2]$$

$$+ (n_{ps}-1)A_{ps}(\bar{y} - d_p)^2$$

### b. Moment of Inertia of Cracked Section:

Solve the quadratic  $c = \frac{-B + \sqrt{B^2 - 4Ac}}{2A}$  to find the

distance "c" from the top of the beam to the neutral axis.

Case 1: Neutral Axis in Top Flange:

$$A = \frac{b_t}{2}$$

$$B = (n-1)A_{st} + n(A_{sb} + A_{ps})$$

$$C = -[(n-1)A_{st}d_t + n A_{sb}(d_{tot} - d_b) - n_{ps}A_{ps}(d_{tot} - d_p)]$$

Check that:  $c \leq b_t$

$$I_{cr} = \frac{b_t c^3}{3} + (n-1)A_{st}(c - d_t) + nA_{sb}(d_{tot} - c - d_b)^2 \\ + n_{ps}A_{ps}(d_{tot} - c - d_p)^2$$

Case 2: Neutral Axis in Web:

$$A = \frac{t_w}{2}$$

$$B = t_t(b_t - t_w) + (n-1)A_{st} + n(A_{sb} + A_{ps})$$

$$C = -\left[\frac{t_t^2}{2}(b_t - t_w) + (n-1)A_{st}d_t \right. \\ \left. + nA_{sb}(d_{tot} - d_b) - n_{ps}A_{ps}(d_{tot} - d_p)\right]$$

$$I_{cr} = \frac{t_w c^3}{3} + \frac{(b_t - t_w)}{12} t_t^3 + (b_t - t_w) t_t \left(c - \frac{t_t}{2}\right)^2 \\ + (n-1)A_{st}(c - d_t)^2 + nA_{sb}(d_{tot} - c - d_b)^2 \\ + n_{ps}A_{ps}(d_{tot} - c - d_p)^2$$

c. Average Moment of Inertia and Stiffness:

$$I_{avg} = \frac{I_g + I_{cr}}{2}$$

$$K = \frac{384 E_c I_{avg}}{5 L^3}$$

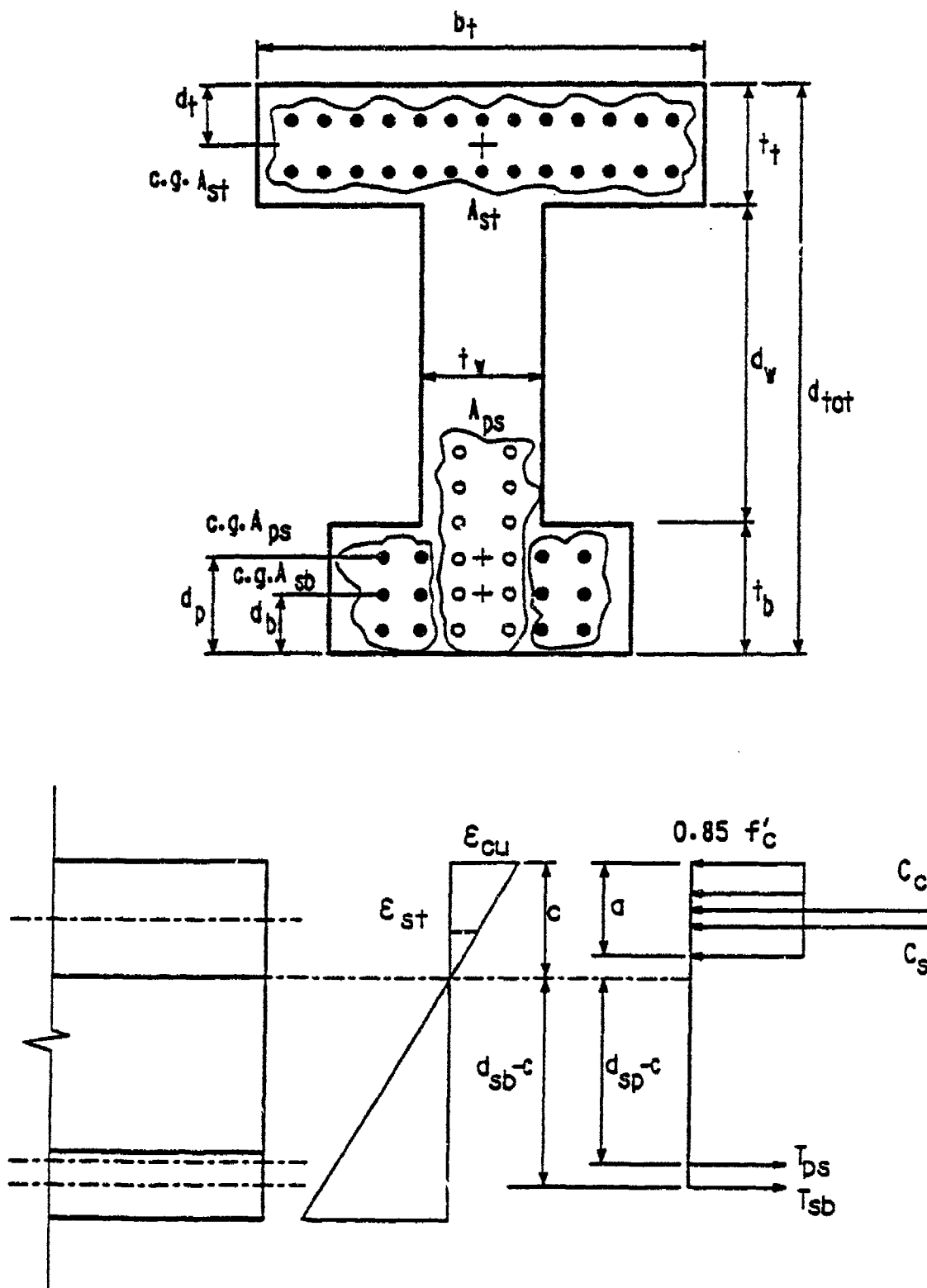


Figure A-2. Definition of Formula Symbols for Prestressed Concrete Concept.



## C. STEEL - CONCRETE COMPOSITE

Refer to Figure A-3 for definition of symbols.

### 1. Flexural Resistance:

#### Case 1: Neutral Axis in Web:

$$C_s = 0.85f'_c b_s t_s$$

$$C_{tf} = f_{yg} b_{tf} t_{tf}$$

$$C_w = f_{yg} 2t_w (c - t_s - t_{tf})$$

$$T_w = f_{yg} 2t_w (d_{tot} - c - t_{bf})$$

$$T_{bf} = f_{yg} b_{bf} t_{bf}$$

Summation of forces and solving for "c" gives:

$$c = t_s + t_{tf} + \frac{d_w}{2} + \frac{b_{bf} t_{bf} - b_{tf} t_{tf}}{4t_w} - \frac{0.85f'_c b_s t_s}{4f_{yg} t_w} \geq (t_s + t_{tf})$$

$$M = C_s \left( c - \frac{t_s}{2} \right) + C_{tf} \left( c - t_s - \frac{t_{tf}}{2} \right) + C_w \left( \frac{c - t_s - t_{tf}}{2} \right) \\ + T_w \left( \frac{d_{tot} - c - t_{bf}}{2} \right) + T_{bf} \left( d_{tot} - c - \frac{t_{bf}}{2} \right)$$

#### Case 2: Neutral Axis in Top Flange:

$$C_s = 0.85f'_c b_s t_s$$

$$C_{tf} = f_{yg} b_{tf} (c - t_s)$$

$$T_{tf} = f_{yg} b_{tf} (t_s + t_{tf} - c)$$

$$T_w = f_{yg} 2t_w d_w$$

$$T_{bf} = f_{yg} b_{bf} t_{bf}$$

Summation of forces and solving for "c" gives:

$$c = t_s + \frac{t_{tf}}{2} + \frac{t_w d_w}{b_{tf}} + \frac{b_{bf} t_{bf}}{2b_{tf}} - \frac{0.85f'_c b_s t_s}{2f_{yg} t_{tf}} \geq (t_s + t_{tf})$$

$$M = C_s(c - \frac{t_s}{2}) + C_{tf}(\frac{c - t_s}{2}) + T_{tf}(\frac{t_s + t_{tf} - c}{2}) \\ + T_w(\frac{d_w}{2} + t_s + t_{tf} - c) + T_{bf}(d_{tot} - c - \frac{t_{bf}}{2})$$

If  $c < t_s$ , the girder should be modified.

## 2. Stiffness:

### a. Location of Neutral Axis from Top:

$$\bar{y} = \frac{\sum A \cdot y}{\sum A}$$

$$\sum A \cdot y = (\frac{b_s}{n})(t_s)(\frac{t_s}{2}) + b_{tf}t_{tf}(t_s + \frac{t_{tf}}{2}) + 2t_w d_w(t_s + t_{tf} + \frac{d_w}{2}) \\ + b_{bf}t_{bf}(t_s + t_{tf} + d_w + \frac{t_{bf}}{2})$$

$$\sum A = (\frac{b_s}{n})(t_s) + b_{tf}t_{tf} + 2t_w d_w + b_{bf}t_{bf}$$

### b. Moment of Inertia and Stiffness:

$$I = \frac{1}{12} \left( \frac{b_s}{n} t_s^3 + b_{tf} t_{tf}^3 + 2t_w d_w^3 + b_{bf} t_{bf}^3 \right) \\ + \frac{b_s}{n} t_s \left( \bar{y} - \frac{t_s}{2} \right)^2 + b_{tf} t_{tf} \left( \bar{y} - t_s - \frac{t_{tf}}{2} \right)^2 \\ + \left[ 2t_w d_w (t_s + t_{tf} + \frac{d_w}{2} - \bar{y})^2 + b_{bf} t_{bf} (t_s + t_{tf} + d_w + \frac{t_{bf}}{2} - \bar{y})^2 \right]$$

$$K = \frac{384 E_s I}{5 L^3}$$

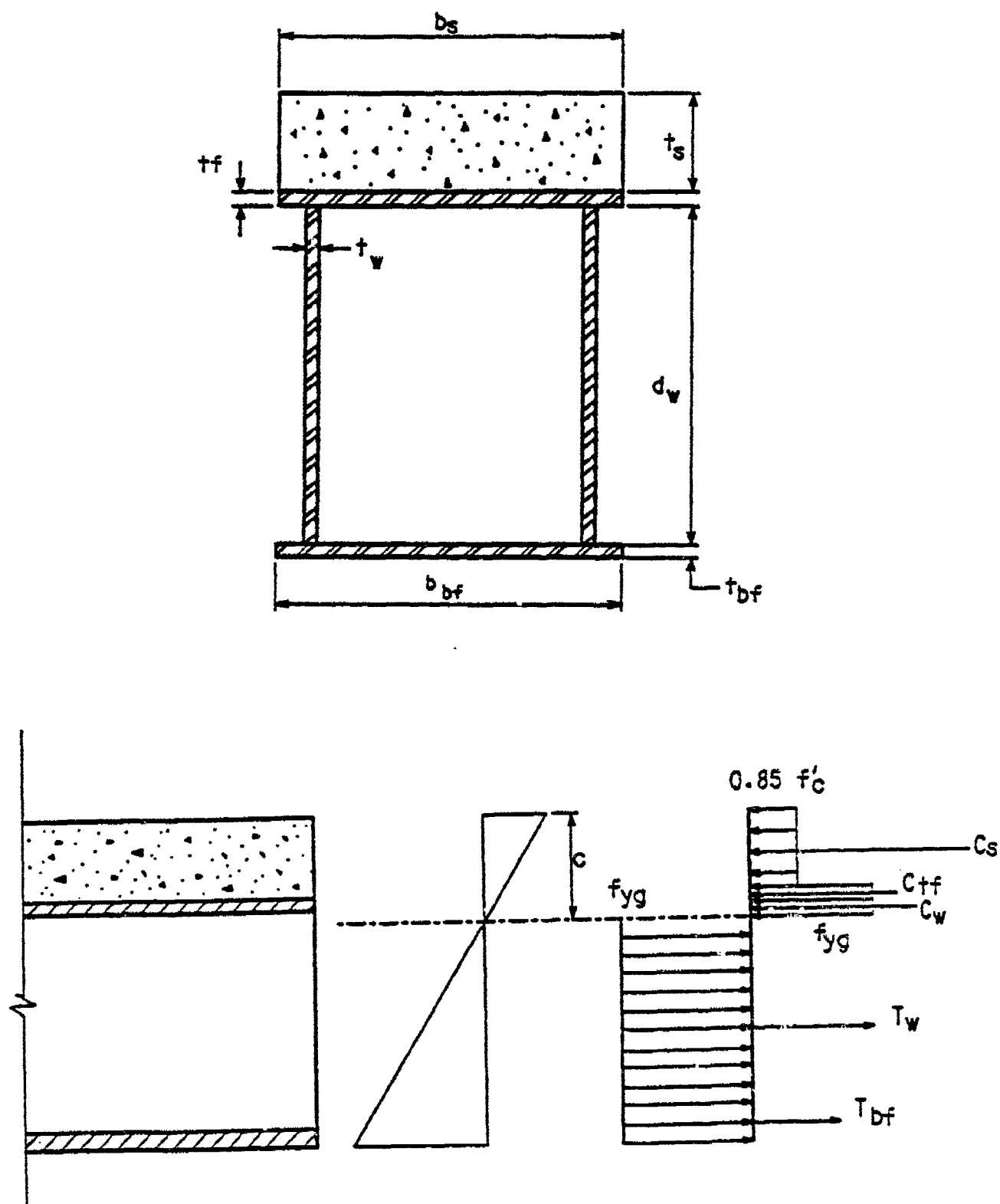


Figure A-3. Definition of Formula Symbols for Steel-Concrete Composite Concept.

D. MASS OF ROOF BEAMS AND OVERLYING SOIL

1. Reinforced Concrete

$$W_{\text{beam}} = [(b_t t_t + t_w d_w + b_b t_b) w_c + (A_{st} + A_{sb}) w_s] L$$

2. Prestressed Concrete

$$W_{\text{beam}} = [(b_t t_t + t_w d_w + b_b t_b) w_c + (A_{st} + A_{sb} + A_{ps}) w_s] L$$

3. Steel -Concrete Composite

$$W_{\text{beam}} = [(b_s t_s) w_c + (b_{tf} t_{tf} + 2 t_w d_w + b_{bf} t_{bf}) w_s] L$$

4. Overlying Soil

$$W_{\text{soil}} = d_{\text{soil}} b_{\text{beam}} L w_{\text{soil}}$$

5. Mass

$$\text{Mass} = \frac{W}{384.6 \times 10^{-6}} \quad \text{lb-msec}^2/\text{in.}$$

## E. DYNAMIC ANALYSIS

### 1. Equivalent Mass and Net Resistance:

$$M_E = \text{Mass} \times K_{LM}$$

where:

$K_{LM}$  = for elastic response

= for plastic response

$$R_{net} = \frac{8M_p}{L} - W_{beam} - W_{soil}$$

where:

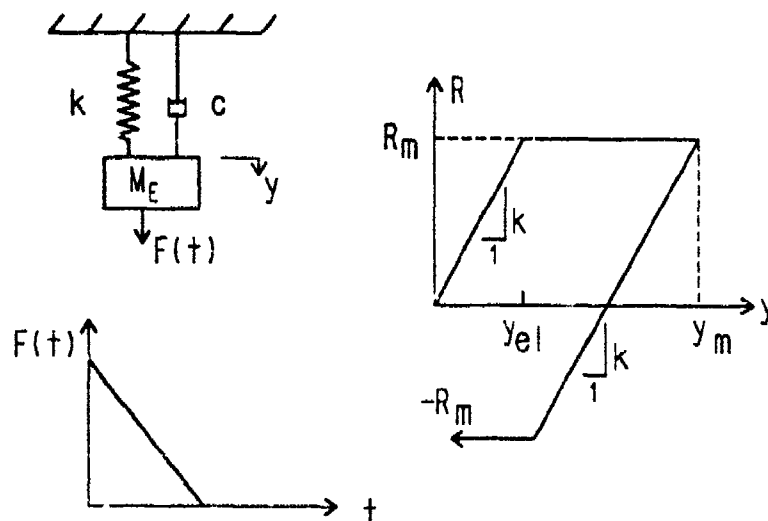
$R_{net}$  = net resistance of beam (lb.)

$M_p$  = moment capacity of beam (in-lb)

$W_{beam}$  = weight of beam (lb)

$W_{soil}$  = weight of overlying soil (lb)

### 2. Equation of Motion



Equation of Motion:

Elastic Range  $y < y_{el}$

$$M_E \ddot{y} + c \dot{y} + ky - F(t) = 0$$

Plastic Range  $y_{el} < y < y_m$

$$M_E \ddot{y} + c \dot{y} + R_m - F(t) = 0$$

After  $y_m$  has been reached  $(y_m - 2y_{el}) < y < y_m$ :

$$M_E \ddot{y} + c \dot{y} + R_m - k(y_m - y) - F(t) = 0$$

Integration of the equation of motion can be performed using any well-known procedure, such as the simple constant-velocity method:

$$y^{(s+1)} = y^{(s)} + \dot{y}_{av} \Delta t$$

$$\dot{y}_{av} = \frac{y^{(s)} + y^{(s-1)}}{\Delta t} + \ddot{y}^{(s)} \Delta t$$

To start the procedure, use the special equation:

$$y^{(1)} = \frac{2\ddot{y}^{(0)} + \ddot{y}^{(1)}}{6} \Delta t^2$$

which must be solved iteratively because  $\ddot{y}^{(1)}$  depends on  $y^{(1)}$ .

### 3. Dynamic Shear Force

#### a. Approximate Method:

Elastic Range:

$$V(t) = 0.39R(t) + 0.11F(t)$$

Plastic Range

$$V(t) = 0.38R_m + 0.12F(t)$$

b. Modal Analysis - Elastic Range Only

$$V(t) = \frac{4\pi EI p_1}{mL^3} \sum_{n=1}^{\infty} \frac{n^2}{\omega_n^2} DLF_n(t)$$

where:

- $P_1$  = magnitude of uniform load at time zero (lb/in)
- $E, I$  = modulus of elasticity and moment of inertia
- $m$  = mass per unit length (lb-m sec<sup>2</sup>/in/in)
- $n$  = mode number; 1,3,5,....
- $\omega_n$  = natural frequency for mode  $n$

$DLF(t)$  = dynamic load factor corresponding to natural frequency  $\omega_n$

Natural frequency  $\omega_n$

$$\omega_n = \frac{n^2 \pi^2}{L^2} \sqrt{\frac{EI}{m}}$$

Dynamic Load Factor  $DLF_n$

$t < t_d$ :

$$DLF_n = 1 - \cos(\omega_n t) + \frac{\sin(\omega_n t)}{\omega_n t_d} - \frac{t}{t_d}$$

$t > t_d$ :

$$DLF_n = \frac{1}{\omega_n t_d} (\sin(\omega_n t) - \sin \omega_n (t - t_d)) - \cos \omega_n t$$

The above calculations are performed for normal modes 1,3, and 5 for each time step of the numerical integration procedure (even numbered modes do not contribute for symmetric loading). The shear calculated by modal analysis is compared with the dynamic reaction calculated from the approximate method, and the larger value is used for designing the shear reinforcement.

## APPENDIX B - PROTOTYPE BEAM TEST DATA

### Deflection Between Support & Load

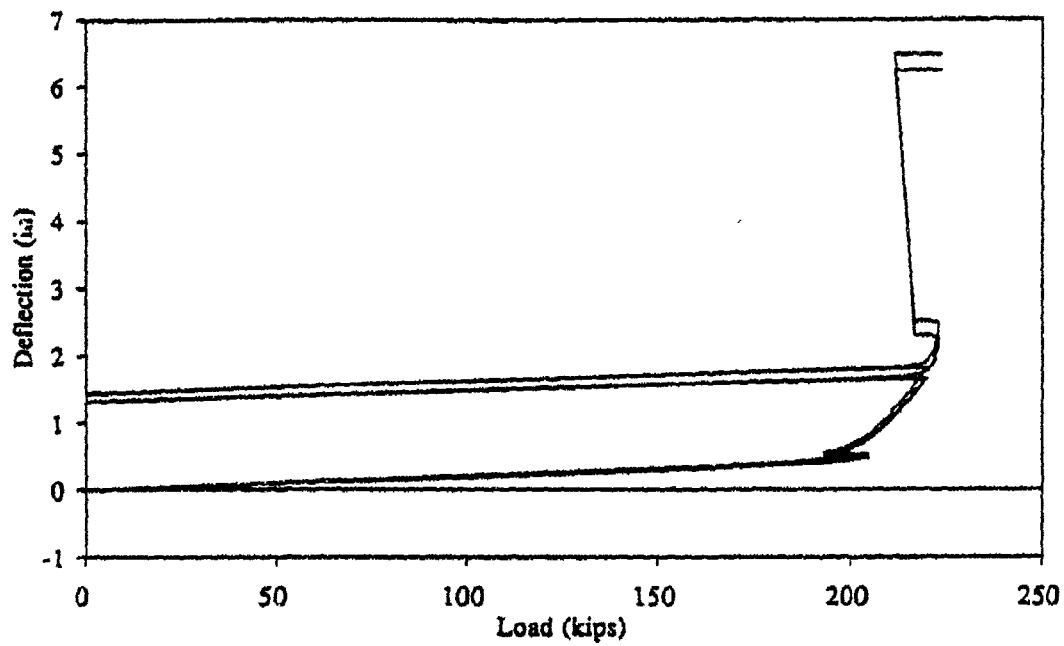


Figure B-1. Beam 10A Load Deflection Data Between Load and Support Points.

### Deflection at Load Points

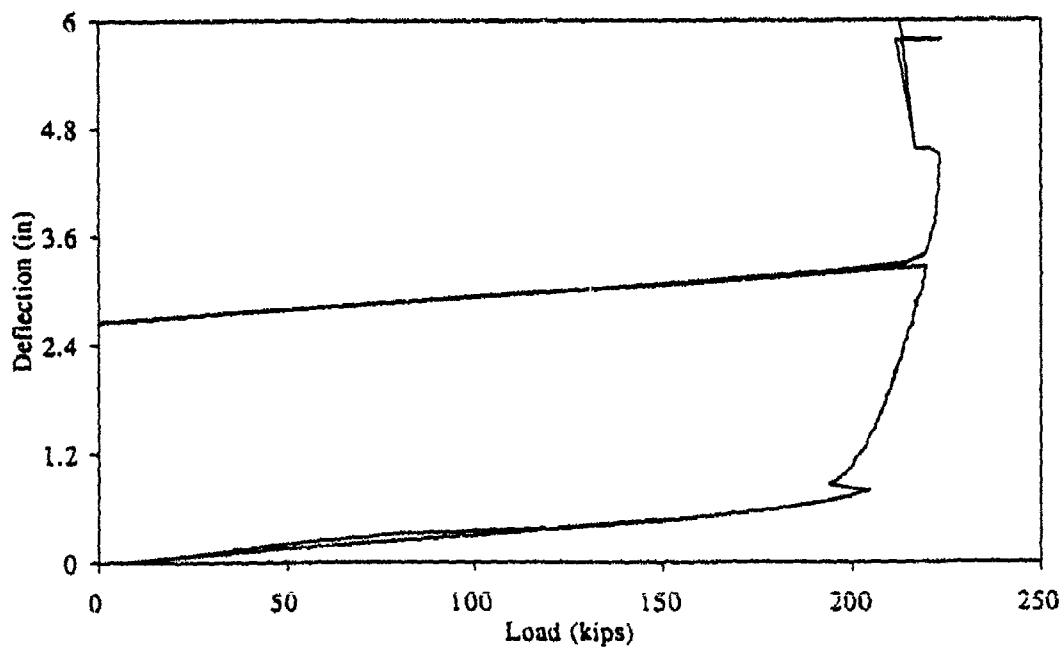


Figure B-2. Beam 10A Load Deflection Data at Load Point.



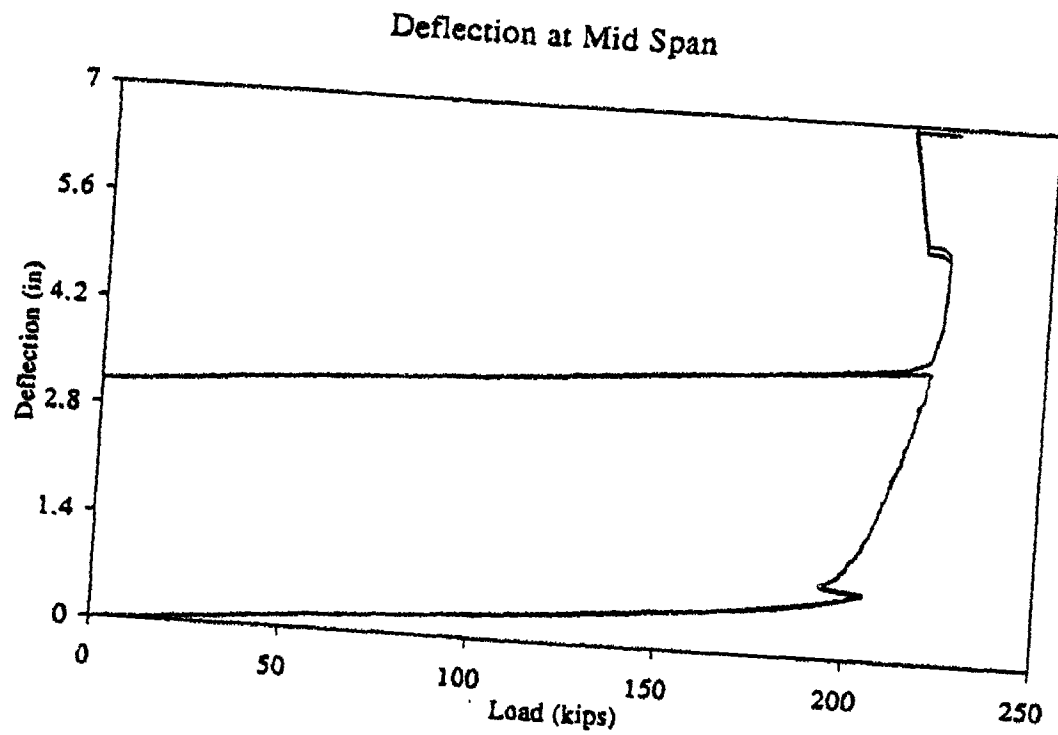


Figure B-3. Beam 10A Load Deflection Data at Midspan.

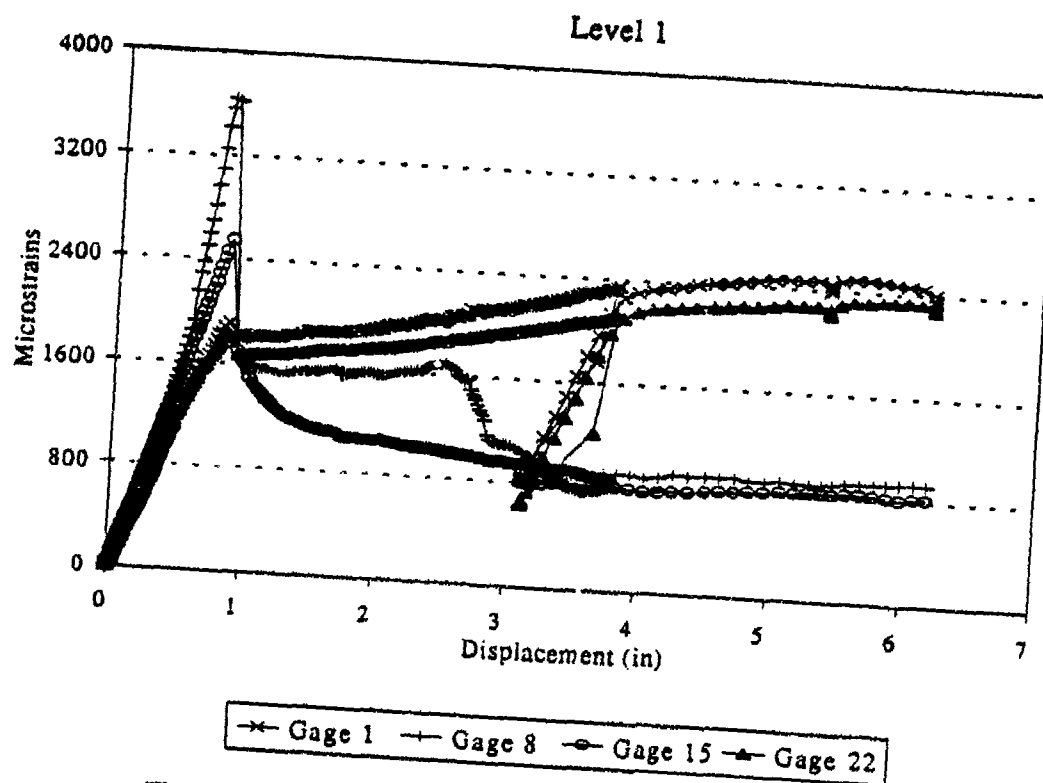


Figure B-4. Beam 10A Strain Gage Data for Level 1 Gages.

### Level 2

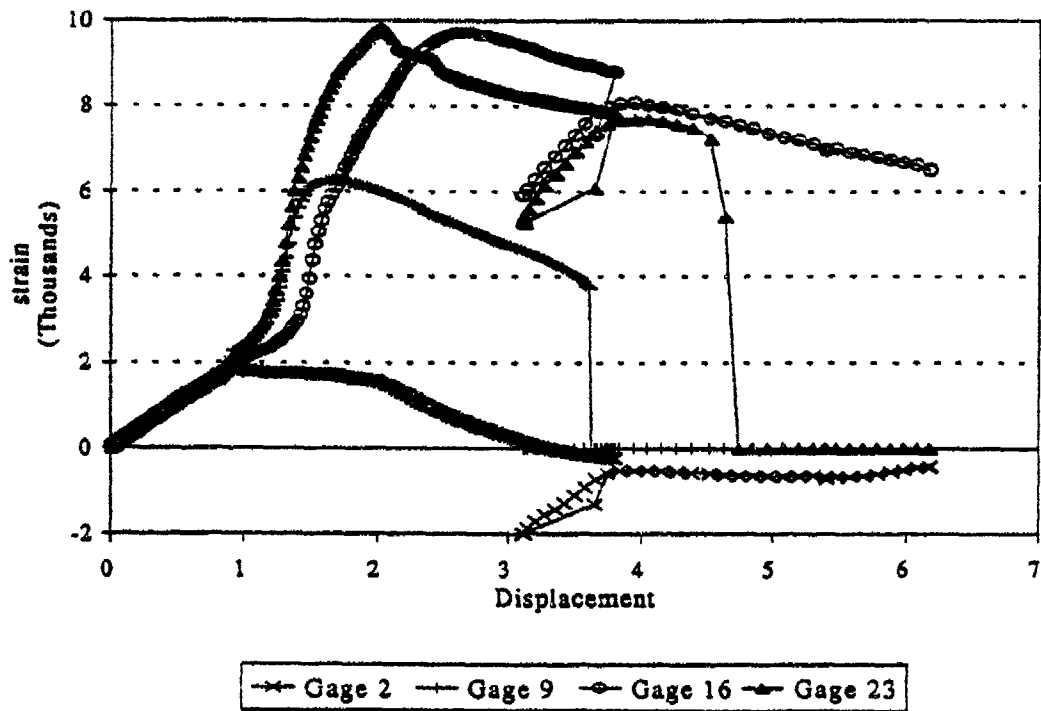


Figure B-5. Beam 10A Strain Gage Data for Level 2 Gages.

### Level 3

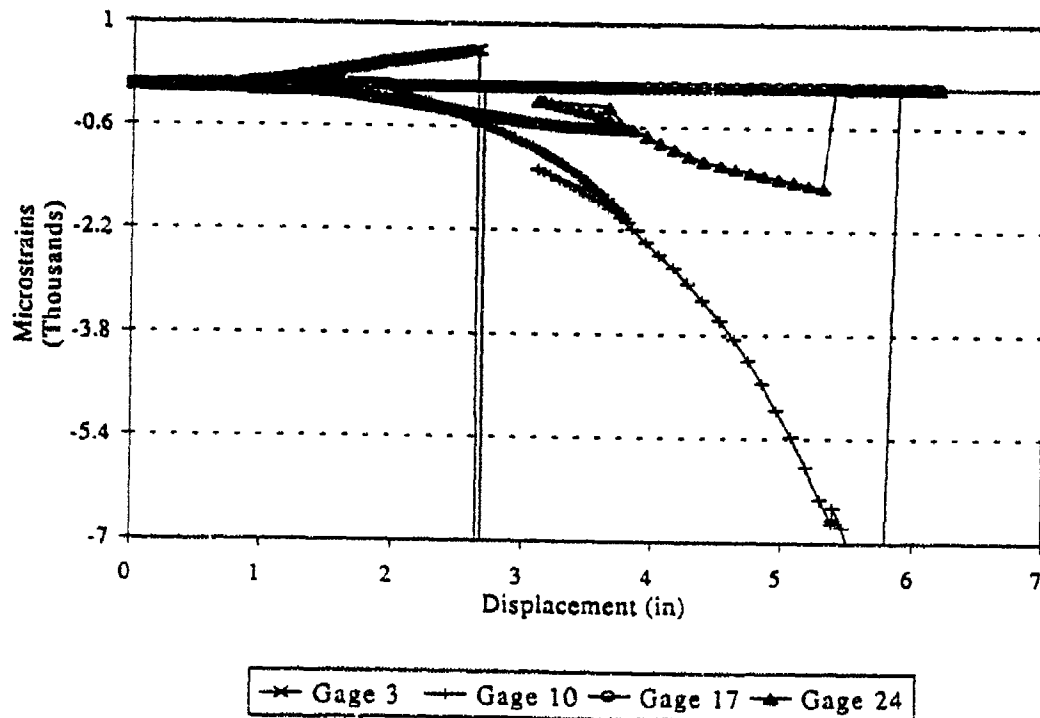


Figure B-6. Beam 10A Strain Gage Data for Level 3 Gages.

# Level 4

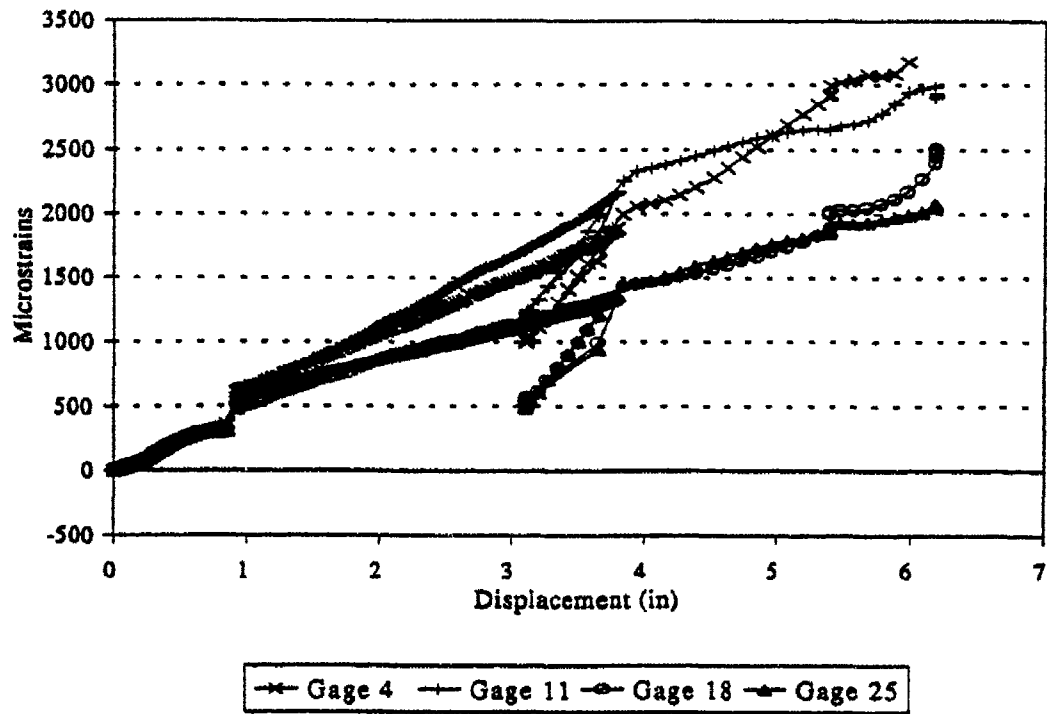


Figure B-7. Beam 10A Strain Gage Data for Level 4 Gages.

# Level 5

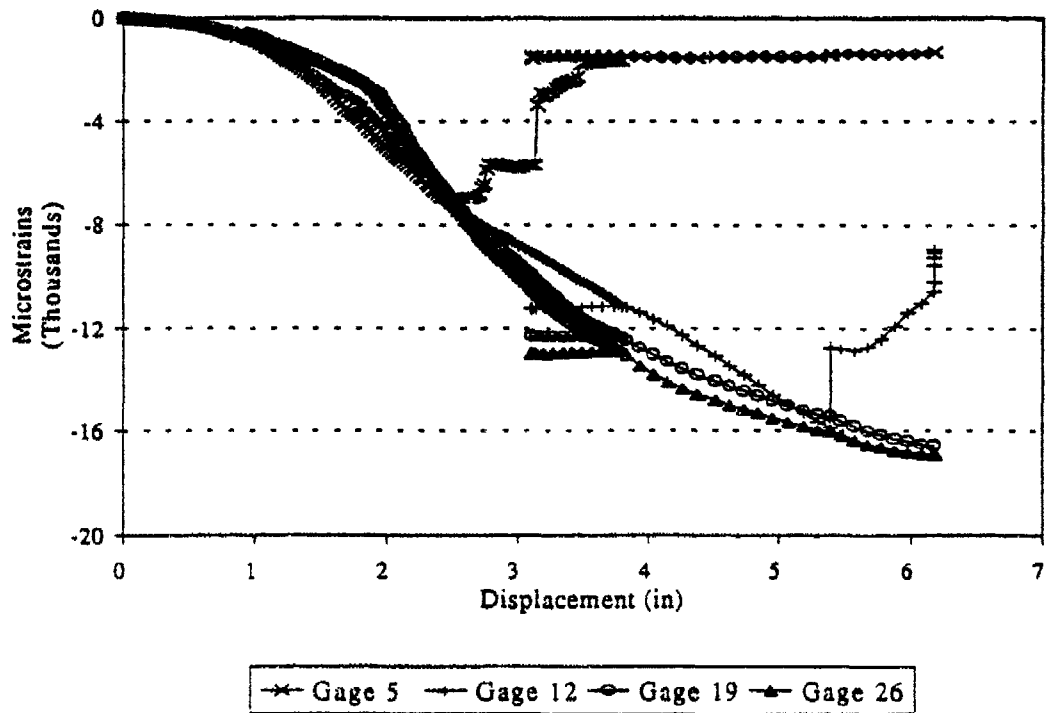


Figure B-8. Beam 10A Strain Gage Data for Level 5 Gages.

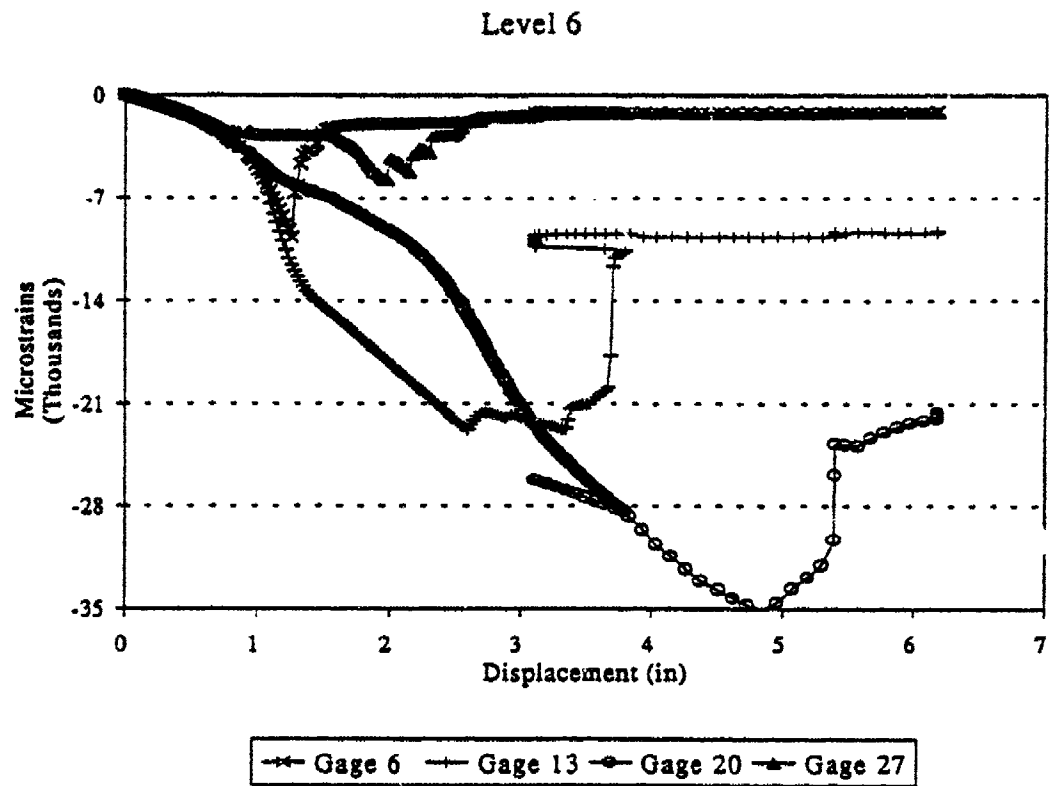


Figure B-9. Beam 10A Strain Gage Data for Level 6 Gages.

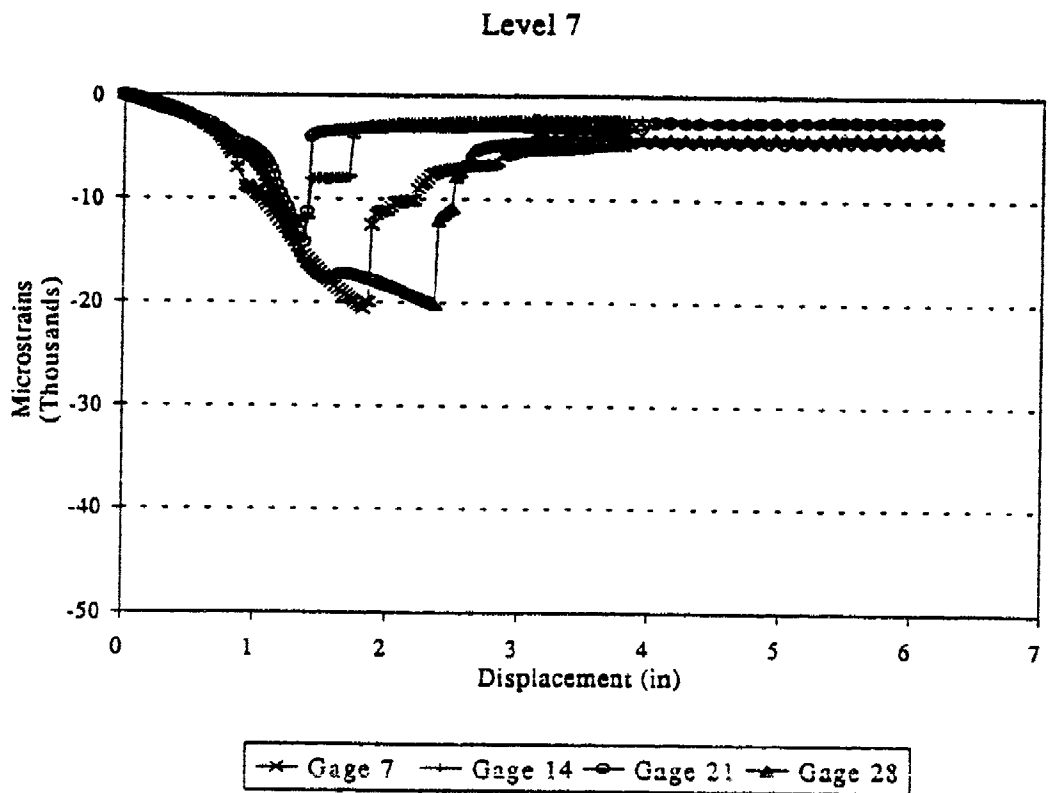


Figure B-10. Beam 10A Strain Gage Data for Level 7 Gages.

### Deflection Between Support & Load

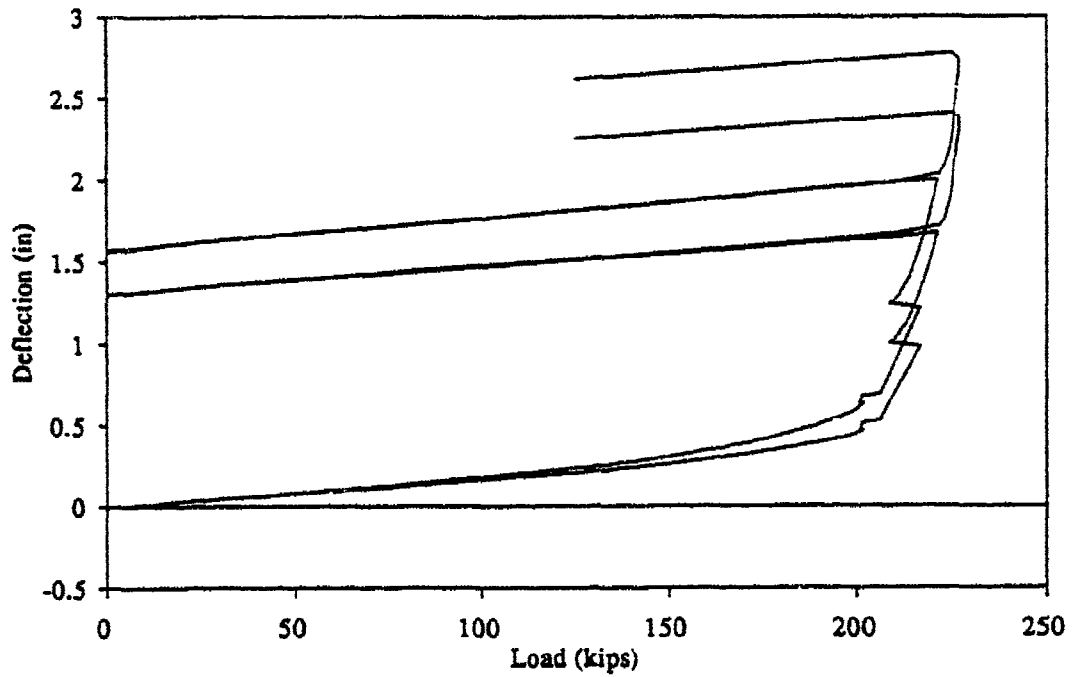


Figure B-11. Beam 10B Load Deflection Data Between Load and Support Points.

### Deflection at Load Points

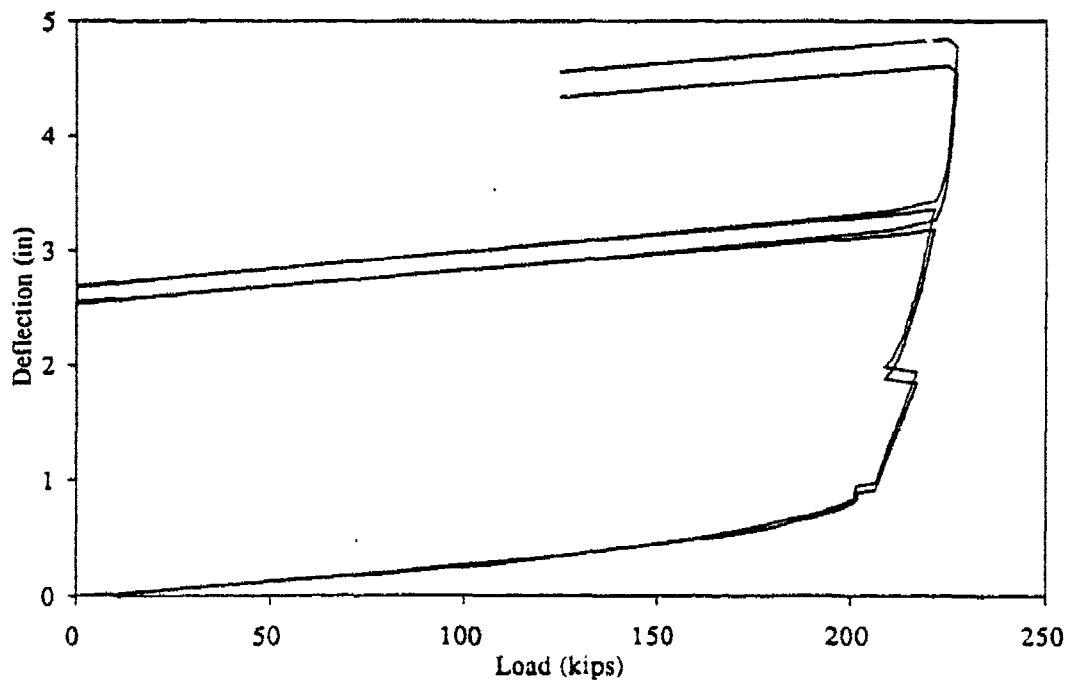


Figure B-12. Beam 10A Load Deflection Data at Load Point.

# Deflection at Mid Span

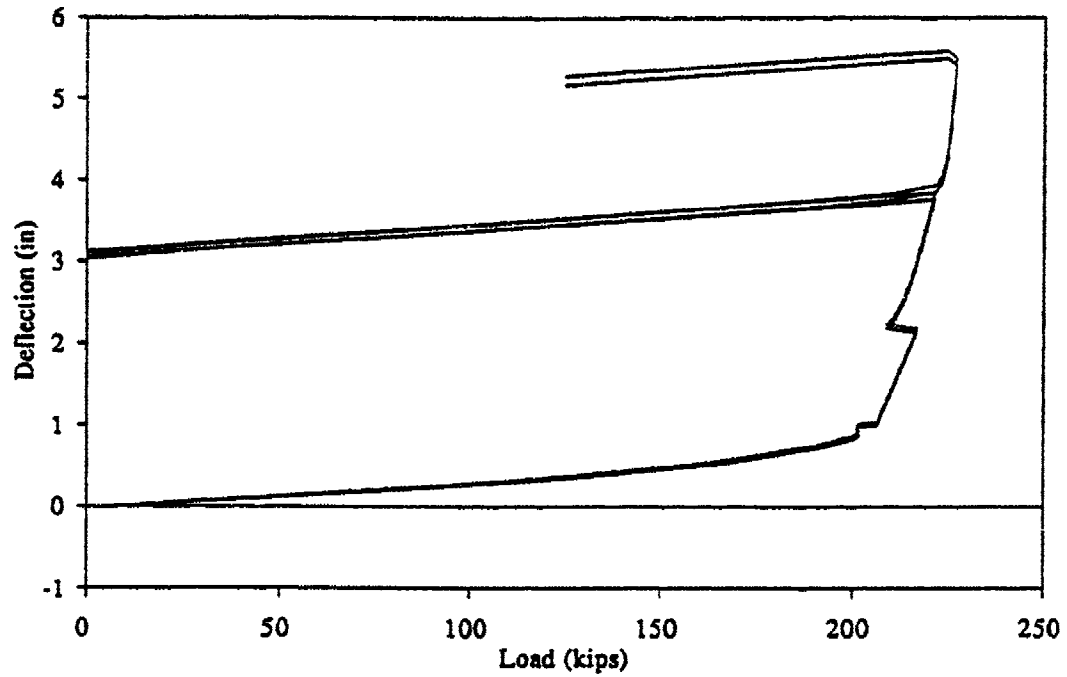
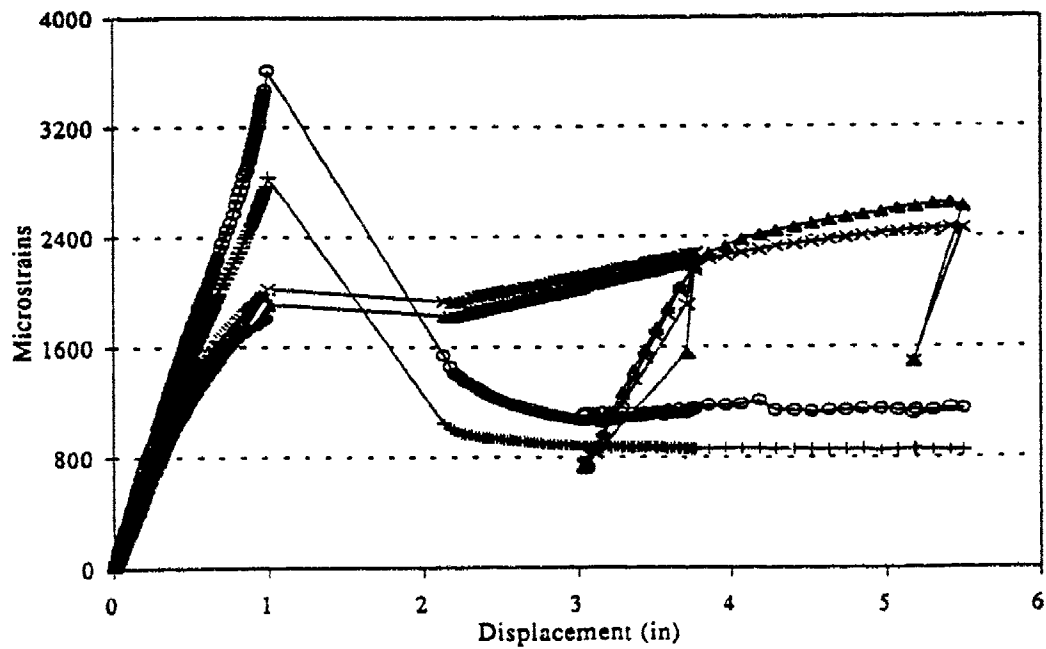


Figure B-13. Beam 10A Load Deflection Data At Midspan.

## Level 1



—x— Gage 1    —+— Gage 8    —o— Gage 15    —△— Gage 22

Figure B-14. Beam 10A Strain Gage Data for Level 1 Gages.

# Level 2

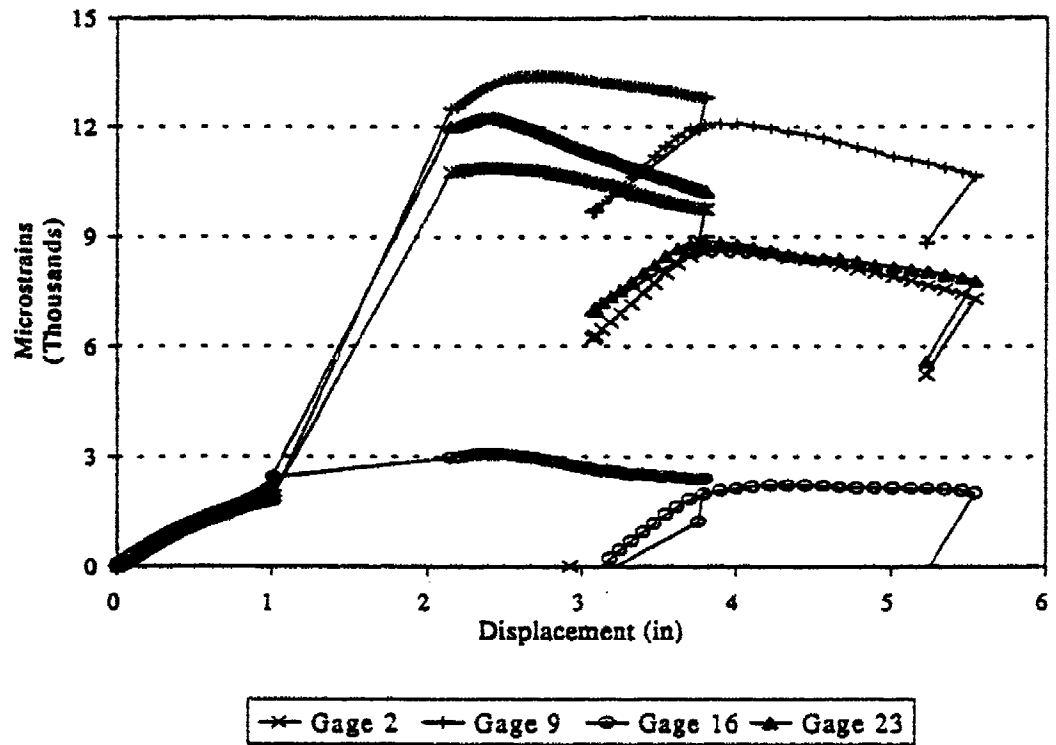


Figure B-15. Beam 10B Strain Gage Data for Level 2 Gages.

# Level 3

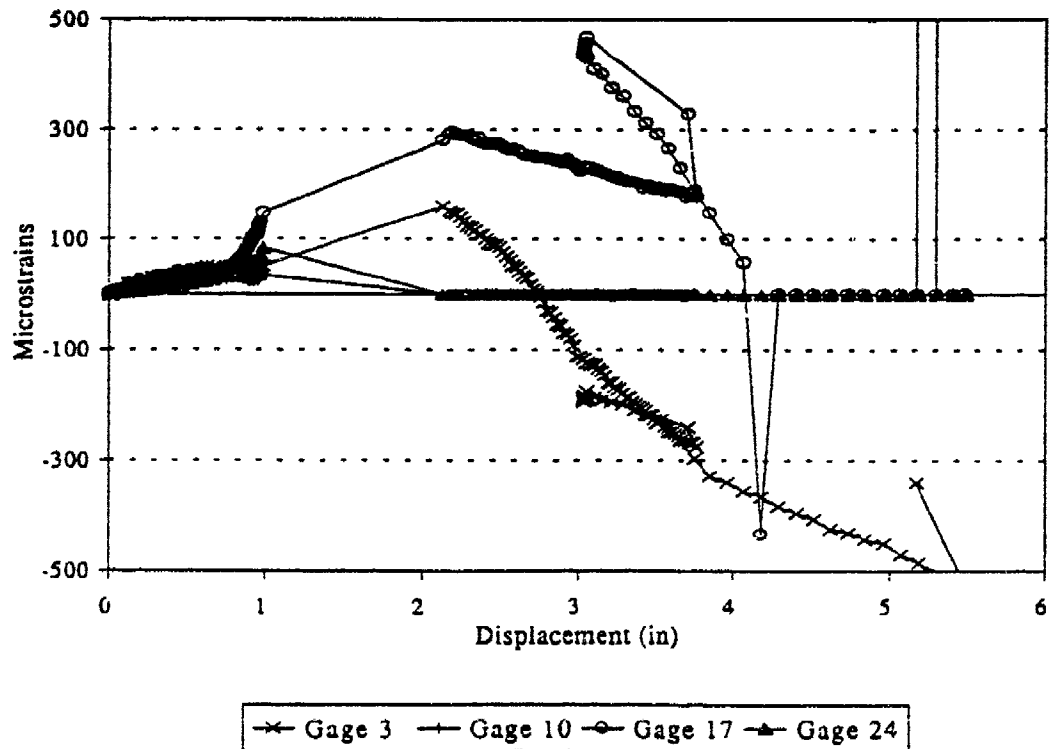


Figure B-16. Beam 10B Strain Gage Data for Level 3 Gages.

# Level 4

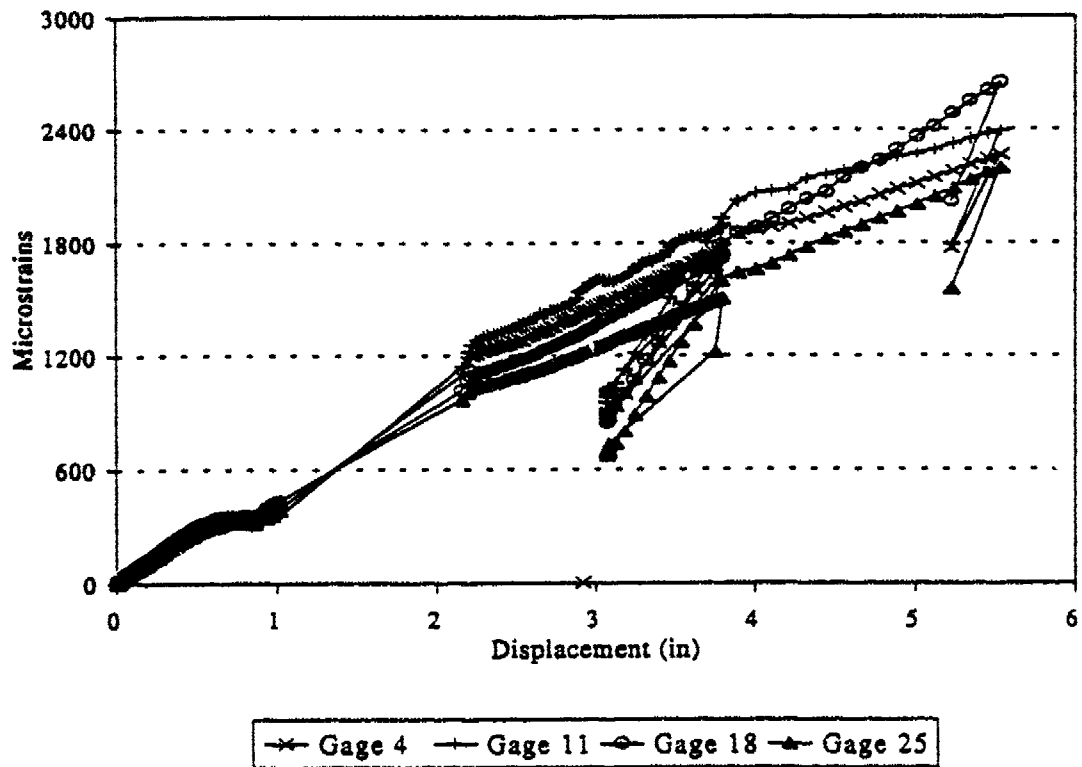


Figure B-17. Beam 10B Strain Gage Data for Level 4 Gages.

# Level 5

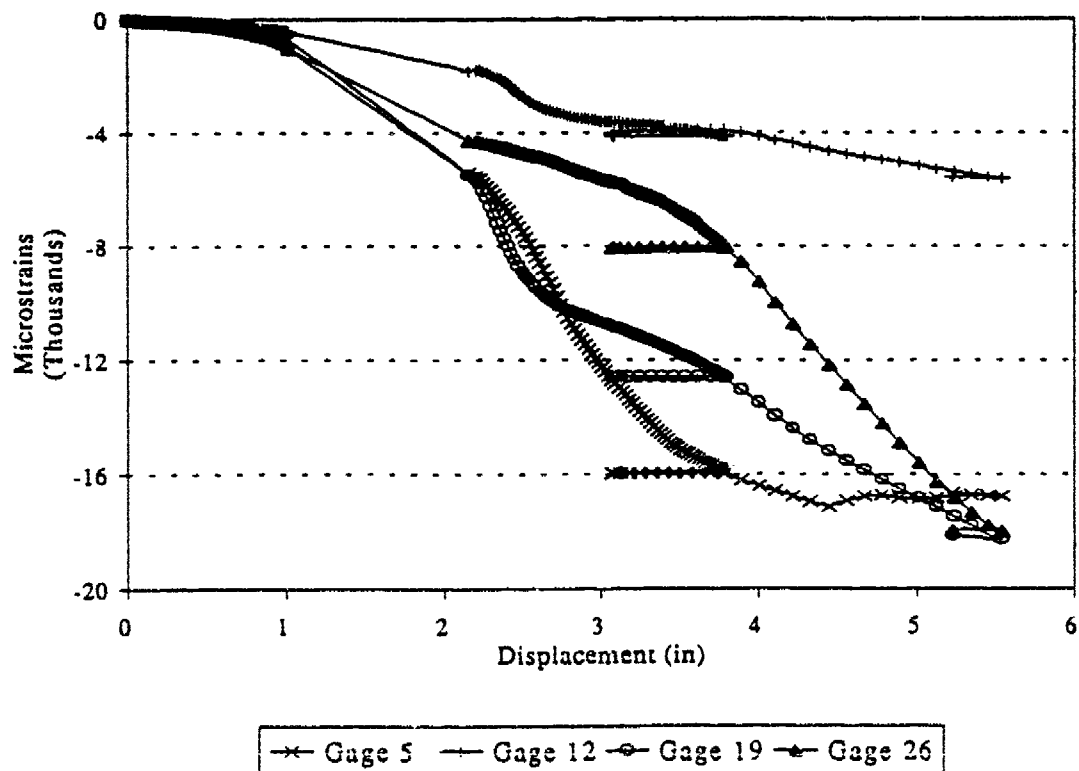


Figure B-18. Beam 10B Strain Gage Data for Level 5 Gages.



# Level 6

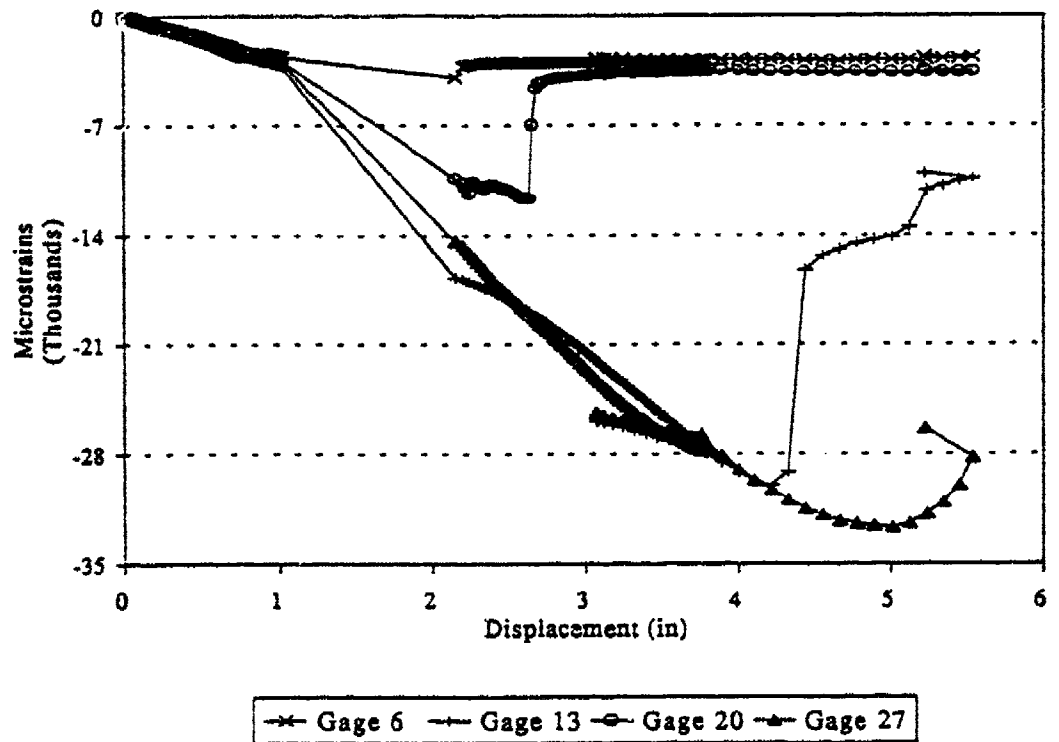


Figure B-19. Beam 10B Strain Gage Data for Level 6 Gages.

# Level 7

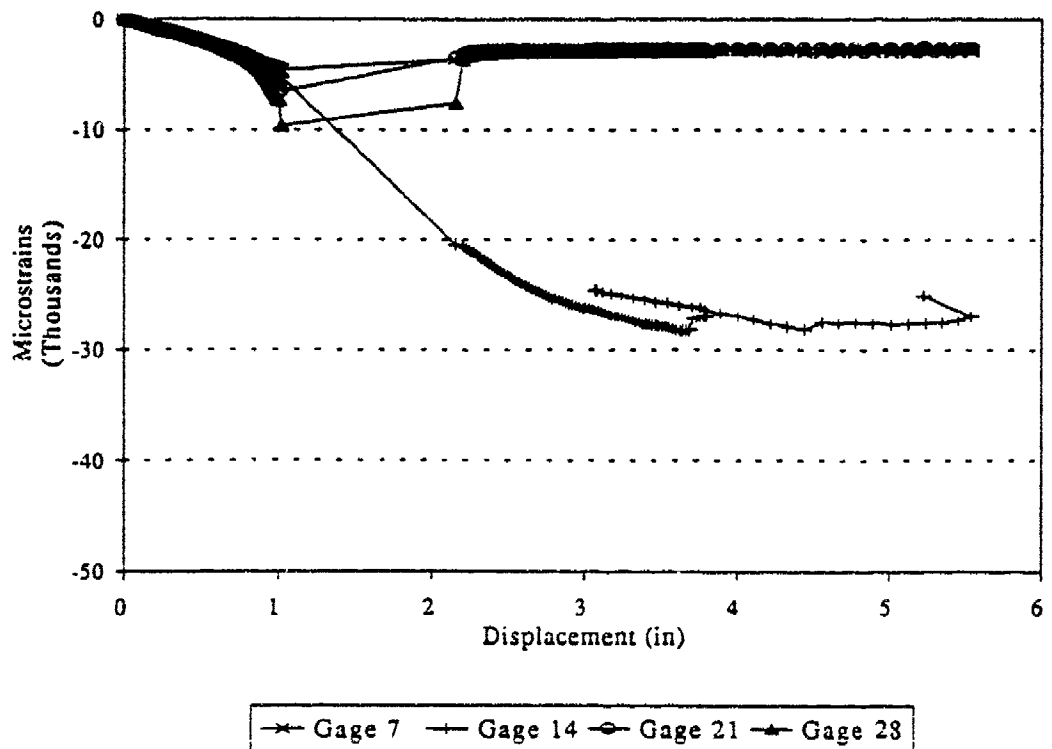


Figure B-20. Beam 10E Strain Gage Data for Level 7 Gages.

### Deflection Between Support & Load

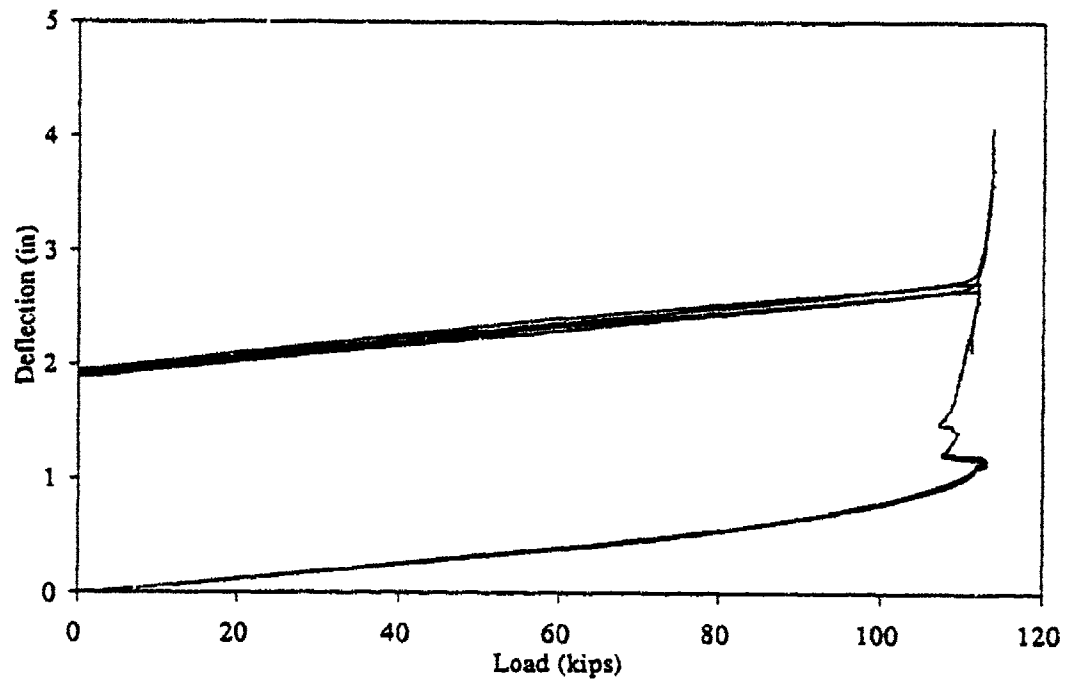


Figure B-21. Beam 16A Load Deflection Data Between Load and Support Points.

### Deflection at Load Points

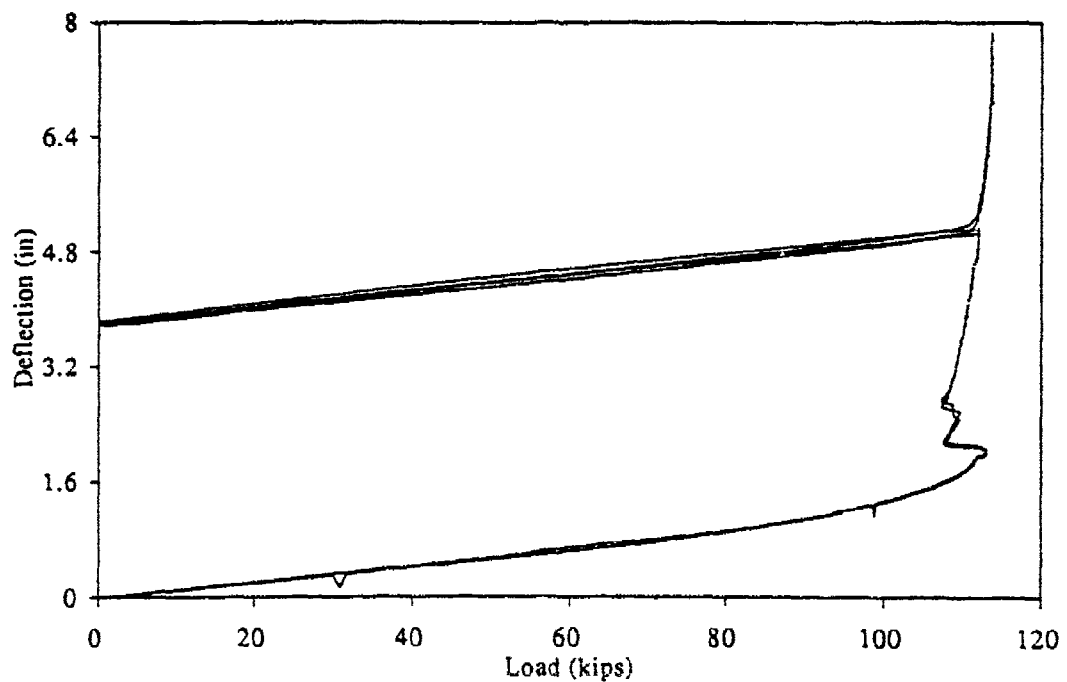


Figure B-22. Beam 16A Load Deflection Data at Load Point.

### Deflection at Mid Span

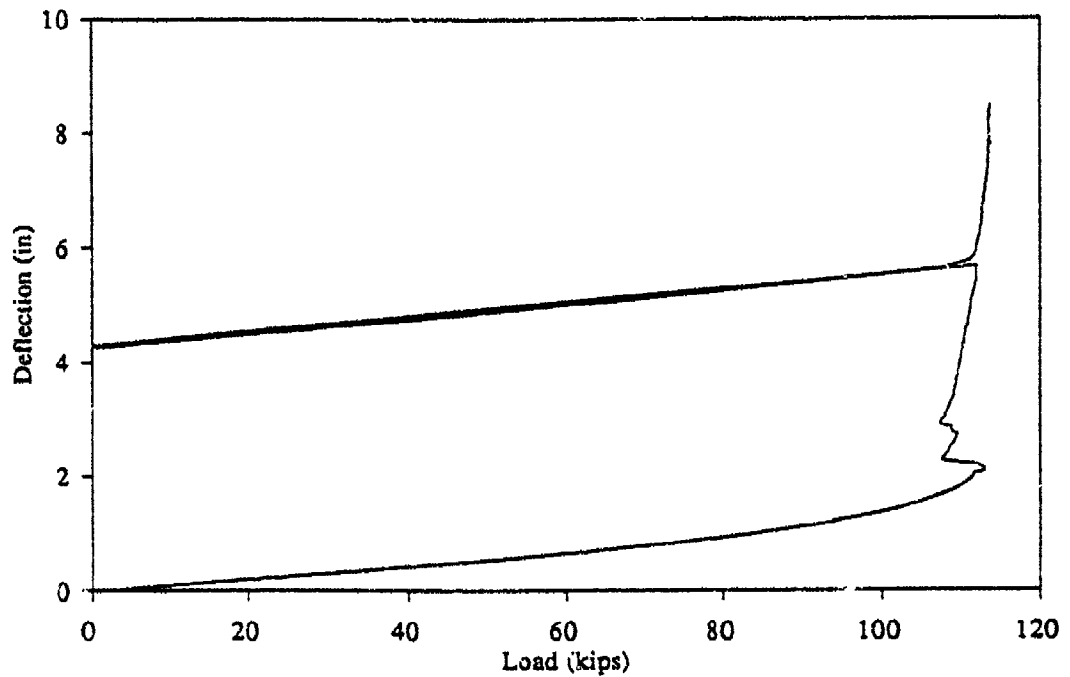


Figure B-23. Beam 16A Load Deflection Data at Midspan.

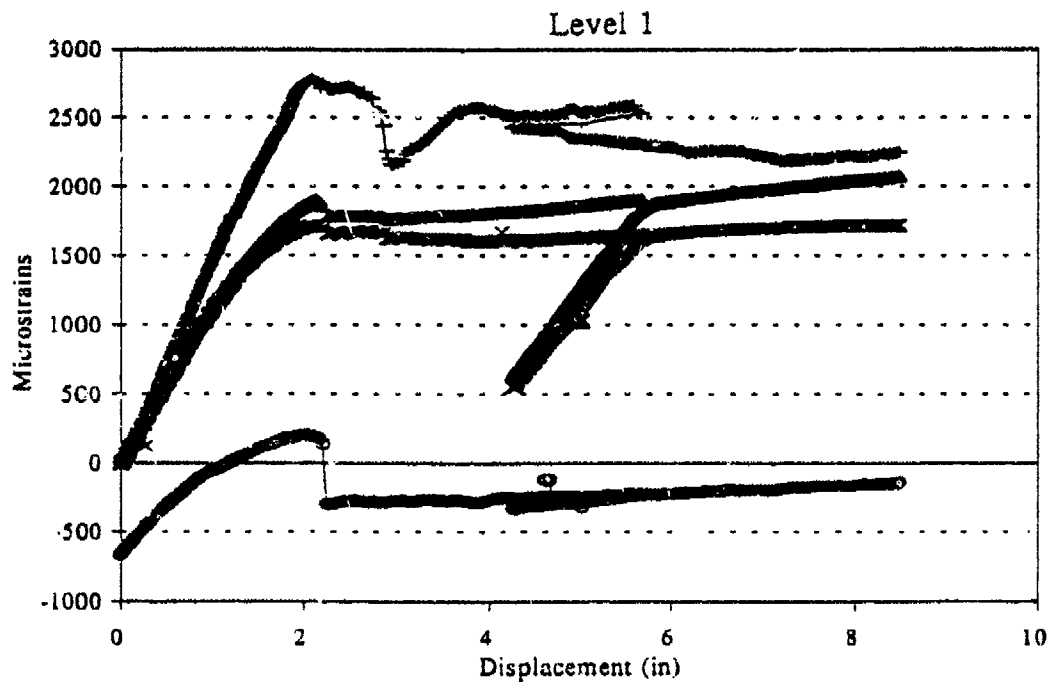


Figure B-24. Beam 16A Strain Gage Data for Level 1 Gages.

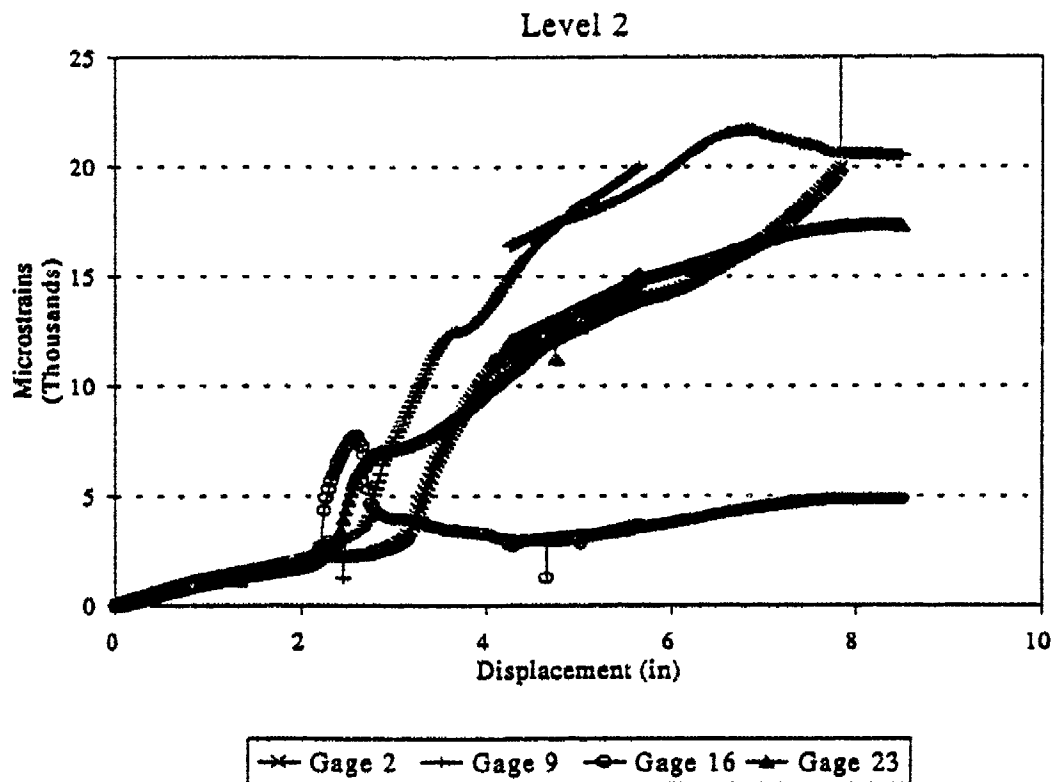


Figure B-25. Beam 16A Strain Gage Data for Level 2 Gages.

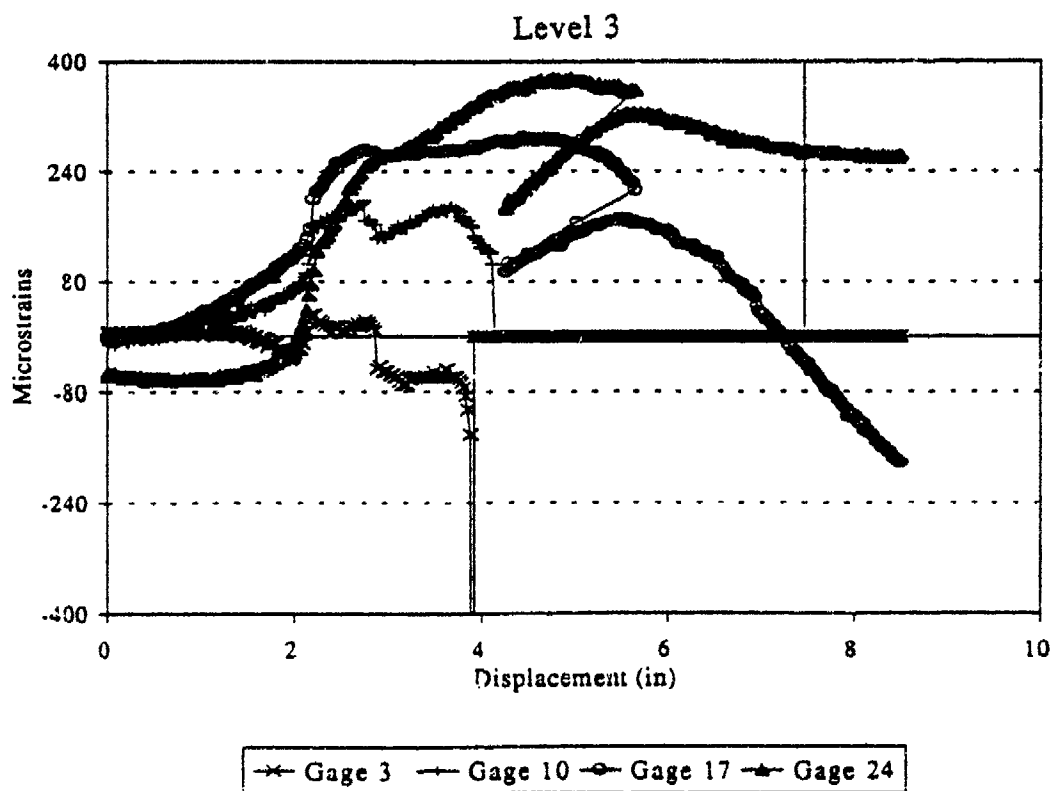


Figure B-26. Beam 16A Strain Gage Data for Level 3 Gages.

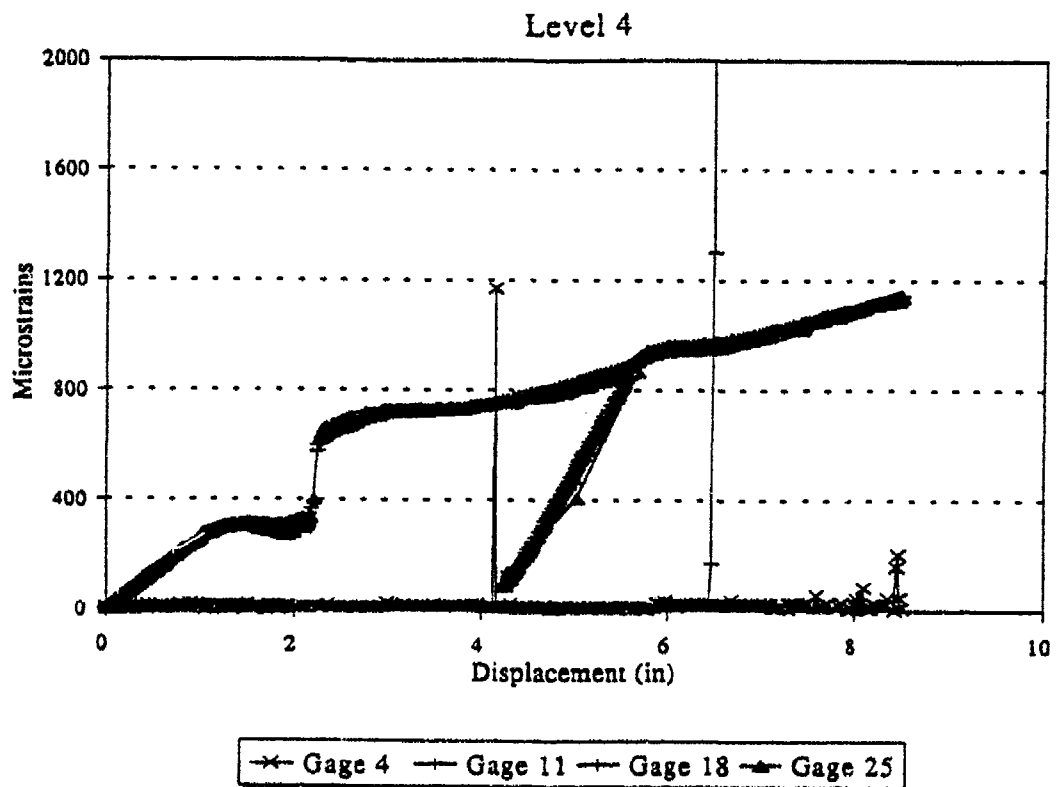


Figure B-27. Beam 16A Strain Gage Data for Level 4 Gages.

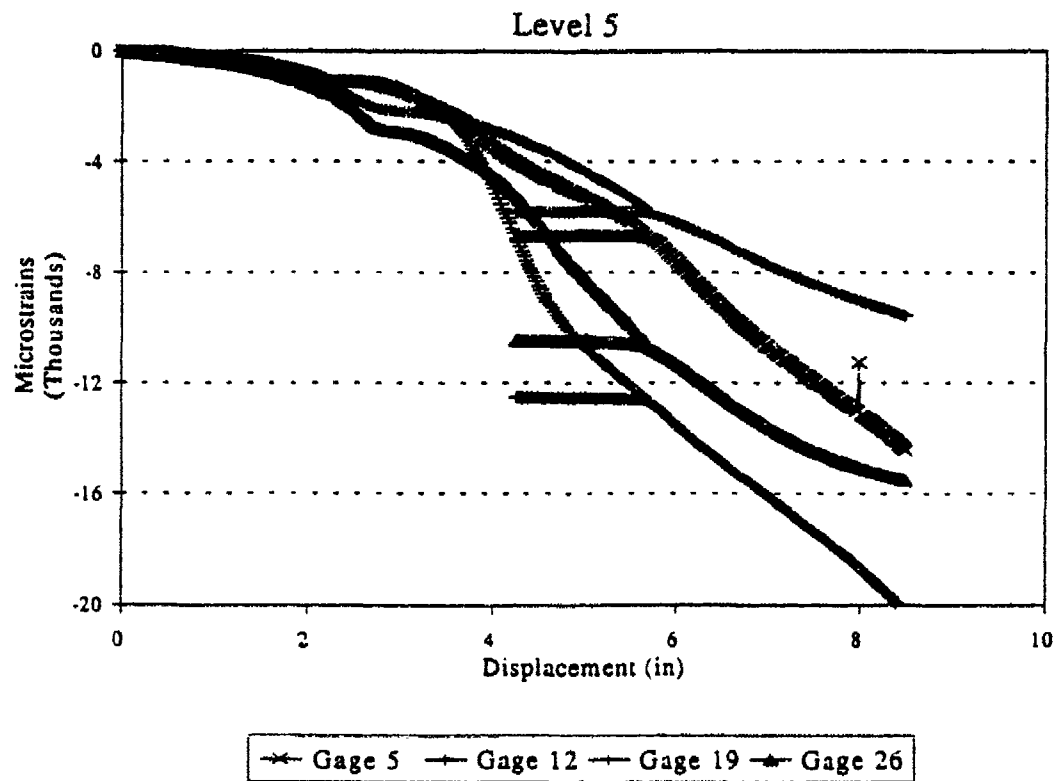


Figure B-28. Beam 16A Strain Gage Data for Level 5 Gages.

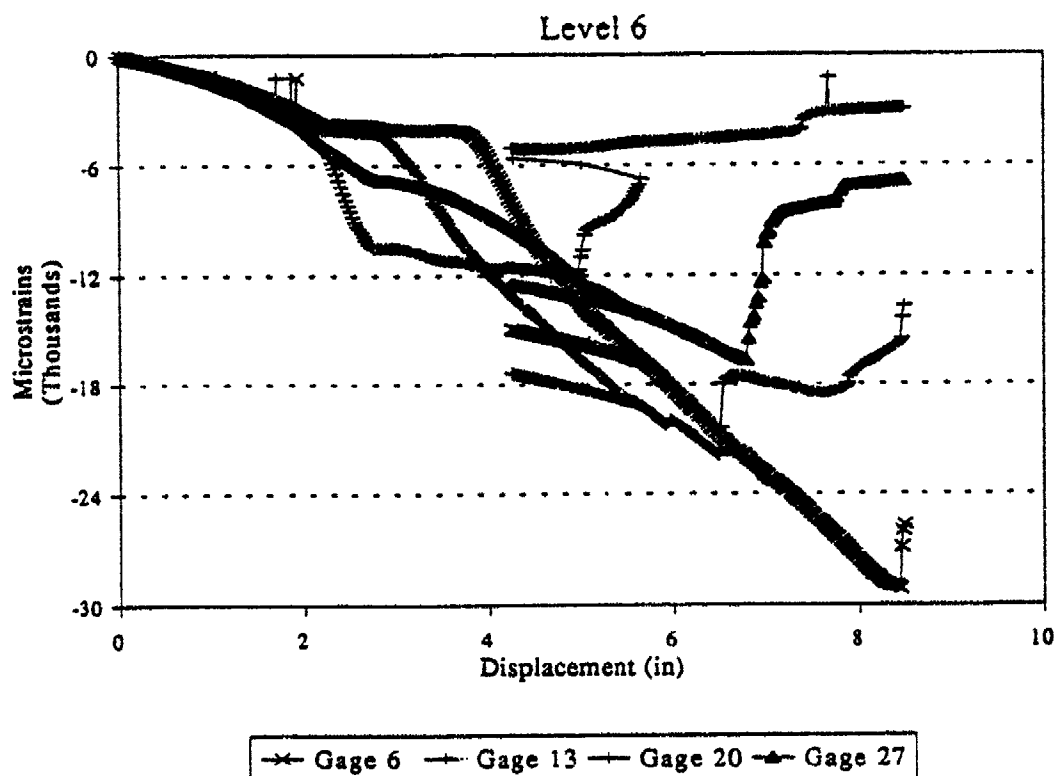


Figure B-29. Beam 16A Strain Gage Data for Level 6 Gages.

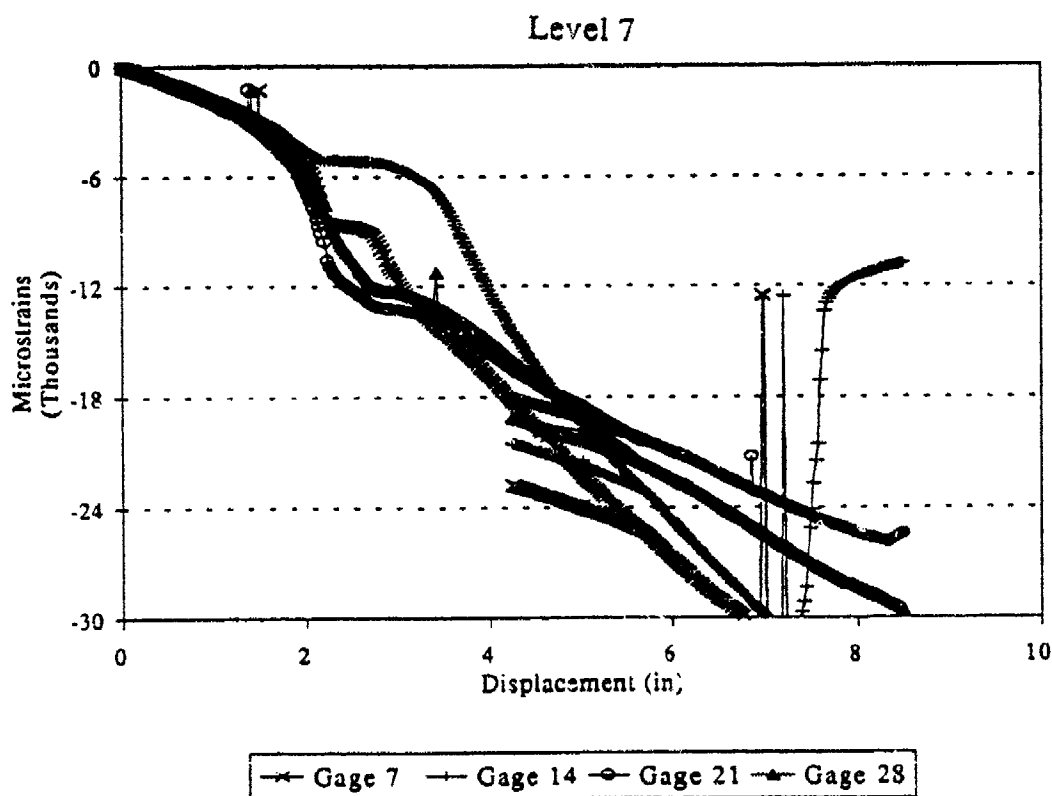


Figure B-30. Beam 16A Strain Gage Data for Level 7 Gages.

### Deflection Between Support & Load

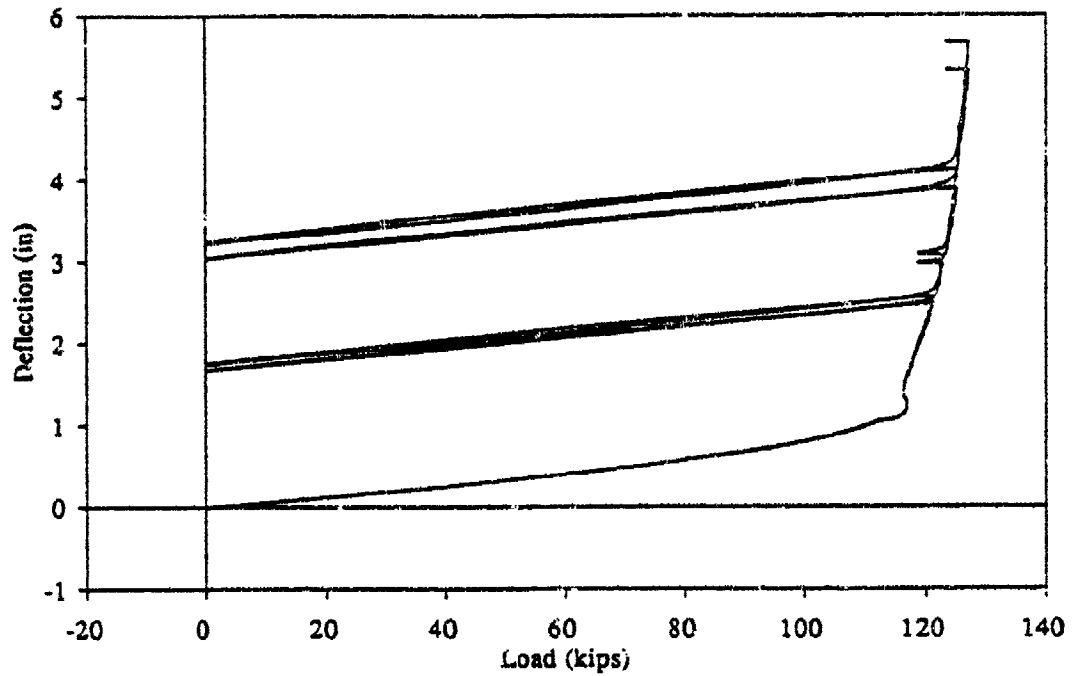


Figure B-31. Beam 16B Load Deflection Data Between Load and Support Points.

### Deflection at Load Points

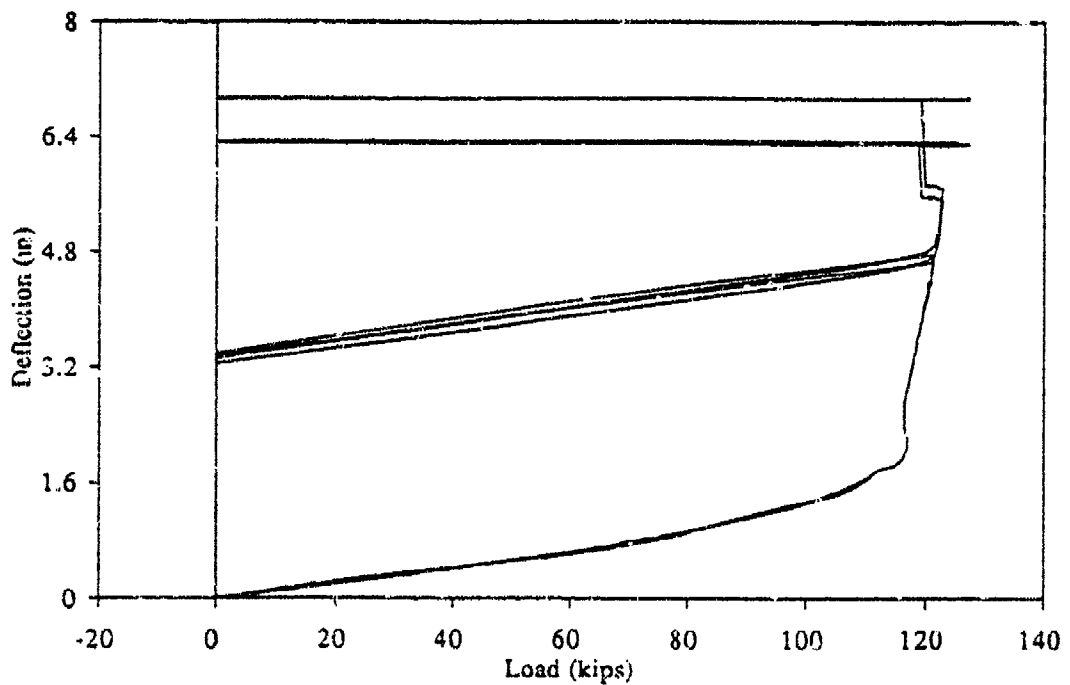


Figure B-32. Beam 16A Load Deflection Data at Load Point.

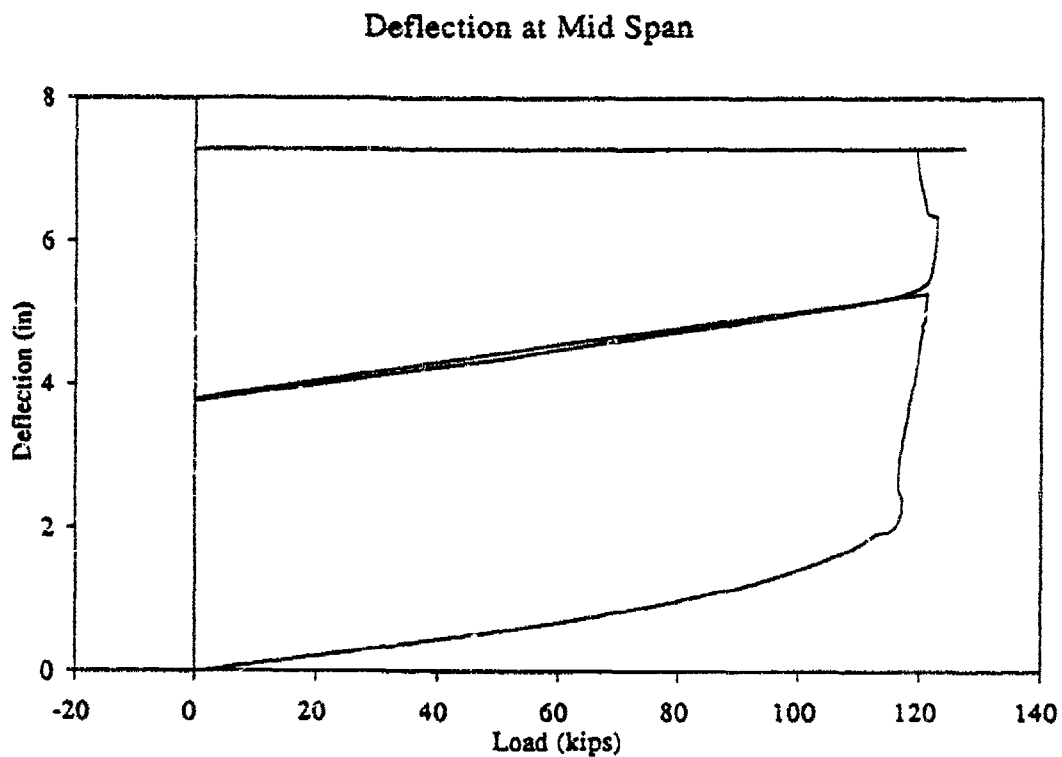


Figure B-33. Beam 16A Load Deflection Data at Midspan.

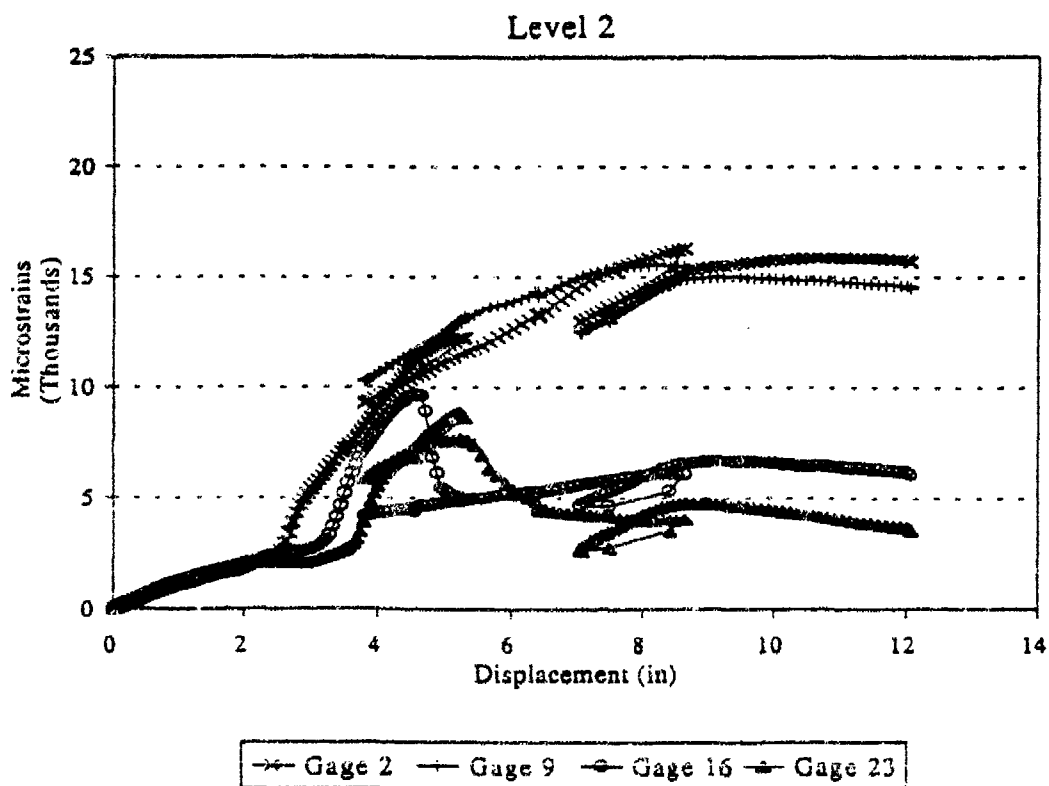


Figure B-34. Beam 16B Strain Gage Data for Level 2 Gages.



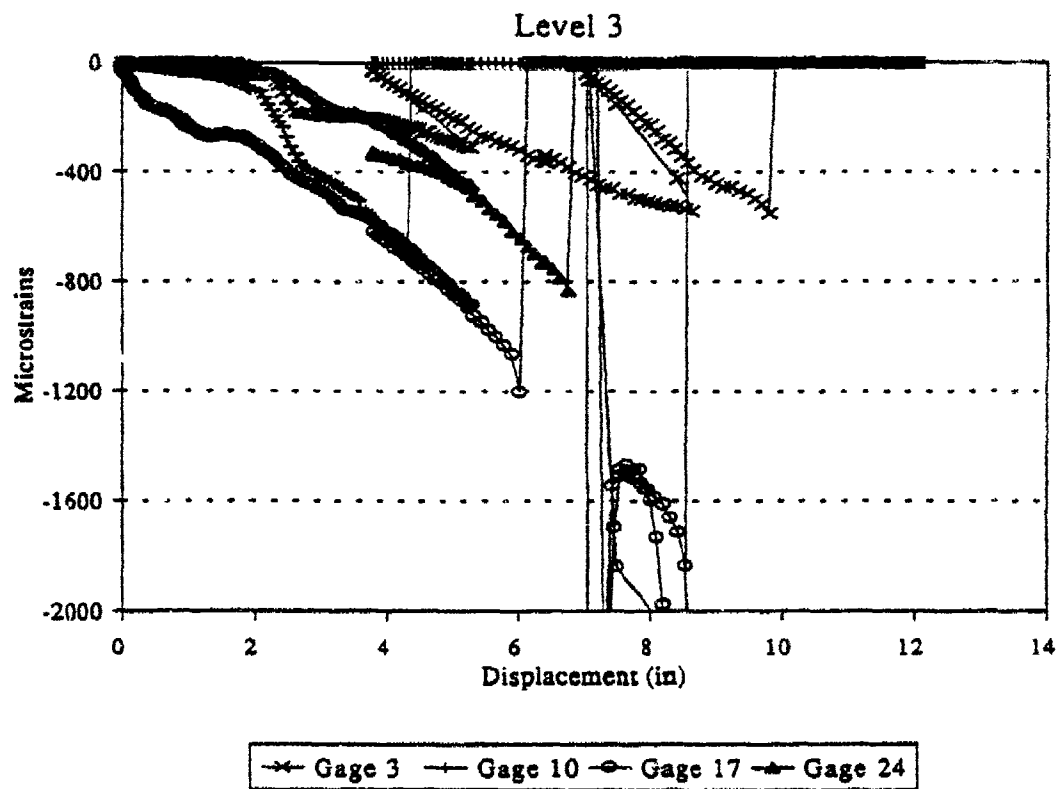


Figure B-35. Beam 16B Strain Gage Data for Level 3 Gages.

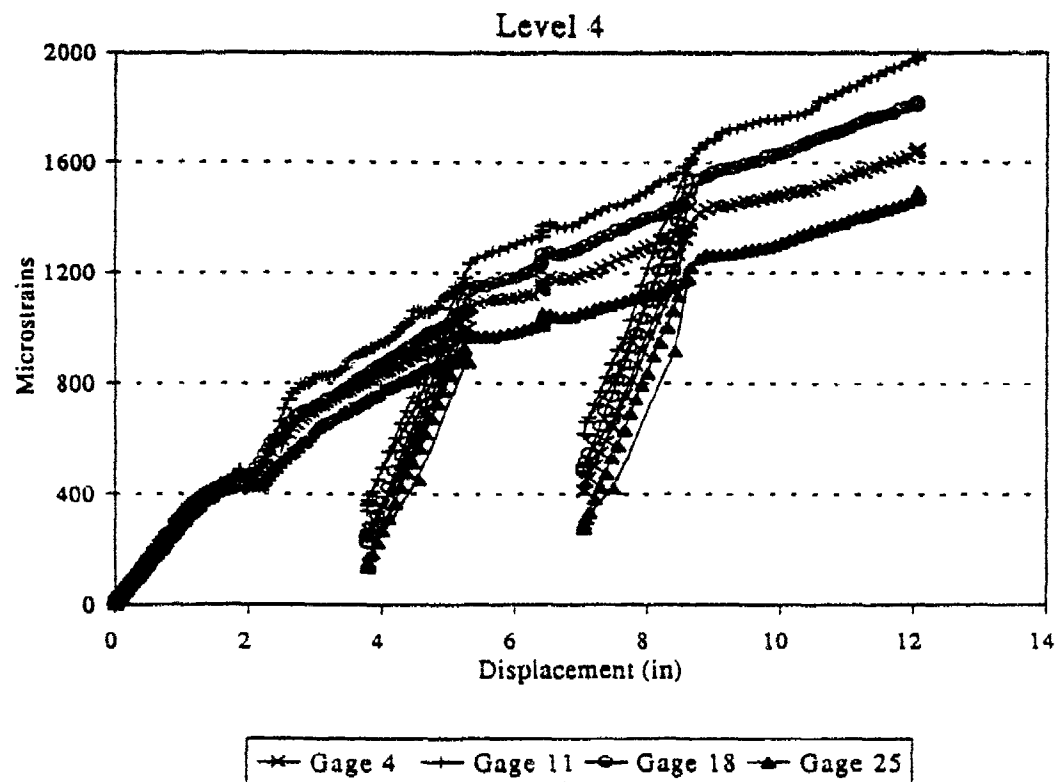


Figure B-36. Beam 16B Strain Gage Data for Level 4 Gages.

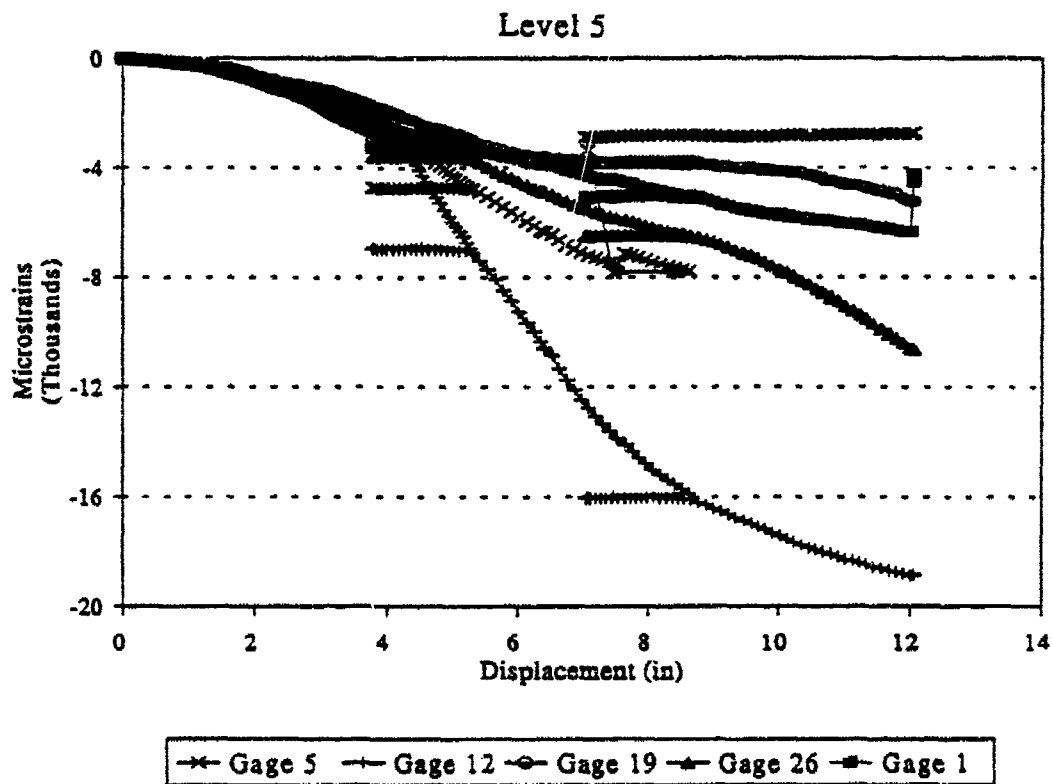


Figure B-37. Beam 16B Strain Gage Data for Level 5 Gages.

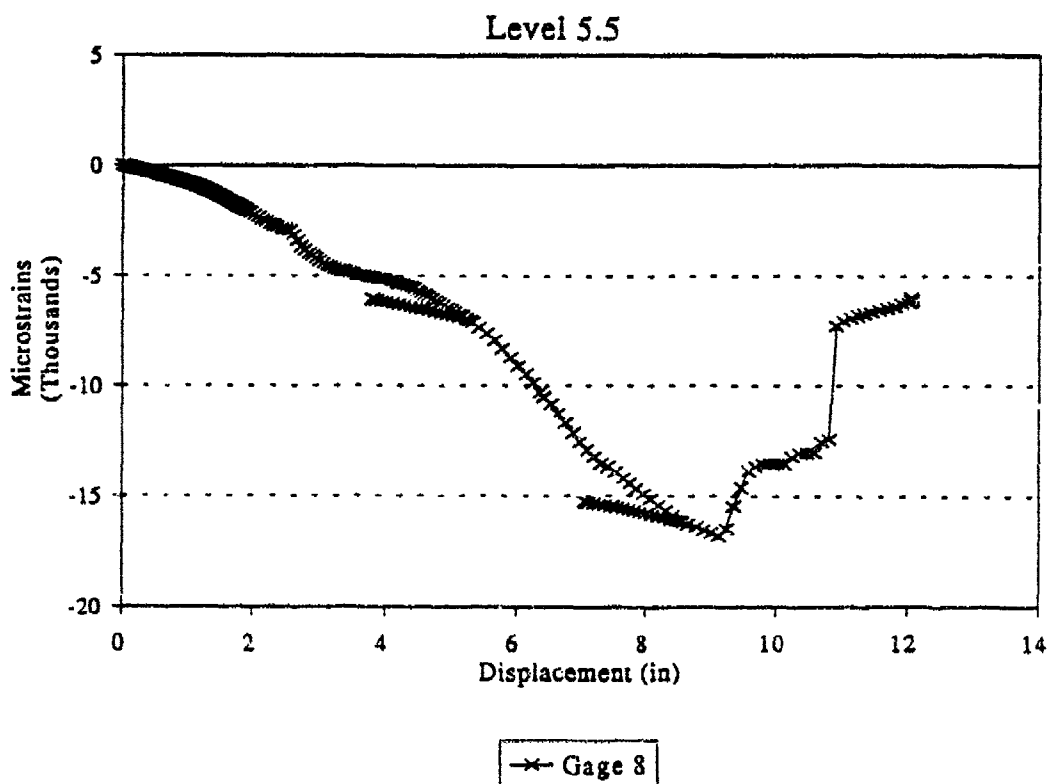


Figure B-38. Beam 16B Strain Gage Data for Level 5.5 Gage.

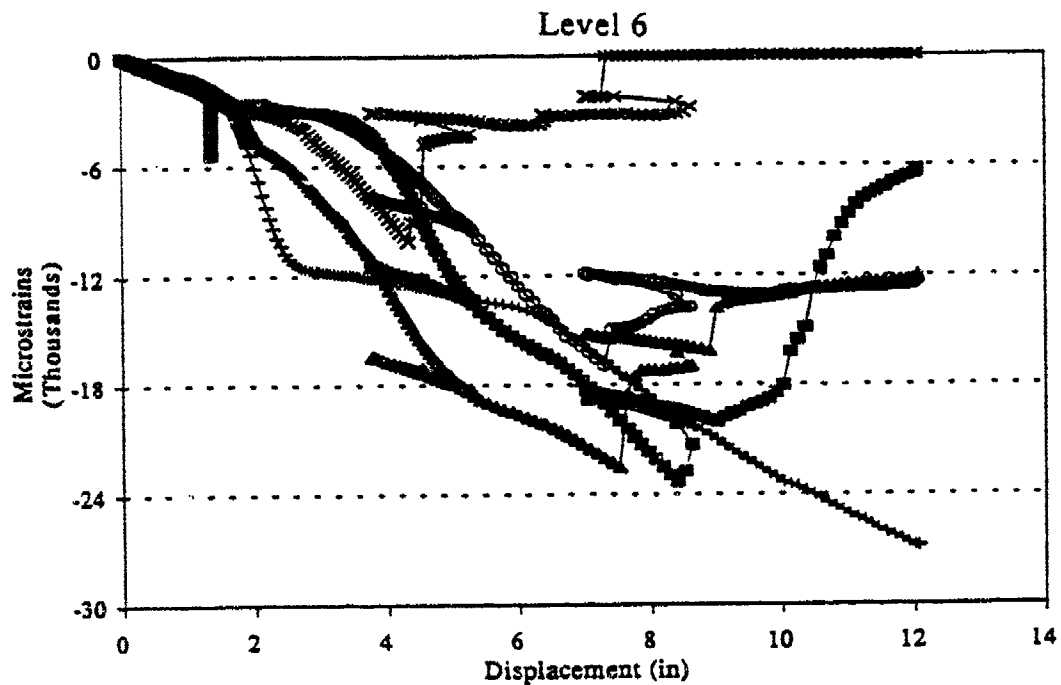


Figure B-39. Beam 16B Strain Gage Data for Level 6 Gages.

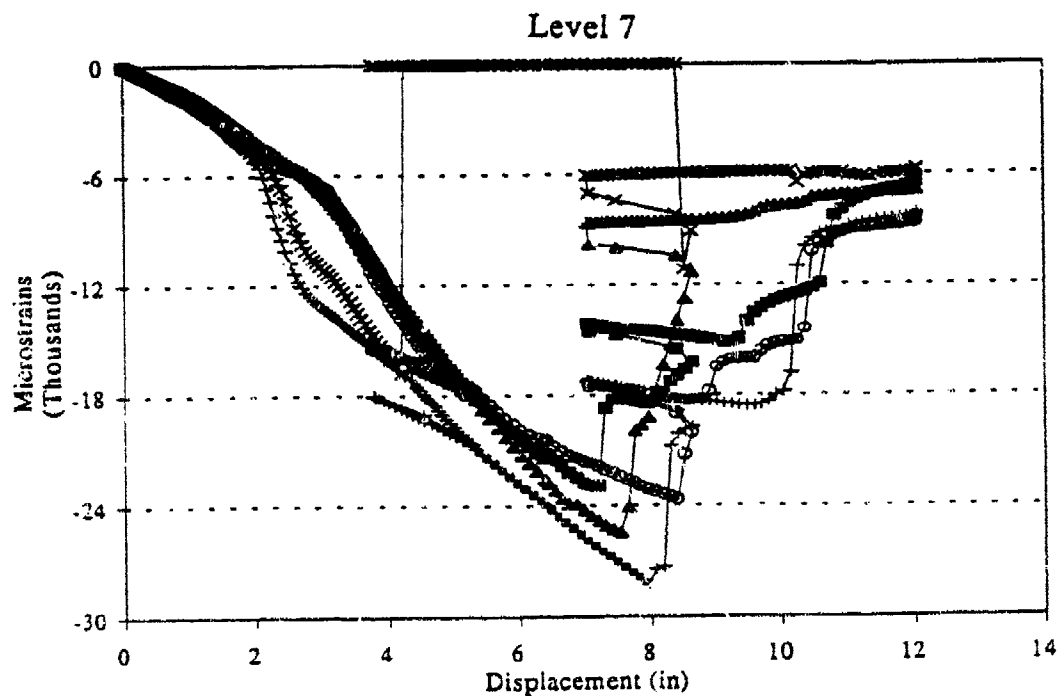


Figure B-40. Beam 16B Strain Gage Data for Level 7 Gages.